OPTIMAL DESIGN AND CONTROL OF STATIONARY ELECTROCHEMICAL DOUBLE-LAYER CAPACITORS FOR LIGHT RAILWAYS

by

TOSAPHOL RATNIYOMCHAI

A thesis submitted to The University of Birmingham for the degree of

DOCTOR OF PHILOSOPHY

School of Engineering

Department of Electronic, Electrical and Systems Engineering

The University of Birmingham, UK

March 2016

Abstract

DC railways are fed by transformer-rectifier substations and, therefore, the energy regenerated by a train during braking can be used only if another train is accelerating nearby. The energy efficiency of the railway could be improved by adding storage devices, which could absorb the braking energy and help the substations during train's acceleration. Storage devices are preferably stationary, as the modification of existing rolling stock requires a significant redesign effort, and have to have high power density, as braking and acceleration last for tens of seconds and up to few minutes. Nevertheless, storage devices add a significant additional cost to the electrification system and, hence, their storage capacity should be minimised. However, the storage capacity is dependent on the service of the trains, the characteristics of the track and the feeders and the position of the storage devices themselves, which make not easy the design of the optimal capacity. Additionally, even when the optimal storage has been designed, a suitable control of the storage is required to effectively reduce the energy consumption, because real train conditions are normally different from the designed case.

This thesis proposes a new method to optimise the capacity of the storage devices for a DC railway with reference to stationary electrochemical double-layer capacitors (EDLCs) and a new piece-wise linear state of charge control algorithm that optimises the energy consumption of trains by controlling the state of charge of EDLCs.

The capacitances and positions of the stationary energy storage have been optimised using the theory of calculus of variations. This unique approach links together the capacitances and positions of the storage within an objective function. The optimal capacitances are

therefore those minimising the objective function. This method requires the modelling of a DC railway electrification system, which includes rolling stock, electrical substations and the stationary EDLCs. The electrical powers of the substations have been obtained using the Single Train Simulator of Birmingham Centre for Railway Research and Education, which permits the simulation of different characteristics of the train in terms of speed, acceleration and mechanical power.

The optimisation algorithm has been further investigated to understand the influence of the weight coefficients that affect the solution of all the optimisation problems and it is very often overlooked in the traditional approach. In fact, the choice of weight coefficients leading to the optimum among different optimal solutions also presents a challenge and this specific problem does not give any a priori indications. This challenge has been tackled using both genetic algorithms and particle swarm optimisations, which are the best methods when there are multiple local optima and the number of parameters is large. The results show that, when the optimal set of coefficients are used and the optimal positions and capacitances of EDLCs are selected, the energy savings can be up to 42%.

The second problem of the control of the storage has been tackled with a linear state of charge control based on a piece-wise linear characteristic between the current and the voltage deviation from the nominal voltage of the supply at the point of connection of the storage. The simulations show that, regardless of the initial state of charge, the control maintain the state of charge of EDLCs within the prescribed range with no need of using the on-board braking resistor and, hence, dissipating braking energy. The robustness of the control algorithm has been verified by changing the characteristics of the train loading and friction force, with an energy saving between 26 – 27%.

Acknowledgements

I wish to express my sincere gratitude to my supervisors Dr Pietro Tricoli and Dr Stuart Hillmansen for their invaluable advice, supervision and support throughout my study. I have greatly benefitted from their knowledge, experience and understanding of traction systems, DC electrification systems, light railway systems and energy storage devices. I am also grateful for their encouragement when I faced difficulties with my study and for their patience in helping me to improve my English.

I also wish to express my sincere gratitude to Prof. Clive Roberts for giving me the opportunity to study my PhD at the Birmingham Centre for Railway Research and Education at the University of Birmingham and for his encouragement and valued discussions throughout my study.

I acknowledge the Office of the Civil Service Commission, Thailand for providing financial support toward the cost of tuition fees and student general maintenance costs during my PhD study and also the Office of Educational Affairs, the Royal Thai Embassy, London for taking care of both education and welfare.

I am grateful to everybody at the Birmingham Centre for Railway Research and Education for their continuous help, support, encouragement and friendship, and also to everyone who allowed me to use MATLAB programming at their computer desk.

I also wish to express my sincere gratitude to Katherine Slater for anglicising this thesis.

Lastly, I would like to express my gratitude to everyone in my family for their understanding, sincere encouragement and never-ending support.

Table of Contents

List of Figures

List of Tables

List of Acronyms

Term	Explanation / Meaning / Definition
ADEME	French Environment and Energy Management Agency
CJRC	Central Japan Railway Company
CPU	Central Processing Unit
DC	Direct Current
EDLCs	Electrochemical Double Layer Capacitors
FEM	Finite Element Method
GA	Genetic Algorithm
HES	Hybrid Energy Storage
JR	Japan Railway
KCL	Kirchhoff Current Law
KVL	Kirchhoff Voltage Law
Li – ion	Lithium – ion
LUL	London Underground Limited
LRV	Light Rail Vehicle
MTS(a)	Metro Transports do Sul
MTS(b)	Multi Train Simulator
NEC	Nippon Electric Company
Ni – MH	Nickel Metal Hydride
PB	Permanent Battery
PSO	Particle Swarm Optimisation
RAM	Random Access Memory
RATP	Régie Autonome des Transports Parisiens / Autonomous Operator of Parisian Transports

SES	Stationary Energy Storage
SOC	State of Charge
STEEM	Maximise Energy Efficiency Tramway System
STS	Single Train Simulator
SWIMO	Smooth Win Mover
TB	Temporary Battery
USSR	Union of Soviet Socialist Republics

Chapter 1 Introduction

1.1 Overview of DC Railway Systems

DC electric traction power supply, which it uses DC for the final supply to the train via parts of the conductor system along the track, distributes the power to the track from the trackside substations. In all cases, this power can be derived from the industrial utility supply at a level within the grid system which is suitable to the power being drawn at 11, 22 or 33 kV for light railways and metros. The DC railway systems in common use are as follows:

- 600 – 1000 V. Implemented for metros, light rail transit, street-cars and suburban railways. A conductor arrangement is a third rails at the side or third and fourth rails (exceptionally, London Underground Limited: LUL), otherwise an overhead for street running;
- 1500 V overhead. Implemented for most economic solution of heavy metros;
- 3000 V overhead. Implemented for extensive installations of the exist suburban and mainline, especially in Italy, former Union of Soviet Socialist Republics (USSR), South Africa, etc. It is generally out of dated by 25 kV AC.

The power supply of DC electrified railways generally comes from electrical substations placed along the route, based on transformer rectifiers. These are diode rectifiers and hence not bidirectional in power, as shown in Figure 1.1. The mainline power of DC railway vehicles is derived from the grid system of the industrial utility supply with a voltage of 11, 22 or 33 kV and then equipped with rectifiers with a voltage of 630/750 V_{dc}

in the UK, and 1.5 and 3.0 kV in other countries such as European countries, South Africa and India, etc. The main components of DC substations are as follows (Goodman, 2010):

- **Duplicated distribution transformers:** to transfer the 3-phase AC input voltage of the grid distribution system from 22 kV to 11 kV and then from 11 kV to the DC voltage with rectifiers of 630 – 1500 Vdc;
- **AC circuit breaker:** for protection from over load and fault conditions;
- **AC switches/ isolators:** for power supply selection of the incoming feeder and transformer in cases of maintenance access and emergency feeding conditions;
- **6- pulse diode bridge rectifier:** to rectify the AC voltage to become the DC voltage via the uncontrollable rectifier, this is non-bidirectional power;
- **DC switches/ isolators:** for selecting the rectifier section and isolating track sections;
- **High-speed DC circuit breakers:** for protecting the train and track from a large DC current of an induction circuit.

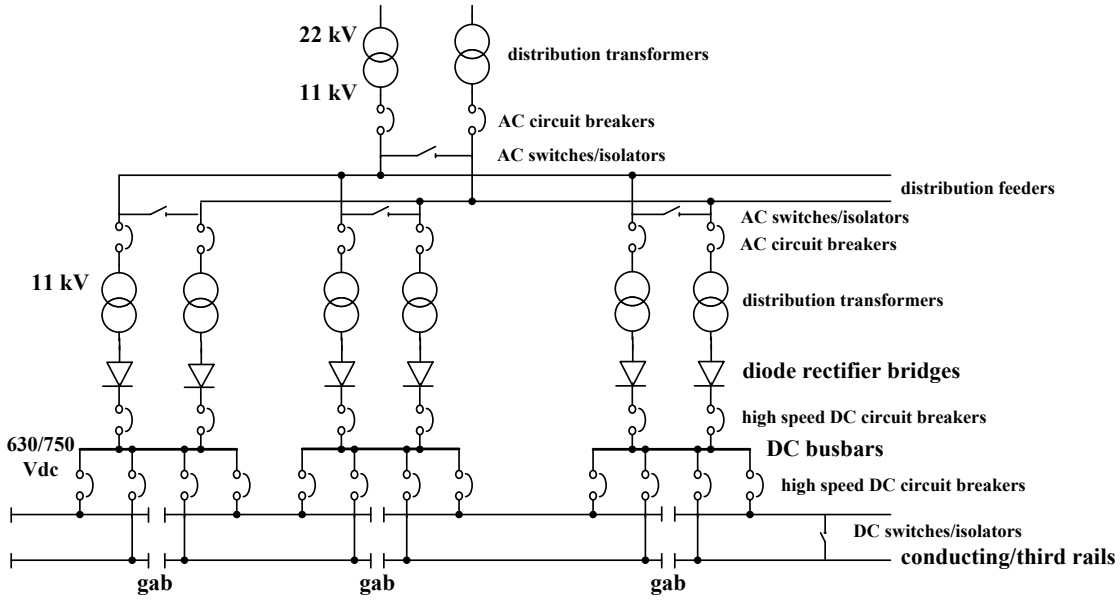

Figure 1.1: Schematic of the DC substation (Goodman, 2010)

Based on the traffic density of DC railway systems, the distance between the substations is in the range of 3 to 9 km. The resistance of the overhead conductor system is 35-90 mΩ/km whereas the third rail system provides 8-20 mΩ/km. In the simulation, the resistances of the conductor (catenary or third-rail) and rail are normally combined together at the middle between substations.

There is a problem with stray current within the DC system as the rails are connected to the ground, therefore the current can eventually return back to the substation via the earth mat. Stray current has caused electrolytic corrosion damage of gas pipes and metal parts of the tracks. This problem can be solved by connecting the rails directly to the negative busbar of the substations without connecting to the ground or insulating the rails.

Based on the duplicated diode bridge rectifier, only one direction of power can flow from the DC power substation to support the train motoring. However, the power from a regenerating train is unable to flow back to the substations, so this power has to be dissipated by the on-board electric resistors. Alternatively, the reuse of regenerative braking energy can improve the efficiency of a DC railway system in terms of energy consumption saving, peak power reduction and voltage profile regulation by applying the inverting substation, appropriate train timetables and energy storage devices.

DC railway systems mainly include the light railway and heavy railway systems. Light railway systems are recently more popular than the heavy railway systems in terms of high capacity, low capital costs and high reliability. Therefore, light railway systems are a special case of the DC railway systems for a passenger service.

Light railways are DC electrified railways operating train services for passengers in urban areas. Examples of light railways are trams, suburban railways and rapid transits that are

characterised by the presence of a large number of stations within a distance of a few kilometres. Therefore, the headway between successive trains on the same route is expressed in a few minutes and the dwell time of trains at the stations is expressed in seconds.

Definition 1.1 (Light railway): An electric railway with a light volume traffic capacity compared to a heavy railway. A light railway may use shared or exclusive rights-of-way, high or low platform loading and multi-car train or single cars. It is also known as a streetcar, trolley car or tramway.

Definition 1.2 (Heavy railway): An electric railway with the capacity for a heavy volume of traffic and characterised by exclusive rights-of-way, multi-car trains, high speed and rapid acceleration, sophisticated signalling and high platform loading. It is also known as a rapid rail, subway, elevated (railway), or metropolitan railway (metro).

Definition 1.3 (Headway): The time interval between the passing of the front ends or successive train units moving along the same track in the same direction, usually expressed in minutes.

Definition 1.4 (Dwell time): The time that a train spends at a station or stop, measured as the interval between its stopping and starting.

1.2 Motivation of the work

Energy consumption reduction or energy saving are the main aims of railway efficiency, especially in DC light railways because their applications have many frequent stops along the route where energy saving can be achieved with the benefit of regenerative energy from the trains braking. The traction energy flow of DC light railway systems is illustrated

in Figure 1.2; it can be seen that about 33% of traction energy can be recovered back to the DC power supply by regenerative braking. In practice, if there are no trains running in the neighbourhood area and the DC substation is not bi-directional in power, then the surplus regenerative braking energy that remains from the primary use of the auxiliary and comfort functions on-board will be dissipated by the braking resistor on-board the train (Gonzalez-Gil et al., 2015). The auxiliary loads and comfort functions on-board are the electrical systems that consume energy on trains and at substations, including signalling systems, ventilation systems, lighting systems, heating systems, air-conditioning systems and other electrical systems.

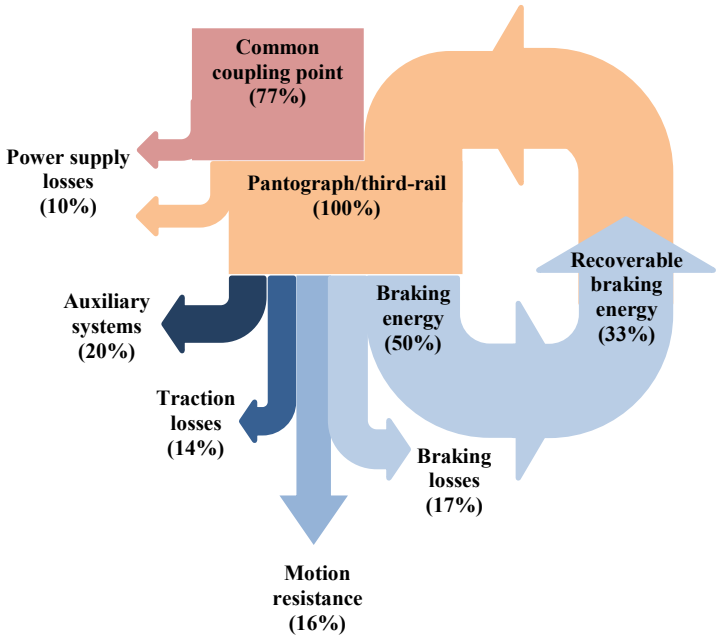

Figure 1.2: Traction energy flow diagram for DC light railway systems (Gonzalez-Gil et al., 2015)

There are many research and practical solutions to tackle the problem of energy saving for DC light railway systems with the reuse of regenerative braking energy, such as

optimised timetables, reversible substations and the application of energy storage systems.

In this thesis, the research is based on the application of energy storage devices and energy saving for DC light railway systems is achieved with the use of electrochemical double-layer capacitors (EDLCs). This is because the characteristics of EDLCs are suitable for DC light railways in terms of high power density, quick recharge/discharge, low internal resistance, long life cycle and low maintenance.

1.3 Solutions for Saving Energy

Based on Figure 1.2, energy saving for DC light railway systems, which have the characteristic of numerous and frequent stops, is most likely to be achieved by technology that recovers and reuses the braking energy. The braking energy is recuperated as it is supplied back to either the power network or substations, or it is used to support the simultaneous acceleration of trains, with the following currently available options:

- **Energy-optimised timetables:** to synchronise the time of trains motoring and braking by means of timetable optimisation. This method is quite easy to implement, as it does not require any extra components and can increase energy savings up to 14% (Gonzalez-Gil et al., 2014, Nasri et al., 2010);
- **Inverting substations:** to change conventional DC substations to inverting substations, replacing the diode rectifiers with thyristor/IGBT rectifiers. This technology presents relatively high investment costs with a 7-11% energy saving (Gonzalez-Gil et al., 2014, Cornic, 2011);

- **Energy-efficient driving:** to use eco-driving techniques by optimising the speed profiles (Alves and Pires, 2010), coasting (Bocharnikov et al., 2007) and using the track gradients (Hoang et al., 2003);
- **Energy-efficient traction systems:** to reduce energy in the power supply network by limiting the power peak of the simultaneous train acceleration (Gonzalez-Gil et al., 2014), to reduce losses in on-board traction equipment, mainly in the traction motors by using permanent magnet synchronous motors (PMSM) (Kondo, 2010), and to reduce the vehicle mass (Carruthers et al., 2009);
- **Reducing the energy consumption of comfort functions:** rolling stock related measures for the service mode include reducing the heat transfer to outdoors (Baetensa et al., 2010), rolling stock related measures for the parked mode include optimising the setup and control of the comfort functions in terms of temperature (Gunselmann, 2005). Infrastructure related measures are also used, such as maximising the natural ventilation in the tunnels of underground stations (Raines, 2009);
- **Energy measurement and smart management:** metering and optimising energy usage within the system (Stewart et al., 2011), micro-generation within the system by using renewable energy generation sources at substations or along the track (Faranda and Leva, 2007), and smart energy management by using both regenerative braking and renewable energy generation (Barsali et al., 2011);
- **Energy storage systems:** the use of energy storage devices to store energy during train braking and then discharge the regenerated energy to support train acceleration, which can achieve an energy saving of 15-30% (Gonzalez-Gil et al., 2014).

1.4 Energy Storage Solutions

There have been some outstanding developments in both the technology of energy storage systems and power electronic devices, such that they are now appropriate energy saving solutions for recuperating the braking energy of trains in DC light railway systems. The applications of energy storage systems can be installed wayside along the track, at the stations or on-board trains. In the on-board application, trains temporarily store their own braking energy and then reuse it with the next acceleration, whereas in the wayside application the storage device stores the braking energy regenerated by any trains in the neighbourhood area and, subsequently, it supplies it to the accelerating trains (Gonzalez-Gil et al., 2014).

When they are properly designed, both wayside and on-board energy storage systems lead to not only considerable traction energy savings in light railway systems, but they also contribute to the regulation of the network voltage profile and the reduction of power peak demands (Barrero et al., 2010, Steiner et al., 2007, Chymera et al., 2008). Another advantage of the on-board application is that it enables vehicles to run catenary-free without the power supply for a short distance (Allègre et al., 2010). Generally, on-board storage systems operate with higher efficiency than their wayside counterparts because of the absence of line losses. Nevertheless, a large space is usually needed to accommodate the storage on the train and the train mass is significant increased; these are the main drawbacks of installing on-board storage systems in existing rolling stock. Alternatively, stationary energy storage systems can be installed with no practical restrictions of mass and volume and no modifications to the existing rolling stock are required. Moreover, their maintenance and installation do not affect the train service.

Considering the available energy storage system technologies for DC light railways, electrochemical double-layer capacitors (EDLCs), flywheels and batteries are the most appropriate options (Vazquez et al., 2010). EDLCs have high power density, quick recharge/discharge times, a long life cycle of millions of recharge/discharge cycles, low internal resistance and low maintenance. For these characteristics, they are widely used in DC light railway systems (Gonzalez-Gil et al., 2013). However, their energy density is very low in comparison to other storage devices, therefore they can be either replaced or combined with high specific energy density Li-ion or NiMH batteries in the on-board systems that provide a high level of autonomy and catenary-free operations (Ogasa, 2010a, Ogura et al., 2011, Meinert, 2009). Flywheels also present attractive characteristics for energy saving in DC light railway systems (Bolund et al., 2005, Tzeng et al., 2006), even though their commercial wayside application to date is limited to few trials (Gonzalez-Gil et al., 2013).

1.5 Main advantages of stationary EDLCs for DC railways

Batteries are particularly suitable for on-board applications when catenary-free operations are required or they are the main source of energy of the train. For stationary applications, where the main objective is to recuperate the braking energy, they are not recommended as they have recharging times of hours due to the internal chemical reactions, which also reduces the recharge efficiency. Conversely, EDLCs have negligible chemical reactions at the electrodes, they offer very low internal resistance and therefore have a very high efficiency around 95% (Gonzalez-Gil et al., 2013). EDLCs present a high power density and have a very fast response to recharge/discharge energy with a high current and they are able to operate in a wide range of environmental conditions (Sharma and Bhatti,

2010). They have an excellent lifetime of up to 10^6 recharge/discharge cycles, because the storage process is of electrostatic type (Hammar et al., 2010), compared to 10^3 cycles of batteries.

Flywheels have characteristics similar to those of EDLCs and are, therefore, a valid competitor for railway applications. Their main disadvantages are the additional step of converting electrical energy into kinetic energy with the motor/generator, the presence of friction requiring the use of a vacuum chamber and pump and maintenance of the moving parts. This results in a storage system that is more complicated than one based on EDLCs and the review of the literature has confirmed that EDLC systems are the most widely utilised energy storage system in DC light railways. Examples of application of EDLCs to light railway systems are presented in Chapter 2.

1.6 Research Hypotheses

The main hypotheses of this research are:

1) Can energy storage devices enhance the efficiency of DC electrified railways?
   This question has been addressed by analysing the energy demand, energy losses and voltage regulation of the light railway with stationary EDLCs in comparison with normal light railways.
2) Is the optimal design of capacitances and locations of stationary EDLCs essential to improve the performance of DC light railways?
   The addition of EDLCs to the electrification system implies additional costs and complications that need to be repaid by the cost savings introduced by the storage devices**.** The analysis is devoted to understanding how it is possible to

maximise the capital investment in terms of cost savings for light railways**.** It is expected that the minimum energy consumption and losses will be achieved by the optimal design of EDLC capacitances and their positions on each section of the track**.**

3) Does a new control strategy for the state of charge of stationary EDLCs improve the performance of DC light railways?

   This question will be addressed by varying the state of charge of EDLCs with different control laws to see if there are any benefits in terms of energy consumption and energy losses**.**

1.7 Objectives and Methodology

The objectives of this research are as follows:

1) to develop a mathematical model of DC electrified railways with stationary EDLCs with a single train travelling on the route in order to determine the efficiency of the entire system and evaluate the performance of only one train service, without sharing energy with other trains (the case of real railways with multi-train services will be subject to study in further works);
2) to develop an optimisation algorithm to design the optimal capacitances and locations of stationary EDLCs;
3) to develop a piece-wise state of charge control algorithm based on the rated voltages, currents and energy capacities of stationary EDLCs obtained from the optimisation algorithm;

4) to verify the robustness of the piece-wise state of charge control algorithm and the design of stationary EDLCs by varying the train loading and friction forces.

The research is based on theoretical analysis and numerical simulations obtained by use of the MATLAB program.

1.8 Assumptions of the Research

The work done for this thesis is based on the following assumptions:

1) The light railway has been simulated with the single train simulator (STS) developed by the Birmingham Centre for Railway Research and Education at the University of Birmingham, UK. There is only one train travelling on the line for the entire duration of the simulation. Using the STS, there are errors in some phases of the train motion (acceleration, coasting and braking) because the STS applies the Euler method to solve the differential equations to keep a constant acceleration for the duration of each distance step. This error has an effect on the results in terms of, for example, distance less than 10 m, time less than 1 sec and energy less than 1 kWh (Douglas et al., 2016). Even though the STS error can be reduced by reducing the step size of the discrete distance steps from the default setting of 10 m, this thesis retains the default discrete distance step of 10 m for the STS. This is because, if the step size is smaller than 10 m (if it becomes 1 m or less), then the calculation time of the optimisation algorithm will be greater than 1 day, and the STS results do not give significant differences based on the results of the optimisation

algorithm. For a low frequency railway, there is limited interaction between trains, as such a single train simulator provides a good approximation. Only a single train is used in the simulation; using only one train the regenerative braking energy of a single train can be clearly evaluated and the efficiency of the entire DC railway network can be studied with only one train in service. This study can be referred to DC light railway systems with multi-train services, for which the trend of results is similar to that of single train services. A study of more than one train in motion on the same route will be included in the further works after this thesis;

2) The route of the train journey is divided into sections, each of which lies between two electrical substations. This means that only the two substations adjacent to the train contribute to the power supply of the train, as found in practice with good approximation. The optimal design of the stationary EDLCs has been considered section by section;

3) There is only one track in the simulation, which is 22 km long, with 5 substations and 9 stations. The train uses the same track during the return journeys;

4) The position of the stationary EDLCs has been varied every 500 metres between substations. The small step size of the position of EDLCs will increase the time of calculation, however, the results of the simulation do not give significant differences if the EDLCs are positioned 300-400 metres closer together or at a distance greater than 500 metres;

5) The train loading and friction force variations are taken into account to verify the robustness of the piece-wise linear state of charge control algorithm of the stationary EDLCs.

1.9 Thesis Structure

The thesis consists of 7 chapters as follows:

- Chapter 1 is a general introduction to the research and presents the background, thesis assumptions, research hypothesis, objectives and methodology.
- Chapter 2 provides a literature review of the applications and developments of energy storage devices for electrified railways.
- Chapter 3 focuses on the model of the railway electrification system and rolling stock.
- Chapter 4 provides the theories behind the optimisation techniques, based on the classical theory of calculus of variations with constraints and Lagrange multipliers, and meta-heuristic methods. In addition, Chapter 4 also describes the algorithm of the optimisation technique used to find the optimal capacitances and locations of stationary EDLCs and provides the results.
- Chapter 5 presents the piece-wise state of charge control of stationary EDLCs based on the linear relation between the voltage deviation and the current of the stationary EDLCs. Chapter 5 also provides the results and discussions of the piece-wise state of charge control for variations in the loading of the train and friction forces.
- Chapter 6 gives the conclusions and identifies future research work in this area.

Chapter 2 Applications of Energy Storage Devices for Electrified Railways

2.1 Introduction

Energy storage devices provide a numerous of energy saving, cost saving and beneficial services to the electric utility systems, and other institutions deployed storage technologies for a number of different purposes. At present, energy storage devices also allow electrical system to run significantly more efficiently in terms of lower prices, less emissions and more reliable power. There are many applications of energy storage devices in the electric utilities, for example; connecting to low-voltage microgrids for power quality improvement and energy management (Wasiak et al., 2014), increasing efficiency to utilise renewable generation and reducing the costs of energy consumption (Li and Hennessy, 2013); connecting with renewable energy integration to enhance the reliability and operability of wind integration (Ghofrani et al., 2013) and counteracting variant and unpredictable power generation (Ye et al., 2014, Bocklisch, 2015). Furthermore, the applications of energy storage devices in the electric vehicles, such as trolley-bus and electrified railways, achieve the energy saving by reusing the regenerative energy of the vehicle braking. The applications of energy storage devices in the electric utilities and electric vehicles are different. An energy that is stored in the energy storage devices of the electric utility systems is supplied from the renewable energy sources connecting to the grid, and then this energy will be supplied back to the grid system for compensating the active and reactive power and finally improving the efficiency of the grid system. On the other hand, an energy that is stored in the energy storage devices of

the electric vehicles applications is supplied from the regenerative energy of the vehicle braking and sometime from the power substations, and then this energy will be supplied to DC system to support the vehicles acceleration. Based on the motivation, therefore, the applications of energy storage devices in the electric vehicles, especially electrified railways, will be subsequently reviewed and highlighted in this chapter.

It is likely that the revolutionary contribution of power electronics in electric vehicles, such as electric cars and trains, will partly replace conventional internal combustion engine vehicles in the near future because of the significant issue of shortage of traditional energy sources and the environmental impact of non-renewable fuels. Energy storage systems such EDLCs, batteries, flywheels and fuel cells are widely used as electric power sources or storage units in electric and plug-in hybrid electric vehicles (Amjadi and Williamson, 2009). Energy storage systems can recharge energy during low demand and discharge energy during high demand, acting like a catalyst to provide an energy boost. In addition, they can recharge energy from the vehicle braking, for example, the applications used for energy saving which are in trolley-buses (Falvo et al., 2012) and urban rail systems (Gonzalez-Gil et al., 2013), and then discharge this energy to support the vehicle for the next acceleration phase.

Based on the advantage of the railway applications in terms of number of passengers, this chapter focuses on the applications of energy storage systems used in the electrified railway by presenting a survey of the technical papers. This review mainly considers the mechanism of regenerative braking, the characteristics of different energy storage devices and the associated control strategies. Part of the work presented in this chapter has been published in a journal paper (Ratniyomchai et al., 2014b).

2.2 Regenerative Braking of Trains

The dynamic braking of electric vehicles converts the kinetic energy into electric energy by means of the traction machines that temporarily operate as electrical generators. The regenerated electric energy can be either dissipated by on-board electric resistors (rheostatic braking) or regenerated to support other vehicles on the same network (regenerative braking). In previous decades, there was no availability of power electronic devices to support the train to use regenerative braking to reduce energy consumption, thus rheostatic braking was used or trains sometimes supported adjacent trains. Today, with the currently available technologies of energy storage systems and power electronic devices, regenerative braking is preferred for energy saving and rheostatic braking is only used when the power supply line is not receptive. The recuperation of the braking energy is particularly effective for light railway systems, which are characterised by numerous and frequent stops, with many phases of acceleration and deceleration (Gonzalez-Gil et al., 2013).

Regenerative braking energy is fundamentally used to support the auxiliary loads and comfort functions on-board when the train is braking, and then the surplus energy is fed back to the power line to support other vehicles within the same network. Since light railways are supplied by transformer rectifier substations, the braking energy is confined in the power line, because diodes are not bidirectional in power. Therefore, regenerative braking is possible only when other vehicles are motoring in the vicinity of the stopping train. If there are no other trains, all the braking energy is dissipated by the on-board rheostat (Gonzalez-Gil et al., 2013).

The performance and efficiency of electrified railway systems could be improved by better use of the regenerative braking energy, minimising the need for on-board rheostats. To tackle this problem, four alternative solutions have been studied and developed.

The first solution uses energy storage devices on-board the train to accumulate the surplus of regenerative braking energy and support acceleration during motoring, see Table 2.1.

The second solution is focussed on improving the receptivity of the electrified network by using an appropriate train timetable. Some studies have focussed on timetables that synchronise the time of vehicles braking and motoring as far as possible, see Table 2.1.

The third solution is focussed on improving the receptivity of the electrified network by installing inverting substations by replacing diodes with thyristors. This would enable the surplus energy to be fed back to the power distribution network, see Table 2.1.

The fourth solution focuses on improving the receptivity of the electrified network by adding stationary energy storage devices at the substations or at the trackside. The stationary storage can also share the power supply to trains with the electrical substations, see Table 2.1.

Table 2.1: Alternative solutions to recuperate the regenerative braking energy

Applications	References
On-board energy storage devices	(Barrero et al., 2008, Domínguez et al., 2011, Barrero et al., 2010, Chymera et al., 2008, Miyatake and Matsuda, 2009, Ciccarelli et al., 2012, Destraz et al., 2007, Iannuzzi and Tricoli, 2012, Iannuzzi and Tricoli, 2010, Iannuzzi and Tricoli, 2011, Mir et al., 2009, Allègre et al., 2010, Steiner and Scholten, 2004, Steiner et al., 2007, Lhomme et al., 2005, Moskowitz and Cohuau, 2010, Henning et al., 2005, Ogasa, 2010a, Jeong et al., 2011b, Meinert, 2009)
Timetable optimisation	(Albrecht, 2004, Chen et al., 2005, Nasri et al., 2010, Peña-Alcaraz et al., 2011, Boizumeau et al., 2011)
Reversible substations	(Ortega and Ibaiondo, 2011, Gelman, 2009, Mellitt et al., 1984, Warin et al., 2011, Cornic, 2011)
Stationary energy storage devices	(Barrero et al., 2010, Iannuzzi et al., 2012b, Battistelli et al., 2009, Brenna et al., 2007, Battistelli et al., 2011, Iannuzzi et al., 2012a, Iannuzzi et al., 2013, Teymourfar et al., 2012, Lee et al., 2011b, Konishi et al., 2004, Morita et al., 2008, Rufer et al., 2004, Garcia-Tabares et al., 2011, Richardson, 2002, Ogura et al., 2011, Konishi et al., 2010)

Depending on the method used to enable regenerative braking, the total energy consumption can be reduced by 10-45% (Adinolfi et al., 1998, Falvo et al., 2011, Lee et al., 2011a, Kim and Lee, 2009, Foiadelli et al., 2006, López-López et al., 2011). In addition, the problems of high power-peaks and voltage-drop of the feeder line can be significantly mitigated (Ciccarelli et al., 2012, Iannuzzi et al., 2012a). The reduction in the energy dissipated by braking rheostats can have a significant impact on underground applications, where the removal of heat in tunnels and at stations requires expensive additional equipment (Ampofo et al., 2011, Thompson et al., 2006).

2.3 Energy Storage Devices for Electrified Railway Systems

The energy storage devices available for electrified railway systems are: batteries, flywheels, EDLCs and hybrid energy storage devices. The characteristics of the different energy storage devices can be graphically compared using the Ragone plot shown in Figure 2.1 (Christen and Carlen, 2000). The axes of the Ragone show the power and energy densities on a log-log scale. The discharging time of the energy storage devices is

represented by the lines at 45 degrees in Figure 2.1. It is clear to note that, of the available energy storage devices (batteries, flywheels and EDLCs), EDLCs are the most appropriate for storing and regenerating braking energy in electrified railway applications because they are quick to recharge/discharge energy. The applications of each energy storage device are reviewed in the following sections.

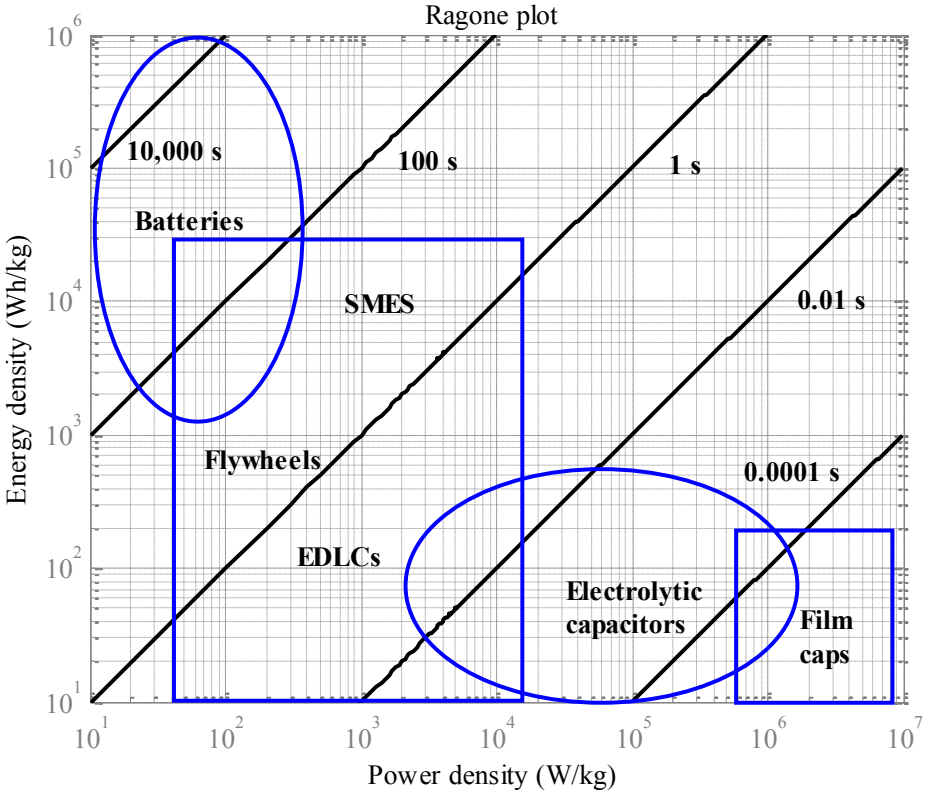

Figure 2.1: Typical Ragone plot (Christen and Carlen, 2000)

Definition 2.1 (cycle of recharge/discharge): The lifecycle of energy storage is the number of recharge-discharge cycles when the capacity degrades to 80% of the nominal capacity.

2.3.1 Electrochemical Batteries

Electrochemical batteries are the most traditional method of storing electrical energy and their characteristics have been well known for many years. Due to the characteristic

discharge and recharge times of electrified railway systems, the preferred battery technologies are lithium-ion and nickel metal hydride.

2.3.1.1 Lithium-ion Batteries for Electrified Railways

Lithium-ion (Li-ion) batteries were initially presented to the commercial market in the 1990s by Sony and they were based on the application of Li-intercalation compounds (Chen et al., 2009a, Dunn et al., 2011, Shionuma et al., 1991, Nagamine et al., 1992). Li-ion batteries are considered a relatively new energy storage technology in comparison to conventional lead-acid and Ni-Cd batteries. The advantages of Li-ion batteries are their high specific energy, light weight, fast recharge/discharge capabilities, long lifetime and low self-discharge rate. Other significant advantages of Li-ion batteries are that they can be operated at high current and they have high-capacity usability (Budde-Meiwes. et al., 2013).

Due to these characteristics Li-ion batteries have quickly become the preferred storage technology for portable electronic devices. Recently, Li-ion batteries have also been introduced in the automotive market for hybrid and fully electric vehicles, with stationary energy storage applications used as the power back-up.

The applications of Li-ion batteries in electrified railways are presented as follows:

A. Energy Saving and Voltage Drop Compensation

Stationary Li-ion batteries were installed in electrified railways in Japan to reduce the energy consumption of trains. The installation was divided into two subsequent phases: the first phase used temporary batteries (TB) for the initial testing and the second phase

used full-scale permanent batteries (PB) for the train service. The rated capacities of the TB and PB are shown in Table 2.2 (Okui et al., 2010, Konishi et al., 2010).

Table 2.2: Specific capacity of the TB and PB for energy saving (Ratniyomchai et al., 2014b)

Companies	Rated Power (kW)	Rated Energy (kWh)
Nagoya Railroad Co., Ltd. (TB)	500	18.7
Kobe Municipal Transportation Bureau (PB)	1,000	37.4
West Japan Railway Company (PB)	1,050	140
Kagoshima City Transportation Bureau (PB)	250	18.1
Japan Railway East (PB)	2,000	76

The verification tests of the Li-ion batteries for a TB with the rated power of 500 kW and the rated energy of 18.7 kWh were installed in the Shin-Anjo station on the Nagoya line, which was a long distance from the DC substation. The initial testing was aimed at verifying the energy saving and the voltage drop compensation. The PB was installed at Myodani substation on the Seishin-Yamate line of the Kobe Municipal Transportation Bureau in May 2005. This section had an average slope of 2.9% continuously along the track length of 4 km between Myodani substation and the next station. Therefore, the recuperation of the braking energy was necessary for this section. In February 2007, Li-ion batteries were installed at the Itayado substation on the same line, with a double rated capacity compared to that of the Myodani substation, which saved over 300 MWh per year (Okui et al., 2010, Konishi et al., 2010). Further Li-ion batteries were installed at the Shin-Hikida substation on the Hokuriku line of the West Japan Railway Company with the purpose of line voltage regulation and voltage drop compensation in the autumn of 2006. In addition, Li-ion batteries were installed to improve the voltage drop and power line efficiency at the Sakurajimasanbashidori station and the Nakasudori station of the Kagoshima City Transportation Bureau in March 2007 (Okui et al., 2010, Konishi et al., 2010). Finally, Li-ion Batteries with a capacity of 76 kWh and 2,000 kW power rating

were operated at Haijima substation on the OME line of JR East on 20th February 2013. The functions of the Li-ion batteries at the Haijima substation were to compensate the voltage drop, to improve regenerative braking and to provide a back-up power supply. An analysis of the efficiency has shown energy savings of up to 400 MWh per year (Hayashiya et al., 2014).

B. Catenary-Free Operations

At cross sections of the track, such as bridges and tunnels, it may be difficult to install power conductors to supply the vehicles., It is not always possible, especially in city centres, to deploy power conductors either as overhead wires, due to the presence of historical buildings, or as a third rail, due to pedestrian safety concerns. In these situations, catenary-free operations are the best choice to satisfy both transportation bureaus and city councils (Ogasa, 2010b). Catenary-free operations are possible with Li-ion batteries, due to their high energy density and applications can be found on two tramways: the "Lithey-Tramy" and the "Hi-Tram", installed in 2003 and 2007, respectively (Ratniyomchai et al., 2014b). The on-board Li-ion batteries on the first tram had a rated energy of 33 kWh and consisted of 168 cells in series. The operating voltage was 605 V, the total track length was 17.4 km, the distance between the substations was 250 m and the maximum tram speed was 40 km/h. The Lithey-Tramy was operated for public service from August 2003 to January 2005, and subsequently with a new electrified system operating at 750 V and 1500 V (Ogasa and Taguchi, 2007, Ogasa, 2010b). The on-board Li-ion batteries on the second tram had a rated energy of 72 kWh and consisted of 672 cells in series. The operating voltage was 605 V, the total track length was 25.8 km and the maximum tram speed was 40 km/h. The Hi-tram was operated from November 2007 to March 2008 by

Sapporo Municipal Transport. The battery was recharged at the station with a current of approximately 1000 A over a period of 60 s to cover approximately 4 km catenary-free. In November 2009, the Hi-Tram was modified to operate at both 605 and 1500 V of the electrification system. The maximum speed of the new Hi-Tram increased to 80 km/h and it was capable of covering the full 49.1 km of the track within an hour (Ogasa, 2010b).

2.3.1.2 Nickel Metal Hydride Batteries for Electrified Railway Systems

Nickel Metal Hydride (Ni-MH) batteries are the first type of advanced rechargeable battery technology that has dominated both the consumer electronic and the industrial market because of their good characteristics in terms of energy and power densities, cost and environmental impact (Ovshinsky et al., 1993, Gibbard, 1993). The first Ni-MH battery was introduced in 1991 in the form of a cylindrical cell with an energy density of 54 Wh/kg. Today, commercially available Ni-MH battery cells have energy densities of 100 Wh/kg. Over the last two decades, the power densities have increased from 200 to 1200 W/kg (Fetcenko, 2005). These improvements have recently enabled the use of Ni-MH batteries for electric vehicles and hybrid electric vehicles (Tsais and Chan, 2013).

The applications of Ni-MH batteries in electrified railways are presented as follows:

Ni-MH batteries have been mostly used for the power supply of hybrid and electric cars, whereas the applications to electrified railways are outnumbered by those of Li-ion batteries, due to the smaller power and energy densities. However, Ni-MH batteries were installed to reduce the energy consumption at the Komagawa substation on the Tanimachi line operated by Osaka Municipal Transportation Bureau, with a rated energy of 576 kWh and power of 5.6 MW (Okui et al., 2010, Konishi et al., 2010). In addition, a prototype electric tram called “SWIMO” (Smooth Win MOver) by Sapporo Municipal Transport

and Kawasaki Heavy Industry had Ni-MH batteries installed on-board. The tram was operated with a voltage of 600 V from December 2007 to March 2008. The Ni-MH batteries on-board unit consisted of 480 cells having capacity of 274 Ah, with a total rated power and energy of the storage unit of 250 kW and 120 kWh respectively. SWIMO was able to travel catenary free for 10 km with the maximum speed of 40 km/h (Ratniyomchai et al., 2014b, Kawasaki, 2008). On-board Ni-MH batteries were also used in the Citadis tram by Alstom transportation, which was operated in the city of Nice, France. The vehicle travelled catenary free up to a maximum speed of 30 km/h over a length of 1 km (Rufer, 2010). This performance was sufficient to get past a distance of 500 m in the historic squares of Place Massena and Place Garibaldi (Lacote, 2005).

2.3.2 Flywheels

Flywheels are mechanical energy storage devices which consist of a large wheel spinning around an axle supported by a low-friction bearing. Therefore, flywheels store energy in the form of kinetic energy, which is dependent on the inertia of the wheel and the square of the rotating speed. Flywheel-based systems have been used for over a thousand years in millstones, potters wheels and hand looms. More recently, flywheels have been used as energy storage devices in the crankshaft to smooth out the rotating speed of the engine (Breeze, 2014). When they are coupled with an electric machine, flywheels convert mechanical energy into electrical energy and vice versa (Salameh, 2014).

In traditional flywheels, the rotor disk is made of either iron or steel, which is capable of spinning at low speed. With the introduction of composite materials, such as carbon or glass fibres, the rotor speed has been increased up to 10,000-100,000 rpm (Breeze, 2014). The high speed of the rotor disk causes a significant increase in mechanical friction losses

and air drag. In order to overcome these problems, some flywheels use magnetic bearings and are sealed in a vacuum enclosure. Flywheels also need a strong external container to prevent scattering of pieces in case of failure. A cross-sectional view of a flywheel is shown in Figure 2.2.

The electric machine is normally placed inside the flywheel and is operated with a bidirectional power converter (2 or 3 levels) to exchange electrical energy with the external circuit (Salameh, 2014).

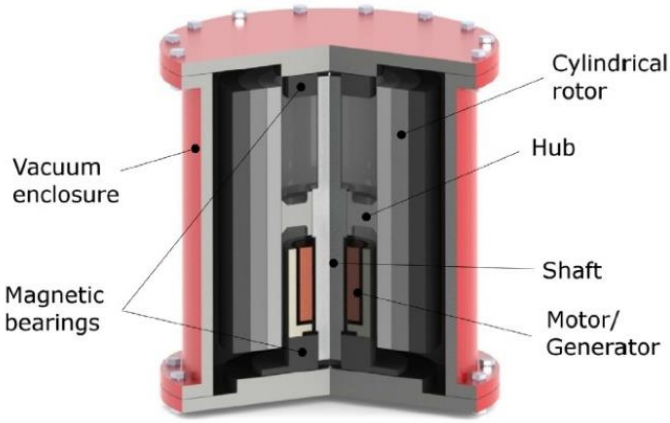

Figure 2.2: A cross-section of a flywheel (Salameh, 2014)

2.3.2.1 Flywheels for Electrified Railway Systems

Flywheels were first installed in 1988 to store the regenerative braking energy of trains travelling at Zushi post in the Keihin Electric Express Railway, Japan. The power and energy of the flywheels were 2 MW and 25 kWh, respectively. The study showed an energy saving of 12% during normal passenger service (Okui et al., 2010). Another flywheel storage system of 300 kW was installed in London Underground in October 2000 for demonstration. The operating voltage of the underground line is 630 V, although it can drop down to 450 V during peak times. The verification test of the flywheels

improved the voltage of the power line up to 530 V with the same load at peak times. However, the actual capability of the regenerative braking was higher than 300 kW, therefore, the specific power of the flywheels was estimated by the manufacturer to be at least 1 MW for completely recovering regenerative braking energy. The flywheels were bigger than the measured regenerative braking of 300 kW to cover future regenerative braking which might exceed this level. Considering the estimated costs in 2000, the annual electricity cost of a London Underground substation was £195,000, which was reduced by 26%, i.e. £50,000 per year. Since the cost of a 1 MW flywheel was £210,000 and the maintenance cost was approximately £2,500 a year, the investment cost was paid back within 5 years (Radcliffe et al., 2010). This reasonable estimation does not take into account the benefit of demand reduction in the local electricity grid during peak periods.

Another two energy storage systems based on flywheels were developed in Spain for ADIF Railways by CEDEXs, the Experimentation Centre of Public Works and Transportation Ministry and the Centre for Energy, Environment and Technology Research. The first project, called "ACE2", started in 2003 and the prototype flywheels had power and energy of 350 kW and 56 kWh respectively. The second project, called "SA2VE", started in 2006 and the flywheels had a power of 5.6 kW and energy of 0.9 kWh with a discharge time of 9.5 minutes (Iglesias et al., 2008).

Flywheels have also been used in catenary-free operations for the tramway service in Rotterdam, Netherlands. The flywheels were installed on the roof of the trams and had a power of 325 kW, an energy of 4 kWh and top speed of 20,000 rpm (Lacote, 2005). A second test with similar flywheels was trialled on the Citadis trams, with a total weight of the vehicle of approximately 40 tonnes. The test showed that the tram travelled

catenary-free for nearly 2 km, including three intermediate stops, with a maximum speed of 50 km/h. The Citadis tram also travelled across the Erasmus Bridge over a distance of 900 m and a difference in height of 15 m (Lacote, 2005, Citadis, 2005). Recently, an agreement between Alstom Transportation and Williams group was signed to further develop the flywheel systems on-board Citadis trams, called "Williams hybrid power flywheels", to reduce energy consumption (Glickenstein, 2013).

Finally, three flywheels of 200 kW each were installed on the rolling stock of the Lyon metro to improve voltage regulation during train braking between 850-860 V. After 4 months of operation, the overvoltage of the Lyon metro line was continuously prevented by the operation of the flywheels; one of them was even temporarily stopped. (Wheeler, 2004).

2.3.3 Electrochemical Double-Layer Capacitors

Electrochemical double-layer capacitors (EDLCs) are also known as supercapacitors, ultracapacitors, electrochemical capacitors, or pseudocapacitors, and they store energy into an electric field (Salameh, 2014). EDLCs were first commercially introduced by Nippon Electric Company (NEC) in 1978 (Kurzweil, 2015).

EDLCs differ from conventional capacitors because the electrodes are separated by a liquid electrolyte and a separator. According to the Helmholz theory, a double layer is created at the interfaces of the positive and negative electrodes, as shown in Figure 2.3 (a). These double-layers of charges are equivalent to two capacitors connected in series, as shown in Figure 2.3 (b). The electrodes are made of porous activate carbon and designed to maximise the energy storage capacity. Based on the double layer of charges, the total capacitance of an EDLC cell is generated by regulating and adjusting the pore

size of each carbon electrode and optimising the interactions between the electrolyte materials (Salameh, 2014).

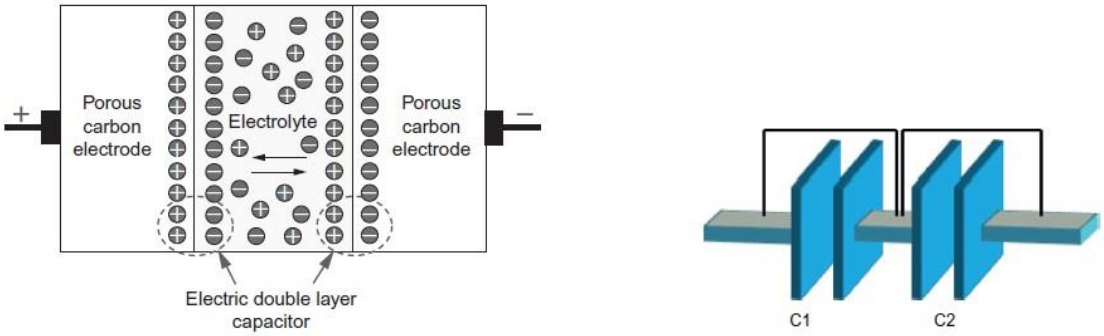

(a) (b)

Figure 2.3: EDLCs; (a) Schematic of an EDLC (b) Series capacitor behaviour in an EDLC (Breeze, 2014, Salameh, 2014)

2.3.3.1 EDLCs for Electrified Railways

EDLCs have been extensively used as the energy storage for electrified railway systems and especially for light DC railways with traditional diode rectifier substations (Son et al., 2009, Iannuzzi, 2008). EDLCs have a function similar to batteries, although they can significantly contribute to the power supply for a short time and have a much longer lifetime. EDLCs have been used both for prototype and real passenger services (Ratniyomchai et al., 2014b) to reduce energy consumption, improve the voltage regulation and regenerative braking capability of trains, and for catenary-free operation. Both stationary and on-board applications have been tested. Commercial products with EDLCs which are available in the market are the MITRAC Energy Saver by Bombardier Transportation (Steiner et al., 2007), the SITRAS SES by Siemens Transportation Systems (SIEMENS, 2004) and the STEEM by Alstom Transport (Moskowitz and Cohuau, 2010), as better described in the following subsections.

A. Stationary EDLCs

The first installation of EDLCs was in December 2007 in the Agono and Shumaru substations of the Seibu Railway Co. Ltd in Japan, operating at 1500 V DC. The EDLC system had a rated energy of 6.86 kWh and power of 2.56 MW. This particular section of the line has a gradient of 2.5% for 7.15 km and, therefore, the reuse of regenerative braking energy is particularly effective. The results of the experiment showed a recovery of 7.7 kWh from each train in the EDLCs module and 77% of this energy was delivered to support other trains (Okui et al., 2010, Konishi et al., 2010).

Another EDLC system with rated energy of 10.39 kWh and power of 1.87 MW was installed at the Daedong substation of the Daejeon Metropolitan Rapid Transit Corporation, Korea, operating at 1500 V DC. After satisfactory preliminary tests in the laboratory, the EDLC modules were installed in the railway and they were capable of maintaining the catenary voltage around the nominal value in any traffic conditions (Lee, 2010).

B. On-Board EDLCs

On-board EDLCs were installed for the first time in January 2005 on the Central Japan Railway Company (CJRC) rolling stock series 313, which serviced between Nagoya and Jinryo on the Chuo line in Japan, to improve the dynamic braking performance of trains. The EDLCs module specifications were roughly estimated from the braking energy dissipated by the mechanical braking. The EDLC system was formed by two modules with a rated energy of 0.28 kWh, power of 180 kW, total capacitance of 1.4 F, weight of 430 kg and operating voltage between 700 V and 1425 V. The results showed that 8% of the regenerative braking energy was stored in the EDLCs, which contributed to 1.6% of

the energy used for motoring. Consequently, the peak braking force was effectively reduced, with benefits for brake cylinders and the temperature of the wheel treads (Sekijima et al., 2006).

Another application of on-board EDLCs connected to the traction drive with a new DC-DC power converter was developed for the Blackpool tram system in the UK. The EDLC system had rated power of 50 kW, capacitance of 17.8 F with 65 mΩ equivalent series resistance. The results of the testing demonstrated an energy saving of 0.38 kWh/km, which is equivalent to a reduction of 23% with 100 passengers and 28% with no load. There is an extra energy saving of up to 8% or 0.09 kWh/km with a new DC-DC power converter, depending on the passenger loading (Chymera et al., 2011).

C. MITRAC Energy Saver

The schematic of the MITRAC Energy Saver unit is shown in Figure 2.4 and includes EDLCs modules connected to the DC-link of the traction inverter by means of a bi-directional DC-DC converter (Steiner et al., 2007). The MITRAC Energy Saver can be used for energy saving, infrastructure investment reduction, power supply optimisation and catenary-free operations (Bombardier-Transportation, 2009). A prototype of a light rail vehicle (LRV) with the MITRAC Energy Saver on-board was built for the German operator Rhein-Neckar-Verkehr Gmbh in Mannheim, Germany and was in service between 2003 and 2008 (Steiner et al., 2007). The specifications of the MITRAC Energy Saver are presented in Table 2.3 (Bombardier-Transportation, 2009). The results of the experimentation showed that a 30% reduction of the traction energy consumption was achieved. At the maximum speed of 50 km/h, a significant reduction of the peak line

current and voltage drop in the LRVs with MITRAC Energy Saver was measured in comparison to the rolling stock without storage (Bombardier-Transportation, 2009).

Table 2.3: The specification of the MITRAC Energy Saver unit

Quantities/Applications	LRV 2003	LRV 2008
Energy capacity (kWh)	1	1
Power capacity (kW)	300	300
Weight (kg)	477	428
Dimensions (mm^3)	1900×950×455	1700×680×450 (partly 550)
Typical installations	2 boxes of a 30 m long LRV	2 boxes of a 30 m long LRV

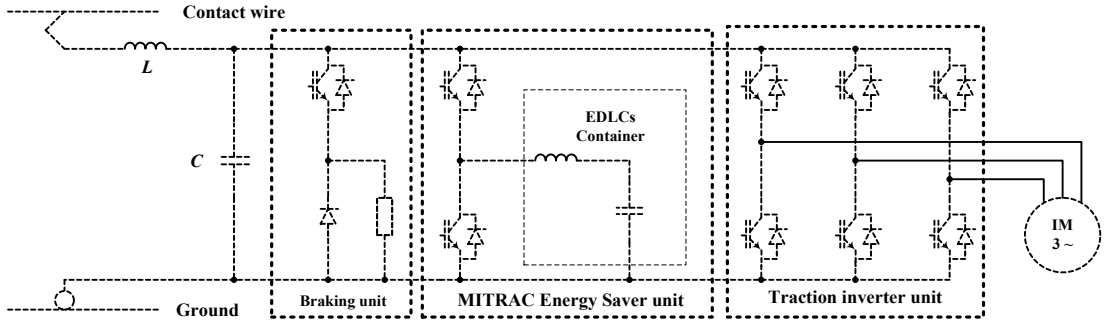

Figure 2.4: Schematic of MITRAC Energy Saver unit (Steiner et al., 2007)

The MITRAC Energy Saver was also used for catenary-free operation of the LRV in the city centre square, an area of historical buildings and tunnels, and even during outages. In the verification tests the LRV with the MITRAC Energy Saver travelled catenary-free for 500 m with a maximum speed of 26 km/h. The charging system of the MITRAC Energy Saver was an overhead busbar feeder at the charging station, instead of an overhead wire. The charging station was capable of a quick recharge 3 kWh within 20 s with a maximum current of 1 kA. The mass of the LRV increased by approximately 2% and the additional space required to accommodate the on-board energy storage reduced the vehicle capacity in terms of the number of passengers. Based on the dimensions in Table 2.3, the space taken up by the on-board energy storage is equivalent to about 2-3 lines of seats.

D. SITRAS SES

The SITRAS SES is a stationary energy storage system based on Maxwell EDLC modules developed by Siemens Transportation Systems for light railway applications (Maher, 2006). Figure 2.5 shows the schematic of SITRAS SES connected to the DC power supply via a bi-directional DC-DC converter (SIEMENS, 2004). This energy storage system can be used to improve the voltage regulation on metro trains and tramway systems and has shown an energy saving of approximately 30%. Generally speaking, the benefits of the stationary energy storage system SITRAS SES are similar to those of the on-board energy storage system MITRAC Energy Saver. However, the SITRAS SES can sustain the DC power supply for a short time during failures and regulate the voltage of the line. On the other hand, they contribute to the short-circuit current and increase the fault levels on the line. From 2001-2003, SITRAS SES was operated at the Kölner Verkehrsbetriebe AG in Cologne, Germany on the basis of simulations and verification tests for 1 year of vehicle services. SITRAS SES achieved a 500 MWh reduction in the energy consumption. The SITRAS SES had a power of 1 MW and consisted of 2,600 F BOOSTCAP capacitors, with its overall dimensions being 3 m long and 2.7 m tall. The SITRAS SES supported the electrified line within a radius of 3 km of the installation site.

In addition, the SITRAS SES was installed for public services on the new Trimet Portland-Milwaukie light rail transit line, in Oregon, USA in 2002; and on the Metro de Madrid SA, in Madrid, Spain in 2003 (Maher, 2006). The results showed that the SITRAS SES achieved an energy saving of 320 MWh per station per year in comparison with traditional feeding systems (Ratniyomchai et al., 2014b, Maher, 2006).

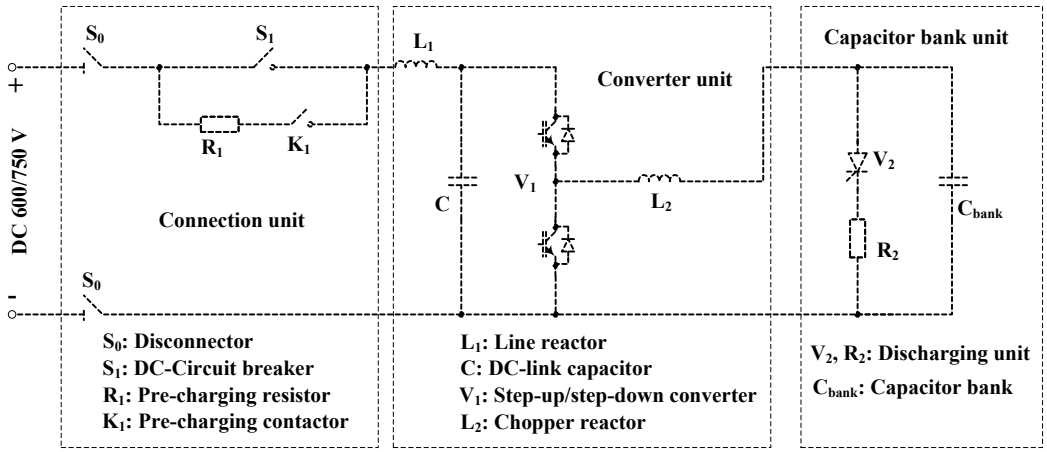

Figure 2.5: Schematic of SITRAS SES system (SIEMENS, 2004)

E. Maximised Energy Efficiency Tramway System (STEEM)

The STEEM is an on-board energy storage system based on EDLCs which was developed as a cooperation between the public transport operator in Paris, France (RATP), Alstom transport and the public research laboratory ADEME under the French Framework Program on Research Experimentation and Innovation in Land Transport (PREDIT) (Moskowitz and Cohuau, 2010). The STEEM energy storage has 48 EDLC modules connected in series and in parallel, each having capacitance of 130 F, voltage of 54 V and weight of 15 kg. The energy storage system was accommodated on the roof of the trams and included a DC-DC converter and a complete traction control. The schematic of the STEEM project is similar to the MITRAC Energy Saver shown in Figure 2.4. Twenty-one "Citadis 402" trams, each 40 m long, have operated for passenger services on the T3 line of RATP in Paris since 2009. The T3 line is about 7.9 km long with a headway of 4 minutes. During peak time 16 trams run with a ratio of more than 2 trams/km and less than 1.5 trams/km on average, therefore, this line has very high receptivity. However, using the on-board energy storage system did not result in a significant reduction in energy consumption in winter or summer. The majority of the regenerative braking

energy was typically used to supply the auxiliary loads on-board, mainly the air conditioning units and heaters, whereas only minor surplus energy was stored in the energy storage system. The results of the STEEM project show that there was a small energy saving in winter and in summer because the energy demand for the auxiliary loads is high in comparison to the available regenerative braking energy, therefore there is less energy available to recharge the energy storage system. On the other hand, in spring an average 13% energy saving was achieved (Moskowitz and Cohuau, 2010). Catenary-free operations were tested between Porte d'Italie and Porte de Choisy stations for a total length of 300 m.

2.3.4 Hybrid Energy Storage Devices

The Sitras HES is a hybrid energy storage device consisting of a Ni-MH battery and an EDLC module (Ogasa and Taguchi, 2007). This storage device has been designed to integrate the characteristics of batteries and EDLCs in terms of high energy and power densities. In comparison to other storage devices based on only one technology, the Sitras HES has better a performance for both energy saving and length of catenary-free operations. The product features 18 kWh of high energy density traction batteries and 1 or 2 kWh of EDLCs. The general specifications of the Sitras HES are presented in Table 2.4 (Meinert, 2009).

The Sitras HES can be recharged both from the vehicle braking and a dedicated quick charging unit located at stations. According to Table 2.4, the recharging current of the traction battery is 10 times smaller than the discharging current, which means that the largest proportion of the braking energy is stored in the EDLCs.

The Sitras HES was installed on the roof of the trams operated by the Portuguese company Metro Transports do Sul, S.A. (MTS(a)), called "Combino plus MTS(a)", and it travelled between Almada and Seixal in Lisbon. The storage system enabled the tram to travel catenary-free for a maximum length of 2.5 km.

Table 2.4: Specification of the Sitras HES: EDLCs unit and traction batteries (Meinert, 2009)

Quantities	EDLCs	Battery
Nominal voltage (V)	190 – 480	528
Specific current (A)	600	220 for discharging, 22 for recharging
Specific power (kW)	288	85
Specific energy (kWh)	0.85	18
Dimension (mm^3)	2000×1520×630	1670×1025×517
Weight (kg)	820	826

2.3.5 Comparison of Energy Storage Devices

The data available from manufacturers of energy storage normally refer to single cells or single modules. On the basis of the analysis of the literature review, a similar diagram has been developed for practical applications of energy storage in real railways and tramways, as shown in Figure 2.6 (Ratniyomchai et al., 2014b).

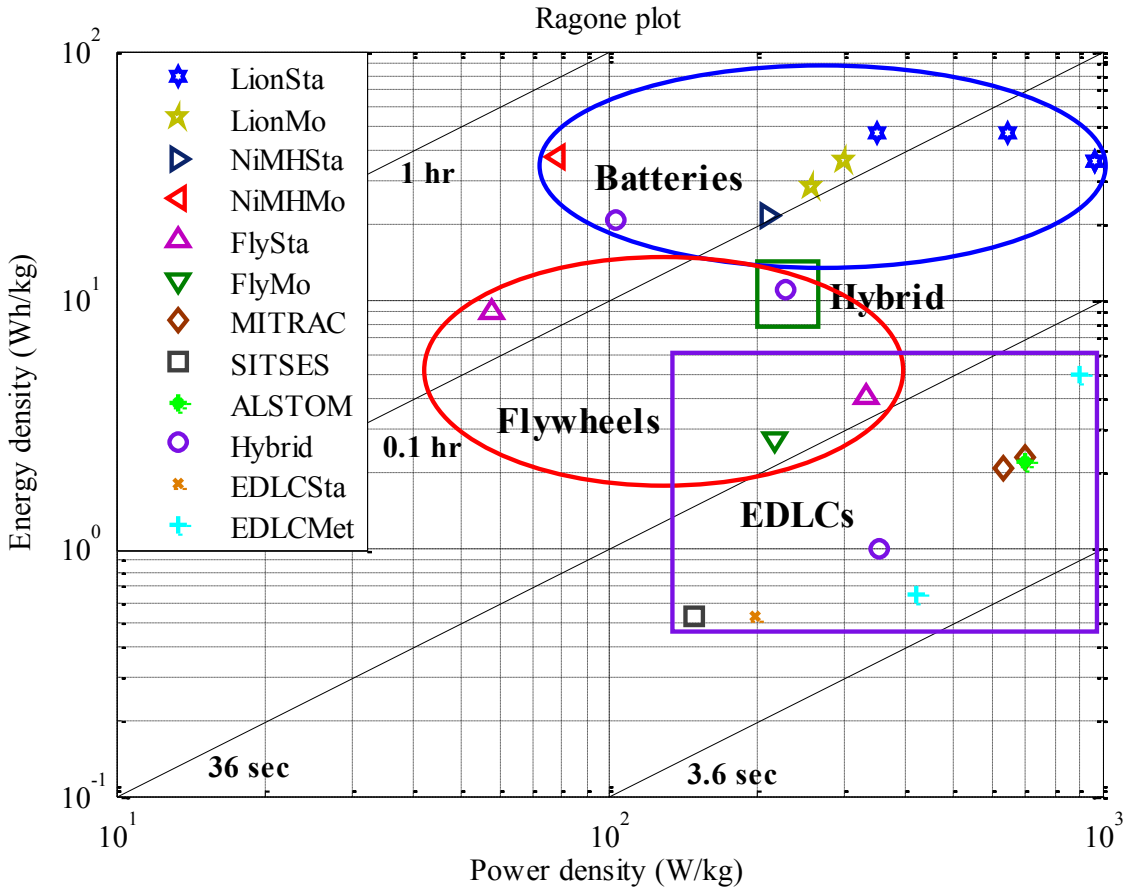

Figure 2.6: Ragone plot of the recent energy storage devices employed in electrified railways (Ratniyomchai et al., 2014b)

From this diagram, the equivalent average discharge time of the storage devices can be extrapolated. This information is important to understand which function of the energy storage is more emphasised. High discharge time implies better catenary-free operations but reduced capabilities for storing the braking energy and supporting the motoring phase, and vice versa. The average discharge time of Li-ion batteries is approximately 5 minutes. For Ni-MH batteries, the average discharge time is about 6 minutes for stationary applications and 30 minutes for on-board applications. The discharge time of flywheels varies between 0.8 and 10 minutes for stationary applications and is about 0.8 minutes for on-board applications. For EDLCs, the discharge time varies between 3.6 and 36 seconds. The discharge time is 12 seconds for the on-board MITRAC Energy Saver, 13 seconds for the

stationary SITRAS SES and 11 seconds for the STEEM project. With reference to the hybrid SITRAS HES, the discharge time is 12 minutes for the Ni-MH traction batteries and 10 seconds for the EDLCs. Reviewing the entire energy system as a whole, the average discharge time in the Ragone plot would be 3 minutes.

From this analysis it is clear that the discharging time of EDLCs is around 5-15 seconds, which is much shorter than that of batteries (5-30 minutes) and flywheels (0.8-10 minutes) in both on-board and stationary applications. EDLCs are effectively used for supplying power peak demands and for voltage stabilisation purposes, requiring a rapid response discharge period. In addition, the power density characteristic of EDLCs (100-1000 W/kg) is higher than that of flywheels (50-200 W/kg) and some batteries (80-300 W/kg). This means that EDLCs are capable of recharging and discharging the state of charge with a high power and also a high current within a short period of time. Therefore, EDLCs can be used effectively to store the braking energy during a short period of train braking and then discharge the regenerated energy to support the train acceleration in the next phase of the train motion. This can increase the efficiency of the light railway system by reducing the energy consumption. Other advantages of EDLCs are long life cycles, low internal resistance, and low maintenance costs compared to flywheels and batteries.

Flywheels have characteristics which are similar to EDLCs, in terms of discharging time, power density and life time, whereas the energy density is higher than EDLCs. However, flywheels are bigger and heavier than EDLCs, and they need more maintenance due to the presence of rotating parts. For railway applications, flywheels have a high risk of explosive shattering in case of overload and they have high self-discharge rates caused

by internal friction or orientation changes drawn by train movements. Regarding investment costs, flywheels for use in railway applications are quite expensive.

Batteries (both Li-ion and Ni-MH batteries) have a high discharge time and high energy density, however, they are low in power density. For railway applications, they are more suitable for large catenary-free operations, rather than the recovery of braking energy and the provision of support to the power supply, because they can temporarily act like a power supply. On the other hand, batteries have a short life cycle and a high cost for the protection and maintenance.

Hybrid energy storages have both the high power and energy density that are provided by EDLCs and batteries in only one storage system. They can recharge and discharge the state of charge with high power and current within a short time, which is carried out by EDLCs, and can also support a large energy use for catenary-free operations, which is carried out by batteries. The combination of uses of hybrid energy storage systems make them suitable for railway applications, however, the investment cost is quite high in comparison to individual energy storage.

From this evidence, it is clear to note that EDLCs are appropriate for implementation in the DC light railway system to improve energy efficiency in terms of energy saving by regenerating the train braking energy.

2.4 State of Charge Control of Storage Devices

The practical control algorithm for recharging and discharging the energy storage, based on the stationary flywheel application in the New York City Transit Authority with a DC track system of 900 V is shown in Figure 2.7 (Richardson, 2002). The purposes of this

control are to reduce the peak power demand of the power supply, to regulate the DC track voltage, and also to save energy, in the case of the regenerating train. In Figure 2.7, the power profile control includes three control areas: recharge, recovery and discharge, and presents the typical no-load voltage of around 630 V. During train motoring, the DC track voltage is under 620 V, the flywheel discharges energy to support train acceleration in proportion to the voltage down to 600 V, and at the maximum rated power under 600 V. On the other hand, during train braking, the DC track voltage is above 650 V, the braking energy from the traction is charged by the flywheel in proportion to the voltage up to 690 V and at the maximum rated power above 690 V.

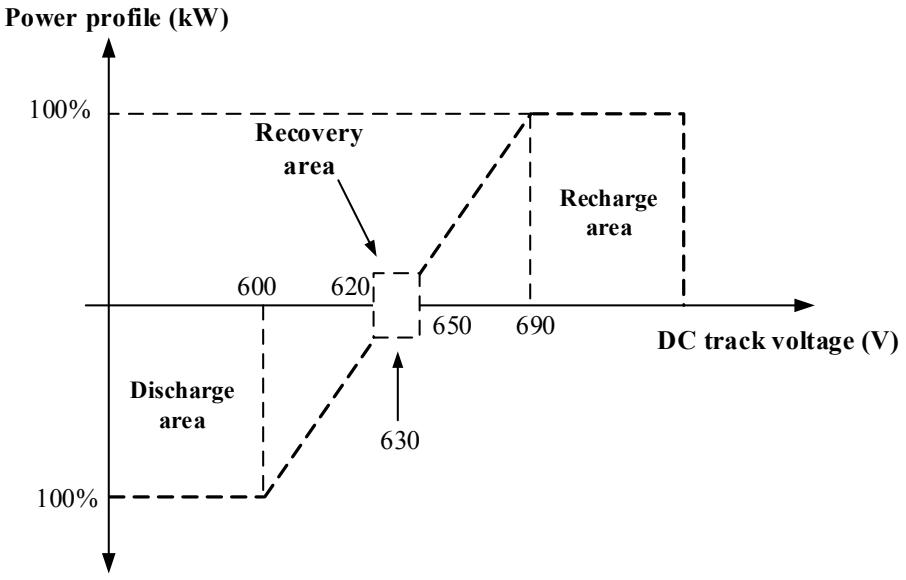

Figure 2.7: Power profile control of the flywheel with the DC track system of 900 V (Richardson, 2002)

With the recovery area, the DC track voltage is between 620 and 650 V. In this area, the speed of the flywheel is controlled to generate energy at the mid-point equivalent, which is a pre-defined power level. The DC track voltages given in Figure 2.7 are actually simplified voltages, for explanation. In practice, all of the DC track voltage can be varied

around the nominal no-load voltage level, as in the recovery area it depends on the system power demand.

In this thesis, only two principles of state of charge (SOC) control for energy storage devices are proposed, for on-board application and stationary application. The purpose of SOC control for on-board energy storage is energy saving and catenary-free operation, whereas the purpose of SOC control for stationary energy storage is energy saving and line voltage regulation. The SOC control strategy of the stationary energy storage is based on the following subsection, and the power profile control presented in Figure 2.7 is developed and implemented in this thesis, and is presented in Chapter 5. The characteristics of each control strategy are summarised in the following subsections.

2.4.1 On-board SOC Control Strategy

The concepts of on-board SOC control strategies for storage devices in DC electrified railways are generally divided into four classifications (RSSB, 2010). The criteria is based on the number and length of the catenary gaps, speed profiles and the amount of kinetic braking energy. The characteristics of each control strategy are described in the following subsections.

A. Control Strategy to Maintain the Maximum SOC

The controller scheme relates the SOC to the power supplied by the storage devices to keep the storage fully charged at all times, as shown in Figure 2.8. The main purpose of this control strategy is to maximise the distance covered by the vehicle during catenary-free operations. When the vehicle enters a section of the line which is not electrified, the storage provides power to the traction drive, reducing its SOC down to the discharging limit. As soon as there is a brake or the vehicle approaches an electrified section, the storage is recharged until full charge is reached. The recharge power can be reduced when the storage reaches a certain level, called the charging limit. The recharge power has two different levels, the highest is from the vehicle braking during travel through gaps in the electrified line or under the contact wire and the lowest is only from the vehicle travelling under the contact wire. In both cases, at the charging limit the energy of the storage devices is reduced until full charge is reached.

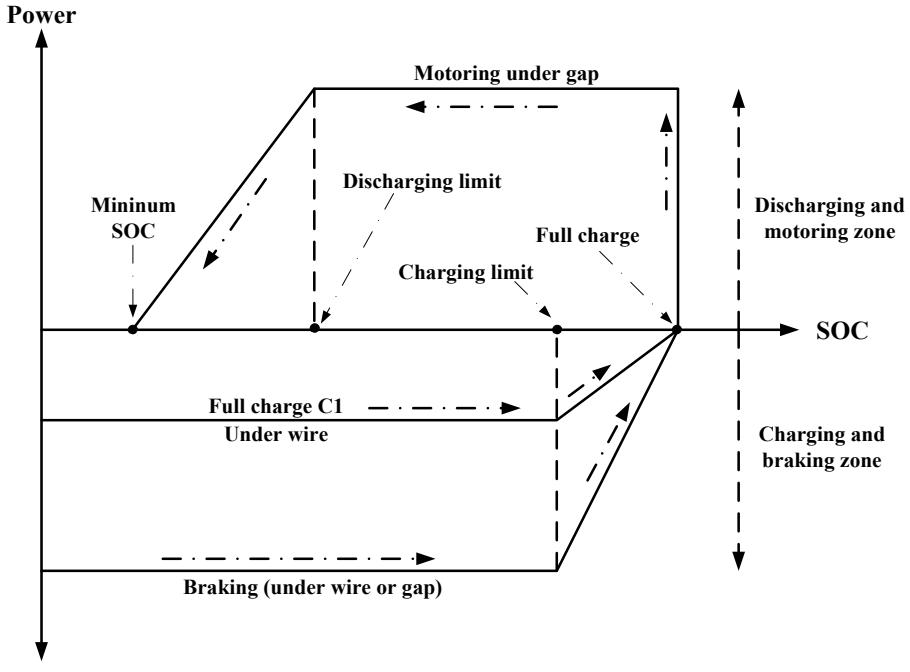

Figure 2.8: Control strategy to maintain the maximum SOC (RSSB, 2010)

B. Control Strategy to Maintain Minimum SOC

The objective of this controller scheme is to keep the minimum SOC of the storage at all times, as shown in Figure 2.9. The main purpose of this control is to maximise the energy available from regenerative braking. Therefore, in this control strategy there are no limits to the braking power up to the charging limit, and reduced power from the charging limit to full charge. For the discharging mode, the power has two different levels; the highest is used to support the vehicle travelling through gaps in the electrified line and the lowest is used to support the vehicle when it is under the contact wire. In both cases, energy from the storage devices is used until the minimum SOC is reached.

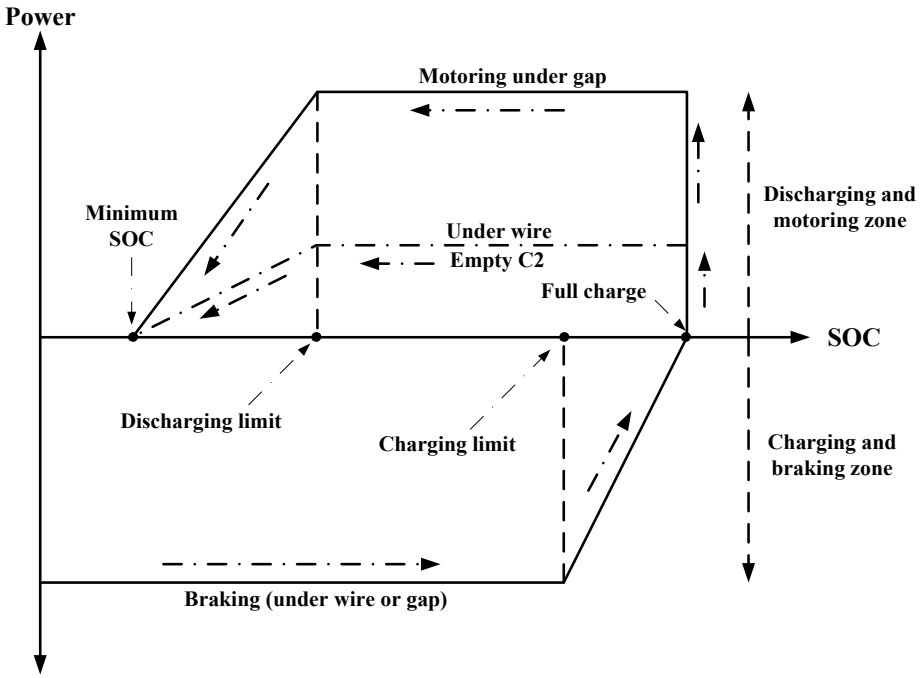

Figure 2.9: Control strategy to maintain the minimum SOC (RSSB, 2010)

C. Speed-Based Dependent Control Strategy

Unlike other strategies, this control is based on the speed profile of the vehicle and is shown in Figure 2.10 (a). In the charging mode, there are two levels of charging power, similar to the control strategy that maintains the maximum SOC. For the discharging mode, there are two levels of discharging power, similar to the control strategy that maintains the minimum SOC. In the shaded area where the train is travelling under the contact wire, the control strategy is based on the characteristic speed profile of the train. Where the SOC is above the minimum of the storage devices, it is in proportion to the train speed as shown in Figure 2.10 (b).

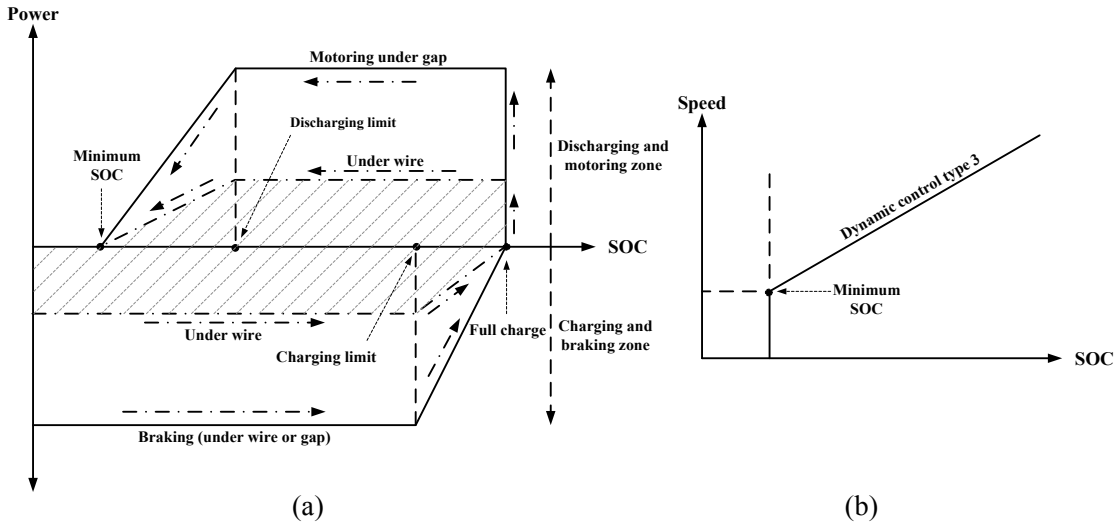

Figure 2.10: Speed dependent control strategy; (a) SOC and power (b) SOC and speed (RSSB, 2010)

D. Look Ahead Control Strategy

This control is based on the strategy of maintaining minimum and maximum SOC of the energy storage devices and the track profile. In fact, the number of gaps and the stop pattern is likely to be known in advance. Therefore, the controller can be adjusted to maximise the SOC when the vehicle is approaching a gap and minimise the SOC when the vehicle is approaching a stop.

2.4.2 Stationary SOC Control Strategy

Based on the fixed stationary energy storages employed in LRV systems, the capacity and lifetime are limited depending on the type of energy storage. Therefore, appropriate control of the charge and discharge of storage devices is able to solve that problems due to the driving styles: motoring or braking of the LRV. The control strategies based on the relationship between line voltage and charge/discharge of storage devices are described in the following subsections.

A. Static Control Strategy

Figure 2.11 shows the principle static control strategy for storage devices. If the line voltage is more than the charge starting voltage, the storage devices are recharged with the maximum charge current. On the other hand, if the line voltage is lower than the discharge starting voltage, the storage devices are discharged with the maximum discharge current. If the line voltage is between the charge and discharge starting voltage, the storage devices are on standby for recharging or discharging, depending on the driving styles. A high SOC for energy storages on standby mode is preferred for compensating the line voltage drop, whereas a low SOC is preferred for storing the braking energy (Okui et al., 2010, Konishi et al., 2010).

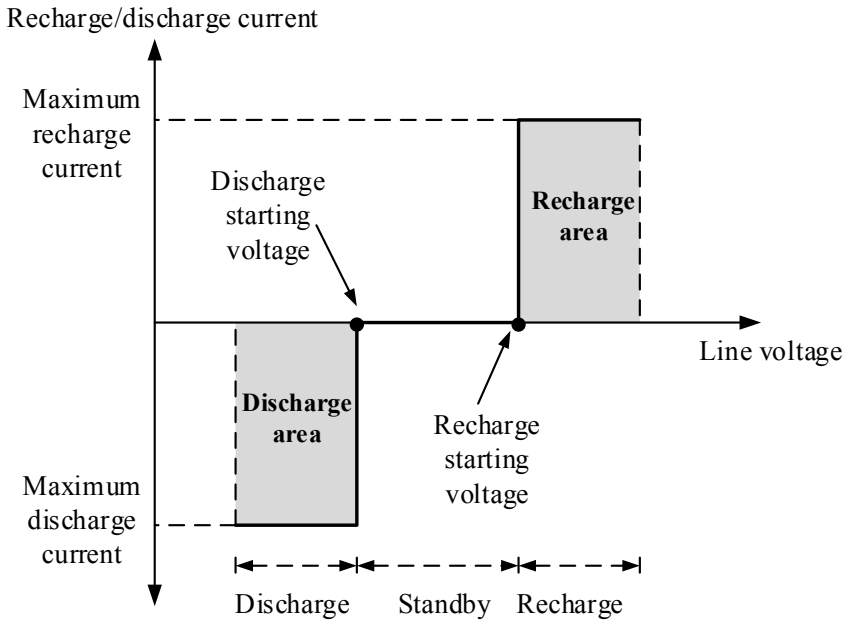

Figure 2.11: Principle static control strategy

In this control, the line voltage can oscillate around the two boundaries dividing discharge, standby and recharge operations and this would cause that the storage switch continuously from discharge to standby or from standby to recharge. To avoid this

problem, this control strategy requires hysteresis bands at the borders between the standby mode and discharge mode and the standby mode and recharge mode. The width of these bands can be adjusted case by case on the basis of the typical oscillations of the line voltage.

B. Supplementary Recharge/Discharge Control Method

Figure 2.12 shows the concept of the supplementary recharge/discharge control strategy for storage devices. This strategy is developed from the static control method, but it is different in the standby mode. If the purpose of the recharge/discharge control is both line voltage drop compensation and storing braking energy, the SOC of the storage devices must be constantly maintained at the medium, or 50% SOC, on standby mode for covering the charge and discharge simultaneously. The standby mode in this method is called the supplementary charge/discharge area, and the medium SOC of the storage devices should be kept within this area (Konishi et al., 2010).

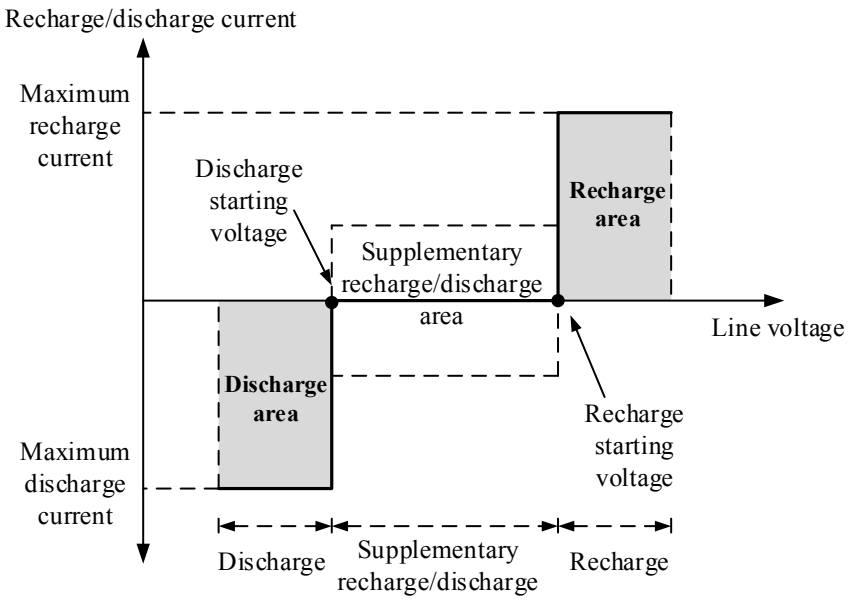

Figure 2.12: Supplementary recharge/discharge control method

C. Current Regulation Control Strategy

Figure 2.13 shows the concept of the current regulation control strategy for storage devices. This strategy is developed from the static control strategy, but it is different in the recharge and discharge area. The fluctuation of the large charge/discharge current is slightly limited by the linear equation until the maximum charge/discharge current around the charge/discharge area (Okui et al., 2010). This control strategy is developed in Chapter 5.

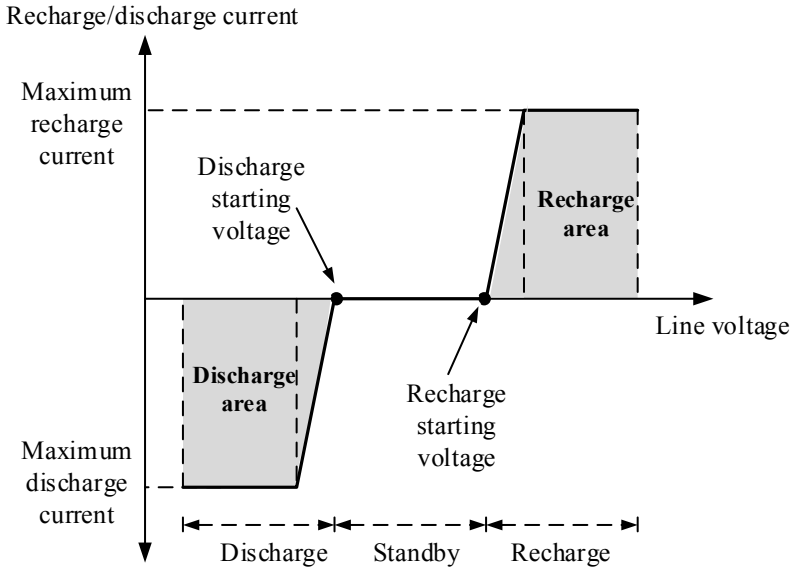

Figure 2.13: Current regulation control strategy

D. Standby Current Regulation Control Strategy

Figure 2.14 shows the concept of the standby current regulation control strategy. This control method is developed from the current regulation control strategy but it is different in the standby mode and discharge area. The maximum discharge current and standby current are able to vary higher or lower than the nominal values. The SOC of storage devices in the discharge area and standby mode based on this control strategy are easy to adjust. The degradation of storage devices is suppressed by the appropriately adjustable SOC (Okui et al., 2010).

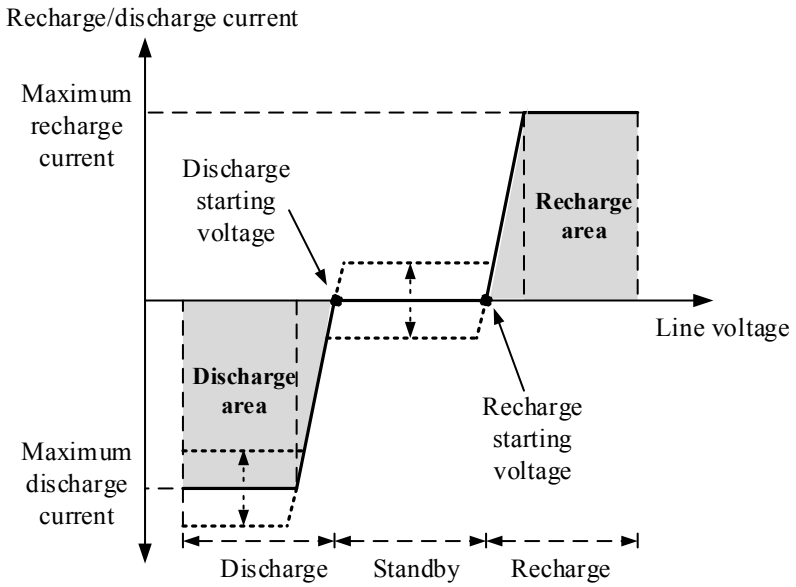

Figure 2.14: Standby current regulation control strategy

However, the line voltage fluctuation of DC electrified railways is affected by the train motoring and braking. These principle controls are not effective all the time. Therefore, the new SOC control for stationary storage devices is expected to cover any condition of the train motoring or braking.

2.5 Summary

This chapter reviews the benefits of the use of regenerative braking energy, which is generated when vehicles brake, in DC light railway systems with non-bi-directional power. The reuse of surplus braking energy by the auxiliary and comfort functions can increase the efficiency of the light railway systems in terms of energy saving by employing reversible substations, timetable optimisation of adjacent trains and on-board and wayside energy storage systems.

This chapter also provides a review of the applications and developments of energy storage devices for electrified railway systems, including batteries, flywheels, EDLCs and hybrid energy storage for both stationary and on-board applications. The analysis is focussed on both research prototypes and commercial products. The main characteristics of the storage technologies have been reviewed and compared in terms of energy density, power density and discharging time by using the Ragone plot. This analysis was extended from single cells and modules to entire storage systems to point out the main areas of application of the storage technologies. The contributions of the Ragone plot analysis based on the available energy storage systems reviewed in this chapter show that EDLCs present the characteristics of high power density and rapid discharging time in comparison with batteries, flywheels and hybrid energy storage. In addition, other typical characteristics of EDLCs are that they are well known as having high efficiency due to low internal resistance, they have long life cycles and low maintenance cost. These excellent characteristics make EDLCs suitable for worldwide use in electrified railway systems, with the main purpose of energy saving by recuperating the braking energy. Even though EDLCs do have disadvantages, such as low energy density and a high self-discharge rate, they are still good for enhancing the efficiency of light railway

applications. Moreover, flywheels have characteristics similar to EDLCs in terms of high power density, quick discharging time and long life cycles. They are also suitable for use to save energy in electrified railway systems, however, they are typically expensive in terms of investment and protection, and there is a high risk of explosion due to over load and failure in comparison to EDLCs and batteries. Batteries present the characteristics of high energy density and low discharging time, which means that they are able to support vehicles for catenary-free operations. Furthermore, the new technology of power electric devices combines both EDLCs and batteries together to become hybrid energy storage. The characteristics of hybrid energy storage combine the benefit of EDLCs and batteries into one energy storage system that will be very suitable for use in electrified railways in the future for both energy saving and catenary-free operations. However, this device may have a high investment cost in comparison with the individual energy storage devices.

Energy storage devices, both on-board and trackside applications, could significantly improve the efficiency of DC light railways in terms of energy saving by regenerating the train braking energy. Among the different types of storage devices which are available, EDLCs present the most appropriate characteristics for railway application in terms of high power density, quick recharge/discharge, long life cycle and low maintenance costs. In addition, stationary EDLCs allow more flexibility in the design of the storage system, because weight and volume have a much lower impact in comparison with on-board applications and the current design of trains.

The principal SOC controls for stationary and on-board applications of energy storage devices were also presented in this chapter. The purpose of the SOC control of on-board energy storage is energy saving and catenary-free operations. The control approach is based on the relationship between train energy and the SOC of energy storages. The

recharge and discharge modes of this control strategy depend on the position of vehicles travelling under or without catenary, whereas the purpose of the SOC control of stationary energy storage is voltage regulation and energy saving. The strategy of the stationary storage control approach is based on the relationship between the line voltage and current of the energy storage.

In this thesis, the SOC control of stationary energy storage devices has been studied and developed from the current regulation control strategy. This approach has been chosen because the standby mode is defined to avoid fluctuation of the line voltage and the current of the energy storage is limited by the linear equation for both recharge and discharge mode. The line voltage is modified by the deviation voltage between the voltage of the energy storage at the point of connection and the nominal voltage. The boundaries of the linear current of the recharge and discharge zones are designed by the minimum and maximum deviation voltage. This SOC control will be called "Piece-wise linear SOC control of stationary EDLCs", and it is presented in more detail in chapter 5.

Chapter 3 Model of the Railway Electrification System and the Rolling Stock

3.1 Introduction

An electrical model of a DC light railway is developed in this chapter. The electrification system consists of two electrical substations at the end of each section of the track. The trains travelling on the track are modelled as variable resistors, drawing power on the basis of the dynamic train motion given by the single train simulator at the University of Birmingham. The modelling of the railway is based on only one train because it is the best indicator of the performance of the line and the specific train with EDLCs, and the results would be similar in the case of a railway with multiple trains. The traction drives and the motors of the train are considered using an average model of the traction inverters. In the average model it is assumed that the inverter currents are perfectly sinusoidal and the DC current is perfectly smooth. The contribution of the stationary EDLCs is also considered using an average model of the DC-DC converters.

Regarding the auxiliary loads and comfort functions on-board the train, they are the electrical systems that consume energy on trains and at substations, including signalling systems, ventilation systems, lighting systems, heating systems, air-conditioning systems and other electrical systems. In addition, they are not considered in this model of the railway electrification system and rolling stock in this thesis, because, for example, the amount of energy they use is very small about 2.2% in comparison with the amount of regenerative braking energy of the London Underground.

The models described in this chapter were used in part of the work published in the conference proceedings papers reported in Appendix B.

3.2 Single Train Simulator

The single train simulator or STS was developed with the MATLAB-based simulator by the Birmingham Centre for Railway Research and Education at the University of Birmingham, UK (Hillmansen and Roberts, 2007). The STS simulates a single train travelling along a certain route based on the discrete distance steps. The gradient and curve data of the detailed track geometry given for the route are considered by the simulator, whereas signalling and block section information, which can be neglected for a single train, are not defined in the STS.

The STS employs the Euler method, which is the simplest method to solve differential equations given an initial value, to keep a constant acceleration for the duration of each distance step. The Euler method is implemented with the train simulators as follows. Firstly, the acceleration is calculated at the beginning of the step, taking into account the speed, traction force and gradient at that point and assuming it is constant for the whole step. For each step, the velocity of the train is calculated from the "suvat" equation: $v^2 = u^2 + 2as$, where v is the final velocity, u is the initial velocity, a is the acceleration and s is the displacement. The travelling time is then found, implementing the distance divided by the average speed, $\Delta t = 2s/(u + v)$. The distance step of the STS defines the displacement of the train travelling each step.

The STS focuses on the energy efficiency of dynamic train motion. In previous research the optimisation of single train trajectories has been solved by the STS in order to

minimise the energy consumption with the introduction of coasting (Lu et al., 2013) and to investigate the hybridisation of diesel vehicles (Hillmansen and Roberts, 2007). However, the STS has a small error in terms of distance, time and energy due to the length of the distance step, which can be solved by reducing the size of the distance step (Douglas et al., 2016). The Pendolino vehicle model as defined in the STS, which has the characteristic shown in Table 3.1, is used in the analytical calculations and the simulation test for validating the train motion used for passenger rail vehicle simulation. The gradient has been changed by 0% and 1% during the simulation on the track length of 2 km.

Table 3.1: Vehicle parameters for the STS Pendolino vehicle model

Parameter	Unit	Quantity
Mass	tonnes	592.8
Lambda	-	0.1
Maximum speed	km/h	260
Maximum traction force	kN	204.4
Maximum power	kW	6,000
Davis coefficient a	N	5421.6
Davis coefficient b	Nm/s	69.03
Davis coefficient c	Nm^2/s^2	10.31

3.3 Modelling of the Substations and the Electrification System

A simplified electrical model of a single-track light railway can be represented by the electric circuit shown in Figure 3.1 (Ratniyomchai et al., 2014a, Ratniyomchai et al., 2015). The three-phase feeders of the electric power distribution system are connected to the DC substations of the railway system by the main busbars and protected by circuit breakers. Generally speaking, a substation (ss) consists of two transformers, each of which has two rectifiers connected in parallel to form a 12-pulse AC-DC converter. The transformer rectifiers supply power to the conductor rail, or third rail (tr). These are

electrically separated by gaps, but they can be connected together by the transfer busbar and the switch/isolator. This switch/isolator can be normally open or normally closed, depending on the network operators, to enable dual-end feeding or mesh feeding, respectively. In the case of dual-end feeding, the switch/isolator can be closed to enable feeding from an adjacent substation in case of faults. The negative feeders of transformer rectifiers are connected to the negative busbars, which are electrically connected with the running rails (rr). The running rails are not normally earthed, to avoid the circulation of stray currents that are responsible for corrosion of metal parts next to the railway. In some other systems, such as London Underground, there is a return conductor and, hence, the return current does not circulate through the running rails.

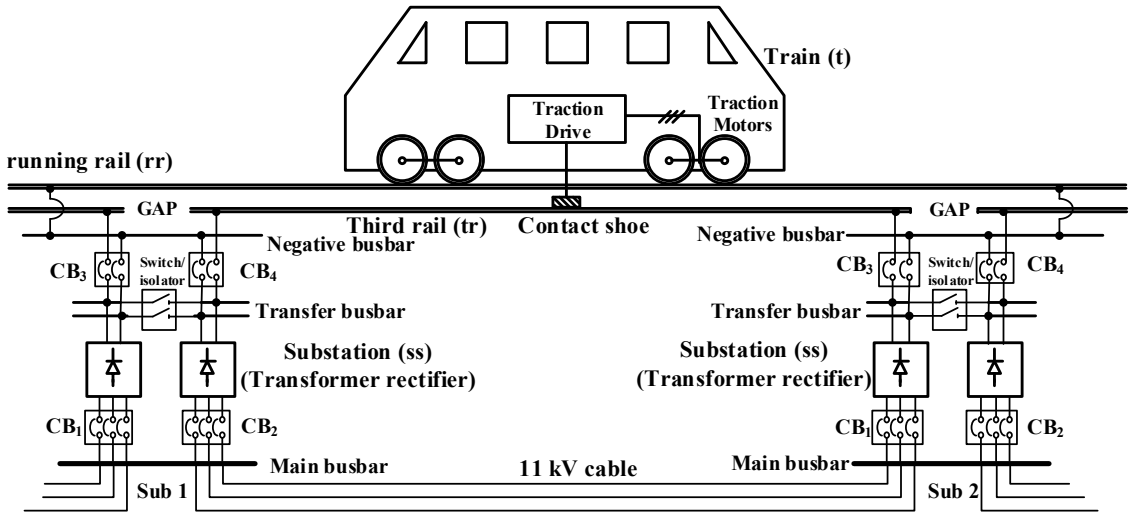

Figure 3.1: Schematic of the general electrification system of a DC light railway

The equivalent circuit of a DC light railway with substations and a train is shown in Figure 3.2. The DC voltages of substations 1 and 2 are represented by two ideal voltage sources generating voltages E_{ss1} and E_{ss2}. The equivalent resistances of substations 1 and 2 are represented by R_{ss1} and R_{ss2}. The portion of conductor rail and the running rails between the train and the substations are represented by R_{tr1} and R_{tr2}, and R_{rr1} and R_{rr2}, respectively.

The train is modelled as an ideal current source i_{train} and has a voltage v_{train}. The currents supplied by substations are $i_{ss}1$ and $i_{ss}2$.

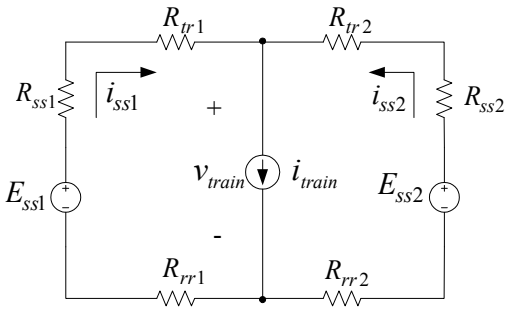

Figure 3.2: Equivalent circuit of a DC light railway

In Figure 3.2, the resistances $R_{ss}1$, $R_{tr}1$ and $R_{rr}1$ are connected in series within the loop, therefore, they can be combined in one resistance R_{L1}. Similarly, R_{L2} is the summation of resistances $R_{ss}2$, $R_{tr}2$, and $R_{rr}2$. With these considerations, the equivalent circuit of Figure 3.2 can be redrawn as in Figure 3.3.

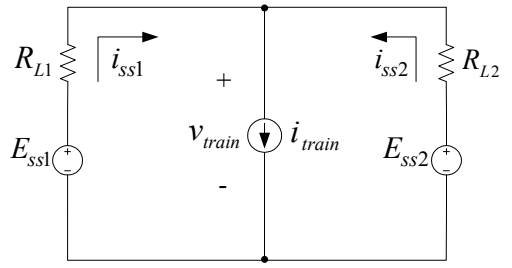

Figure 3.3: Equivalent circuit of a DC light railway with combined resistors

The train voltage v_{train} is given by the Kirchhoff voltage law (KVL) and Kirchhoff current law (KCL):

$$v_{train} = \frac{R_{L2}}{R_{L1}+R_{L2}} E_{ss1} + \frac{R_{L1}}{R_{L1}+R_{L2}} E_{ss2} - \frac{R_{L1}R_{L2}}{R_{L1}+R_{L2}} i_{train} \tag{3.1}$$

Then the electric power of the train P_{train} is:

$$P_{train} = -\frac{R_{L1}R_{L2}}{R_{L1}+R_{L2}} i_{train}^2 + \left(\frac{R_{L2}E_{ss1} + R_{L1}E_{ss2}}{R_{L1}+R_{L2}} \right) i_{train} \tag{3.2}$$

Solving (3.2) for the train current i_{train} yields:

$$i_{train} = \frac{R_{L1}E_{ss2} + R_{L2}E_{ss1} \pm \sqrt{\left(R_{L1}E_{ss2} + R_{L2}E_{ss1}\right)^2 - 4R_{L1}R_{L2}\left(R_{L1}+R_{L2}\right)P_{train}}}{2R_{L1}R_{L2}} \tag{3.3}$$

The positive result in the square root of (3.3) refers to a very high train current i_{train} and is discarded. Using the negative result, the train voltage v_{train} from (3.1) is obtained. According to (3.3) the train current i_{train} is a function of the electric power of the train P_{train}, which is dependent on the mechanical power of the train. The power P_{train} can be calculated from the model of traction motors described in the following section.

3.4 Model of Traction Motors

This thesis refers to the model of induction motors, which is widely used for light railway rolling stock. The power P_{train} in (3.2) is the sum of the electric powers of the individual traction motors. After a preliminary definition of the electrical parameters of the induction motors, the electrical power of the traction motors is calculated from the torque-speed curve characteristic.

3.4.1 Electrical Parameters of Traction Motors

The equivalent circuit of induction motors, referred to a phase of the stator winding, is shown in Figure 3.4, where $\bar{E}_s$ is the stator voltage, $\bar{I}_s$ is the stator current, $\bar{I}_r$ is the rotor current referred to a stator phase winding, R_s and L_s are the stator resistance and stator

leakage inductance, R'_r and L'_r are the rotor resistance and rotor leakage inductance referred to the stator phase winding, L_m is the mutual inductance and s is the slip.

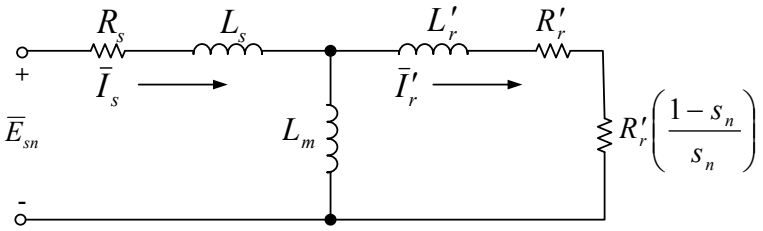

Figure 3.4: Equivalent circuit of the induction motor referred to the stator phase winding

The specifications of the induction motor, i.e. the nominal voltage, nominal current, nominal power, nominal speed, number of pole pairs and motor efficiency, are given by the manufacturer. The parameters of the induction motor in the equivalent circuit in Figure 3.4 are normally calculated from the locked-rotor and no-load tests. When the results of these tests are not available, an alternative procedure can be used to calculate the parameters using the data in nominal conditions. The mutual inductance L_m is significantly larger than the leakage inductances of the stator and rotor winding L_s and L'_r and, hence, the current drawn by this inductance can be neglected. Then the stator current is equal to the rotor current, $\bar{I}_s \approx \bar{I}'_r$. In this thesis, the stator resistance is assumed to be equal to the rotor resistance referred to the stator phase winding, $R_s \approx R'_r$, and also the stator leakage inductance is assumed to be equal to the rotor leakage inductance referred to the stator phase winding, $L_s \approx L'_r$, as recommended by IEEE standard 112-2004 (IEEE, 2004). Using KVL the stator current $\bar{I}_s$ is:

$$\bar{I}_s \approx \bar{I}'_r = \frac{\bar{E}_s}{R_s + \frac{R'_r}{s} + j\omega\left(L_s + L'_r\right)} = \frac{s\,\bar{E}_s}{sR_s + R'_r + js\omega\left(L_s + L'_r\right)} \tag{3.4}$$

where ω is the angular frequency of the supply voltage.

The relationship between the mechanical power of the motor $P_{m,output}$ and the motor torque T_{motor} is:

$$P_{m,output} = T_{motor}\omega_r = 3\left|\bar{I}'_r\right|^2 R'_r\left(\frac{1-s}{s}\right) \tag{3.5}$$

where, ω_r is the rotor angular speed in rad/sec. The relation between the rotor speed and the synchronous speed ω_s is $\omega_r = (1 - s)\,\omega_s$. Furthermore, ω_s is related to the angular frequency of the supply voltage by the relation $\omega_s = \omega/p$, where p is the number of pole pairs. On the basis of these relations, the motor torque of (3.5) can be expressed as follows:

$$T_{motor} = \frac{3R'_r}{s\omega_s}\left|\bar{I}'_r\right|^2 = \frac{3pR'_r}{s\omega}\left|\bar{I}'_r\right|^2 \tag{3.6}$$

If (3.4) is substituted in (3.6), the motor torque is rewritten as:

$$T_{motor} = \frac{3p\left|\bar{E}_s\right|^2}{\omega}\frac{sR_r}{\left[R_s^2 s^2 + \omega^2\left(L_s + L'_r\right)^2 s^2 + 2R_s R'_r s + R'^2_r\right]}$$

Putting:

$$K = 3p|\bar{E}_s|^2/\omega$$

$$X_{sr} = \omega(L_s + L'_r).$$

The previous equation becomes:

$$T_{motor} = K\frac{sR_r}{\left[\left(R_s^2 + X_{sr}^2\right)s^2 + 2R_s R'_r s + R'^2_r\right]} \tag{3.7}$$

The maximum value of the motor torque for a given supply voltage can be obtained by calculus:

$$\frac{\partial T_{motor}}{\partial s} = 0$$

And the solution is:

$$s = \pm \frac{R'_r}{\sqrt{R_s^2 + X_{sr}^2}} \tag{3.8}$$

The negative solution refers to generator operations of the machine and is discarded. Using the positive solution, the maximum torque $T_{motor,\max}$ is:

$$T_{motor,\max} = K \frac{1}{2\left(R_s + \sqrt{R_s^2 + X_{sr}^2}\right)} \tag{3.9}$$

In (3.9), the stator resistance R_s is very small in comparison with the reactance of the stator and rotor winding X_{sr} and can be neglected. Therefore, the maximum torque is simplified as:

$$T_{motor,\max} \cong \frac{3p\left|\overline{E}_s\right|^2}{\omega} \frac{1}{2X_{sr}} = \frac{3p\left|\overline{E}_s\right|^2}{2\omega^2\left(L_s + L'_r\right)} \tag{3.10}$$

When the machine operates in nominal conditions, (3.10) can be used to calculate the stator and rotor leakage inductances:

$$L_s \approx L'_r = \frac{3p\left|\overline{E}_s\right|^2}{4\omega^2 T_{motor,\max}} \tag{3.11}$$

Recalling the assumption $R_s \approx R'_r$, the stator and rotor resistances can be calculated from (3.4) when the machine operates in nominal conditions:

$$\overline{E}_s = \left(R_s + \frac{R'_r}{s} + j\omega\left(L_s + L'_r\right)\right)\bar{I}_s$$

$$R_s \approx R'_r = \frac{s}{1+s}\sqrt{\frac{\left|\overline{E}_s\right|^2}{\left|\bar{I}_s\right|^2} - \omega^2\left(L_s + L'_r\right)^2} \tag{3.12}$$

Finally, the mutual inductance L_m is calculated to match the torque of the motor in nominal conditions.

3.4.2 Power Input of the Traction Motor

The electric power input of the induction motor can be easily calculated once the parameters of the induction motor are known. According to Figure 3.4, the rotor current $\bar{I}'_r$ is equal to:

$$\bar{I}'_r = \frac{j\omega L_m}{\frac{R'_r}{s} + j\omega\left(L'_r + L_m\right)}\bar{I}_s \tag{3.13}$$

And substituting (3.13) into (3.6), the motor torque is:

$$T_{motor} = 3pR'_r\frac{s\omega L_m^2}{R_r'^2 + s^2\omega^2\left(L'_r + L_m\right)^2}\left|\bar{I}_s\right|^2 = 3pR'_r\frac{s\omega L_m^2}{R_r'^2 + s^2\omega^2 L_{rm}{}^2}\left|\bar{I}_s\right|^2 \tag{3.14}$$

where, $L_{rm} = L'_r + L_m$.

The torque has to be calculated in a different way if the motor speed is below or above the nominal speed, also called the base speed ω_{mb}. The details of the two cases are presented in the following subsections.

A. $\omega_m < \omega_{mb}$

Considering the torque-speed curve of the induction motor in Figure 3.5, the slip frequency $s_f\omega_f$ is constant and equal to the nominal slip frequency $s_n\omega_n$:

$$s_f\omega_f = s_n\omega_n = \text{constant} \tag{3.15}$$

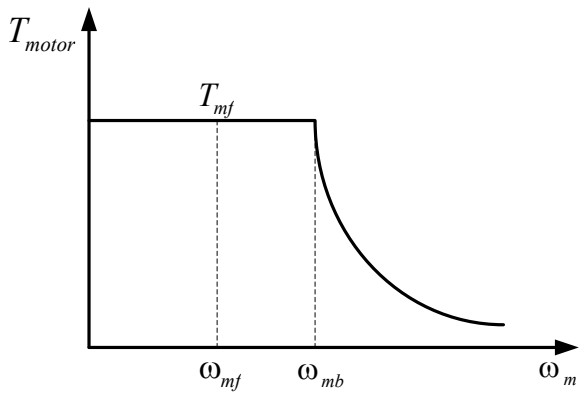

Figure 3.5: Torque-speed curve of the induction motor, $\omega_m < \omega_{mb}$

where s_f is the generic slip and ω_f is the generic angular frequency of the motor operating below the base speed.

Based on the slip frequency, the generic slip s_f is:

$$s_f = \frac{\omega_f - p\omega_{mf}}{\omega_f} \tag{3.16}$$

where, ω_{mf} is the generic speed of the induction motor.

From (3.15) and (3.16), the generic angular frequency ω_f can be calculated as follows:

$$\omega_f = s_n \omega_n + p\omega_{mf} \tag{3.17}$$

From (3.14), the magnitude of the stator current $\bar{I}_{sf}$ is:

$$\left|\bar{I}_{sf}\right| = \sqrt{\frac{T_{mf}\left(R_r'^2 + s_n^2 \omega_n^2 L_{rm}{}^2\right)}{3pR_r' s_n \omega_n L_m^2}} \tag{3.18}$$

where, T_{mf} is the motor torque, equal to the nominal value for every speed below the base speed. From Figure 3.4, the stator voltage $\bar{E}_{sf}$ is:

$$\bar{E}_{sf} = \hat{Z}_{eqf}\bar{I}_{sf} = \left[R_s + j\omega_f L_s + \frac{j\omega_f L_m\left(\frac{R_r'}{s_f} + j\omega_f L_r'\right)}{\frac{R_r'}{s_f} + j\omega_f L_{rm}} \right] \bar{I}_{sf} \tag{3.19}$$

where, $\hat{Z}_{eqf} = R_s + j\omega_f L_s + \dfrac{j\omega_f L_m\left(\frac{R_r'}{s_f} + j\omega_f L_r'\right)}{\frac{R_r'}{s_f} + j\omega_f L_{rm}} = R_s + j\omega_f\left[L_s + \dfrac{L_m\left(R_r' + js_f\omega_f L_r'\right)}{R_r' + js_f\omega_f L_{rm}} \right]$

Therefore, the actual power input of the induction motor $P_{m,input}$ is obtained as follows:

$$P_{m,input} = 3\,\mathrm{Re}\left\{\bar{E}_{sf}\bar{I}_{sf}^*\right\} = 3\left|\bar{I}_{sf}\right|^2 \mathrm{Re}\left\{\hat{Z}_{eqf}\right\} \tag{3.20}$$

B. $\omega_m \geq \omega_{mb}$

Considering that above the base speed the torque-speed curve of the induction motor is represented in Figure 3.6, the slip frequency $s_f\omega_f$ is no longer constant. In fact, in this

region the torque is limited by the maximum current that the machine can draw, equal to the nominal value. Thus, the angular frequency ω_f can be calculated by substituting s_f of (3.16) in the motor torque, given by (3.14):

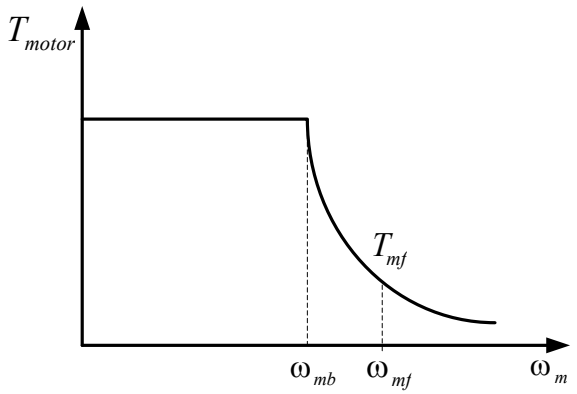

Figure 3.6: Torque-speed curve of the induction motor, $\omega_m \geq \omega_{mb}$

$$T_{mf} = 3pR'_r \frac{s_f \omega_f L_m^2}{R'^2_r + s_f^2 \omega_f^2 L_{rm}{}^2} \left|\bar{I}_s\right|^2 = 3pR'_r \frac{\left(\omega_f - p\omega_{mf}\right) L_m^2}{R'^2_r + \left(\omega_f - p\omega_{mf}\right)^2 L_{rm}{}^2} \left|\bar{I}_{sn}\right|^2 \tag{3.21}$$

where the stator current is equal to the nominal value. From (3.21), a quadratic equation of ω_f is obtained. Then the actual angular frequency ω_f is:

$$\omega_f = \frac{2p\omega_{mf} T_{mf} L_{rm}^2 + 3pR'_r L_{rm}^2 \left|\bar{I}_s\right|^2 \pm \sqrt{R'^2_r \left(9p^2 L_m^4 \left|\bar{I}_{sn}\right|^4 - 4T_{mf}^2 L_{rm}^2\right)}}{2T_{mf} L_{rm}^2} \tag{3.22}$$

Applying the condition that the stator voltage and current have magnitude equal to the nominal value from (3.19) and the solution of the actual angular frequency ω_f from (3.22), the generic slip s_f is obtained by using the positive result in the square root of (3.22). The negative result refers to a very small generic slip s_f in comparison with the nominal slip s_n and is discarded. The power $P_{m,input}$ can be calculated by substituting the actual angular frequency ω_f from (3.22) and the generic slip s_f from (3.16) in $\hat{Z}_{eqf}$ of (3.20).

3.5 Model of the Electrification System with EDLCs

The model presented in Figure 3.3 is modified when a stationary storage system with EDLCs is connected trackside at some points of the line. The train can be between substation 1 on the left and the storage, or between the storage and substation 2 on the right, as indicated by Figure 3.7 and Figure 3.8. For simplicity, these figures refer to the case where the voltages of the substations are equal to E_{ss}. In these figures, the terminal voltage and current of the storage system are v_{Edlc} and i_{Edlc}, the branch currents are i_{L1}, i_{L2} and i_{L3}, the train and storage positions are x_{train} and x_{Edlc}, the track length is L, the resistances, including the rail resistances and the conducting rail resistances, are R_{line}. The internal resistances of substations 1 and 2 are represented by R_{ss1} and R_{ss2}.

Looking at Figure 3.7, the following quantities can be defined:

- $R_{y1} = R_{ss1}+R_{line}\cdot x_{train}/L$ is the sum of the internal resistance of the first substation on the left and the line resistance between the first substation on the left and the train;
- $R_{y2} = R_{line}\cdot(x_{Edlc} - x_{train})/L$ is the line resistance between the train and the storage;
- $R_{y3} = R_{ss2}+R_{line}\cdot(L - x_{Edlc})/L$ is the sum of the internal resistance of the second substation on the right and the line resistance between the storage and the second substation on the right.

Similarly, looking at Figure 3.8, the following quantities can be defined:

- $R_{y4} = R_{ss1}+R_{line}\cdot x_{Edlc}/L$ is the sum of the internal resistance of the first substation on the left and the line resistance between the first substation on the left and the storage;

- $R_{y5} = R_{line} \cdot (x_{train} - x_{Edlc})/L$ is the line resistance between the storage and the train;
- $R_{y6} = R_{ss2} + R_{line} \cdot (L - x_{train})/L$ is the sum of the internal resistance of the second substation on the right and the line resistance between the train and the second substation on the right.

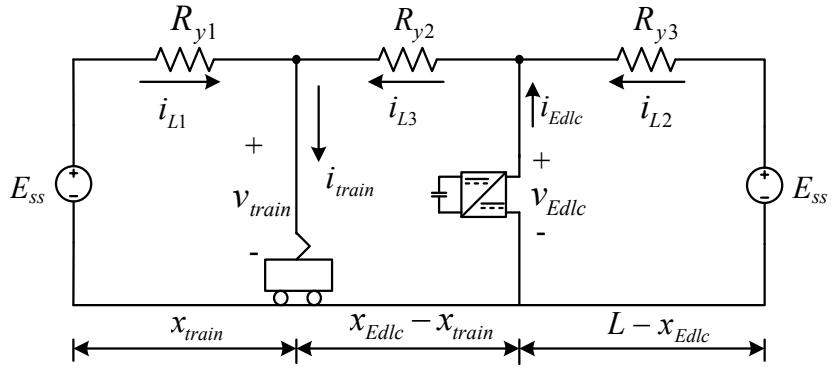

Figure 3.7: A stationary EDLC located after a light railway vehicle, $x_{Edlc} > x_{train}$

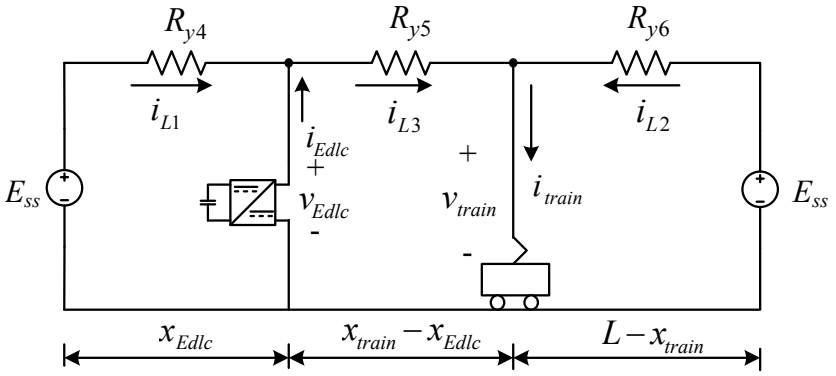

Figure 3.8: A stationary EDLC located before a light railway vehicle, $x_{Edlc} < x_{train}$

Considering Figure 3.7, the following equations are obtained by KVLs and KCLs:

$$v_{train} - E_{ss} + R_{y1} i_{L1} = 0 \tag{3.23a}$$

$$v_{Edlc} - E_{ss} + R_{y3} i_{L2} = 0 \tag{3.23b}$$

$$v_{Edlc} - v_{train} - R_{y2} i_{L3} = 0 \tag{3.23c}$$

$$i_{L1} = i_{train} - i_{L3} \tag{3.23d}$$

$$i_{L2} = i_{L3} - i_{Edlc} \tag{3.23e}$$

Considering Figure 3.8, the following equations are also obtained by KVLs and KCLs:

$$v_{train} - E_{ss} + R_{y6} i_{L2} = 0 \tag{3.24a}$$

$$v_{Edlc} - E_{ss} + R_{y4} i_{L1} = 0 \tag{3.24b}$$

$$v_{Edlc} - v_{train} - R_{y5} i_{L3} = 0 \tag{3.24c}$$

$$i_{L1} = i_{L3} - i_{Edlc} \tag{3.24d}$$

$$i_{L2} = i_{train} - i_{L3} \tag{3.24e}$$

The two sets of equations (3.23c and 3.24c) can be combined into one equation introducing two new parameters, A_s and B_s:

$$v_{Edlc} - v_{train} - R_{y2} i_{L3} A_s - R_{y5} i_{L3} B_s = 0$$

When the storage is after the train, i.e. $x_{Edlc} > x_{train}$, A_s is equal to 1 and B_s is equal to 0; in the other situation, i.e. $x_{Edlc} < x_{train}$, A_s is equal to 0 and B_s is equal to 1. From the previous equation, the current i_{L3} can be calculated:

$$i_{L3} = \frac{v_{Edlc} - v_{train}}{R_{y2} A_s - R_{y5} B_s} = \frac{v_{Edlc} - v_{train}}{C_1} \tag{3.25}$$

where: $C_1 = R_{y2} A_s - R_{y5} B_s$

Combining (3.23a), (3.23d), (3.24a), (3.24e) and (3.25), the train voltage v_{train} and storage voltage v_{Edlc} are related by the equation:

$$C_3 v_{train} + C_4 v_{Edlc} = C_5 \tag{3.26}$$

where: $C_2 = R_{y1}A_s + R_{y6}B_s$, $C_3 = (C_1 + C_2)/C_1$, $C_4 = -C_2/C_1$, $C_5 = E_{ss} - C_2 i_{train}$

Combining (3.23b), (3.23e), (3.24b), (3.24d) and (3.25), the train voltage v_{train} and the storage voltage v_{Edlc} are also related by the equation:

$$C_7 v_{train} + C_8 v_{Edlc} = E_{ss} + C_6 i_{Edlc} \tag{3.27}$$

where: $C_6 = R_{y3}A_s + R_{y4}B_s$, $C_7 = -C_6/C_1$, $C_8 = (C_1 + C_6)/C_1$

The train voltage and the storage voltage can be calculated by solving simultaneously (3.26) and (3.27):

$$v_{train} = C_9 + C_{10} i_{Edlc} \tag{3.28}$$

where: $C_9 = \dfrac{C_5 C_8 - C_4 E_{ss}}{C_3 C_8 - C_4 C_7}$, $C_{10} = -\dfrac{C_4 C_6}{C_3 C_8 - C_4 C_7}$

$$v_{Edlc} = C_{11} + C_{12} i_{Edlc} \tag{3.29}$$

where: $C_{11} = \dfrac{C_3 E_{ss} - C_5 C_7}{C_3 C_8 - C_4 C_7}$, $C_{12} = \dfrac{C_3 C_6}{C_3 C_8 - C_4 C_7}$

Equations (3.28) and (3.29) point out that v_{train} and v_{Edlc} are functions of the storage current i_{Edlc} only. Also the current, i_{L3} is as a function of i_{Edlc} only, if (3.28) and (3.29) are substituted in (3.25):

$$i_{L3} = \frac{C_{11} - C_9}{C_1} + \frac{C_{12} - C_{10}}{C_1} i_{Edlc} = C_{13} + C_{14} i_{Edlc} \tag{3.30}$$

where: $C_{13} = \dfrac{C_{11} - C_9}{C_1}$, $C_{14} = \dfrac{C_{12} - C_{10}}{C_1}$

The same results do apply for the branch currents:

$$i_{L1} = C_{15} + C_{16} i_{Edlc} \tag{3.31}$$

where: $C_{15} = i_{train} A_s - C_{13} A_s + C_{13} B_s$, $C_{16} = C_{14} B_s - C_{14} A_s - B_s$

$$i_{L2} = C_{17} + C_{18} i_{Edlc} \tag{3.32}$$

where: $C_{17} = C_{13} A_s + i_{train} B_s - C_{13} B_s$, $C_{18} = C_{14} A_s - A_s - C_{14} B_s$

In the case where the positions of the train and storage are at the same point $x_{train} = x_{Edlc}$, there is no resistance between the train and storage $R_{y2} = R_{y5} = 0$, and $R_{y1} = R_{y4}$, $R_{y3} = R_{y6}$. Figure 3.7 and Figure 3.8 are modified, as shown in Figure 3.9.

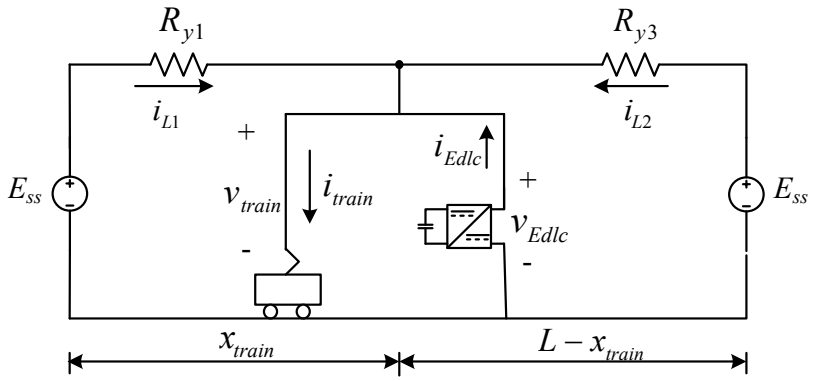

Figure 3.9: A stationary EDLC located at the same position as a light railway vehicle, $x_{Edlc} = x_{train}$

Considering Figure 3.9, the following equations are also obtained by KVLs and KCLs:

$$v_{train} = v_{Edlc} = E_{ss} - R_{y1} i_{L1} = E_{ss} - R_{y2} i_{L2} \tag{3.33a}$$

$$i_{L1} + i_{L2} = i_{train} - i_{Edlc} \tag{3.33b}$$

Combining (3.33a) and (3.33b), the branch current i_{L1} and i_{L2}, the train voltage v_{train} and the storage voltage v_{Edlc} as a function of i_{Edlc} only are:

$$i_{L1} = D_1\left(i_{train} - i_{Edlc}\right) \tag{3.34}$$

where: $D_1 = \dfrac{R_{y2}}{R_{y1} + R_{y2}}$

$$i_{L2} = D_2\left(i_{train} - i_{Edlc}\right) \tag{3.35}$$

where: $D_2 = \dfrac{R_{y1}}{R_{y1} + R_{y2}}$

$$v_{train} = v_{Edlc} = E_{ss} - D_3\left(i_{train} - i_{Edlc}\right) \tag{3.36}$$

where: $D_3 = R_{y1}D_1$

All of the models in section 3.5 are dependent on the current of the storage i_{Edlc} and, hence, these are the variables used for the optimisation. Moreover, these coefficients C_1-C_{18} and D_1-$D3$ are time dependent on the basis of the position $x_{train}(t)$ of the train.

3.6 EDLCs Modelling

The model of the EDLC storage system is based on the series and parallel connection of the basic EDLC, shown in Figure 3.10. The equivalent capacitance of an EDLC system is c_{sc}, and the current and voltage are $i_{sc}(t)$ and $v_{sc}(t)$, respectively. In practical design, there is a small internal resistance which draws a small energy loss from an EDLC system,

which is taken into account in terms of efficiency at the end of the calculation of the total capacitance. Neglecting the effect of the internal resistance of the EDLC at this stage, the EDLC current $i_{sc}(t)$ is (Boylestad, 2007):

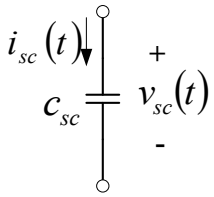

Figure 3.10: A basic EDLC

$$i_{sc}(t) = c_{sc}\frac{dv_{sc}(t)}{dt} \tag{3.37}$$

Then, the power of a basic EDLC is:

$$P_{sc}(t) = v_{sc}(t)i_{sc}(t) \tag{3.38}$$

Using (3.37), (3.38) can be rewritten as:

$$P_{sc}(t) = v_{sc}(t)c_{sc}\frac{dv_{sc}(t)}{dt} = \frac{1}{2}c_{sc}\frac{dv_{sc}^2(t)}{dt} \tag{3.39}$$

The energy of a basic EDLC is the integral of the power given by (3.39):

$$E_{sc}(t) = \int_0^t P_{sc}(t)dt = \frac{1}{2}c_{sc}\int_0^t \frac{dv_{sc}^2(t)}{dt}dt$$

$$E_{sc}(t) = \frac{1}{2}c_{sc}\left[v_{sc}^2(t) - v_{sc}^2(0)\right] \tag{3.40}$$

where $v_{sc}(0)$ is the initial voltage of the basic EDLC.

The EDLC system is connected to the supply line by means of a DC-DC bidirectional converter, whose voltage and current are $v_{Edlc}(t)$ and $i_{Edlc}(t)$, respectively. The efficiency of the DC-DC bidirectional converter and EDLCs are approximately the same, at 90%, which is taken into account in the calculation of the capacitance and expressed in the next subsection on traction efficiency.

The power output of the DC-DC converter is defined as $P_{Edlc}(t)$ and the energy is:

$$En_{Edlc}(t) = \int_0^T P_{Edlc}(t)dt = \int_0^T v_{Edlc}(t)i_{Edlc}(t)dt \tag{3.41}$$

where T is the duration time of the train travelling from the first substation to the second substation and then travelling back to the first substation again.

Based on Figure 3.11, the energy $E_{sc}(t)$ is equal to the opposite of $En_{Edlc}(t)$, since the direction of the $i_{sc}(t)$ is opposite to that of $i_{Edlc}(t)$:

$$E_{sc}(t) = -En_{Edlc}(t)$$

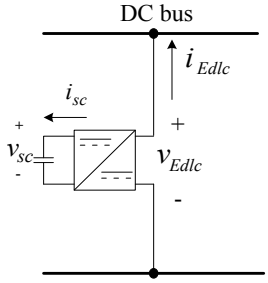

Figure 3.11: EDLC module connected to the DC bus by means of the DC-DC bi-directional converter

Using (3.40) and (3.41):

$$\frac{1}{2}c_{sc}\left[v_{sc}^2(t) - v_{sc}^2(0)\right] = -\int_0^T v_{Edlc}(t)i_{Edlc}(t)dt$$

and solving for $v_{sc}(t)$:

$$v_{sc}(t) = \sqrt{v_{sc}^2(0) - \frac{2}{c_{sc}} \int_0^T v_{Edlc}(t) i_{Edlc}(t) dt} \tag{3.42}$$

In order to keep a reasonable boost ratio of the converter, the nominal voltage of EDLCs $v_{sc,n}$ has been set to one half of the nominal line voltage of the railway. This means that the boost ratio is not greater than 4 when the EDLCs are fully discharged. Additionally, the voltage $v_{sc}(0)$ has been set to $v_{sc,n}$.

Equation (3.42) can be used to design c_{sc}, imposing that the voltage $v_{sc}(t)$ is always equal to or greater than one half of $v_{sc,n}$. Therefore, the capacitance c_{sc} is calculated by satisfying the following inequality:

$$\sqrt{v_{sc,n}^2(t) - \frac{2}{c_{sc}} \int_0^T v_{Edlc}(t) i_{Edlc}(t) dt} \geq \frac{v_{sc,n}}{2} \qquad \text{for any } t$$

$$c_{sc} \geq \frac{8}{3v_{sc,n}^2} \max\left[\int_0^T v_{Edlc}(t) i_{Edlc}(t)\right] dt \qquad \text{for any } t \tag{3.43}$$

In (3.43), the right-side of the equation is slightly modified to cover the whole range of the energy of the EDLC, thus the total capacitance of the EDLC is:

$$c_{sc} \geq \frac{8}{3v_{sc,n}^2} \left[\max\left(\int_0^T v_{Edlc}(t) i_{Edlc}(t) dt\right) - \min\left(\int_0^T v_{Edlc}(t) i_{Edlc}(t) dt\right)\right] \tag{3.44}$$

This is because the state of charge of the EDLC starts at zero, which is, for example, represented as 65% SOC, and then the energy of the EDLC can be both positive and negative during the time in which the train travels from the first substation to the second substation and then back to the first substation again. So the energy range of the EDLC

has to cover peak to peak of the positive and negative sides. The 90% efficiency of each EDLC and the DC-DC bidirectional converter can be taken into account by multiplying in (3.44).

Once the equivalent capacitance of the storage has been calculated by (3.44), the number of modules connected in series N_s, and parallel N_p, can be designed. According to Figure 3.12, the voltage and capacitance of individual modules, which are supposed to be identical, are defined as $v_{sc,m}$ and $c_{sc,m}$.

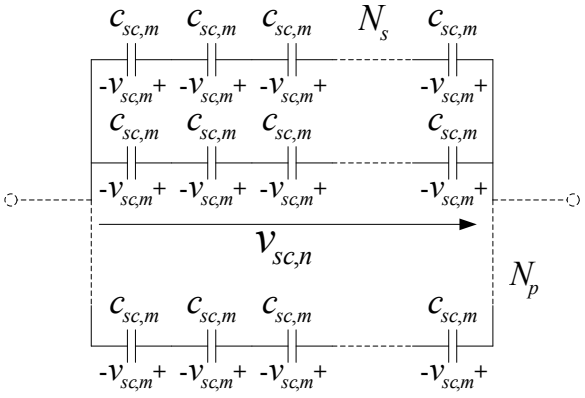

Figure 3.12: EDLC modules connected in series and parallel

The number of modules connected in series is calculated from the voltage requirement of the whole system:

$$N_s = \frac{v_{sc,n}}{v_{sc,m}} \tag{3.45}$$

where $v_{sc,n}$ is the nominal voltage of the storage, equal to one half of the nominal voltage of the railway line.

The number of modules connected in parallel is calculated from the capacitance requirement of the whole system:

$$N_p = ceiling\left(\frac{c_{sc} \times N_s}{c_{sc,m}}\right) \tag{3.46}$$

3.7 Traction Efficiency

In this thesis, the optimisation algorithm takes into account the efficiency of the friction, gearboxes, traction motors, inverters, rails and conducting rails, DC-DC converters and stationary EDLCs during the cycle of stationary EDLCs recharging and discharging energy when the train is braking and accelerating.

In general, the reverse efficiency of a reversible mechanism is not equal to the forward efficiency, however, the forward and reverse efficiencies are only slightly different when the forward efficiency is above 90%. For simplicity, in this thesis all of the reverse efficiencies are considered equal to the forward efficiencies. The diagrams of the energy flow when the train is braking and motoring are shown in Figure 3.13 (a) and (b) for typical values of the different elements involved in the power conversion process (Gonzalez-Gil et al., 2014, Gonzalez-Gil et al., 2015, Douglas et al., 2015). The net efficiency in one cycle of the train braking and motoring is:

$$\eta_{one-cycle} = \left(\prod_{i=1}^{n} \eta_i\right)^2 \cong 25.49\% \tag{3.47}$$

In (3.47), the net efficiency in one cycle of the train braking and motoring indicates that by using EDLCs, 25.49% of the surplus braking energy will be used to support the train motoring in the next cycle of the train journey.

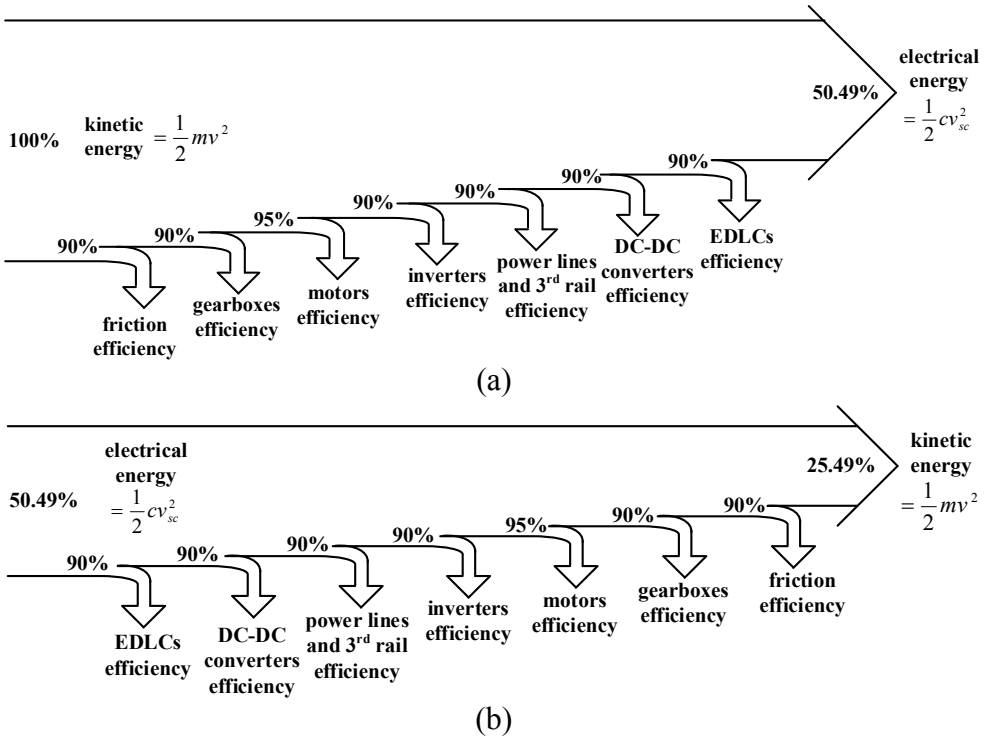

Figure 3.13: Braking energy flows between the train and EDLCs (a) when the train is braking (b) when the train is motoring (Gonzalez-Gil et al., 2014, Gonzalez-Gil et al., 2015, Douglas et al., 2015).

The efficiency of friction is taken into account with the Davis equation in the STS. The efficiency of gearboxes, traction motors and inverters is taken into account in the calculation of the energy of the train during train braking and accelerating. The efficiency of the rails and conducting rails is taken into account in terms of the line losses of the system. The efficiency of the DC-DC converter and EDLCs is taken into account in the calculation of the energy of the EDLCs based on the capacitance design. As mentioned above, the auxiliary loads and comfort functions on-board the train are not considered during train braking and acceleration. This is because the energy drawn by them is very small in comparison with the regenerative braking energy.

3.8 Summary

This chapter has presented a model of a DC electrified railway for light railway vehicles with stationary EDLCs, which refers to a single train travelling on the line. The model of the train includes a detailed model of the traction motors based on the equivalent circuit of three-phase induction machines, and it enables the power drawn by the train to be calculated from the torque-speed characteristic. Moreover, a model of the electrification system with a coupling between the train and EDLC in each section of the route has also been developed in this thesis. The position of the EDLC is fixed at various points along the track, whereas the train can be positioned either at the same point as the EDLC, or before or after the EDLC, depending on how the train moves forward and returns on its journey. This model enables the voltage of the train and EDLCs to be calculated; the branch currents are all considered as a function of the current of the EDLCs. All of the formulas obtained from the models in this chapter are implemented in the cost function of the optimisation technique presented in Chapter 4. In addition, the total capacitance of the EDLCs and the number of EDLC systems connected in series and in parallel are presented and calculated from the modelling. The traction efficiencies of the train braking and motoring have been taken into account in the calculations employed in the optimisation algorithm in the following chapter.

Chapter 4 Optimal Design of Stationary EDLCs for Light Railways

4.1 Introduction

This chapter presents an optimisation algorithm to design the optimal locations and capacitances of stationary EDLCs in a light railway system. The content of this chapter is divided into two main sections, including a review of the theory of optimisation techniques with the optimisation method for stationary EDLCs developed in this thesis, and the optimisation results with a discussion of the case study.

In section 4.2 the theory of the principal optimisation techniques is presented, including the classical theory of calculus of variations and the meta-heuristic methods genetic algorithm and particle swarm optimisation. Both methods are employed in the optimisation algorithm. The calculus of variations is taken into account in the optimal design of capacitances and locations of stationary EDLCs because it is faster than meta-heuristic methods in terms of the number of iterations. However, the fitting weight coefficients $\omega_1 - \omega_4$ between 0 and 1 employed in the optimisation algorithm are found by genetic algorithms and particle swarm optimisation, which is faster than using the calculus of variations because it is not necessary to calculate every possible candidate of the solution when using meta-heuristic methods.

In addition, the model of the railway electrification system, the train and the stationary EDLC storage system developed in chapter 3 has been implemented to design the optimal positions and capacitances of EDLCs along the route. The objective function of the

optimisation algorithm is to minimise the total energy consumption of substations when the train travels a round-trip in each section. The isoperimetric constraint takes into account that the storage system has the initial state of charge at the end of one cycle of the train journey (from the first substation to the second substation and then back to the first substation again).

In section 4.3 the optimisation results are presented based on a case study of a real light railway route with a single train travelling a round trip. Comparisons of the results of the light railway system, both with and without optimal positions and capacitances of EDLCs in terms of the substation currents and EDLCs, the voltages of the train and EDLCs, and energy drawn by substations, train and EDLCs are presented and discussed.

The models and the algorithms in this chapter have been, in part, employed for the work published in the conference proceedings reported in Appendix B.

4.2 Theory of Optimisation Techniques

As mentioned above, the optimal positions and capacitances of the stationary EDLCs are obtained by an optimisation method based on the classical theory of calculus of variations with the cost function presented in section 4.2.4, whereas the fitting weight coefficients $\omega_1 - \omega_4$ implemented in the cost function are found by meta-heuristic methods based on genetic algorithms and particle swarm optimisation. Therefore, the theory of the optimisation techniques based on the classical theory of calculus of variations and the meta-heuristic methods genetic algorithms and particle swarm optimisation is presented in the subsections below.

4.2.1 Classical Theory of Calculus of Variations

The application of optimisation techniques has been of fundamental importance in system design. The main concept which forms the basis of an optimisation technique is to find the function that maximises a given integral once specific limits on either the integral or the function are assigned. The function is called an objective function and includes a number of parameters which are specific to the problem to be solved. In this section, the principles of equality constraints and Lagrange multipliers are presented, together with isoperimetric constraints, which are employed in the optimisation algorithms used in this thesis.

4.2.1.1 Equality Constraints and Lagrange Multipliers

The performance measure M or the objective function of problems that are subject to be extremised by the maximisation or minimisation is assumed and defined as follows (Pierre, 1969):

$$M = f_0(y_1, y_2) \cong f_0 \tag{4.1}$$

The equality constraint related to the objection function is assumed and defined as follows:

$$c_1 = f_1(y_1, y_2) \cong f_1 \tag{4.2}$$

where c_1 is a constant, f_0 and f_1 are supposed to be the continuous function with respect to the parameters y_1 and y_2. The real set value of parameters y_1 and y_2, which are dependent

in practical problems, are considered to exist for satisfying the constraint in (4.2) (Pierre, 1969).

The derivatives of (4.1) and (4.2) can be calculated applying the chain rule of the differentiation with respect to the parameters y_1 and y_2 as follows:

$$\frac{dM}{dy_1} = \frac{\partial f_0}{\partial y_1} + \frac{\partial f_0}{\partial y_2}\frac{dy_2}{dy_1} \tag{4.3}$$

and:

$$\frac{dc_1}{dy_1} = 0 = \frac{\partial f_1}{\partial y_1} + \frac{\partial f_1}{\partial y_2}\frac{dy_2}{dy_1} \tag{4.4}$$

For the extreme function M at a given point, the term dM/dy_1 in (4.3) is equal to zero. Therefore (4.3) is turned into a necessary condition of the extreme function: at a given point, the extreme function M is constant, so the differentiation must be zero.

$$\frac{\partial f_0}{\partial y_1} + \frac{\partial f_0}{\partial y_2}\frac{dy_2}{dy_1} = 0 \tag{4.5}$$

The advantage of this condition for the extreme function is that the term dy_2/dy_1 is independent of the numerical calculation based on the formulas in (4.4) and (4.5). Thus, the term dy_2/dy_1 can be eliminated in (4.4) and (4.5). With the assumptions of having nonzero derivatives, (4.4) and (4.5) yield:

$$\frac{dy_2}{dy_1} = \frac{-\partial f_1/\partial y_1}{\partial f_1/\partial y_2} = \frac{-\partial f_0/\partial y_1}{\partial f_0/\partial y_2} \tag{4.6}$$

From (4.6), the term dy_2/dy_1 is defined as a Lagrange multiplier, h (Pierre, 1969):

$$h \cong \frac{-\partial f_1/\partial y_1}{\partial f_1/\partial y_2} = \frac{-\partial f_0/\partial y_1}{\partial f_0/\partial y_2} \tag{4.7}$$

Therefore, the expression (4.7) can be rewritten as:

$$\frac{\partial f_0}{\partial y_1} + h\frac{\partial f_1}{\partial y_1} = 0 \tag{4.8}$$

and

$$\frac{\partial f_0}{\partial y_2} + h\frac{\partial f_1}{\partial y_2} = 0 \tag{4.9}$$

The augmented performance measure, also called augmented functional f_a, is defined as (Pierre, 1969):

$$f_a = f_0(y_1, y_2) + hf_1(y_1, y_2) \tag{4.10}$$

From the augmented functional in (4.10), (4.8) and (4.9) are replaced by:

$$\frac{\partial f_a}{\partial y_1} = 0 \tag{4.11}$$

and

$$\frac{\partial f_a}{\partial y_2} = 0 \tag{4.12}$$

The Lagrange multiplier h is independent of y_1 and y_2. Therefore, the set of the three equations (4.2), (4.11) and (4.12) can be solved for the three variables y_1, y_2 and h to obtain the optimal solution of the objective function in (4.1).

4.2.1.2 Isoperimetric Constraints

In the calculus of variations, isoperimetric problems refer to the optimisation of a functional under the constraint of an integral (Wang, 2013). The general equation of an isoperimetric constraint for an optimisation problem can be written as (Pierre, 1969):

$$P_1 = \int_{t_a}^{t_b} f_1\left(y, \dot{y}, t\right) dt \tag{4.13}$$

where P_1 is a constant, $y(t)$ satisfies the boundary conditions $y(t_a) = y_a$ and $y(t_b) = y_b$ and $f_1(y,\dot{y},t)$ is a real valued function. Isoperimetric constraints can be used in conjunction with equality constraints and Lagrange multipliers to solve optimisation problems.

4.2.2 Genetic Algorithm

The genetic algorithm (GA) was developed by John Holland and his collaborators in 1975 (Holland, 1975), and it is a model and concept of biological evolution based on Charles Darwin's theory of natural selection. The genetic algorithm was first used by Holland as a problem-solving strategy in terms of crossover and recombination, mutation and selection in the study of adaptive and artificial systems. GA has been subsequently modified and developed to solve a wide range of optimisation problems, for example, from graph colouring to pattern recognition, from discrete systems to continuous systems, and from financial markets to multi-objective engineering optimisation. In practical applications, GA has been used to solve the optimisation problems in the areas set out by the examples in Table 4.1.

Table 4.1: The optimisation problems solved by GA

Problems solved by GA	References
Digital signal processing	(Man et al., 1997, Castillo et al., 2001)
Image processing and computer vision	(Minami et al., 2001, Bosco, 2001, Hussein et al., 2001, Mitsukura et al., 2001)
Control systems	(Man et al., 1997, Bedwani and Ismail, 2001, Visioli, 2001, Melin and Castillo, 2001)
Communication and telecommunication	(Bajwa et al., 2001, Weile and Michielssen, 2001, Arabas and Kozdrowski, 2001)
Electronic applications	(Grimbleby, 2000, Manganaro, 2000, Goh and Li, 2001)
Electrical power systems	(Wong et al., 2000, Poirier et al., 2001, Yong-Hua and Irving, 2001, Kezunovic and Liao, 2001)
Computer and internet systems	(Nick and Themis, 2001, Min-Huang et al., 2001, Kim and Byoung-Tak, 2001)
Medical applications	(Meesad and Yen, 2001, Moller and Zeipelt, 2001, Kin et al., 2001)
Finance applications	(Lam, 2001)
Transport systems	(Srinivasan et al., 2001)
Electrified railway systems	(Adamuthe et al., 2012, Chen et al., 2009c, Xiangzheng et al., 2007, Wei et al., 2009, Bocharnikov et al., 2010, Arenas et al., 2013, Ratniyomchai et al., 2015)

GA is likely to be the most popular evolution algorithm in terms of the diversity of its applications. Moreover, the operations of GA are population-based, and several modern evolutionary algorithms are directly based on GA or have some strong similarities to it, for example, fuzzy-logic systems (Cordon et al., 2001), wavelet systems (Jones et al., 2001) and neural-network systems (Yamazaki et al., 1998), which are used to solve complex optimisation problems involving nonlinear equations (Srikaew, 2009).

The advantages of GA in comparison with traditional optimisation algorithms are its ability to deal with complex problems and parallelism. Firstly, problems with an objective (fitness) function which is stationary or non-stationary, linear or nonlinear, continuous or discontinuous, or with random noise can be solved and satisfied by GA. Secondly, the implementation of parallelism to the algorithm is based on the feature of independent agents of multiple offspring in a population that can explore the search space in several directions simultaneously. This means that different parameters or groups of encoded strings are manipulated at the same time.

However, GA has some minor drawbacks which may include the formation of the fitness function, the use of population size, the rate of mutation and crossover and the selection criteria for a new population, which must be carefully carried out. Unsuitable choices for these parameters will lead to difficulties in solution convergence or meaningless solutions.

The essence of GA is related to chromosomes presented by the encoding of an optimisation function as an array of bit or character strings, the manipulation of the strings by genetic operators and the selection based on their fitness, with the aim of finding the solution to the relevant problem.

The procedures of GA are presented in the following pseudo code (Yang, 2010):

---

*Objective function f (**x**), **x** = $(x_1, \ldots, \underline{x_n})^T$*
Encode the solution into chromosomes (binary strings)
*Define fitness F (eg, F α f (**x**) for maximisation of minimisation)*
Generate the initial population
Initial probabilities of crossover (p_c) and mutation (p_m)
    ***while** (t < Max number of generations)*
        Generate new solution by crossover and mutation
        if** p_c > rand, Crossover; **end if
        if** p_m > rand, Mutate; **end if
        Accept the new solution if its fitness increases
        Select the current best for the next generation (elitism)
    end while
Decode the results and visualisation

The pseudo code above can be generally explained as follows:

1) Encoding of the objective or optimisation functions;
2) Defining a fitness function or selection criteria;
3) Creating a population of individuals;
4) Evaluation cycles or iterations, evaluating the fitness of all the individuals in the population, creating a new population by performing crossover, mutation and

fitness proportionate reproduction, and replacing the old population using the new population;

5) Decoding the results to obtain solutions to the problems.

In general, the encoding and decoding of the objective function are in the form of binary arrays or strings. The crossover, mutation and selection from the population are the genetic operators.

4.2.3 Particle Swarm Optimisation

Particle swarm optimisation, or PSO, is a stochastic population-based metaheuristic method proposed by Kennedy and Eberhart for continuous optimisation problems. It is inspired by swarm intelligence, which is the optimisation of complex models of attitudes, behaviours and cognitions enabled by the interaction among particles (Kennedy and Eberhart, 1995, Kennedy and Eberhart, 2001). The PSO algorithm mimics the social behaviour of natural organisms such birds and fish looking for food. The coordinated motions of these animals, where the members move together, suddenly split out of the group and then re-join, suggest that information can be shared between individual members of the group without a central control. The PSO algorithm was generally used to solve optimisation problems in the areas set out by the examples in Table 4.2

Table 4.2: The optimisation problems solved by PSO

Problems solved by PSO	References
Electric power systems	(Jordehi et al., 2013, Yu and Peng, 2010, Valle et al., 2008, Miranda and Fonseca, 2002, Heo et al., 2011)
Power electronics	(Kouzou et al., 2010, Zhan and Zhang, 2011, Yang et al., 2009, Shindo and Jin'no, 2012, Ray et al., 2009)
Machines	(Yassin et al., 2010, Huynh and Dunnigan, 2010b, Wu et al., 2014, Huynh and Dunnigan, 2010a, Hutchison et al., 2010)
Robotic	(Daş et al., 2013, Vatankhah et al., 2009, Jeong et al., 2011a, Walha et al., 2013)
Sensor modelling	(Li et al., 2009, Dang et al., 2010)
Telecommunications	(Song et al., 2010, Bera et al., 2014, Otevrel and Oliva, 2007, Ho et al., 2012)
Renewable energy	(Liu et al., 2015, Ishaque et al., 2011, Yuan et al., 2015, Ishaque et al., 2011, Hou et al., 2015, Zhu et al., 2012)
Power generations	(Chen et al., 2009b)
Electrified railway systems	(Liu et al., 2014, Zhao et al., 2013, Selamat and Bilong, 2013, Sun et al., 2012, Wang et al., 2009, Liu and Shi, 2014, Li et al., 2011)

The PSO algorithm has some similarities to GA, but it is simpler as it has no mutation or crossover operators. On the other hand, the PSO algorithm implements real random numbers and global communication among the swarm particles instead of encoding and decoding the parameters into binary strings, as is performed by GA. The objective function of the problem is searched for in the search space by adapting the trajectories of individual agents called particles as the piece-wise paths formed by position vectors in a quasi-stochastic manner.

The movement of each swarm particle is based on two major components, a stochastic component and a deterministic component. In addition, each swarm particle is attracted to the current global best g^* and its own best location x_i^* with a tendency for random movement. When the best location has been found by a particle, the new best location is updated for particle i. Moreover, the current best for all n particles at any time t during the iteration is also found. The main aim is to find the global best among the current best solutions until the maximum number of iterations is reached or the objective function no longer improves. The movement of a particle can be schematically presented in Figure

4.1, where the current best for particle i is $\boldsymbol{x}_i^*$, and the current global best is $\boldsymbol{g}^* \approx \min\{f(\boldsymbol{x}_i)\}$ for $(i = 1, 2, \ldots, n)$.

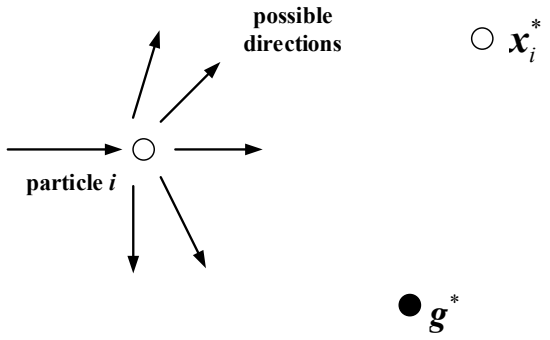

Figure 4.1: Schematic of the motion of a particle in PSO (Yang, 2010)

The procedures and essential steps of the PSO algorithm are summarised as the following pseudo code (Yang, 2010):

Objective function $f(\boldsymbol{x})$, $\boldsymbol{x} = (x_1, \ldots, x_n)^T$
Initialise locations x_i and velocity v_i of n particles
Find $\boldsymbol{g}^*$ from $\min\{f(\boldsymbol{x}_1), \ldots, f(\boldsymbol{x}_n)\}$ (at $t = 0$)
***while** (criterion)*
    $t = t + 1$ (pseudo time or iteration counter)
    ***for loop** over all n particles and all d dimensions*
    Generate new velocity $\boldsymbol{v}_i^{t+1}$ using equation (4.14)
    Calculate new locations $\boldsymbol{x}_i^{t+1} = \boldsymbol{x}_i^t + \boldsymbol{v}_i^{t+1}$
    Evaluate objective functions at new locations $\boldsymbol{x}_i^{t+1}$
    Find the current best for each particle $\boldsymbol{x}_i^*$
    end for
    Find the current global best g^*
end while
Output the final results x_i^* and g^*

---

where x_i and v_i are the position vector and velocity vector of the particle i. The updated velocity vector is calculated as follows:

$$\boldsymbol{v}_i^{t+1} = \boldsymbol{v}_i^t + \alpha\boldsymbol{\varepsilon}_1 \bullet \left(\boldsymbol{g}^* - \boldsymbol{x}_i^t\right) + \beta\boldsymbol{\varepsilon}_2 \bullet \left(\boldsymbol{x}_i^* - \boldsymbol{x}_i^t\right) \tag{4.14}$$

where $\boldsymbol{\varepsilon}_1$ and $\boldsymbol{\varepsilon}_2$ are two random vectors in between 0 and 1. The parameters α and β are the learning parameters or acceleration constants which are typically taken as $\alpha \approx \beta \approx 2$. The initial locations of all particles are uniformly distributed, therefore they can sample many more regions in the search space. The initial velocity of a particle can start at zero and it can be varied up to the maximum velocity. Then the new position of a particle can be updated by:

$$\boldsymbol{x}_i^{t+1} = \boldsymbol{x}_i^t + \boldsymbol{v}_i^{t+1} \tag{4.15}$$

4.2.4 Optimisation Method of Stationary EDLCs System

The design of stationary EDLCs is based on minimising the total energy consumption of substations in a cycle of the train journey with the duration T. One cycle, or a round-trip, of each section is completed when the train travels down from the first substation on the left and stops at the second substation on the right and then travels back to the first substation on the left again. Therefore, the objective function has the following expression (Iannuzzi et al., 2012b, Ratniyomchai et al., 2014a, Ratniyomchai et al., 2015):

$$\varphi = \int_0^T f\left(i_{Edlc}\right)dt = \int_0^T \left[\omega_1\left(v_{train} - E_{ss}\right)^2 + \omega_2 i_{L1}^2 + \omega_3 i_{L2}^2 + \omega_4 i_{Edlc}^2\right]\ dt \tag{4.16}$$

where v_{train} is the train voltage, E_{ss} is the DC substation voltage, i_{L1} and i_{L2} are the branch currents, i_{Edlc} is the storage current and ω_1, ω_2, ω_3 and ω_4 are the fitting weight coefficients. The result of the optimisation is dependent on these coefficients. If one term is more important than the others, the corresponding coefficient will have to be bigger and the optimal solution will be closer to the situation where that selected term has the absolute minimum value. If the coefficients are the same, the optimal solution will

minimise all of the terms, but none of them will be very close to the absolute minimum value. Careful attention must, therefore, be devoted to the choice of the coefficient. A legitimate question is to ask what particular combination of weight coefficients should be used to obtain the optimum possible capacitance of the storage devices. This question is addressed in sections 4.2.2 and 4.2.3 using the GA and PSO algorithms.

'The cost function in (4.16) takes into account the cost of energy loss on the line and the cost of the storage. The cost of energy loss on the line has two contributions: energy loss caused by a low train voltage, because the train requires higher current from the substations for the same amount of power; energy losses caused by the substations currents. Both losses can be reduced by the storage current. However, a larger storage current increases the cost of the storage, which counterbalance the cost function.

Using the model derived in Chapter 3, the four terms of the summation in (4.16) can be manipulated to be the only function of the current i_{Edlc}:

- $(v_{train} - E_{ss})^2$ obtained modifying (3.28):

$$\left(v_{train} - E_{ss}\right)^2 = \left(C_9 + C_{10} i_{Edlc} - E_{ss}\right)^2 = \left(C_9 - E_{ss} + C_{10} i_{Edlc}\right)^2 = \left(C_{19} + C_{10} i_{Edlc}\right)^2$$

$$\left(v_{train} - E_{ss}\right)^2 = C_{19}^2 + 2C_{19}C_{10} i_{Edlc} + C_{10}^2 i_{Edlc}^2 \qquad (4.17a)$$

  where: $C_{19} = C_9 - E_{ss}$

- i^2_{L1} obtained modifying (3.31):

$$i_{L1}^2 = \left(C_{15} + C_{16} i_{Edlc}\right)^2 = C_{15}^2 + 2C_{15}C_{16} i_{Edlc} + C_{16}^2 i_{Edlc}^2 \qquad (4.17b)$$

- i^2_{L2} obtained modifying (3.32):

$$i_{L2}^2 = \left(C_{17} + C_{18} i_{Edlc}\right)^2 = C_{17}^2 + 2C_{17}C_{18} i_{Edlc} + C_{18}^2 i_{Edlc}^2 \tag{4.17c}$$

Substituting (4.17a), (4.17b) and (4.17c) in (4.16), the objective function $f(i_{Edlc})$ is rewritten as follows:

$$\begin{aligned} f\left(i_{Edlc}\right) = \omega_1\left(C_{19}^2 + 2C_{19}C_{10} i_{Edlc} + C_{10}^2 i_{Edlc}^2\right) + \omega_2\left(C_{15}^2 + 2C_{15}C_{16} i_{Edlc} + C_{16}^2 i_{Edlc}^2\right) \\ + \omega_3\left(C_{17}^2 + 2C_{17}C_{18} i_{Edlc} + C_{18}^2 i_{Edlc}^2\right) + \omega_4 i_{Edlc}^2 \end{aligned} \tag{4.18}$$

In order to obtain a realistic result, the state of charge of the storage at the end of a cycle needs to return to the initial value, for example 65% SOC. This constraint needs to ensure that the state of charge of the EDLCs is enough to recharge or discharge energy for the next cycle of the train travelling. This can be taken into account in the optimisation problem by adding an isoperimetric constraint that is equal to zero of the net energy of the stationary EDLC across the period *T*. The isoperimetric constraint based on (4.13) is written as:

$$\int_0^T f_1\left(i_{Edlc}\right) dt = \int_0^T v_{Edlc} i_{Edlc} dt = 0 \tag{4.19}$$

where the function $f_1(i_{Edlc})$ is determined from (3.29):

$$f_1\left(i_{Edlc}\right) = C_{11} i_{Edlc} + C_{12} i_{Edlc}^2 \tag{4.20}$$

The inclusion of the isoperimetric constraint requires a modification of the objective function using the augmented functional and the Lagrange multiplier *h* based on (4.10):

$$f_a\left(i_{Edlc}\right) = f\left(i_{Edlc}\right) + h f_1\left(i_{Edlc}\right) \tag{4.21}$$

Substituting (4.18) and (4.20) in (4.21), $f_a(i_{Edlc})$ is rewritten as:

$$\begin{aligned} f_a(i_{Edlc}) = {} & \omega_1\left(C_{19}^2 + 2C_{19}C_{10}i_{Edlc} + C_{10}^2 i_{Edlc}^2\right) + \omega_2\left(C_{15}^2 + 2C_{15}C_{16}i_{Edlc} + C_{16}^2 i_{Edlc}^2\right) \\ & + \omega_3\left(C_{17}^2 + 2C_{17}C_{18}i_{Edlc} + C_{18}^2 i_{Edlc}^2\right) + \omega_4 i_{Edlc}^2 + h\left(C_{11}i_{Edlc} + C_{12}i_{Edlc}^2\right) \end{aligned} \tag{4.22}$$

Using the classic theory of calculus of variations, the current i_{Edlc} is determined by equalling to zero the derivative of the augmented functional $f_a(i_{Edlc})$ with respect to i_{Edlc} based on (4.11) and (4.12):

$$\frac{\partial f_a(i_{Edlc})}{\partial i_{Edlc}} = 0$$

and using (4.22):

$$\begin{aligned} & \omega_1\left(2C_{19}C_{10} + 2C_{10}^2 i_{Edlc}\right) + \omega_2\left(2C_{15}C_{16} + 2C_{16}^2 i_{Edlc}\right) + \omega_3\left(2C_{17}C_{18} + 2C_{18}^2 i_{Edlc}\right) \\ & + 2\omega_4 i_{Edlc} + C_{11}h + 2C_{12}h i_{Edlc} = 0 \end{aligned}$$

Manipulating the previous equation, we have:

$$i_{Edlc} = \frac{-C_{21} - C_{11}h}{C_{20} + 2C_{12}h} \tag{4.23}$$

where: $C_{20} = 2\omega_1 C_{10}^2 + 2\omega_2 C_{16}^2 + 2\omega_3 C_{18}^2 + 2\omega_4$, $C_{21} = 2\omega_1 C_{19}C_{10} + 2\omega_2 C_{15}C_{16} + 2\omega_3 C_{17}C_{18}$

The Lagrange multiplier h can be found by satisfying the isoperimetric constraint (4.19). Substituting the current i_{Edlc} from (4.23) into (4.20), we have:

$$f_1(i_{Edlc}) = \frac{C_{22}h^2 + C_{23}h + C_{24}}{C_{25}h^2 + C_{26}h + C_{27}} \tag{4.24}$$

where: $C_{22} = -C_{12}C_{11}^2$, $C_{23} = -C_{20}C_{11}^2$, $C_{24} = C_{12}C_{21}^2 - C_{11}C_{21}C_{20}$,

$$C_{25} = 4C_{12}^2, \qquad C_{26} = 4C_{20}C_{12}, \qquad C_{27} = C_{20}^2$$

And, finally, the isoperimetric constraint is:

$$\int_0^T f_1(i_{Edlc})dt = \int_0^T \frac{C_{22}h^2 + C_{23}h + C_{24}}{C_{25}h^2 + C_{26}h + C_{27}} dt = 0 \tag{4.25}$$

In the case where the train and the storage are at the same position $x_{train} = x_{Edlc}$, and the branch currents, the train and storage voltages are obtained in (3.34)-(3.36). The objective function $f(i_{Edlc})$ is rewritten as follows:

$$f(i_{Edlc}) = \left(\omega_1 D_3^2 + \omega_2 D_1^2 + \omega_3 D_2^2\right)\left(i_{train}^2 - 2i_{train}i_{Edlc} + i_{Edlc}^2\right) + \omega_4 i_{Edlc}^2 \tag{4.26}$$

The function $f_1(i_{Edlc})$ is determined from (3.36):

$$f_1(i_{Edlc}) = D_4 i_{Edlc} + D_3 i_{Edlc}^2 \tag{4.27}$$

where: $D_4 = E_{ss} - D_3 i_{train}$

The augmented functional $f_a(i_{Edlc})$ is rewritten as:

$$f_a(i_{Edlc}) = \left(\omega_1 D_3^2 + \omega_2 D_1^2 + \omega_3 D_2^2\right)\left(i_{train}^2 - 2i_{train}i_{Edlc} + i_{Edlc}^2\right) + \omega_4 i_{Edlc}^2 + h\left(D_4 i_{Edlc} + D_3 i_{Edlc}^2\right) \tag{4.28}$$

Using the classic theory of calculus of variations, the current i_{Edlc} is determined by equalling to zero the derivative of the augmented functional $f_a(i_{Edlc})$ with respect to i_{Edlc}:

$$\frac{\partial f_a(i_{Edlc})}{\partial i_{Edlc}} = 0$$

and using (4.28):

$$i_{Edlc} = \frac{D_6 - D_4 h}{D_5 + 2D_3 h} \tag{4.29}$$

where: $D_5 = 2\left(\omega_1 D_3^2 + \omega_2 D_1^2 + \omega_3 D_2^2 + \omega_4\right)$, $D_6 = D_5 i_{train}$

The Lagrange multiplier *h* can be found by satisfying the isoperimetric constraint (4.19). Substituting the current i_{Edlc} from (4.29) into (4.27), we have:

$$f_1\left(i_{Edlc}\right) = \frac{D_7 h^2 + D_8 h + D_9}{D_{10} h^2 + D_{11} h + D_{12}} \tag{4.30}$$

where: $D_7 = -D_3 D_6^2$, $D_8 = -D_4 D_6^2$, $D_9 = D_4 D_5 D_6$, $D_{10} = 4D_3^2$, $D_{11} = 4D_3 D_4$, $D_{12} = D_4^2$

And, finally, the isoperimetric constraint is:

$$\int_0^T f_1\left(i_{Edlc}\right) dt = \int_0^T \frac{D_7 h^2 + D_8 h + D_9}{D_{10} h^2 + D_{11} h + D_{12}} dt = 0 \tag{4.31}$$

Equations (4.25) and (4.31) can be solved for Lagrange multiplier *h*, which gives the optimal solution. Since the quantities C_i (i = 1, 2,…, 27) and D_i (i = 1, 2,…, 12) are time-dependent, the isoperimetric constraints in (4.25) and (4.31) are non-linear equations that can be solved for *h* using the Newton-Raphson method (Grainger, 1994). Therefore, the updated Lagrange multiplier is written as follows:

$$h_i^{(k+1)} = h_i^{(k)} - \frac{f_2\left(i_{Edlc}\right)}{f_2'\left(i_{Edlc}\right)} \tag{4.32}$$

where: $f_2\left(i_{Edlc}\right) = \int_0^T \frac{C_{22} h_i^{2(k)} + C_{23} h_i^{(k)} + C_{24}}{C_{25} h_i^{2(k)} + C_{26} h_i^{(k)} + C_{27}} dt$, for $x_{train} \neq x_{Edlc}$

$$f_2'(i_{Edlc}) = \frac{C_{22}h_i^{2(k)} + C_{23}h_i^{(k)} + C_{24}}{C_{25}h_i^{2(k)} + C_{26}h_i^{(k)} + C_{27}}, \text{ for } x_{train} \neq x_{Edlc}$$

$$f_2(i_{Edlc}) = \int_0^T \frac{D_7h_i^{2(k)} + D_8h_i^{(k)} + D_9}{D_{10}h_i^{2(k)} + D_{11}h_i^{(k)} + D_{12}} dt, \text{ for } x_{train} = x_{Edlc}$$

$$f_2'(i_{Edlc}) = \frac{D_7h_i^{2(k)} + D_8h_i^{(k)} + D_9}{D_{10}h_i^{2(k)} + D_{11}h_i^{(k)} + D_{12}}, \text{ for } x_{train} = x_{Edlc}$$

$h_i^{(k+1)}$, $h_i^{(k)}$ are the Lagrange multiplier at position i of the train and at the iteration k+1 and k, respectively.

The optimal storage current $i_{Edlc,opt1}$ of each position of the train is obtained by substituting the exact Lagrange multiplier $h_{i,opt1}$ in (4.23) and (4.29). Then the optimal train voltage $v_{train,opt1}$ in (3.28) and (3.36), the optimal storage voltage $v_{Edlc,opt1}$ in (3.29) and (3.36), the optimal substation currents $i_{L1,opt1}$ and $i_{L2,opt1}$ in (3.31), (3.32) and (3.34), (3.35) are obtained by the solution of the optimal storage current $i_{Edlc,opt1}$.

For every position of the train, the optimal train voltage $v_{train,opt1}$ and the optimal stationary EDLC voltage $v_{Edlc,opt1}$ are compared with the substation voltage E_{ss} and the relevant circuit is used in cases of $v_{train,opt1} \geq E_{ss}$ and $v_{Edlc,opt1} \geq E_{ss}$:

- $v_{train,opt1} < E_{ss}$ and $v_{Edlc,opt1} \geq E_{ss}$

  If the train is before the storage, the second substation is not active (see Figure 4.2) and the equations of the model are:

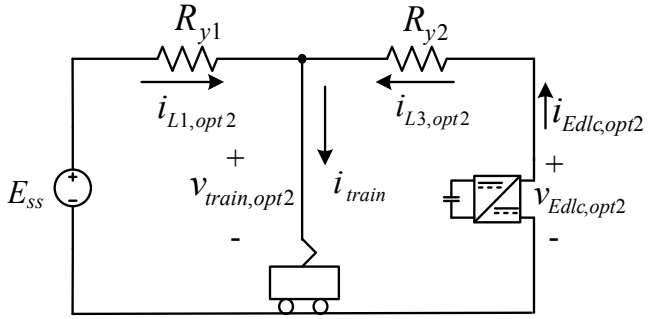

Figure 4.2: $x_{Edlc} > x_{train}$ with $v_{train,opt1} < E_{ss}$ and $v_{Edlc,opt1} \geq E_{ss}$ (modified from Figure 3.7)

$$\begin{aligned} i_{L3,opt2} &= i_{L3,opt1} \\ i_{L1,opt2} &= i_{L1,opt1} \\ i_{L2,opt2} &= 0 \\ i_{Edlc,opt2} &= i_{L3,opt2} \\ v_{train,opt2} &= v_{train,opt1} \\ v_{Edlc,opt2} &= v_{train,opt2} + R_{y2} i_{L3,opt2} \end{aligned} \tag{4.33}$$

If the train is after the storage, the first substation is not active (see Figure 4.3) and the equations of the model are:

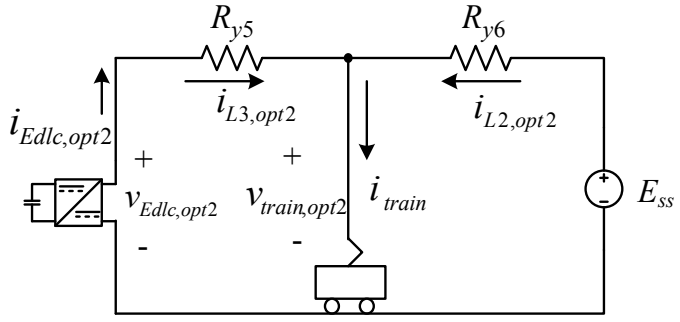

Figure 4.3: $x_{Edlc} < x_{train}$ with $v_{train,opt1} < E_{ss}$ and $v_{Edlc,opt1} \geq E_{ss}$ (modified from Figure 3.8)

$$
\begin{aligned}
i_{L3,opt2} &= i_{L3,opt1} \\
i_{L1,opt2} &= 0 \\
i_{L2,opt2} &= i_{L2,opt1} \\
i_{Edlc,opt2} &= i_{L3,opt2} \\
v_{train,opt2} &= v_{train,opt1} \\
v_{Edlc,opt2} &= v_{train,opt2} + R_{y5} i_{L3,opt2}
\end{aligned}
\tag{4.34}
$$

- $v_{train,opt1} \geq E_{ss}$ and $v_{Edlc,opt1} < E_{ss}$

If the train is before the storage, the first substation is not active (see Figure 4.4) and the equations of the model are:

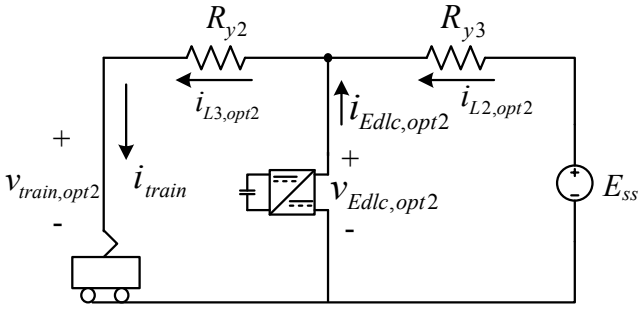

Figure 4.4: $x_{Edlc} > x_{train}$ with $v_{train,opt1} \geq E_{ss}$ and $v_{Edlc,opt1} < E_{ss}$ (modified from Figure 3.7)

$$
\begin{aligned}
i_{L3,opt2} &= i_{train} \\
i_{L1,opt2} &= 0 \\
v_{Edlc,opt2} &= v_{Edlc,opt1} \\
i_{L2,opt2} &= \left(E_{ss} - v_{Edlc,opt2}\right) / R_{y3} \\
i_{Edlc,opt2} &= i_{train} - i_{L2,opt2} \\
v_{train,opt2} &= v_{Edlc,opt2} - R_{y2} i_{L3,opt2}
\end{aligned}
\tag{4.35}
$$

If the train is after the storage, the second substation is not active (see Figure 4.5) and the equations of the model are:

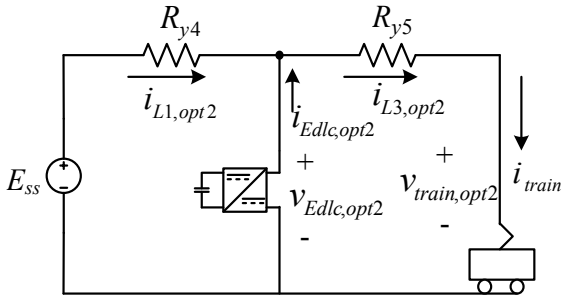

Figure 4.5: $x_{Edlc} < x_{train}$ with $v_{train,opt1} \geq E_{ss}$ and $v_{Edlc,opt1} < E_{ss}$ (modified from Figure 3.8)

$$
\begin{aligned}
&i_{L3,opt2} = i_{train} \\
&i_{L2,opt2} = 0 \\
&v_{Edlc,opt2} = v_{Edlc,opt1} \\
&i_{L1,opt2} = \left(E_{ss} - v_{Edlc,opt2}\right) / R_{y4} \\
&i_{Edlc,opt2} = i_{train} - i_{L1,opt2} \\
&v_{train,opt2} = v_{Edlc,opt2} - R_{y5} i_{L3,opt2}
\end{aligned}
\tag{4.36}
$$

- $v_{train,opt1} \geq E_{ss}$ and $v_{Edlc,opt1} \geq E_{ss}$

  In this case, the two substations are not active. If the train is before the storage, the circuit is shown in Figure 4.6 and the equations of the model are:

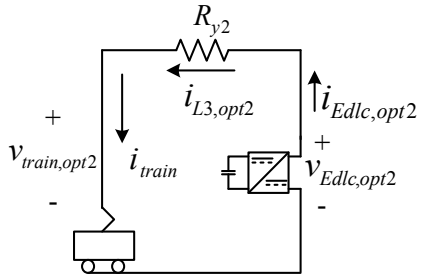

Figure 4.6: $x_{Edlc} > x_{train}$ with $v_{train,opt1} \geq E_{ss}$ and $v_{Edlc,opt1} \geq E_{ss}$ (modified from Figure 3.7)

$$
\begin{aligned}
&i_{L1,opt2} = i_{L2,opt2} = 0 \\
&i_{L3,opt2} = i_{Edlc,opt2} = i_{train} \\
&v_{Edlc,opt2} = v_{Edlc,opt1} \\
&v_{train,opt2} = v_{Edlc,opt2} - R_{y2} i_{L3,opt2}
\end{aligned}
\tag{4.37}
$$

If instead the train is after the storage, the circuit is shown in Figure 4.7 and the equations of the model are:

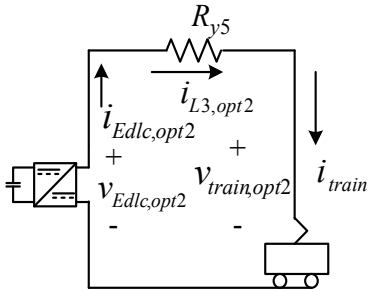

Figure 4.7: $x_{Edlc} < x_{train}$ with $v_{train,opt1} \geq E_{ss}$ and $v_{Edlc,opt1} \geq E_{ss}$ (modified from Figure 3.8)

$$
\begin{aligned}
&i_{L1,opt2} = i_{L2,opt2} = 0 \\
&i_{L3,opt2} = i_{Edlc,opt2} = i_{train} \\
&v_{Edlc,opt2} = v_{Edlc,opt1} \\
&v_{train,opt2} = v_{Edlc,opt2} - R_{y5} i_{L3,opt2}
\end{aligned}
\tag{4.38}
$$

If the train and the storage are at the same position, the circuit is shown in Figure 4.8 and the equations of the model are:

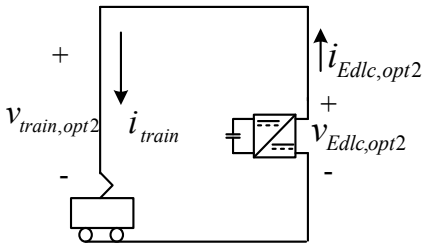

Figure 4.8: $x_{Edlc} = x_{train}$ with $(v_{train,opt1} = v_{Edlc,opt1}) \geq E_{ss}$ (modified from Figure 3.9)

$$\begin{aligned} i_{L1,opt2} &= i_{L2,opt2} = i_{L3,opt2} = 0 \\ i_{Edlc,opt2} &= i_{train} \\ v_{Edlc,opt2} &= v_{train,opt2} = v_{Edlc,opt1} \end{aligned} \tag{4.39}$$

From the results of the optimisation algorithm, the total energy consumption of the substations, the total losses of the conducting rails and the rails, the train energy and the stationary EDLC energy have been determined, depending on the mutual positions of a train and a stationary EDLC in the model of the electrification system with two substations:

- Energy consumption of two substations: En_{sub}

$$En_{sub} = \int_0^T E_{ss} i_{L1,opt2}(t)dt + \int_0^T E_{ss} i_{L2,opt2}(t)dt \tag{4.40}$$

- Energy loss from the conducting rails and rails: En_{line}

$$\begin{aligned} En_{line} = &\int_0^T i_{L1,opt2}^2(t)\left(R_{y1}A_s + R_{y4}B_s\right)dt + \int_0^T i_{L2,opt2}^2(t)\left(R_{y3}A_s + R_{y6}B_s\right)dt \\ &+ \int_0^T i_{L3,opt2}^2(t)\left(R_{y2}A_s + R_{y5}B_s\right)dt \end{aligned} \tag{4.41}$$

- Train energy: En_{train}

$$En_{train} = \int_0^T v_{train,opt2}(t) i_{train}(t)dt \tag{4.42}$$

- EDLC energy: En_{Edlc}

$$En_{Edlc} = \int_0^T v_{Edlc,opt2}(t) i_{Edlc,opt2}(t)dt \tag{4.43}$$

The results of the optimisation algorithm have been verified using the law of conservation of energy, which states that the total energy of the traction system is equal to zero:

$$En_{sub} + En_{Edlc} - En_{train} - En_{line} = 0 \tag{4.44}$$

The constraint in (4.44) expresses that the summation of energy supported by the EDLCs and substations is equal to the energy drawn by the train and line losses at every step of the train travelling. This constraint is used to verify the zero of the summation of the entire energy flow in the DC light railway systems with the additional energy support by EDLCs. At every step of the single train travelling, the current of EDLC i_{Edlc} is obtained and affected by the Lagrange multiplier h in (4.23) for $x_{Edlc} \neq x_{train}$ and (4.30) for $x_{Edlc} = x_{train}$ and then the train voltage v_{train} in (3.28), the EDLC voltage v_{Edlc} in (3.29) for $x_{Edlc} \neq x_{train}$ and both in (3.36) for $x_{Edlc} = x_{train}$ are obtained later. The energy drawn by substations, EDLCs, train and line losses are calculated by (4.40) – (4.43) and checked by the constraint in (4.44). If the constraint is unsatisfied, the Lagrange multiplier h is updated by (4.32) and calculated again until satisfied the constraint.

4.3 Optimisation Results of the Case Study

The procedure used to find the optimal design of stationary EDLCs and the piece-wise linear SOC control of EDLCs is shown in the flowchart in Figure 4.9. The procedure is divided into 22 steps and 2 main parts.

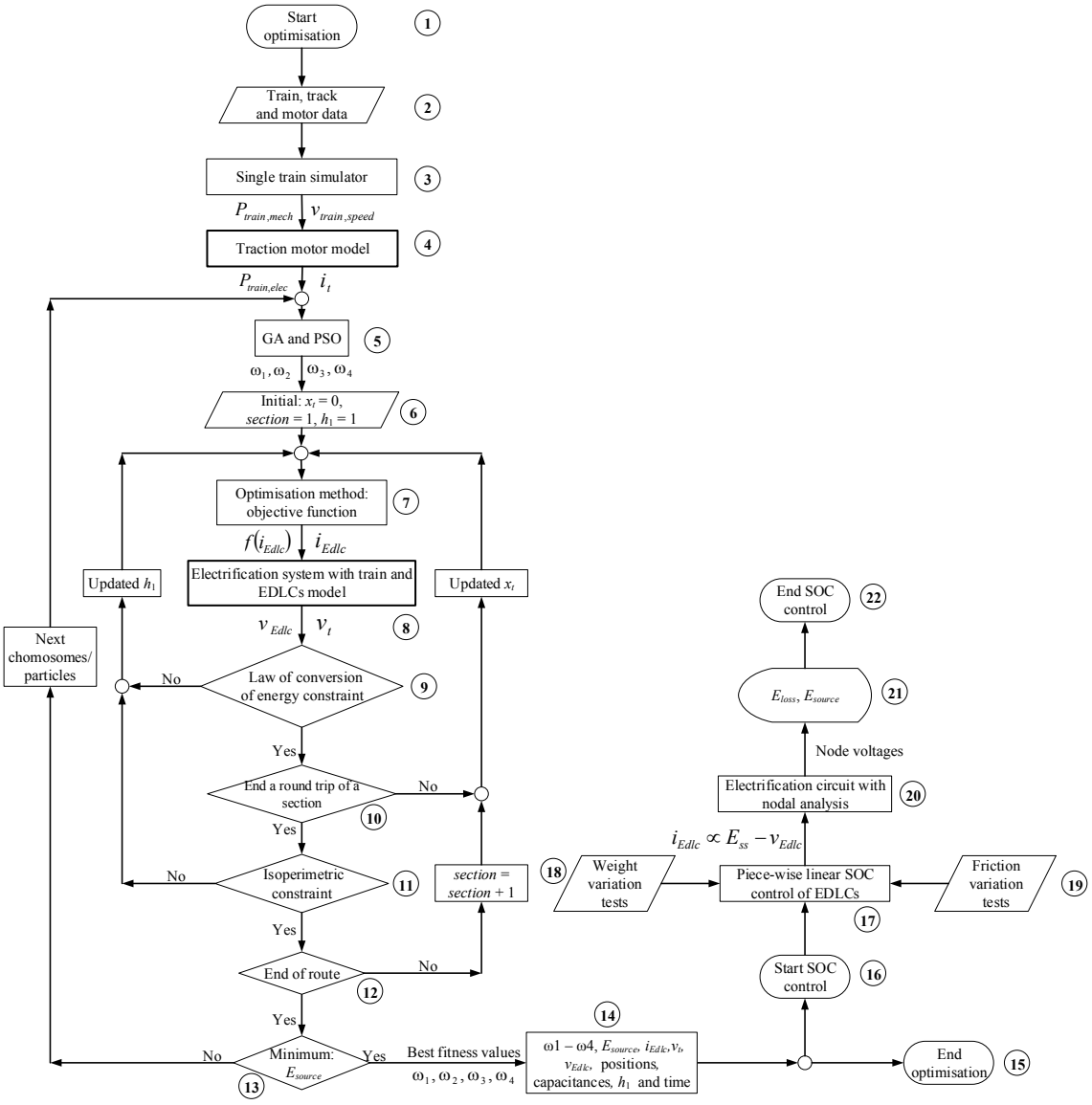

Figure 4.9: The procedure of the optimisation algorithm and the piece-wise linear SOC control of stationary EDLCs

The first part of this thesis is dedicated to the design of an optimisation algorithm to find the optimal capacitances and positions for EDLCs, which is presented in steps 1 to 15 below. Each step of the procedure can be explained as follows:

Step 1: Start the optimisation algorithm;

Step 2: The train, track and motor data presented in Table 4.3, Table 4.4 and Table 4.5 are provided to be input to the STS;

Step 3: The STS presented in section 3.2 simulates a single train running a round-trip along a real route of a DC light railway system. The arrays of the mechanical power of the train $P_{train,mech}$ and the speed of the train $v_{train,speed}$ are obtained by the STS and used as the input to the next step;

Step 4: The model of the substations and electrification system and the model of the traction motors developed in section 3.3 and section 3.4 are implemented to calculate the arrays of the current of the train i_t, and the electrical power of the train $P_{train,elec}$. i_t is calculated by equation (3.3), whereas $P_{train,elec}$ is calculated by equation (3.20);

Step 5: The GA optimisation technique described in section 4.2.2 or the PSO algorithm described in section 4.2.3 is chosen to find the optimal values of the weight coefficient ω_1-ω_4 used in step 7. The objective function of the GA and PSO algorithm is to minimise the total energy consumption of the DC light railway system when a train travels a round-trip. The initial values of ω_1-ω_4 are generated by random numbers in between 0 and 1. Examples of the MATLAB code for calling GA and PSO algorithms are shown as follows:

GA:

```
options = gaoptimset('PopulationSize', 25,'Generations', 25,'TolFun', 1e-1, 'CrossoverFraction', 0.8);
[x,fval,exitflag,output] = ga(@func_name, 4,[],[],[],[],[0 0 0 0],[1 1 1 1], [], options);
```

PSO:

```
opts = psooptimset(opts,'Generations', 25, 'TolFun', 1e-1, 'PopulationSize', 25,'Display','final');
[x,Fval] = pso(@func_name,4,[],[],[],[],[0 0 0 0],[1 1 1 1],[],opts);
```

Step 6: The initial values of some parameters are defined. The train position starts at 0 km, $x_t = 0$. The section of the route is started at 1 in a total of 4, *section* = 1. The Lagrange multiplier is started at 1, $h_1 = 1$;

Step 7: For each independent section of the route, the optimisation method based on the classical theory of calculus of variations described in section 4.2.1 is implemented in this step. The cost function of this optimisation method based on the problems in this thesis is referred to in equation (4.16), with the objective function of voltage regulation of the train, minimisation of the energy consumption and capacitance of the EDLCs in each section of the train travelling a round-trip. The optimal current of the EDLCs i_{Edlc} is obtained by equations (4.23) and (4.29);

Step 8: A model of the electrification system with EDLCs and rolling stock is developed and presented in section 3.5. The voltage of the EDLCs v_{Edlc} and a train v_t are calculated by equations (3.28), (3.29) and (3.36);

Step 9: For each step of the train motion, all parameters obtained from the optimisation method in step 7 have been verified by the law of conversion of energy constraint presented in equation (4.44). If the answer to the constraint is NO, the Lagrange multiplier

h_1 is updated by equation (4.32) and the process goes back to step 7, otherwise the procedures carry on to the next step;

Step 10: This step checks the distance of the train motion at the end of a round-trip of each section. If the answer to the condition is NO, the position of the train is updated depending on the discrete of the distance step in the STS and the process goes back to step 7, otherwise the procedures carry on to the next step;

Step 11: The isoperimetric constraint in equation (4.19) of the SOC of each EDLC is checked at the end a round-trip of each section. If the answer to the constraint is NO, the Lagrange multiplier h_1 is updated by equation (4.32) and the process goes back to step 7, otherwise the procedures carry on to the next step;

Step 12: This step checks the distance of the train motion at the end of a round-trip of the entire route (all sections of the route). If the answer to the condition is NO, the position of the train is updated depending on the discrete of the distance step in the STS and the section is updated by $section = section + 1$ and the process goes back to step 7, otherwise the procedures carry on to the next step;

Step 13: The objective function of the GA or PSO algorithm is checked in this step with the purpose of minimising the total energy consumption of the entire light railway system with a single train travelling a round-trip. A comparison is made between solutions obtained from each generation of the GA and PSO algorithm. If the answer to the constraint is NO, the next generation of parameters is updated by the GA and PSO algorithm and the process goes back to step 5, otherwise the procedures carry on to the next step;

Step 14: The results of the optimisation problem are obtained in this step, including the best fitness values of ω_1-ω_4, the total energy consumption E_{source}, the current and voltage of EDLCs i_{Edlc} and v_{Edlc}, the voltage of the train v_t, the optimal positions and capacitances of EDLCs, Lagrange multiplier h_1 and the time of the entire calculation. The capacitances are calculated by equation (3.44);

Step 15: The end of the optimisation method.

The second part of the thesis is the SOC control of EDLCs based on the piece-wise linear SOC control of stationary EDLCs developed and presented in Chapter 5. The procedures are continuously presented in steps 16 to 22 with the results obtained from the optimisation method. Each step of the procedure can be explained as follows:

Step 16: Start the SOC control;

Step 17: The piece-wise linear SOC control of EDLCs is developed and presented in section 5.2 with the relation between the current of the EDLCs i_{Edlc}, and the deviation voltage Δv of the EDLCs voltage v_{Edlc} and the DC electrification nominal voltage, as shown in Figure 5.1, is used to control the SOC of the EDLCs. The inputs of this control algorithm are obtained from the results of the optimal design of stationary EDLCs:

Step 18: The algorithm of piece-wise linear SOC control is verified by variation of the train loading test which is described in section 5.4 and Table 5.3. The total energy consumption and energy line loss of the light railway system with and without EDLCs are measured in this step;

Step 19: The algorithm of piece-wise linear SOC control is verified by variation of the train friction based on the Davis's equation, which is described in section 5.4 and **Error!**

Reference source not found.. The total energy consumption and energy line loss of the light railway system with and without EDLCs are measured in this step;

Step 20: The node voltages of the train, EDLCs and stations are calculated by nodal analysis of the light railway system explained in section 5.3. The SOC of EDLCs is based on the piece-wise linear SOC control described in section 5.2;

Step 21: The energy consumption of substations and energy line loss of the light railway system with the train travelling two round-trips with and without stationary EDLCs are calculated and compared in this step;

Step 22: The end of the SOC control of EDLCs.

4.3.1 Elaboration of the Initial Data

The principal data on the train, track and motor employed in the simulations in this thesis are presented in Table 4.3. The train has 4 cars with 8 traction motors of 200 kW (Siemens, 2012). A railway line has 5 electrical substations and 9 stations, 5 of which are in the same location as the substations, as shown in Figure 4.10.

Table 4.3: Train, track and motor parameters

Parameter	Unit	Quantity
Track		
Track length	km	22
Conductor and return rail resistance	mΩ/km	40
Substation 1-4 internal resistance	mΩ	12
Substation 5 internal resistance	mΩ	5
Rated voltage	V	750
Number of substations	-	5
Number of stops	-	9
Train		
Number of train	-	1
Train mass	ton	135.95
Maximum train speed	km/h	121
Diameter of wheel	m	0.85
Davis coefficients: $F = a + bv + cv^2$		
a	N	2,202.4
b	Nm/s	48.9
c	Nm^2/s^2	4.3
Motor		
Base speed of the motors	rpm	1490
Number of poles of the motors	-	4
Base frequency of the motors	Hz	50
Rated power of the motors	kW	200
Rated torque of the motors	N·m	1282
Number of motors	-	8

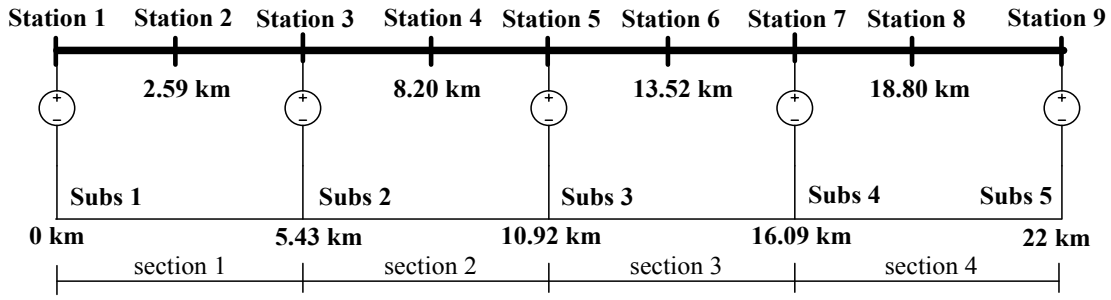

Figure 4.10: Single line diagram of the track with 5 substations and 9 stops

Table 4.4 shows the speed limit of the train on the line, whereas Table 4.5 shows the gradient of the track.

Table 4.4: Speed limits on the line

From	To	Speed (km/h)
0 km	0.3 km	48.28
0.3 km	0.9 km	64.37
0.9 km	21.1 km	120.70
21.1 km	21.6 km	80.47
21.6 km	22 km	32.19

Table 4.5: Gradient of the track

From	To	Slope (%) per km	Accumulated elevation (m)
0 km	0.2 km	0.67	0.13
0.2 km	0.4 km	0	0.13
0.4 km	0.5 km	1.11	0.24
0.5 km	1.1 km	7.50	4.75
1.1 km	1.6 km	1.67	5.57
1.6 km	2.0 km	-1.33	5.05
2.0 km	2.2 km	0.26	5.09
2.2 km	2.4 km	-0.76	4.95
2.4 km	3.0 km	0	4.95
3.0 km	3.5 km	5.32	7.57
3.5 km	4.4 km	-1.66	6.11
4.4 km	4.8 km	1.85	6.84
4.8 km	5.6 km	8	13.21
5.6 km	7.8 km	5.71	25.79
7.8 km	8.2 km	1.51	26.42
8.2 km	9.3 km	0	26.42
9.3 km	9.7 km	-2.27	25.53
9.7 km	11.1 km	5.30	32.94
11.1 km	11.5 km	0	32.94
11.5 km	11.7 km	0.54	33.04
11.7 km	12.9 km	-3.64	28.68
12.9 km	13.4 km	0	28.68
13.4 km	13.6 km	-2.00	28.29
13.6 km	14.1 km	-4.50	26.05
14.1 km	14.9 km	-8.89	18.97
14.9 km	16.3 km	-14.00	-0.61
16.3 km	16.9 km	-4.28	-3.23
16.9 km	17.5 km	-2.31	-4.62
17.5 km	18.5 km	-4.17	-8.78
18.5 km	19.5 km	-3.85	-12.65
19.5 km	19.7 km	0	-12.65
19.7 km	19.9 km	-1.00	-12.85
19.9 km	20.1 km	0	-12.85
20.1 km	20.3 km	2.00	-12.46
20.3 km	20.7 km	2.50	-11.46
20.7 km	22 km	8.12	-0.88

Figure 4.11 shows graphically the speed limit and the elevation of the track over the total distance of the line. At the beginning of the train motion, the track seems to be flat but actually it has a small change of gradient until 0.5 km, as shown in Table 4.5.

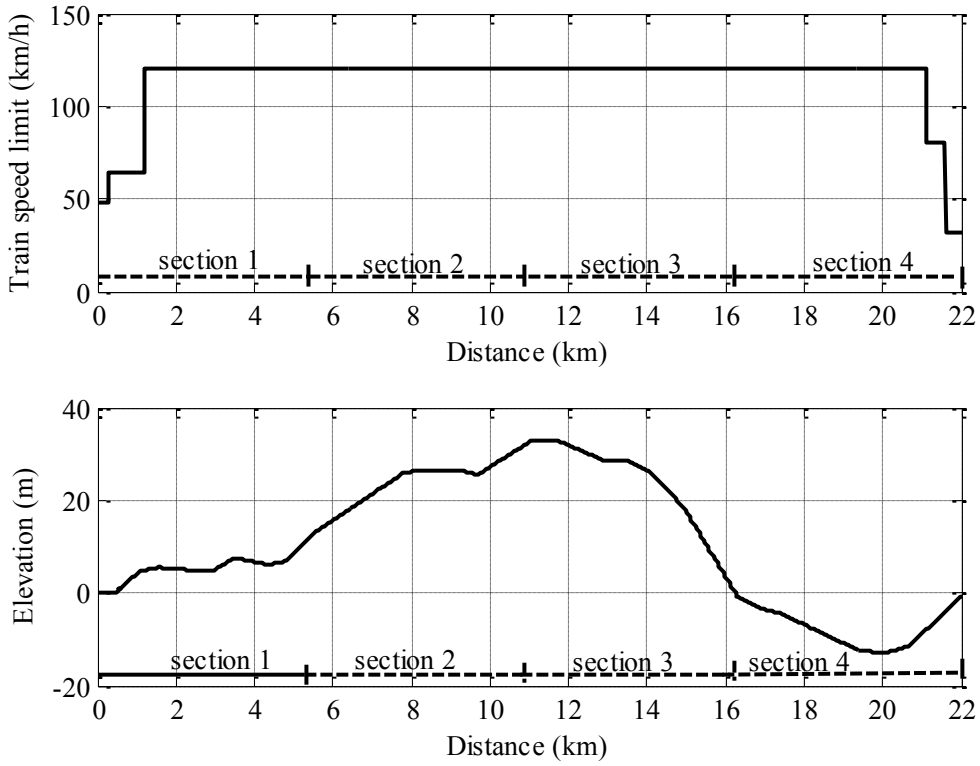

Figure 4.11: The limitation of the train speed and the elevation of the track

These data have been used in the STS and the mechanical power of the train as a function of the distance is shown in Figure 4.12. The mechanical traction and braking power of the train are represented by the solid and dash lines, respectively. The maximum mechanical power for traction and for braking are approximately the same and are equal to 1.6 MW. The diagram shows that a significant use of the field-weakening of the motor is required for this cycle.

Figure 4.13 shows the acceleration of the train with the distance. The maximum acceleration and deceleration of the train motoring and braking are approximately equal to 1.11 m/s^2 and 1.09 m/s^2, of which the average values are equal to 0.44 m/s^2 and 0.52 m/s^2, respectively.

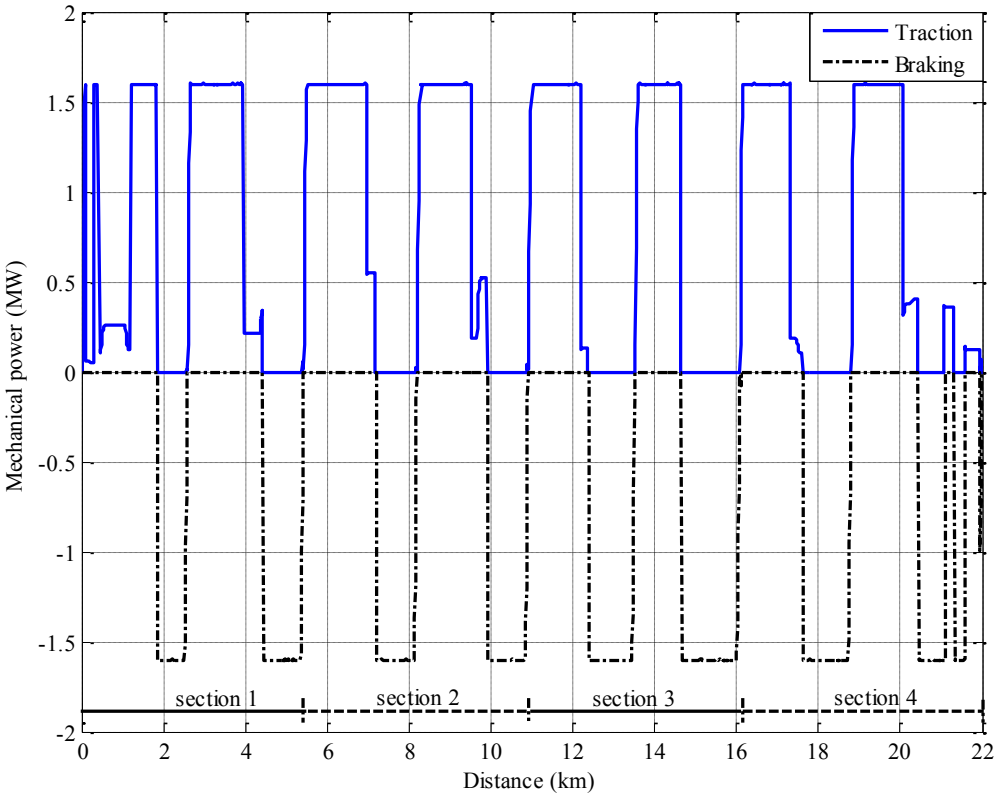

Figure 4.12: The mechanical power of the train as a function of the distance travelled

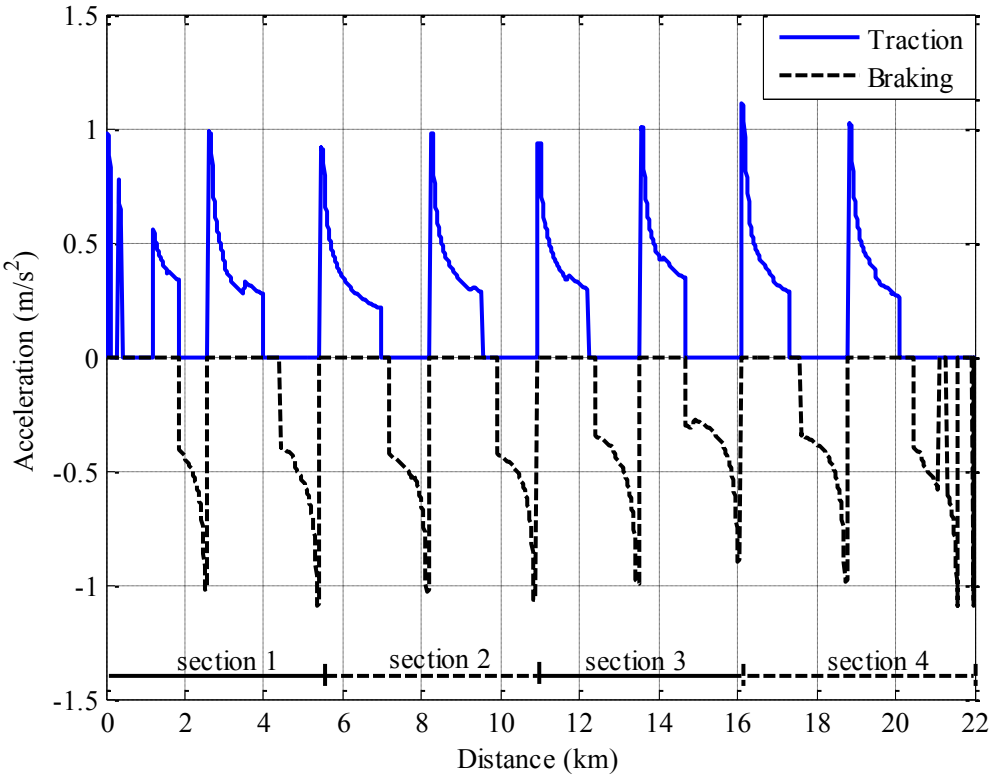

Figure 4.13: The acceleration of the train as a function of the distance travelled

Figure 4.14 shows the actual speed of the train with the track speed limit as a function of the distance. Due to the presence of the intermediate stops, the train travels at the maximum speed for only a short portion of the traction cycle. The speed of the train at the stations is not exactly zero, but it is approximately equal to 3.6 km/h, due to the characteristics of the STS. This is because the distance step of the STS is 10 m and the dwell time of the train at each station is 30 seconds, which means that the train is still running with a speed of 1 m/s along the 30 m track at each station. In fact, the distance step of the STS can be set to be every 0.1 m or smaller to ensure that the train stops or is running with very slow speed at each station, but this would make the calculation of the optimisation algorithms more time consuming. For simplicity, the speed of the train as shown in Figure 4.14 will be employed for the further simulation in this thesis.

Figure 4.15 shows the duration of the journey with the distance travelled by the train. The total time of a single-trip from one end to the other end is about 21.23 minutes when the dwell time of the train at each station is 30 seconds.

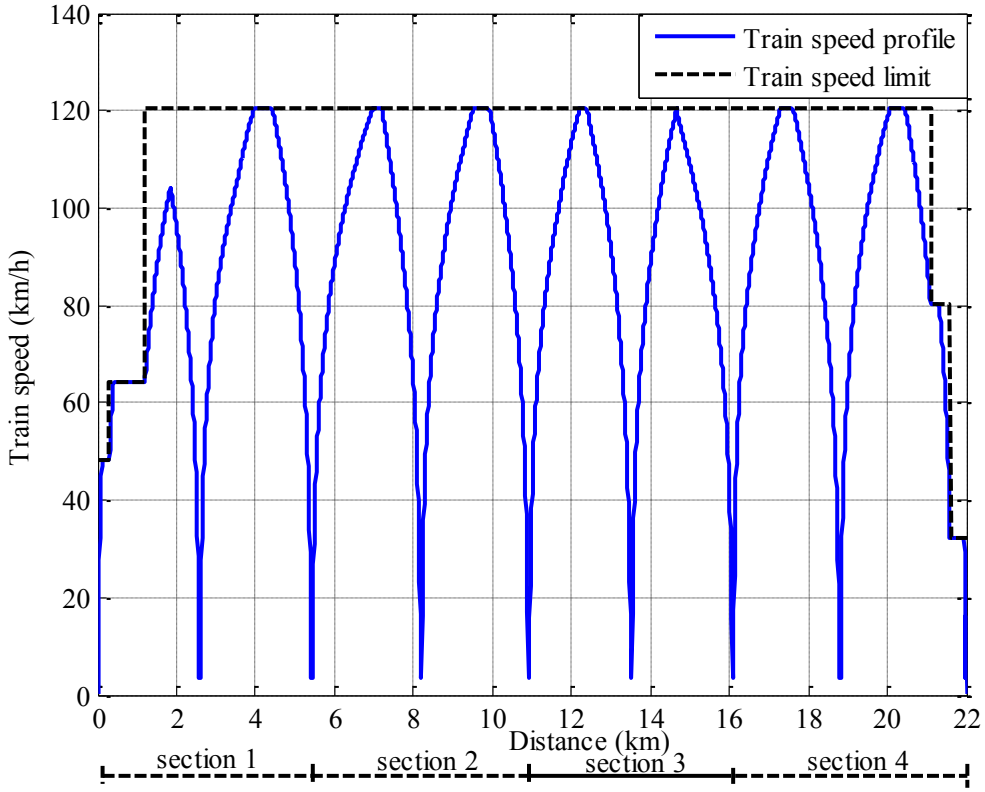

Figure 4.14: Train speed and track speed limit as a function of the distance travelled

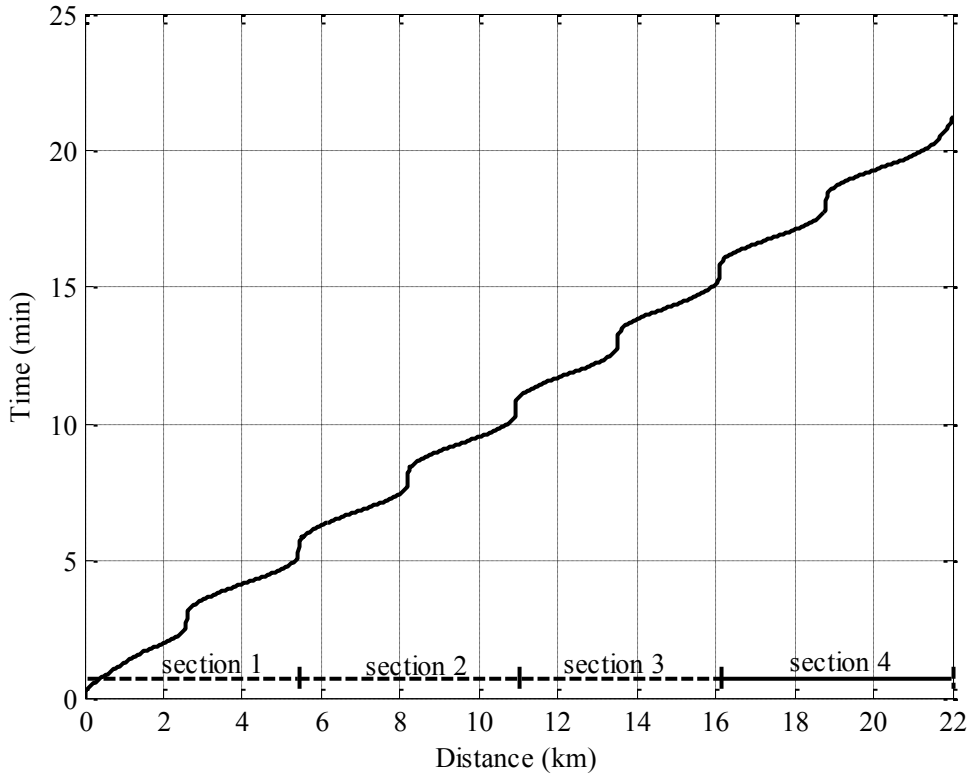

Figure 4.15: Duration of a single journey as a function of the distance travelled

4.3.2 Results from the Optimisation Method and Discussion

In order to apply the optimisation algorithm in (4.16), it is necessary to undertake a preliminary analysis of the system under study. In fact, the fitting weight coefficients ω_1 – ω_4 are unknown and have a strong influence on the final results. For each set of values of the coefficients the objective function has a relative minimum and it is interesting to find the set of coefficients for which the objective function has a global minimum. This optimal set of coefficients is searched for with GA and PSO, starting from a preliminary analysis of the system without EDLCs.

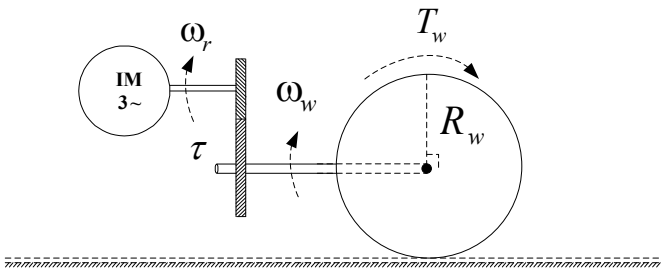

Figure 4.16: Model of the motor, gearbox and wheel

In order to obtain a diagram of the speed of the motors, it is necessary to consider the mechanical transmission system of the train, shown in Figure 4.16. Assuming a gearbox ratio of τ, the angular speed of motor ω_r is related to the angular speed of wheel ω_w by:

$$\tau = \frac{\omega_r}{\omega_w} \tag{4.45}$$

Assuming a base speed of the train equal to one third of the maximum speed, the base speed is approximately 40 km/h and, therefore, the angular base speed of the wheels $\omega_{w,base}$ is:

$$\omega_{w,base} = \frac{v_{base}}{R_w} = \frac{11.11}{0.425} = 26.14 \text{ rad/sec} \tag{4.46}$$

where, v_{base} is the base speed of the train in m/s and R_w is the radius of the wheel.

From the specifications of the traction motor in Table 4.3, the motor has a base speed of 1490 rpm with the operating frequency of 50 Hz, therefore, the base angular speed of the motor $\omega_{r,base}$ is calculated as follows:

$$\omega_{r,base} = \frac{2\pi n_r}{60} = \frac{2\pi}{60}\left(\frac{120f}{p}\right) = \frac{2\pi}{60}\left(\frac{120\times 50}{4}\right) = 157.08 \text{ rad/sec} \tag{4.47}$$

Substituting (4.47) and (4.48) in (4.46), therefore, the gearbox ratio τ is equal to 6. From the train speed diagram of Figure 4.14, the angular speed of the motors based on (4.46) is shown in Figure 4.17.

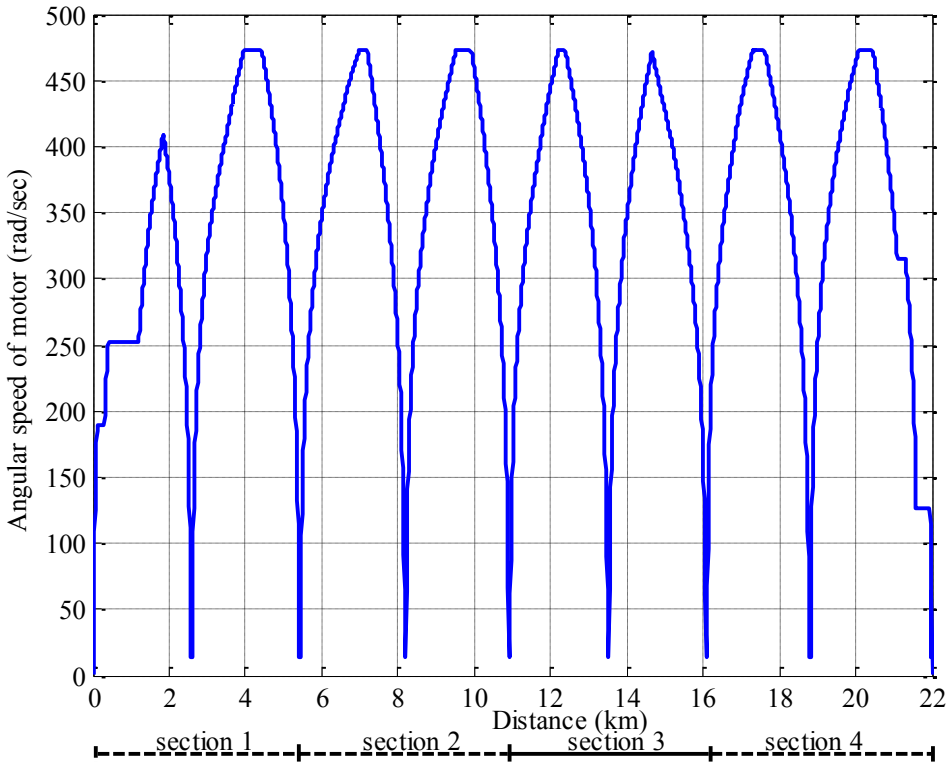

Figure 4.17: Angular speed of motors as a function of the distance travelled

As described in Chapter 3, diagrams of the total electric power P_t when the train is travelling forward and returning are shown in Figure 4.18 and Figure 4.19. The efficiencies of the gearboxes, traction motors and inverters are taken into account in these diagrams for trains both motoring and braking and, hence, the traction power for motoring is larger than the regenerative power for braking. Specifically, the traction power for motoring, represented by a solid-line, has a maximum value of 2.02 MW, whereas the regenerative power for braking, represented by a dash-line, has a maximum value of 1.16 MW.

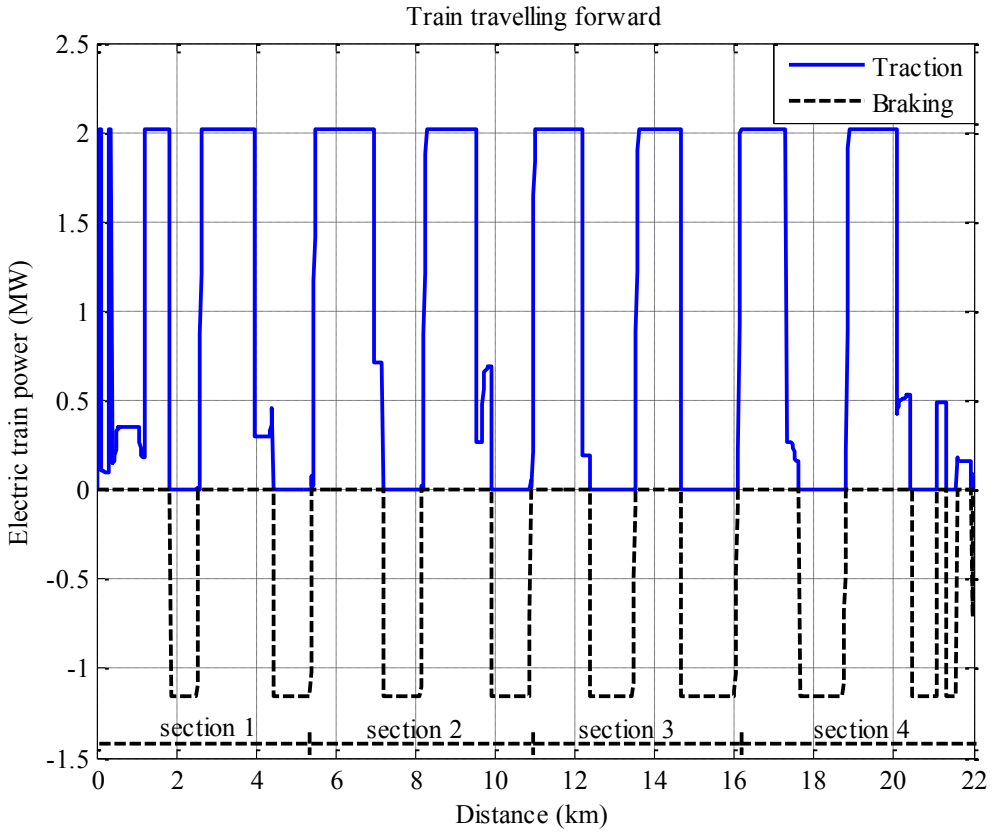

Figure 4.18: Electrical power of the train travelling forward along the track

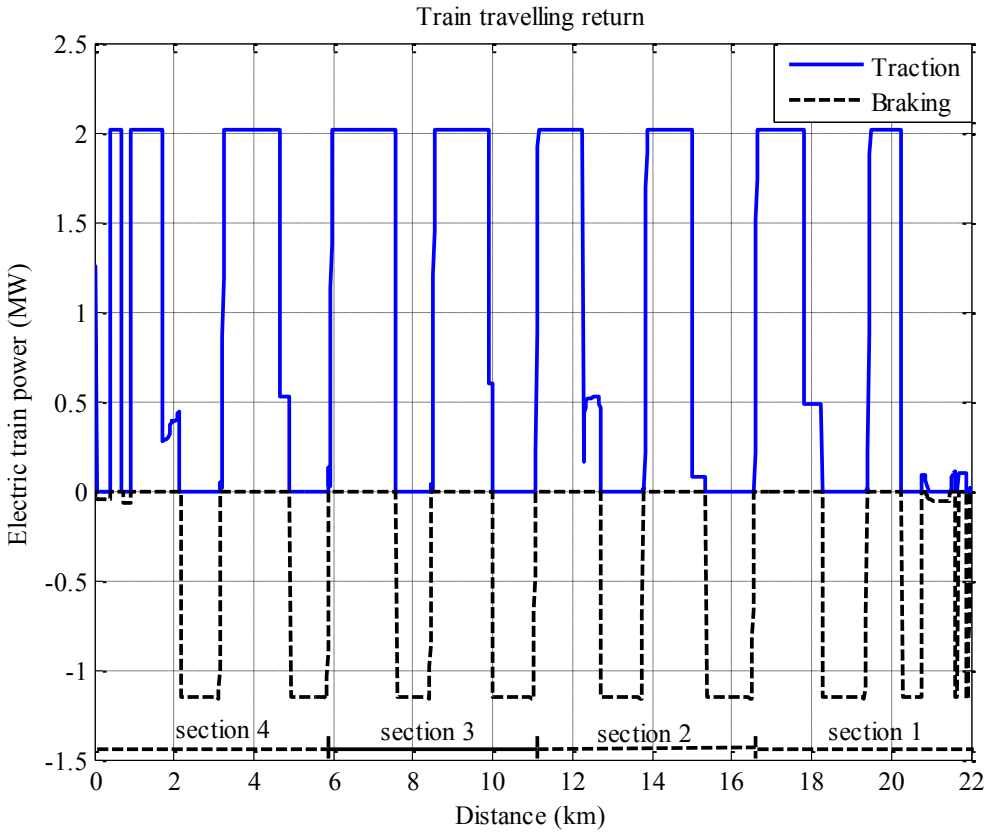

Figure 4.19: Electrical power of the train in the return journey

From the diagram of the electric power of the train, it is possible to calculate the current of the train i_t by (3.3) of Chapter 3, as Figure 4.20 shows for a train travelling forwards. The maximum current for motoring is 3.95 kA and it is represented by a solid-line, whereas the maximum current for braking is 1.50 kA and it is represented by a dash-line. The significant difference of the current value is due to the fact that the line voltage is low when the train is motoring and high when the train is braking.

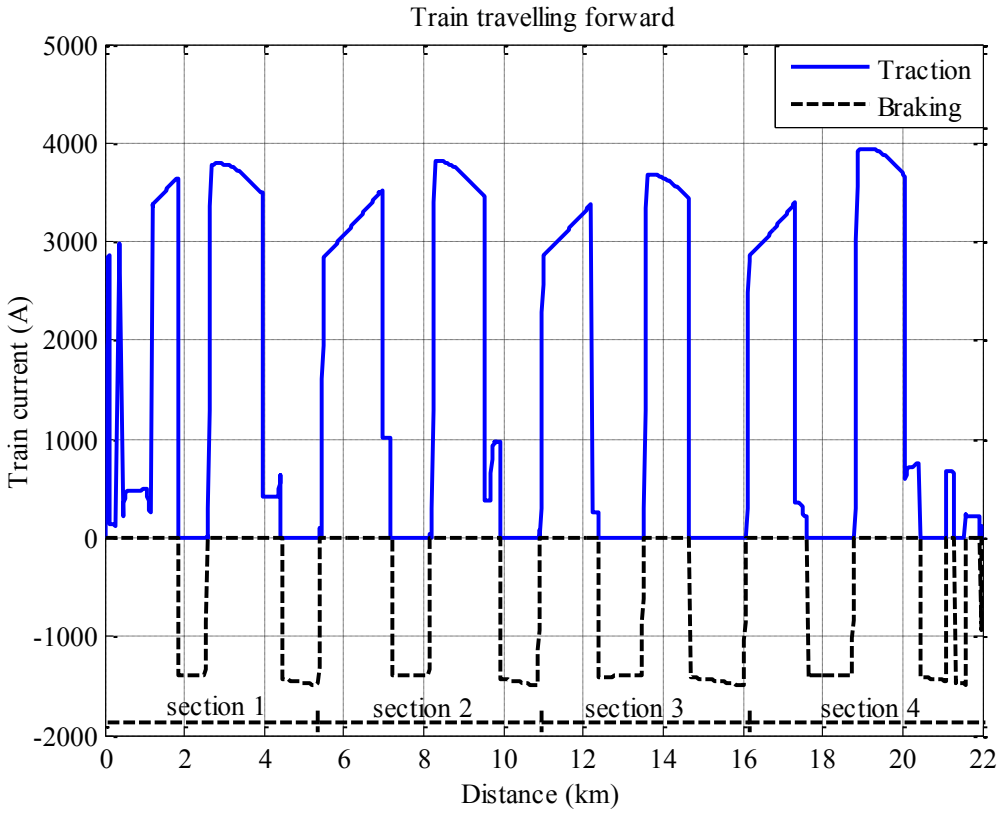

Figure 4.20: Current of the train travelling in the forward direction

Figure 4.21 shows the diagram of the current when the train is travelling in the opposite direction. In this case, using the same types of line for the diagrams, the maximum current for motoring is 4.03 kA, whereas the maximum current for braking is 1.50 kA.

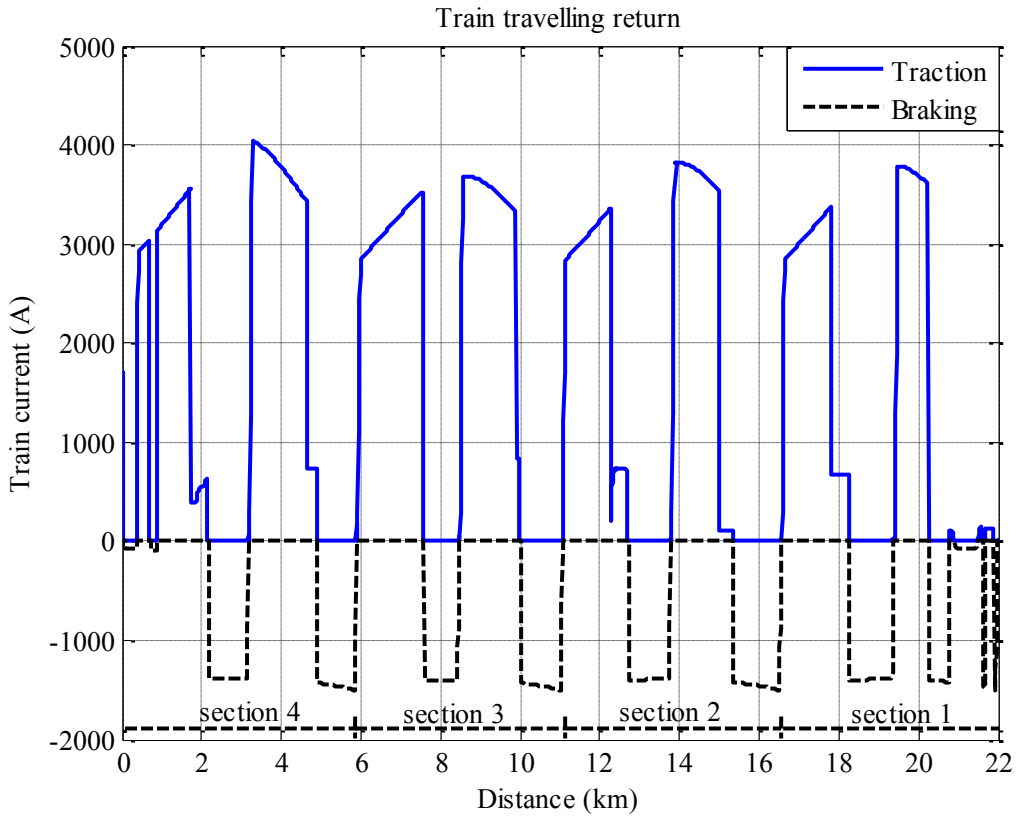

Figure 4.21: Current of the train travelling in the reverse direction.

Based on the optimisation procedures in this thesis, the objective functions of the optimisation algorithm in (4.16) minimising the energy consumption of substations are taken into account in the optimal design capacitances and positions of stationary EDLCs for the train travelling a round-trip of each section. A cycle or a round-trip of each section, T in (4.16) means the duration time that the train travels from the first substation on the left to the second substation on the right, and then travels back to the first substation again. In (4.16), the fitting weight coefficients, $\omega_1 - \omega_4$ are unknown, and can be found by the GA and PSO algorithms with the objective function of minimising the total energy consumption of the substations E_{source}. The boundaries of the fitting weight coefficients, $\omega_1 - \omega_4$ are defined as between 0 and 1 with the initial boundary generated by random numbers. The GA and PSO algorithms have been implemented by the MATLAB GA and

PSO toolboxes, which require to set a maximum number of generations, population size and solution tolerance. These are given by the accuracy required for the solution. For EDLCs there is a difference of 10-20% between the rated and actual capacitance, so the final energy stored calculated from the optimisation algorithm can have the same interval of approximation. After several trials, an acceptable compromise is to use a maximum number of generations of 25, a population size of 25 and a solution tolerance of 0.1 for both the GA and PSO algorithms. For GA, a mutation operator is not set up in this problem because the solutions have bounds, and a crossover fraction operator is set by 0.8. Examples of the MATLAB code for calling GA and PSO algorithms are presented in step 5 of Figure 4.9.

The specifications of the computers which are used for the simulation with the MATLAB toolbox of the GA and PSO algorithms are shown in Table 4.6.

Table 4.6: The specification of computers used for the simulation

Computer	Specification
1	Intel ® Core ™ i5-4590S CPU @ 3.00GHz 2.99 GHz, 8.00 GB of RAM and 64-bit operating system
2	Intel ® Core ™ i5-3570 CPU @ 3.40GHz 3.40 GHz, 8.00 GB of RAM and 64-bit operating system
3	Intel ® Core ™ i5-2500 CPU @ 3.30GHz 3.30 GHz, 4.00 GB of RAM and 64-bit operating system
4	Intel ® Core ™ i5-3570 CPU @ 3.40GHz 3.40 GHz, 8.00 GB of RAM and 64-bit operating system

The results of the top 10 best solutions of the GA and PSO algorithms for the fitting weight coefficients, $\omega_1 - \omega_4$ are presented in the Table 4.7. The minimum energy consumption of substations E_{source} is around 365 kWh for both GA and PSO algorithms and for several different sets of fitting weight coefficients.

Table 4.7: The top ten best solutions of GA and PSO algorithm for a round-trip of the train journey

Method	Energy consumption (kWh)	ω_1	ω_2	ω_3	ω_4	Computer	Time (hours)
GA	365.1196	0.0040	0.0016	0.0038	0.9643	4	24.1
	365.1547	0.1252	0.0025	0.0030	0.9931	4	23.8
	365.1713	0.1303	0	0.0068	0.9043	4	21.4
	365.1754	0.1961	0.0053	0	0.9358	3	19.3
	365.1977	0.0597	0.0011	0.0073	0.9936	3	20.8
	365.2063	0	0.0016	0.0074	0.9715	4	20.0
	365.2936	0.1111	0.0003	0.0132	0.9888	3	16.8
	365.3070	0.0234	0.0111	0	0.9894	3	20.9
	365.6353	0.0657	0.0129	0.0130	0.9966	3	20.0
	365.6744	0.0019	0.0079	0.0206	0.9929	3	22.8
PSO	365.1037	0.1381	0.0002	0.0033	0.8700	2	4.0
	365.1146	0.5538	0.0007	0.0005	0.9313	2	4.5
	365.1155	0.1558	0.0027	0.0001	0.8319	1	3.3
	365.1159	0.3696	0.0008	0	0.5808	1	4.2
	365.1177	0.5902	0.0001	0.0006	0.7602	1	3.5
	365.1491	0.3239	0.0026	0.0011	0.9538	1	2.9
	365.1599	0.4751	0.0017	0.0009	0.7601	2	5.1
	365.1608	0.3158	0.0023	0.0008	0.7561	2	3.9
	365.1624	0.0775	0.0008	0.0034	0.6232	1	2.7
	365.1663	0.3123	0.0016	0.0035	0.9413	2	4.7

The values of the coefficients ω_2 and ω_3 are almost zero, which means that the branch currents i_{L1} and i_{L2} have no effect on energy saving for this optimisation problem. However, energy saving can be achieved by slightly maintaining the train voltage regulation and by significantly reducing the current of the EDLCs regarding the value of coefficients ω_1 and ω_4, respectively.

In practical terms, the solver begins at an initial value x_0 of the solution, performs some intermediate calculations that eventually lead to a new point x_1, and then repeats the process to find successive approximations x_2, x_3, … of the local minimum. Processing stops after some number of iterations k. In this thesis, the number of iteration is the number of objective function evaluations. For GA, the algorithm stops at the maximum number of objective function evaluation and does stop by the solution tolerance, which

means the difference between the subsequent steps is bigger than the solution tolerance. For PSO, the algorithm stops before the maximum number of objective function evaluations is reached if the difference between to subsequent steps is smaller than the solution tolerance. Diagrams showing convergence to the optimal solution by the GA and PSO algorithms are presented in Figure 4.22 and Figure 4.23, with the relation between iterations and the total energy consumption of the substations.

The results show that convergence of the PSO algorithm required 180 function counts and took 4.00 hours, whereas convergence of the GA required 650 function counts and took 24.10 hours. This result shows a clear advantage of the PSO algorithm in terms of the data processing time and memory for this problem.

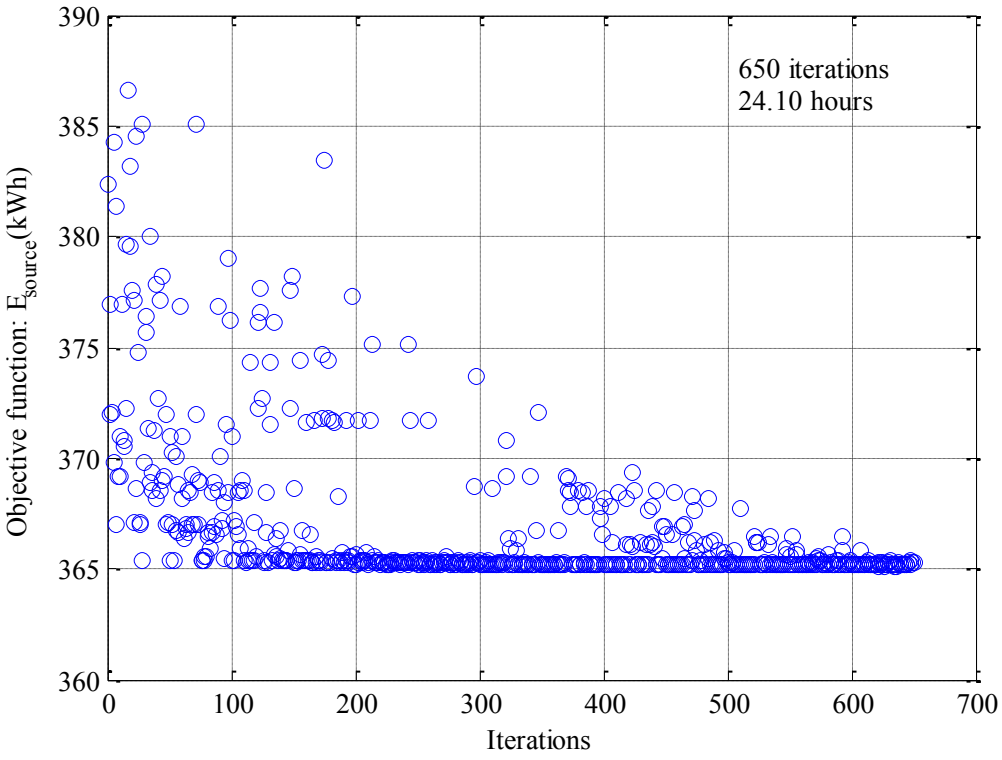

Figure 4.22: Convergence to the optimal solution using GA

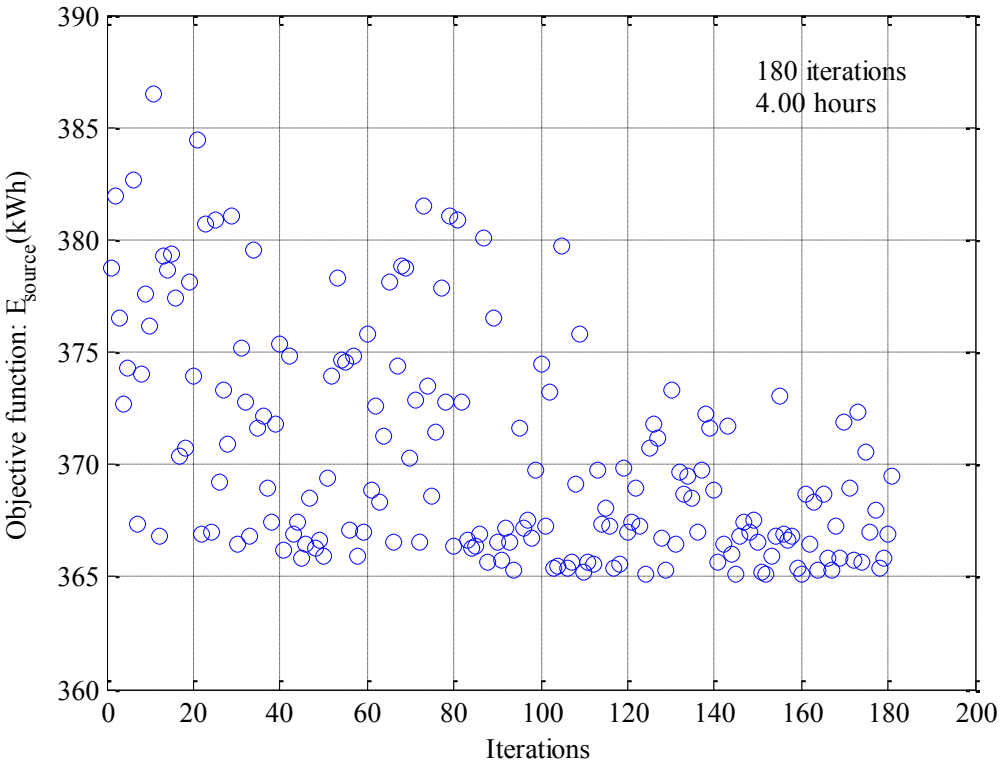

Figure 4.23: Convergence to the optimal solution using PSO

The best fitting weight coefficients are then $\omega_1 = 0.1381\ \Omega^{-1}$, $\omega_2 = 0.0002\ \Omega$, $\omega_3 = 0.0033\ \Omega$ and $\omega_4 = 0.8700\ \Omega$ obtained by the PSO algorithm. The optimal design of capacitances of stationary EDLCs and their positions along the track are obtained with these fitting weight coefficients in the objective function of the optimisation algorithm presented in (4.16).

On the basis of the substation positions, the track of 22 km is divided into four sections: section 1 (0-5.43 km), section 2 (5.43-10.92 km), section 3 (10.92-16.09 km) and section 4 (16.09-22 km). Every section is divided into trunks of 500 m at the end of which the stationary EDLCs can be placed. The train travels across the line of each section and then also returns back to its initial position. Figure 4.24 shows the total energy consumption of the substations as a function of the position of the EDLCs on the track obtained by the optimisation algorithm. The figure shows that the points with the minimum total energy

consumption in sections 1 to 3 are located at 2.5 km, whereas in section 4 this point is at 3.0 km from the substations to the left of each section. This means that the optimal positions of EDLCs are located at the position of each section with the minimum total energy consumption, as shown in Figure 4.24 and Table 4.8. The capacitances of EDLCs in each position are calculated by (3.44).

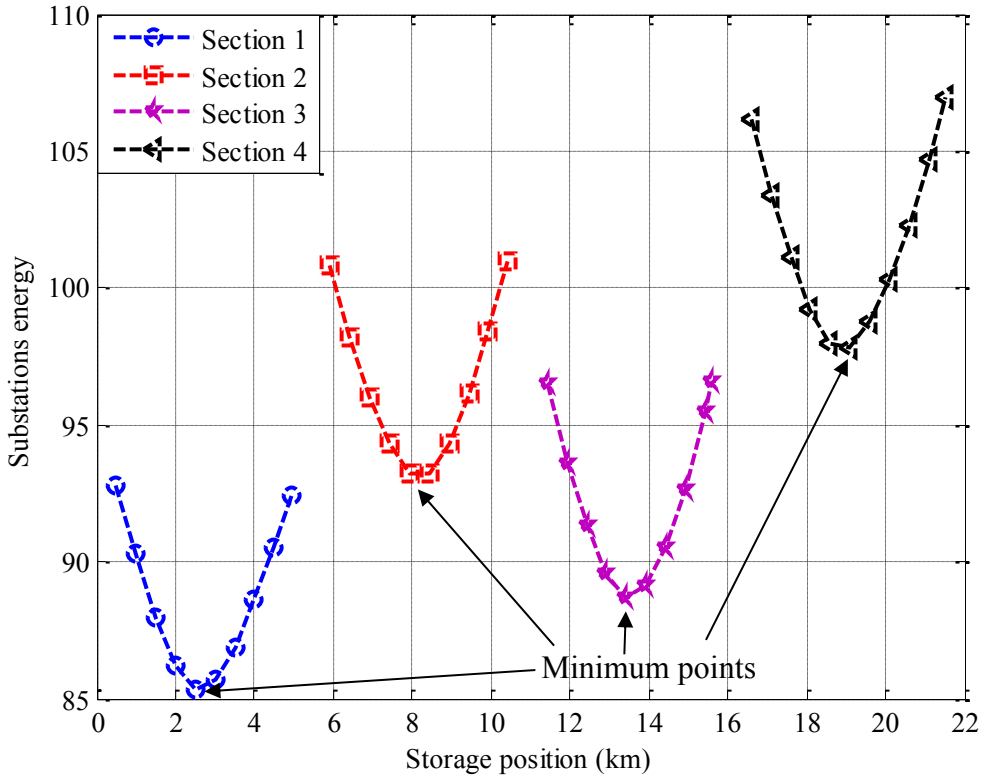

Figure 4.24: The substations energy with each position of stationary EDLCs along the track

Table 4.8 shows the positions, the rated voltages $v_{Edlc,n}$, the energy capacities E_n and the capacitances C_n of the optimal stationary EDLCs. The optimal capacitances of the stationary EDLCs from section 1 to section 4 are 1.03 kF, 1.20 kF, 1.00 kF and 0.99 kF, respectively. The rated voltages $v_{Edlc,n}$ of the EDLC modules are one half of the voltage output of the DC-DC converter v_{Edlc}. It can be observed that the rated voltages $v_{Edlc,n}$ of the minimum stationary EDLCs for all four sections are around 465 – 473 V. The energy

capacity in each EDLC is 32 kWh for section 1, 38 kWh for section 2 and 31 kWh for section 3 and section 4.

From Table 4.8 it is possible to draw a single line diagram of the route with EDLCs, as shown in

Figure **4.25**. For all sections, the optimal EDLCs are located around the middle and not close to the substations.

Table 4.8: Optimal position, capacitance, rated voltage and energy capacity of the optimal stationary EDLCs of a round-trip of the train journey

Track Length (km)	Optimal position (km)	C_n (kF)	$V_{Edlc,n}$ (V)	E_n (kWh)
Section 1 (5.43 km) (EDLC 1): 0–5.43	2.50	1.03	465.95	31.11
Section 2 (5.49 km) (EDLC 2): 5.43–10.92	2.50	1.20	471.87	37.19
Section 3 (5.17 km) (EDLC 3): 10.92–16.09	2.50	1.00	471.06	30.83
Section 4 (5.91 km) (EDLC 4): 16.09–22.00	3.00	0.99	472.72	30.83

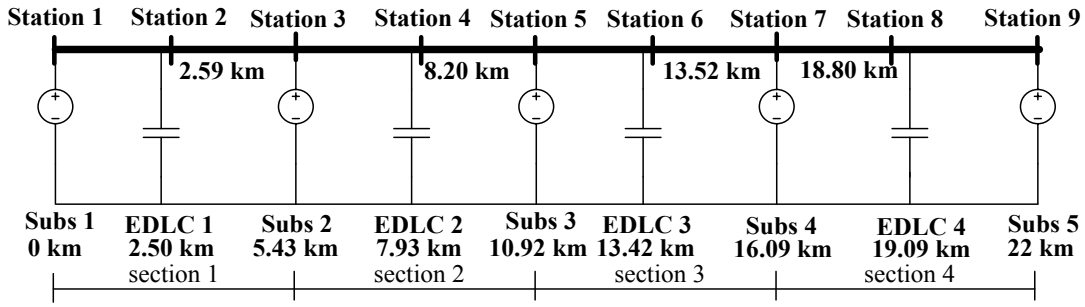

Figure 4.25: Single line diagram of the smallest stationary EDLC positions

Figure 4.26 and Figure 4.27 show the current of the train and the EDLCs when the train is running in two different directions along the track. The current for train motoring is the sum of the substation currents and the EDLC current. Since the substations are not reversible, the current for train braking is fully absorbed by the EDLCs. All the current regenerated during braking is used to charge the EDLCs and not dissipated by the braking choppers.

Based on the single line diagram of the track in Figure 4.25, the train current is the sum of the substation currents of each section; the current of the train is drawn by substations 1 and 2 of section 1, substations 2 and 3 of section 2, substations 3 and 4 of section 3 and substations 4 and 5 of section 4.

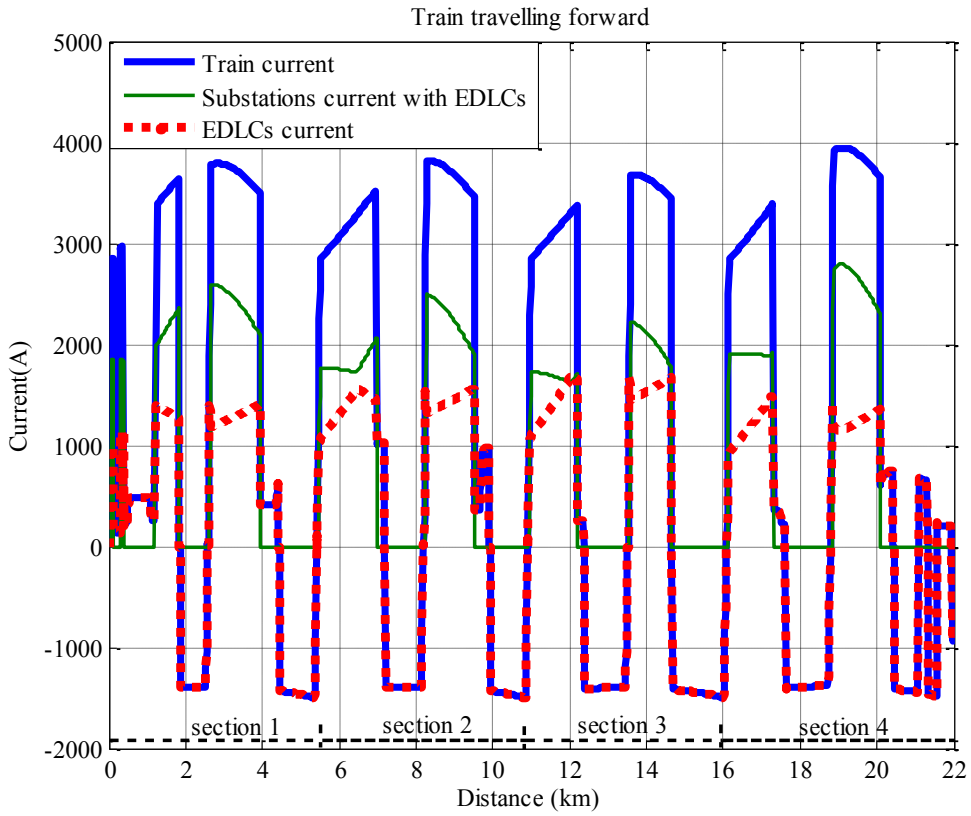

Figure 4.26: Current of the train, substations and EDLCs (train travelling forward)

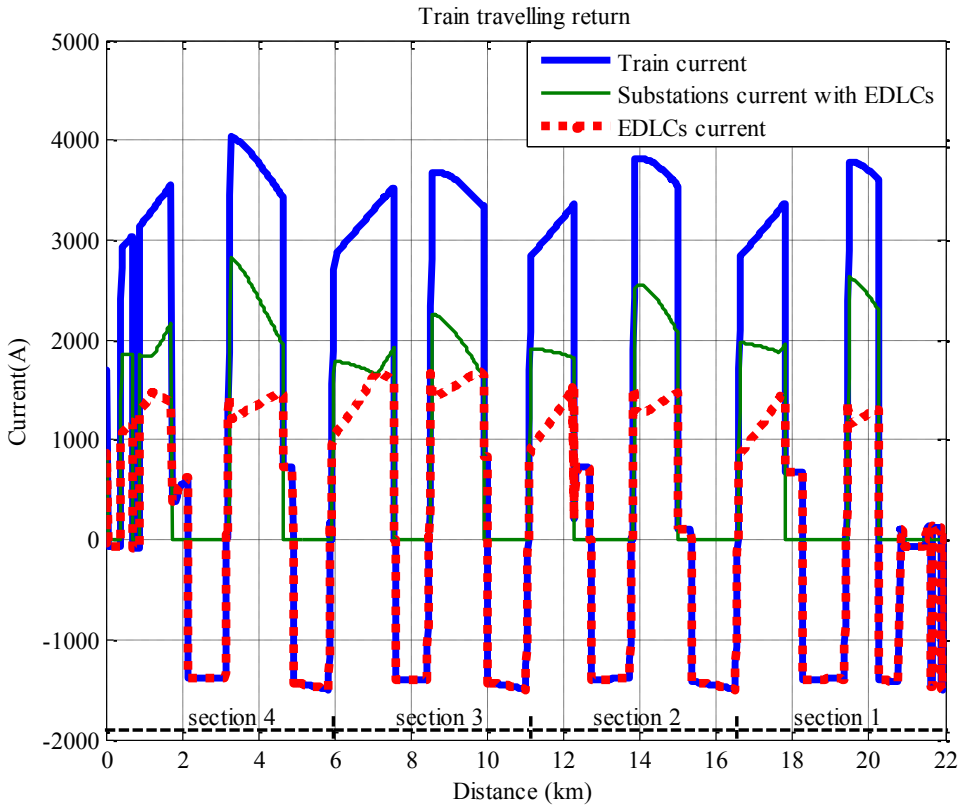

Figure 4.27: Current of the train, substations and EDLCs (return journey)

In order to better appreciate the function of the storage devices, Figure 4.28 and Figure 4.29 compare the currents of the substations with and without the EDLCs. It can be observed that the total current of the substations without EDLCs is equal to the train's current. Therefore, EDLCs help to reduce the average value of the total substation current by 42.4% for the train travelling forward and 41.7% for the train travelling on the return journey, and the peak by 28.9% for the train travelling forward and 29.8% for train travelling on the return journey.

Comparisons of the current of the first and second substations of each section with and without EDLCs for both directions of train travel, which are based on the power supply of the DC light railways in Figure 3.7 and Figure 3.8, are as shown in Figure 4.30. It can

be seen that the current of substations with EDLCs is significantly reduced by the supported current from the EDLCs to the motoring train.

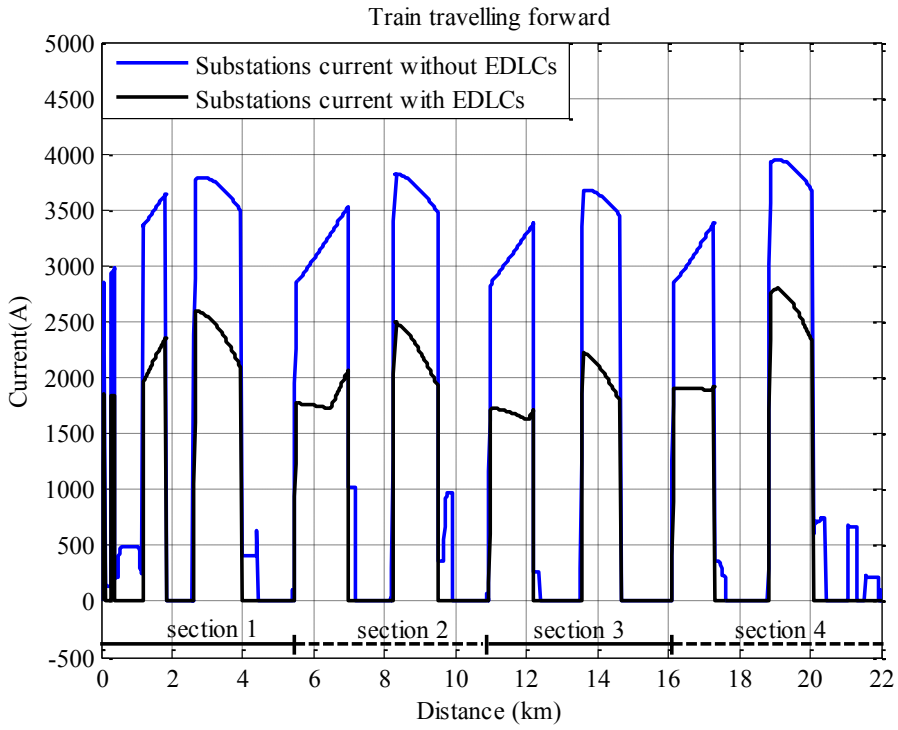

Figure 4.28: Total substation current without and with EDLCs (train travelling forward)

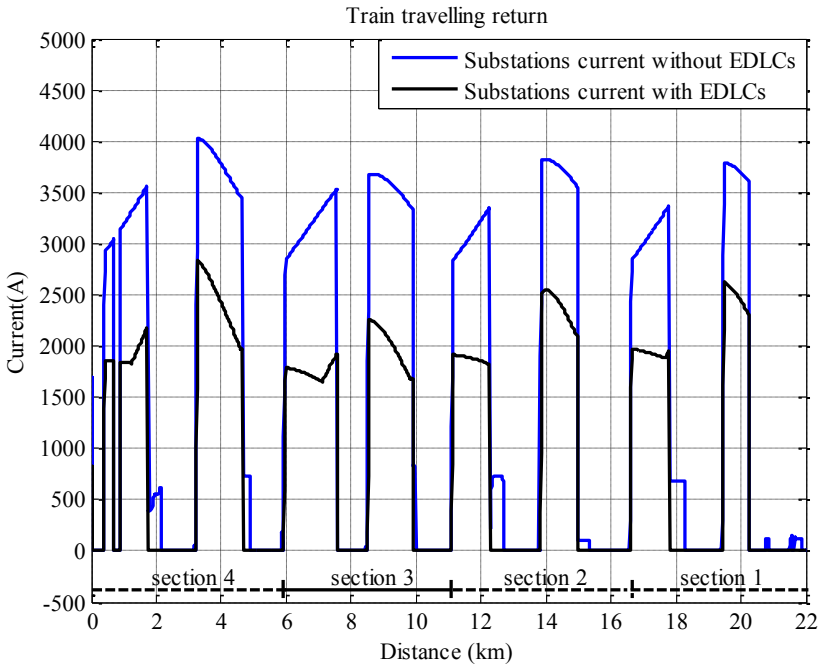

Figure 4.29: Total substation current without and with EDLCs (return journey)

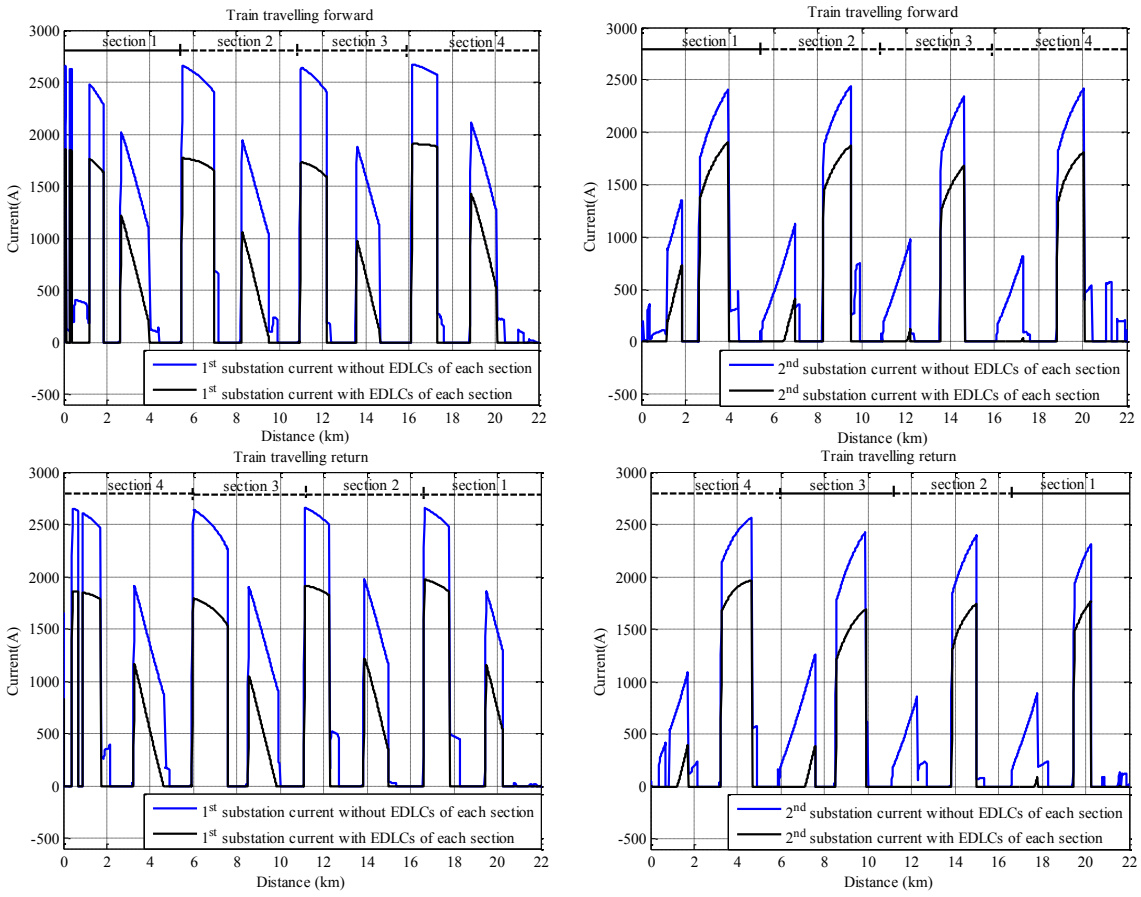

Figure 4.30: Currents of the first and second substations of each section without and with EDLCs of train travelling forward and returning

Figure 4.31 and Figure 4.32 show the voltage of the train without and with the stationary EDLCs as per unit of the nominal voltage at 750 V. Comparing the blue and green lines, it can be seen that the voltage drop during train motoring is improved by 5 – 15% when EDLCs are used. On the other hand, the train voltage during train braking is higher with EDLCs, because for DC systems the voltage of the regenerative source has to be higher than the voltage of the stationary EDLCs to reverse the power flow.

The voltage of the EDLCs at the point of connection to the line is generally lower than the nominal voltage of substations when the train is motoring. Therefore, the storage is actually a support to the substations. In a few cases, the voltage of the EDLCs is higher than the nominal voltage of the substations. This means that the more distant substation

is blocked by the storage and the train is entirely supplied by one substation and the EDLCs. This situation arises when the train is motoring very close to the middle of the section and hence the supply from the storage produces small losses in comparison to the supply from the distant substation.

On the other hand, the voltage of the EDLCs is higher than the nominal voltage of the substations when the train is braking, because no energy can be regenerated to the substations. It is important to note that, when the train is braking, both the voltages of the train and the EDLCs are higher than the nominal voltage of the substations to block any current from the substations themselves. Therefore, the regenerative current circulates only between the train and the storage.

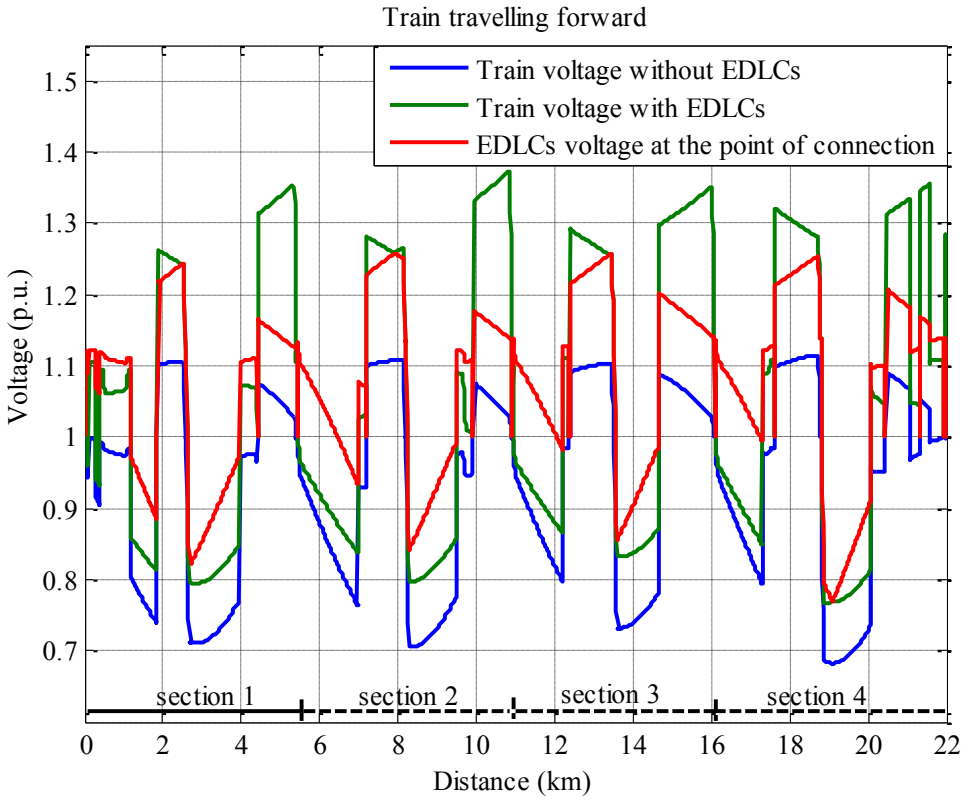

Figure 4.31: Train voltage without and with EDLCs and EDLC voltage at the point of connection (train travelling forward)

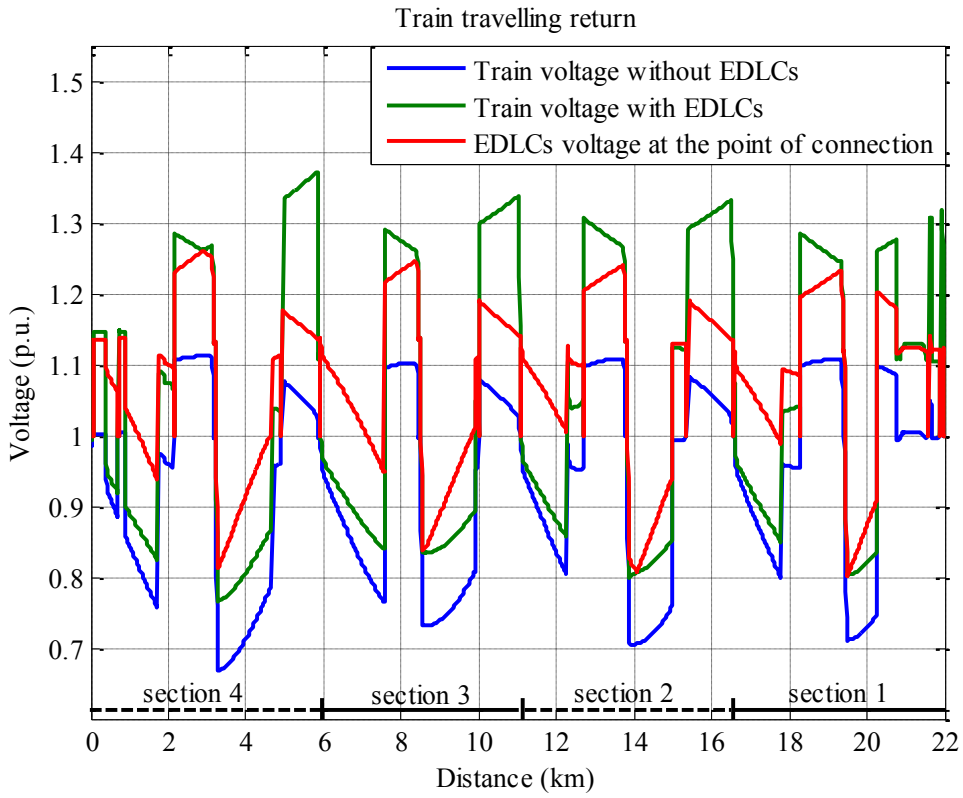

Figure 4.32: Train voltage without and with EDLCs and EDLC voltage at the point of connection (return journey)

Figure 4.33 shows the cumulative energy supplied by the stationary EDLCs and substations, the energy drawn by the train, and the losses on the line during the train travelling forward and returning in each section. The positions of stationary EDLCs are located at 2,500 m from the first substation in section 1 to section 3 and at 3,000 m in section 4. For example, the optimisation algorithm finds the optimal capacitances of the storage to minimise the total energy consumption. This does not necessarily means that the capacitances themselves are the minimum. In fact, the use is 18 kWh which is 56% of the total energy. To prove this, a simulation with a minimum capacitance of 24 kWh (75% of the total energy, obtained from the constraint on the minimum voltage of capacitors equal to 50% of the maximum voltage) leads to an energy consumption of 91 kWh, which is bigger than 85 kWh. When the energy increases, the EDLCs discharge

energy to support the train motoring; when the energy decreases, the EDLCs recover energy from the regenerative braking. From the isoperimetric constraint given in (4.19), the net energy of the EDLCs in one cycle has to be zero and this is confirmed by Figure 4.33.

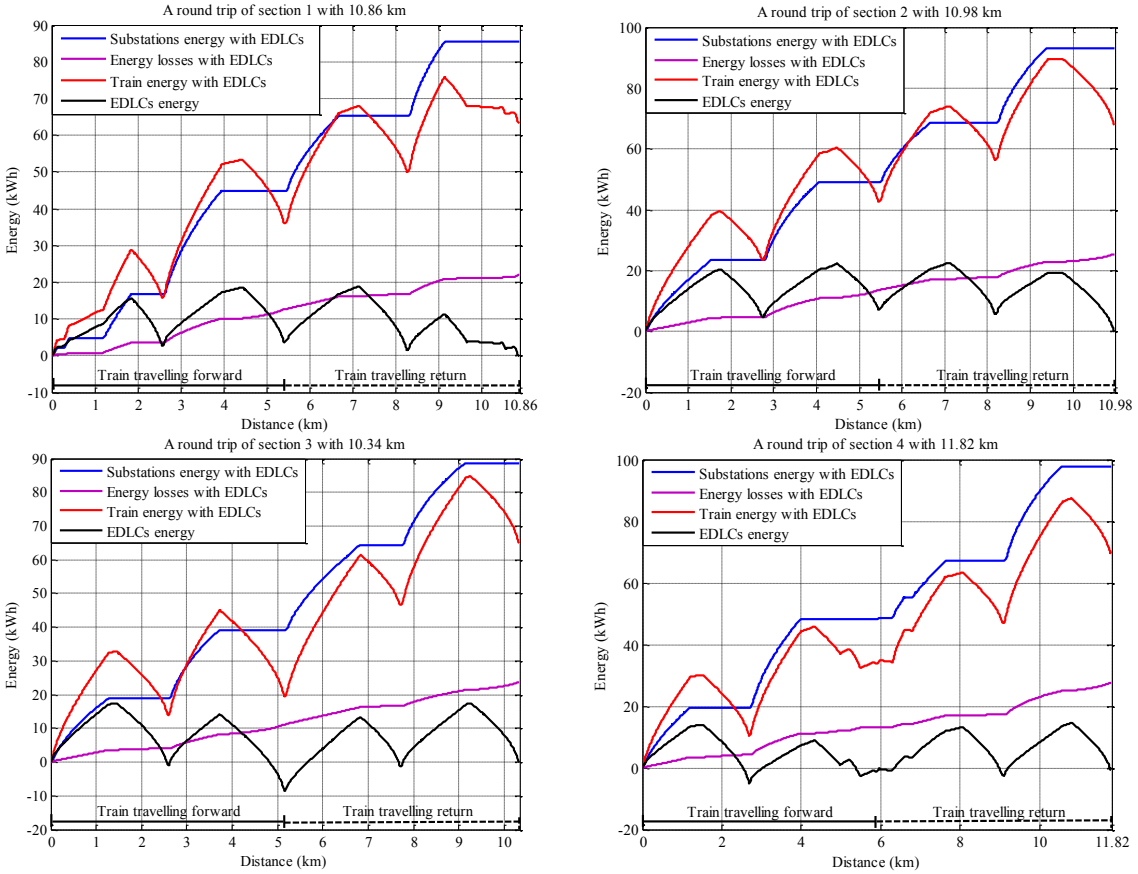

Figure 4.33: Energy of substations, trains, line losses and EDLCs of a round-trip of the train travelling in each section

Figure 4.34 shows a comparison of the cumulative energy supplied by the substations, the energy drawn by the train and the energy losses consumed by the conductor rail, running rail and on-board braking resistance without EDLCs for a round-trip of the train. The energy from the substations increases only when the train is motoring, because there is no regeneration when the train is braking and no energy consumption when the train is at the stations.

The entire cumulative energy supplied by the substations, the energy drawn by the train, the energy supplied by storage and the energy losses consumed by the conductor rail and running rail with EDLCs and the energy supplied by EDLCs for a round-trip of the train travelling in each section are shown in Figure 4.35.

In the model and the results in Figure 4.34 and Figure 4.35, the energy losses are caused by the on-board braking resistance, when in use, and the resistance of rails and conducting rails. The train energy takes into account kinetic energy and friction, hence, it decreases when the train approaches a station. The simulation shows that the energy losses in the traditional system are 267% larger than those with EDLCs. This is because, in the case of only one train travelling on the line, there is no energy saved through regenerative braking. If there is more than one train travelling on the line whilst a train is braking, some of the regenerative braking energy will be distributed to support other trains (Iannuzzi et al., 2012b). The storage device is recharged and discharged cyclically to support the train. The storage is discharged 87% by the kinetic energy of the train and 13% by the feeder stations. With the efficiency assumed in this simulation, the average efficiency of energy regeneration is equal to 53%.

The previous figure also shows that the net energy supplied by the EDLCs is zero at the end of the cycle, in accordance with the isoperimetric constraint in (4.19).

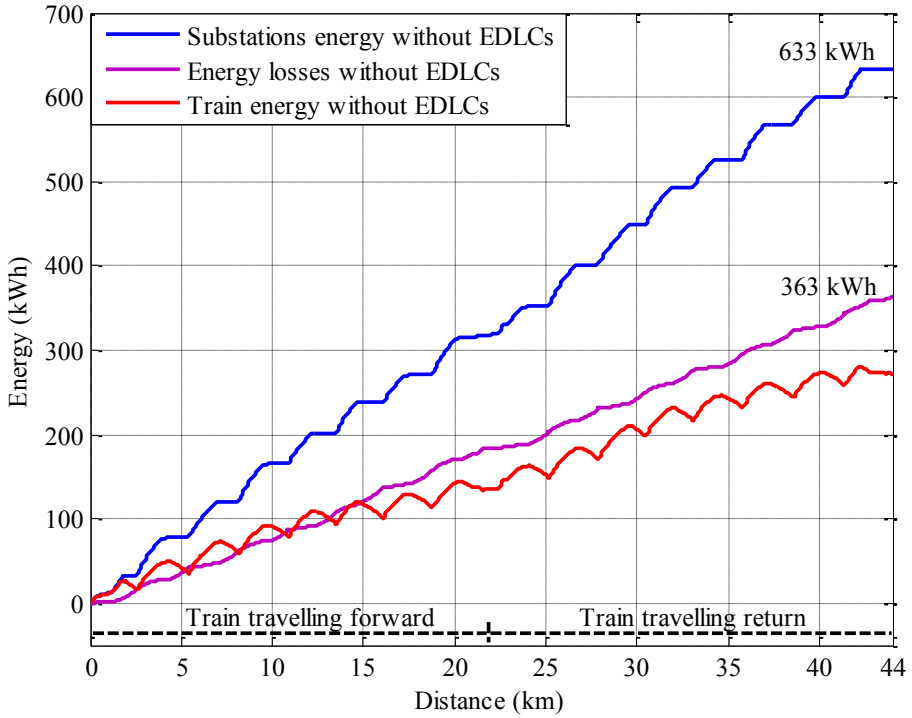

Figure 4.34: Energy of all substations, mechanical energy consumed by the train and energy losses without EDLCs for a complete round-trip of the train

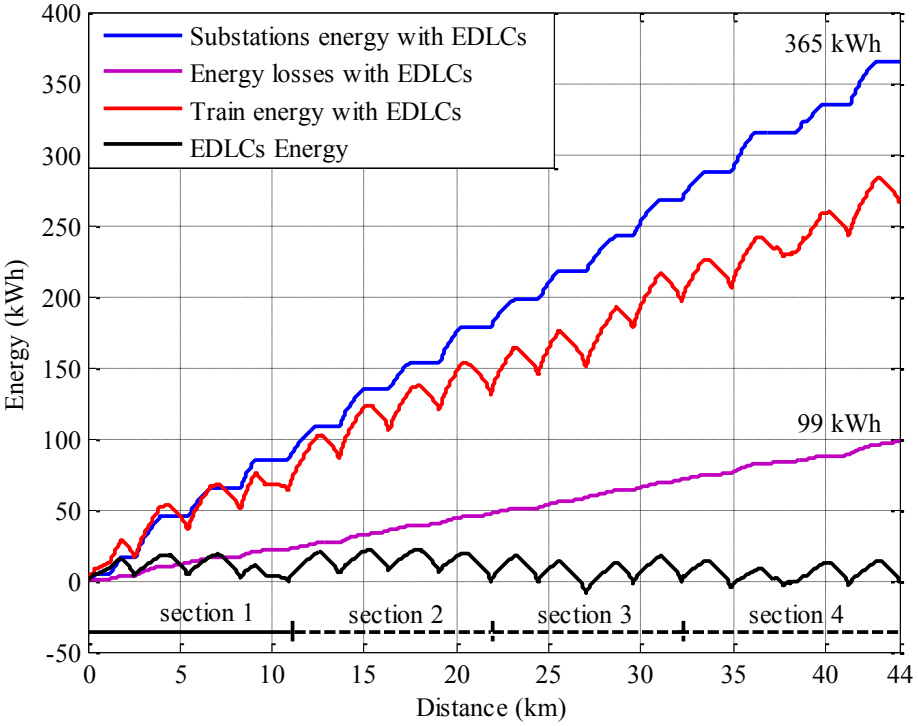

Figure 4.35: Energy of all substations, mechanical energy consumed by the train, energy supplied by the storage (when present) and energy losses with EDLCs for a complete round-trip of each section

The requirements of the EDLCs can be used to specify the commercially available modules, as shown in Table 4.9, where the nominal voltage is V_n, the nominal capacitance is C_{nc}, the nominal current is I_n and the maximum current is $I_{\max}$.

Table 4.9: Main features of commercially available modules (Iannuzzi et al., 2012b)

Producer	Module	V_n (V)	C_{nc} (F)	I_n (A)	$I_{\max}$ (A)	Weight (kg)	Energy (kWh)
Maxwell	BMOD0063 P125	125	63	150	750	59	102
	BMOD0063 P75	75	94	50	150	25	73
LS Ultra-capacitor	LMSU134	180	42	-	-	-	-
	LMSU201	120	62	-	-	-	-
NessCAP	EMHSP0051	340	51	-	3800	384	818
	EMHSP00238	52	238	-	2500	32	89

Using the characteristics of these modules, the number of modules connected in series N_s, and parallel N_p, the peak voltage V_p, the total capacitance C_{Edlc} and the nominal current $I_{Edlc,n}$, can be calculated and the results are reported in Table 4.10.

Table 4.10: Specification of stationary EDLC systems for each section of the considered application

Track	Producer	Module	V_p (V)	C_{Edlc} (kF)	$I_{Edlc,n}$ (kA)	N_s	N_p	Weight (ton)	Energy (kWh)
Section 1	Maxwell	BMOD0063 P125	500	1.07	10.2	4	68	16.0	27.7
		BMOD0063 P75	525	1.06	3.9	7	79	13.8	40.4
	LS Ultracapacitor	LMSU134	540	1.06	-	3	76	-	-
		LMSU201	600	1.07	-	5	86	-	-
	NessCAP	EMHSP0051	680	1.07	-	2	42	32.3	68.7
		EMHSP00238	520	1.07	-	10	45	14.4	40.1
Section 2	Maxwell	BMOD0063 P125	500	1.24	11.9	4	79	18.6	32.2
		BMOD0063 P75	525	1.25	4.7	7	93	16.3	47.5
	LS Ultracapacitor	LMSU134	540	1.25	-	3	89	-	-
		LMSU201	600	1.24	-	5	100	-	-
	NessCAP	EMHSP0051	680	1.25	-	2	49	37.6	80.2
		EMHSP00238	520	1.26	-	10	53	16.9	47.2
Section 3	Maxwell	BMOD0063 P125	500	1.10	10.5	4	70	16.5	28.6
		BMOD0063 P75	450	1.10	4.1	7	82	14.4	41.9
	LS Ultracapacitor	LMSU134	540	1.11	-	3	79	-	-
		LMSU201	480	1.10	-	4	71	-	-
	NessCAP	EMHSP0051	680	1.12	-	2	44	33.8	72.0
		EMHSP00238	520	1.12	-	10	47	15.0	41.8
Section 4	Maxwell	BMOD0063 P125	500	1.02	9.8	4	65	15.3	26.5
		BMOD0063 P75	525	1.02	3.8	7	76	13.3	38.8
	LS Ultracapacitor	LMSU134	540	1.02	-	3	73	-	-
		LMSU201	600	1.03	-	5	83	-	-
	NessCAP	EMHSP0051	680	1.02	-	2	40	30.7	65.4
		EMHSP00238	520	1.02	-	10	43	13.8	38.3

Based on the considered application of stationary EDLCs for each section of the track, as presented in Table 4.10, it is interesting to note that the recommended EDLC modules

that are suitable for this light railway system are BMOD0063 P75 produced by Maxwell and EMHSP00238 produced by NessCAP**.**

4.4 Summary

This chapter has reviewed the principal optimisation methods used in engineering problems. Classical methods are based on the calculus of variations and permit the addition of various constraints using calculus. The meta-heuristic methods, the GA and PSO algorithms, are based on evolutionary algorithms which try to find the optimal solution with a step-by-step refinement of the parameters based on well-defined searching rules. These methods have been implemented in the analysis of the fitting weight coefficient used in the cost function of the optimisation method, based on the calculus of variation with the isoperimetric constraint.

This chapter has also presented a method to design the optimal capacitances and positions of stationary EDLCs. The optimisation technique takes into account the minimisation of the total energy consumption of the light railway and it is based on the model of a light railway system with stationary energy storage developed in chapter 3. The objective function has four weight coefficients which can be designed using the GA and PSO algorithms presented above in sections 4.2.2 and 4.2.3. The optimisation problem also takes into account that the state of charge of the storage has to return to the initial value when the train has completed a journey from the first substation to the second substation and back to the first substation again. This is mathematically described by adding an isoperimetric constraint that requires the modification of the objective function and the determination of a Lagrange multiplier.

The STS provides the mechanical power and the speed of the train, which are employed in the model of the railway electrification system and rolling stock. The results of the optimisation algorithm show that the fitting weight coefficients employed in the objective function are found by the GA and PSO algorithms. Based on the round-trip journey of the train, the optimal design of the capacitances and positions of stationary EDLCs for each section is satisfied by the optimisation algorithm. It can be observed that the optimal capacitance of each stationary EDLC is located at around the middle of the route, or close to the middle station between two substations for each section of the route.

Chapter 5 Piece-wise Linear SOC Control of Stationary EDLCs

5.1 Introduction

This chapter illustrates a method to control the SOC of stationary EDLCs under the specifications of capacitances and positions obtained from the optimisation algorithm. The characteristic of the control of the storage is divided into five zones, depending on the current demand of the traction system, using a piece-wise function.

5.2 Piece-wise Linear SOC Control of Stationary EDLCs

The SOC control has been defined in this thesis as a relationship between the voltage deviation of the stationary EDLCs Δv and the current of the EDLCs i_{Edlc} as shown in Figure 5.1. The voltage deviation Δv is the difference between the nominal voltage of the electrified system E_{ss} and the output voltage of the DC-DC converter v_{Edlc}:

$$\Delta v = E_{ss} - v_{Edlc} \tag{5.1}$$

The characteristic is a piece-wise function with five zones. There are two areas where the EDLCs are active and three areas where the EDLCs are idle. The active discharging area is when the current i_{Edlc} is positive. This area is limited by a minimum and maximum value of the voltage deviation. Therefore, the EDLCs are not activated until the voltage deviation is greater than $\Delta v_{d,\min}$. The EDLC current increases linearly with slope m_d for larger values of Δv until the maximum current of EDLCs $i_{Edlcd,\max}$ is reached. This limit

also defines the maximum voltage deviation $\Delta v_{d,\max}$. For any voltage deviation larger than this limit, the EDLC current is capped to $i_{Edlcd,\max}$ until the minimum SOC of EDLCs is reached and they are disconnected from the line. A similar characteristic has been defined for the recharge region, when the current i_{Edlc} and the voltage deviation are both negative. The voltage limits are $\Delta v_{c,\min}$ and $\Delta v_{c,\max}$, the current limit is $i_{Edlcc,\max}$ and the slope is m_c and they are, in general, different from the values of the discharge.

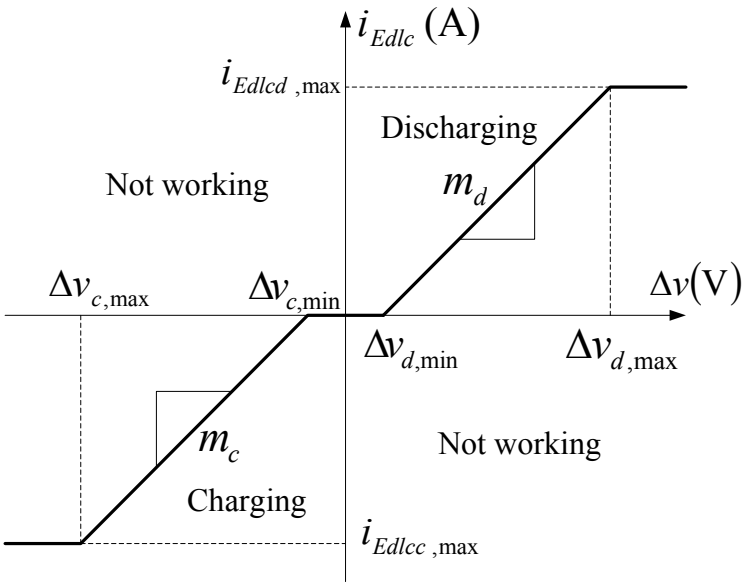

Figure 5.1: The characteristic of the linear SOC control of stationary EDLCs

With reference to Figure 5.1, the characteristic is mathematically described as follows for the five zones.

A. Discharging zone:

- $\Delta v_{d,\min} < \Delta v < \Delta v_{d,\max}$

The current i_{Edlcd} is proportional to the voltage deviation:

$$i_{Edlcd} = m_d\left(\Delta v - \Delta v_{d,\min}\right) \tag{5.2}$$

The slope of the characteristic is:

$$m_d = \frac{i_{Edlcd,\max}}{\Delta v_{d,\max} - \Delta v_{d,\min}} \tag{5.3}$$

and finally, substituting (5.1) and (5.3) into (5.2)

$$i_{Edlcd} = m_{d2} - m_d v_{Edlc} \qquad ;\text{if } \Delta v_{d,\min} < \Delta v < \Delta v_{d,\max} \tag{5.4}$$

where: $m_{d2} = m_d(E_{ss} - \Delta v_{d,\min})$

- $\Delta v \geq \Delta v_{d,\max}$

  In this area the current i_{Edlcd} is equal to the maximum discharge current of the EDLCs:

$$i_{Edlcd} = i_{Edlcd,\max} \qquad ;\text{if } \Delta v \geq \Delta v_{d,\max} \tag{5.5}$$

B. Charging zone

- $\Delta v_{c,\min} < \Delta v < \Delta v_{c,\max}$

  The current i_{Edlcc} is proportional to the voltage deviation:

$$i_{Edlcc} = m_c\left(\Delta v - \Delta v_{c,\min}\right) \tag{5.6}$$

The slope of the characteristic is:

$$m_c = \frac{i_{Edlcc,\max}}{\Delta v_{c,\max} - \Delta v_{c,\min}} \tag{5.7}$$

and finally:

$$i_{Edlcc} = m_{c2} - m_c v_{Edlc} \qquad ;\text{if } \Delta v_{c,\min} < \Delta v < \Delta v_{c,\max} \tag{5.8}$$

where: $m_{c2} = m_c(E_{ss} - \Delta v_{c,\min})$

- $\Delta v \geq \Delta v_{c,\max}$

  In this area the current i_{Edlcc} is equal to the maximum recharge current of the EDLCs:

$$i_{Edlcc} = i_{Edlcc,\max} \qquad ;\text{if } \Delta v \geq \Delta v_{c,\max} \tag{5.9}$$

C. Idling zone:

- $\Delta v_{c,\min} \leq \Delta v \leq \Delta v_{d,\min}$

  In this area discharged current is zero:

$$i_{Edlcd} = 0 \qquad ;\text{if } 0 \leq \Delta v_d \leq \Delta v_{d,\min} \tag{5.10}$$

and also the recharged current is zero:

$$i_{Edlcc} = 0 \qquad ;\text{if } \Delta v_{c,\min} \leq \Delta v_c \leq 0 \tag{5.11}$$

5.3 Modified Mathematical Model of the DC Railway for the Verification of the SOC Control of EDLCs

In order to assess the performance and characteristics of EDLCs with the proposed control, the mathematical model presented in Chapter 3 has been modified to consider that all the substations are electrically connected together. The modified model of the DC railway with stationary EDLCs consists of n-nodes and is presented in Figure 5.2. The node voltages $v_{n\text{-}4}$ and $v_{n\text{-}3}$ are connected to the substations, which are modelled by a voltage source E_{ss} and internal conductances $g_{n\text{-}4,0}$ and $g_{n\text{-}3,0}$, respectively. The node n-2 is introduced to model a station where there is no substation and its voltage is $v_{n\text{-}2}$. The stationary EDLCs are connected to the node n-1 with voltage $v_{n\text{-}1}$. If a train is travelling in this section, a new node n is introduced, with voltage v_n. The conductance of the line between the node voltages v_i and v_j is represented by $g_{i,j}$, where i and j are positive integer numbers from 1 to n. The train current and the stationary EDLCs current are i_{train} and i_{Edlc},

respectively. The node voltages $v_{n\text{-}4}$, $v_{n\text{-}3}$,…, v_n are calculated by taking into account the KCLs:

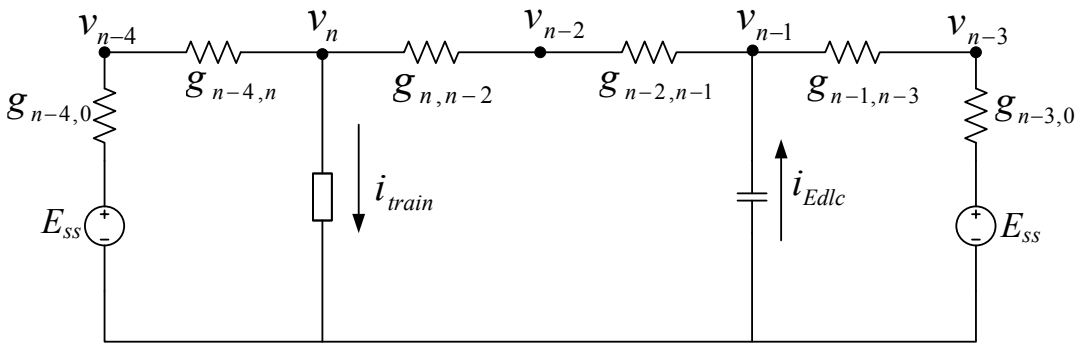

Figure 5.2: The modified model of the DC railway with the train and the stationary EDLCs

- **Node $v_{n\text{-}4}$:** $i_{n\text{-}4,0} = i_{n\text{-}4,n}$

$$\left(E_{ss} - v_{n-4}\right)g_{n-4,0} = \left(v_{n-4} - v_n\right)g_{n-4,n}$$

$$\left(g_{n-4,0} + g_{n-4,n}\right)v_{n-4} - g_{n-4,n}v_n = g_{n-4,0}E_{ss} \tag{5.12}$$

- **Node $v_{n\text{-}3}$:** $i_{n\text{-}3,0} = i_{n\text{-}1,n\text{-}3}$

$$\left(E_{ss} - v_{n-3}\right)g_{n-3,0} = \left(v_{n-3} - v_{n-1}\right)g_{n-1,n-3}$$

$$\left(g_{n-3,0} + g_{n-1,n-3}\right)v_{n-3} - g_{n-1,n-3}v_{n-1} = g_{n-3,0}E_{ss} \tag{5.13}$$

- **Node $v_{n\text{-}2}$:** $i_{n,n\text{-}2} + i_{n\text{-}2,n\text{-}1} = 0$

$$\left(v_{n-2} - v_n\right)g_{n,n-2} + \left(v_{n-2} - v_{n-1}\right)g_{n-2,n-1} = 0$$

$$\left(g_{n,n-2} + g_{n-2,n-1}\right)v_{n-2} - g_{n-2,n-1}v_{n-1} - g_{n,n-2}v_n = 0 \tag{5.14}$$

- **Node $v_{n\text{-}1}$:** $i_{n\text{-}2,n\text{-}1} + i_{n\text{-}1,n\text{-}3} = i_{Edlc}$

$$\left(v_{n-1} - v_{n-2}\right)g_{n-2,n-1} + \left(v_{n-1} - v_{n-3}\right)g_{n-1,n-3} = i_{Edlc}$$

$$-g_{n-1,n-3}v_{n-3} - g_{n-2,n-1}v_{n-2} + \left(g_{n-2,n-1} + g_{n-1,n-3}\right)v_{n-1} = i_{Edlc} \tag{5.15}$$

- **Node v_n:** $i_{n,n-4} + i_{n,n-2} + i_{train} = 0$

$$\left(v_n - v_{n-4}\right)g_{n-4,n} + \left(v_n - v_{n-2}\right)g_{n,n-2} = -i_{train}$$

$$-g_{n-4,n}v_{n-4} - g_{n,n-2}v_{n-2} + \left(g_{n-4,n} + g_{n,n-2}\right)v_n = -i_{train} \tag{5.16}$$

From (5.12) – (5.16), the equations can be written in matrix form of $[\boldsymbol{G}][\boldsymbol{V}] = [\boldsymbol{I}]$:

$$\begin{bmatrix} g_{n-4,0} + g_{n-4,n} & 0 & 0 & 0 & -g_{n-4,n} \\ 0 & g_{n-3,0} + g_{n-1,n-3} & 0 & -g_{n-1,n-3} & 0 \\ 0 & 0 & g_{n,n-2} + g_{n-2,n-1} & -g_{n-2,n-1} & -g_{n,n-2} \\ 0 & -g_{n-1,n-3} & -g_{n-2,n-1} & g_{n-2,n-1} + g_{n-1,n-3} & 0 \\ -g_{n-4,n} & 0 & -g_{n,n-2} & 0 & g_{n,-4,n} + g_{n,n-2} \end{bmatrix} \begin{bmatrix} v_{n-4} \\ v_{n-3} \\ v_{n-2} \\ v_{n-1} \\ v_n \end{bmatrix} = \begin{bmatrix} y_{n-4,0}E_{ss} \\ y_{n-3,0}E_{ss} \\ 0 \\ i_{Edlc} \\ -i_{train} \end{bmatrix} \tag{5.17}$$

where $[\boldsymbol{G}]$ is the conductance matrix, $[\boldsymbol{V}]$ is the node voltage vector, $[\boldsymbol{I}]$ is the current vector and :

$$\begin{aligned} \boldsymbol{G}_{jk} &= -g_{jk} = -g_{kj} \\ \boldsymbol{G}_{jj} &= \sum_{k=0}^{n_y} g_{jk} \end{aligned} \quad , n_y = \text{total number of conductance connected at node } j \tag{5.18}$$

The node voltages v_{n-4}, v_{n-3},…, v_n are calculated from the node voltage vector $[\boldsymbol{V}]$ as follows:

$$[\boldsymbol{V}] = [\boldsymbol{G}]^{-1}[\boldsymbol{I}] \tag{5.19}$$

From (5.15) and (5.17), the currents of the stationary EDLCs change depending on the piece-wise linear SOC control described in the previous section.

The solution of the set of equation of (5.19) gives the nodal voltages of the network, which in turn allows the calculation of the energy consumption of the substations, the

losses of the conducting rails and rails, the internal losses of the substations, the energy absorbed by the train and the energy of the storage.

- Energy consumptions of substations: $En_{sub,con}$

  From Figure 5.2, the currents of the substations are calculated as follows:

$$\begin{aligned} i_{s,n-4} &= (E_{ss} - v_{n-4}) g_{n-4,0} \\ i_{s,n-3} &= (E_{ss} - v_{n-3}) g_{n-3,0} \end{aligned} \tag{5.20}$$

  The energy consumptions of substations are written as follows:

$$En_{sub,con} = \int_0^t E_{ss} i_{s,n-4}(t)dt + \int_0^t E_{ss} i_{s,n-3}(t)dt \tag{5.21}$$

- Energy losses by the conducting rails and rails and the internal losses of the substations: $En_{line,con}$

$$\begin{aligned} En_{line,con} = &\int_0^t (E_{ss} - v_{n-4}(t))^2 g_{n-4,0} dt + \int_0^t (E_{ss} - v_{n-3}(t))^2 g_{n-3,0} dt \\ &+ \int_0^t (v_{n-4}(t) - v_n(t))^2 g_{n-4,n} dt + \int_0^t (v_n(t) - v_{n-2}(t))^2 g_{n,n-2} dt \\ &+ \int_0^t (v_{n-2}(t) - v_{n-1}(t))^2 g_{n-2,n-1} dt + \int_0^t (v_{n-1}(t) - v_{n-3}(t))^2 g_{n-1,n-3} dt \end{aligned} \tag{5.22}$$

- Train energy: $En_{train,con}$

$$En_{train,con} = \int_0^t v_n(t) i_{train}(t)dt \tag{5.23}$$

- EDLCs energy: $En_{Edlc,con}$

$$En_{Edlc,con} = \int_0^t v_{n-1}(t) i_{Edlc}(t)dt \tag{5.24}$$

The results of the optimisation algorithm have been verified using the law of conservation of energy, which states that the total energy of the traction system is equal to zero:

$$En_{sub,con} + En_{Edlc,con} - En_{train,con} - En_{line,con} = 0 \tag{5.25}$$

The constraint in (5.25) is expressed such that the summation of energy supported by the EDLCs and substations is equal to the energy drawn by the train and line losses at every step of the train travelling. This constraint is used to verify the zero of the summation of the entire energy flow in the DC light railway systems with the additional energy support by EDLCs. If the constraint is unsatisfied, it will have something wrong in the algorithm which needs carefully to recheck and modify the equations and algorithm of the piece-wise linear SOC control.

5.4 Results from the Piece-wise Linear SOC Control and Discussion

The performance of the piece-wise linear SOC control of stationary EDLCs has been evaluated by two criteria: the impact of normal conditions with a different initial SOC and a different average steady state SOC of the EDLCs; and the impact of the variations in train loading and friction force with a different initial SOC of the EDLCs with only steady state SOC at 100%, as presented in the following subsection.

5.4.1 Evaluation with Normal Conditions of Train Motion

The initial SOC of the EDLCs, including 100%, 50% and 0%, is implemented to the criteria of the different average steady state SOC of the EDLCs, which is 100% and other in this thesis. These criteria can evaluate and compare the performance of EDLCs based on the proposed controller to improve the efficiency of the DC light railway in terms of energy saving and energy loss reduction.

A. Steady state at 100% SOC

The minimum and maximum currents and the deviation voltages of stationary EDLCs, shown in Table 5.1, can be obtained from the current profiles of the stationary EDLCs when the train is travelling forward and returning, which are presented in Figure 4.26 and Figure 4.27, and the voltage profiles of stationary EDLCs, presented in Figure 4.31 and Figure 4.32. The optimal positions of stationary EDLCs are fixed and based on the positions indicated in the single line diagram of Figure 4.25. The results show that the discharging current of the stationary EDLCs in the section 3 is the highest, whereas the maximum recharge current is almost the same for all the EDLCs. The maximum voltage deviation is 197 V, which is 26% of the nominal voltage.

Table 5.1: Actual currents and voltage deviations of stationary EDLCs placed at the optimal positions

EDLCs	Location (km)	Discharging				Recharging			
		$\Delta v_{d,\min}$ (V)	$\Delta v_{d,\max}$ (V)	$I_{Edlcd,\min}$ (A)	$I_{Edlcd,\max}$ (A)	$\Delta v_{c,\min}$ (V)	$\Delta v_{c,\max}$ (V)	$I_{Edlcc,min}$ (A)	$I_{Edlcc,max}$ (A)
1	2.50	10	150	0	1,438	-20	-183	0	-1,502
2	7.93	6	147	0	1,562	-24	-195	0	-1,502
3	13.42	4	124	0	1,692	-15	-194	0	-1,502
4	19.09	5	175	0	1,480	-23	-197	0	-1,502

From Table 5.1, the piece-wise linear characteristics of the SOC control can be calculated, as shown in Figure 5.3 and Figure 5.4, for a train travelling in the forward and reverse direction, respectively. The solid lines show the piece-wise linear SOC control of the stationary EDLCs for both the train travelling forward and returning, based on the criteria of discharging and recharging energy shown in Table 5.1. The mark symbols of each EDLC present the actual currents for both discharging and recharging energy when the train travels forward and when it returns. It is clear that the actual currents of each EDLC are controlled by the piece-wise linear SOC controls presented along the linear solid lines.

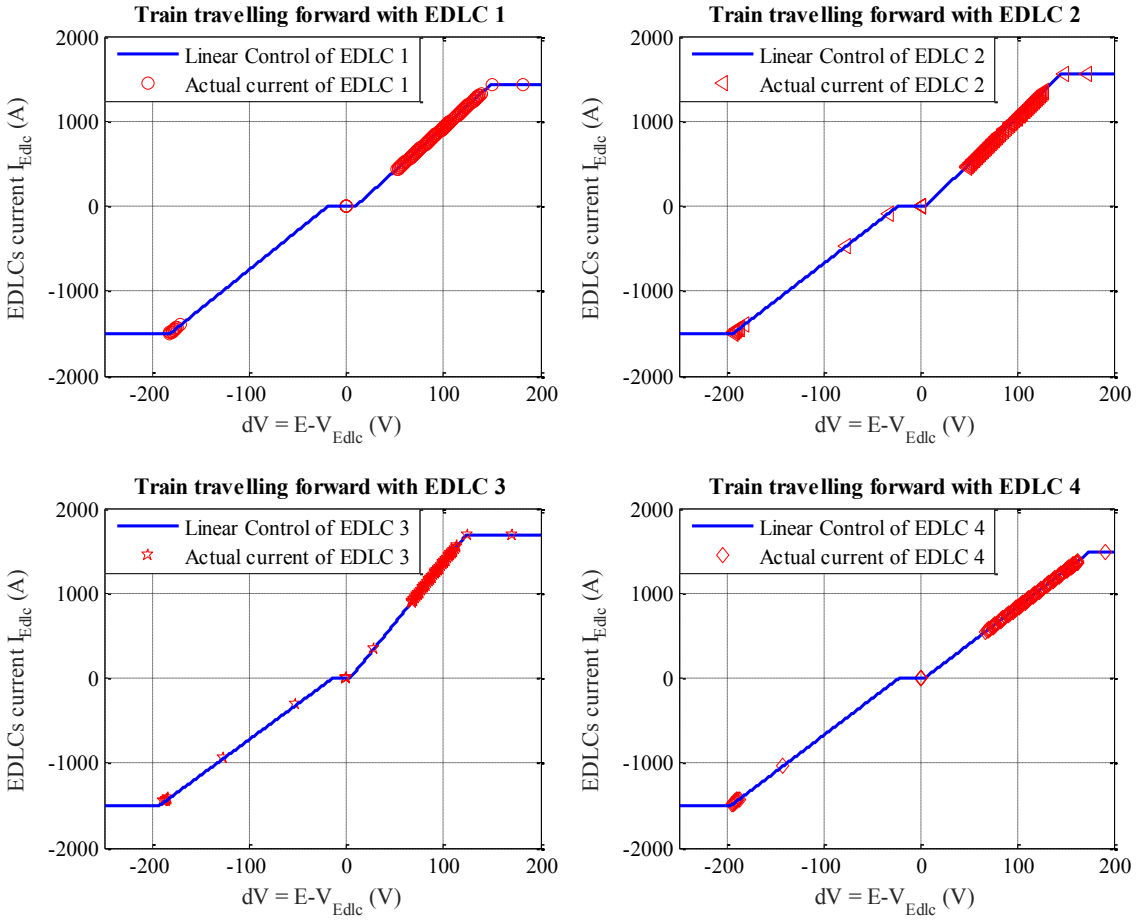

Figure 5.3: Characteristic of piece-wise linear SOC control of stationary EDLCs of the train travelling forward: all EDLCs start from 100% SOC

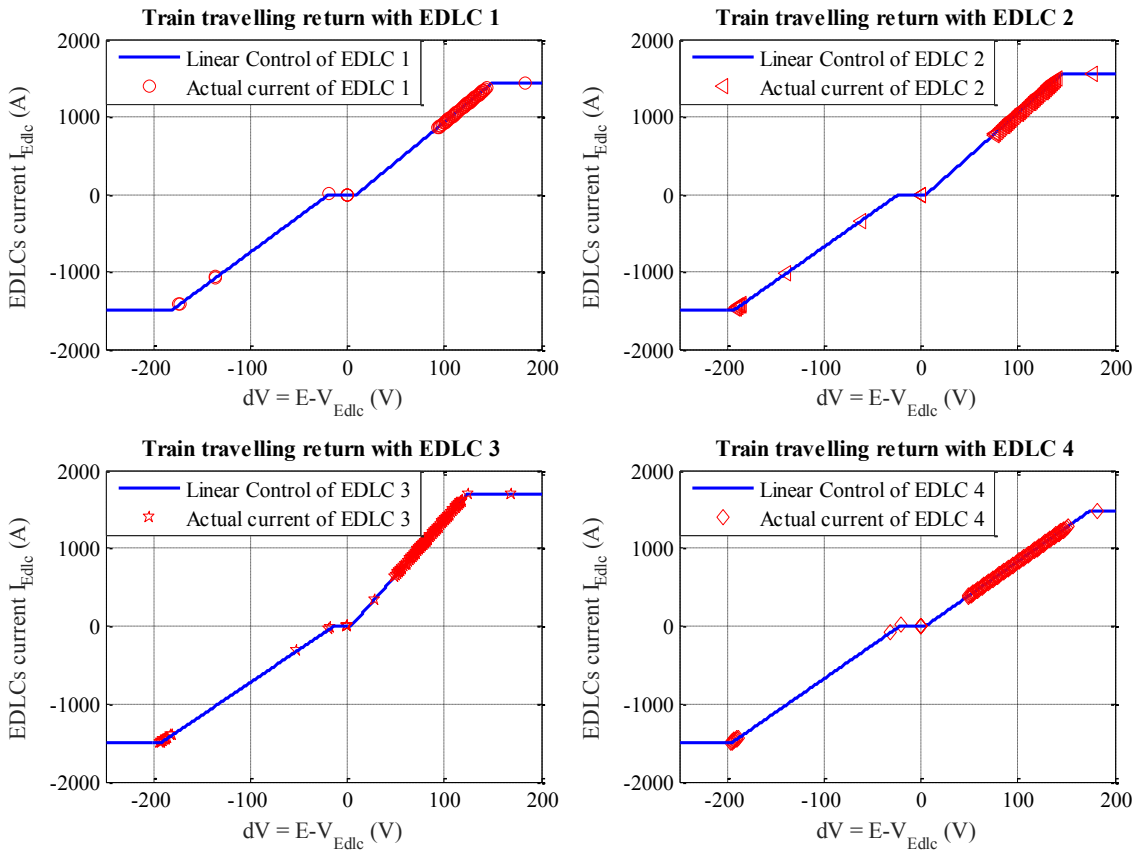

Figure 5.4: Characteristic of piece-wise linear SOC control of stationary EDLCs of the return journey: all EDLCs start from 100% SOC

Figure 5.3 and Figure 5.4 show the slopes of the characteristics and the voltage deviations are basically the same, regardless of the direction of travel of the train. In order to see the impact of the initial SOC of the EDLCs on the control, the simulations are repeated for different initial levels of SOC, i.e. 100%, 50% and 0% for all the storage devices. For all the simulations, it is assumed that the train starts at the first substation and completes several round-trip journeys, i.e. the train travels from section 1 to section 4 and then goes back in the opposite direction. The journey time of the train on a single trip is about 21.23 minutes (22 km) and for a round -trip it is about 42.46 minutes (44 km).

The results of the simulation for an initial SOC of 100% and one single round-trip are shown in Figure 5.5. This means that the initial energies stored in the EDLCs are 32, 38, 31 and 31 kWh, respectively.

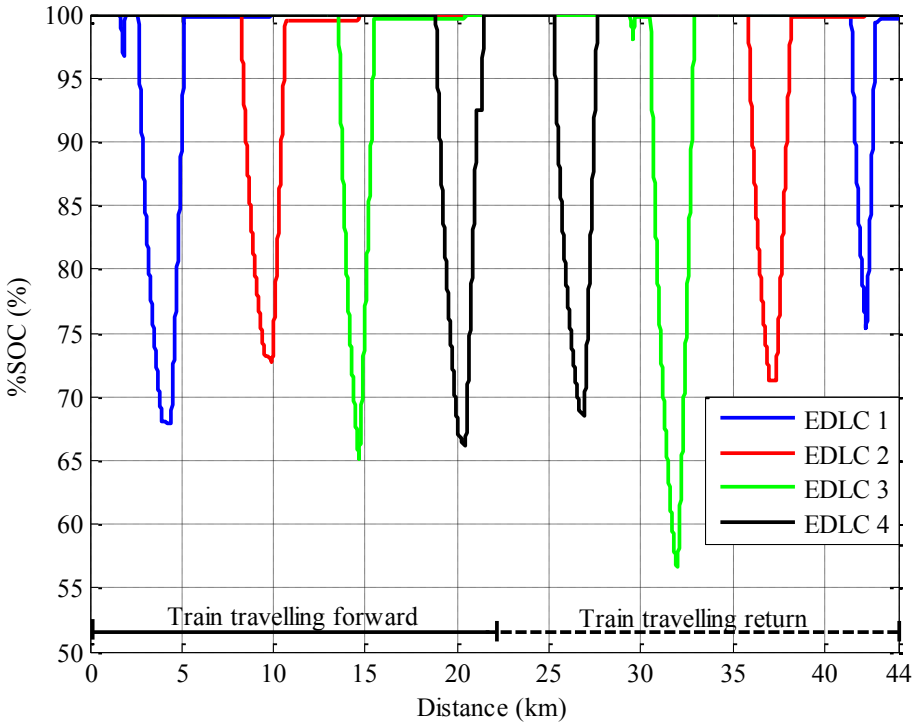

Figure 5.5: Percentage SOC of stationary EDLCs for a round-trip of the train journey: all EDLCs start from 100% SOC and steady state of SOC at 100%

The amount of energy discharged and recharged by each individual EDLC depends on the position of the train and the characteristic piece-wise linear SOC control. The results show that the EDLCs operate with little overlap. This is because there is only one energy storage per section and the contribution of the storage of the other section is strongly limited by the presence of substations. This confirms our hypothesis that the optimisation process does not need to consider the influence of the other sections of the railway electrification.

It can be seen from the simulation that when all stationary EDLCs are fully charged at the beginning, not all the braking energy can be recovered and the surplus regenerative energy is dissipated by the on-board electrical braking resistors.

The return journey of the train, depicted in the second half of the figure, shows a similar diagram of the SOCs, but obviously in a reverse sequence. The maximum percentages of energy used by the EDLCs for a complete round-trip for this simulation are 32%, 28%, 43% and 33%, respectively. This result shows that the optimisation algorithm made a good prediction of the energy needed by each EDLC, since they are discharging with similar proportions.

In order to better understand the impact of the initial SOC of EDLCs on the discharge-recharge cycles, the round-trip journey of the train is repeated twice, as shown in Figure 5.6. The SOCs in the second-trip are the same as those of the first round-trip, highlighting that if the initial SOC is 100% a steady state is achieved within one round-trip.

It is not appropriate that the SOC of EDLCs reaching the steady state at 100% because EDLCs have no an available capacity for storing either uncertain or certain regenerative braking energy. This means that the surplus energy from the train braking will be dissipated by the electric braking resistance. A reason why SOC of EDLCs reaching the steady state at 100% based on the piece-wise linear SOC control of EDLCs in (5.2) – (5.11) is that the recharging energy rate of EDLCs is higher than the discharging energy rate. Therefore, the SOC of EDLCs is always reached the steady state at 100% fully charged even the initials SOC of EDLCs are 0% or 50%. To improve the algorithm of the piece-wise linear SOC control and to avoid the SOC of EDLCs reaching the steady state

at 100%, the recharging energy rate of EDLCs is limited with the proportional gain controller K_{soc} will be presented in the next subsection.

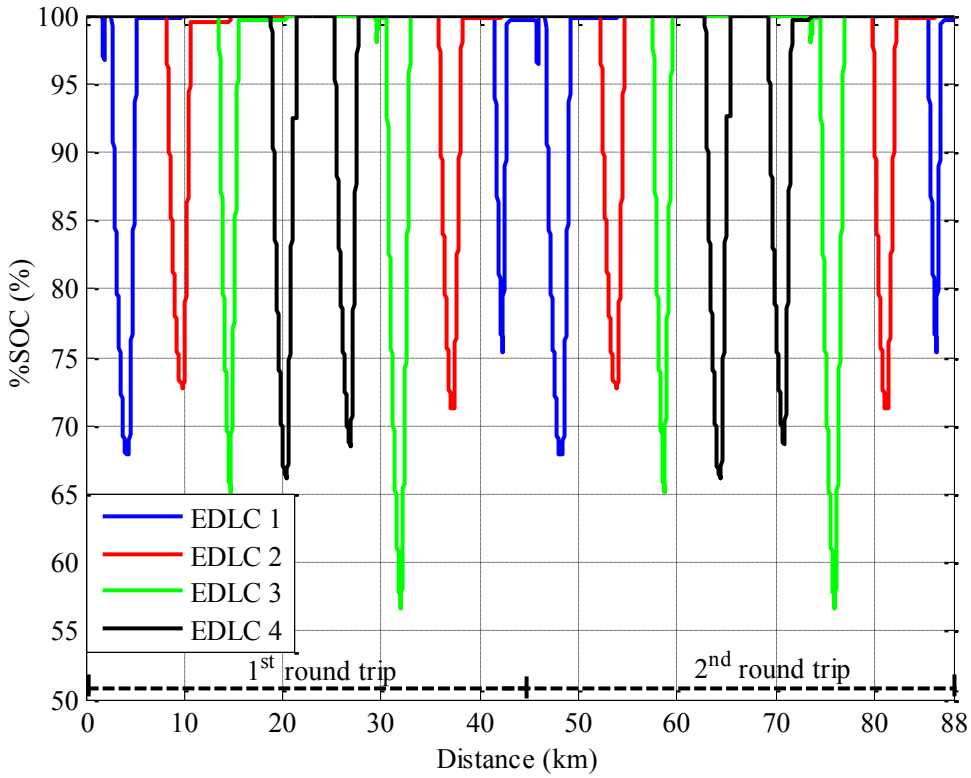

Figure 5.6: Percentage SOC of stationary EDLCs for two round-trips of the train journey: all EDLCs start from 100% SOC and steady state of SOC at 100%

A second case has been simulated with the initial SOC equal to 50% for all the stationary EDLCs and two round-trips, as shown in Figure 5.7. During the first round-trip, there is not much support from the EDLCs and, hence, the higher voltage drops on the line pushes more current to recharge the storage. All EDLCs are 100% fully charged at the end of the first single-trip (after 22 km). EDLCs 3 and 4 are fully charged before EDLCs 1 and 2. This can be explained by the fact that EDLCs 3 and 4 are active only when the train is going past sections 3 and 4, whereas they are recharged from the beginning of the journey. Steady-state conditions are obtained at the end of the first single-trip (after 22 km), when the SOC of all EDLCs is at 100% full charge. During the second round-trip of the train,

the SOC diagrams for all the EDLCs are the same as those presented in Figure 5.6 for an initial SOC of 100%.

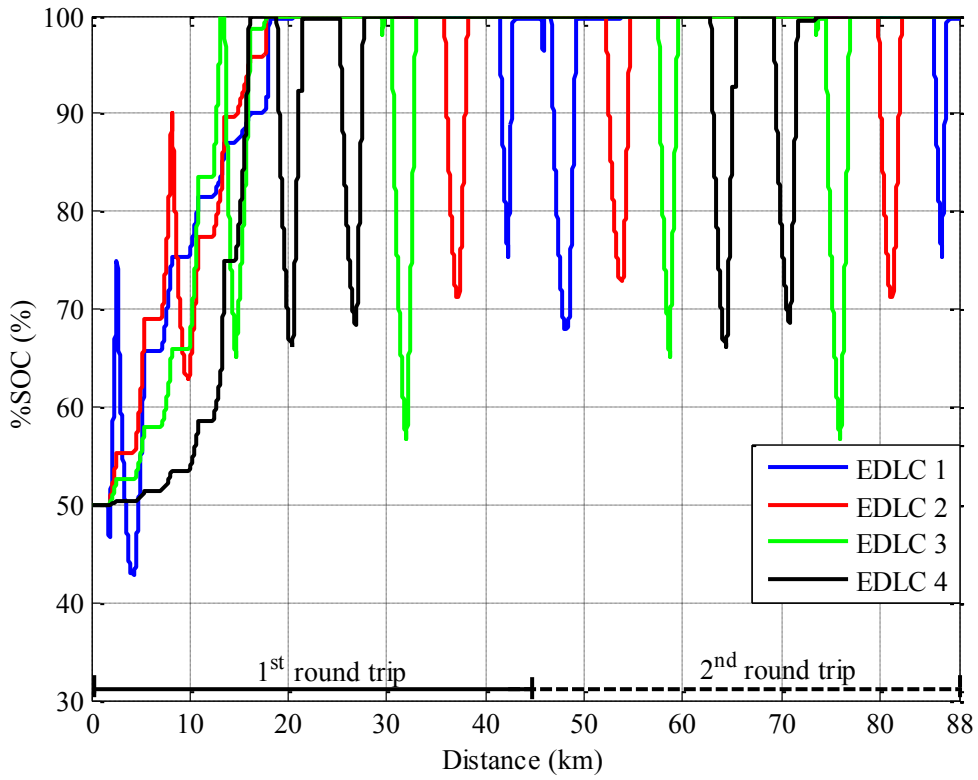

Figure 5.7: Percentage SOC of stationary EDLCs for the two round-trips of the train journey: all EDLCs start from 50% SOC and steady state of SOC at 100%

Figure 5.8 and Figure 5.9 present the characteristic of the piece-wise linear SOC control for an initial SOC of 50% and the train travelling forward and returning only on the first round-trip. The results show that the characteristic of the piece-wise linear SOC control of the stationary EDLCs is the same as those in Figure 5.3 and Figure 5.4, although, when the initial SOC is 50%, the EDLCs are recharged with a low current and voltage drop for the first round-trip of the train.

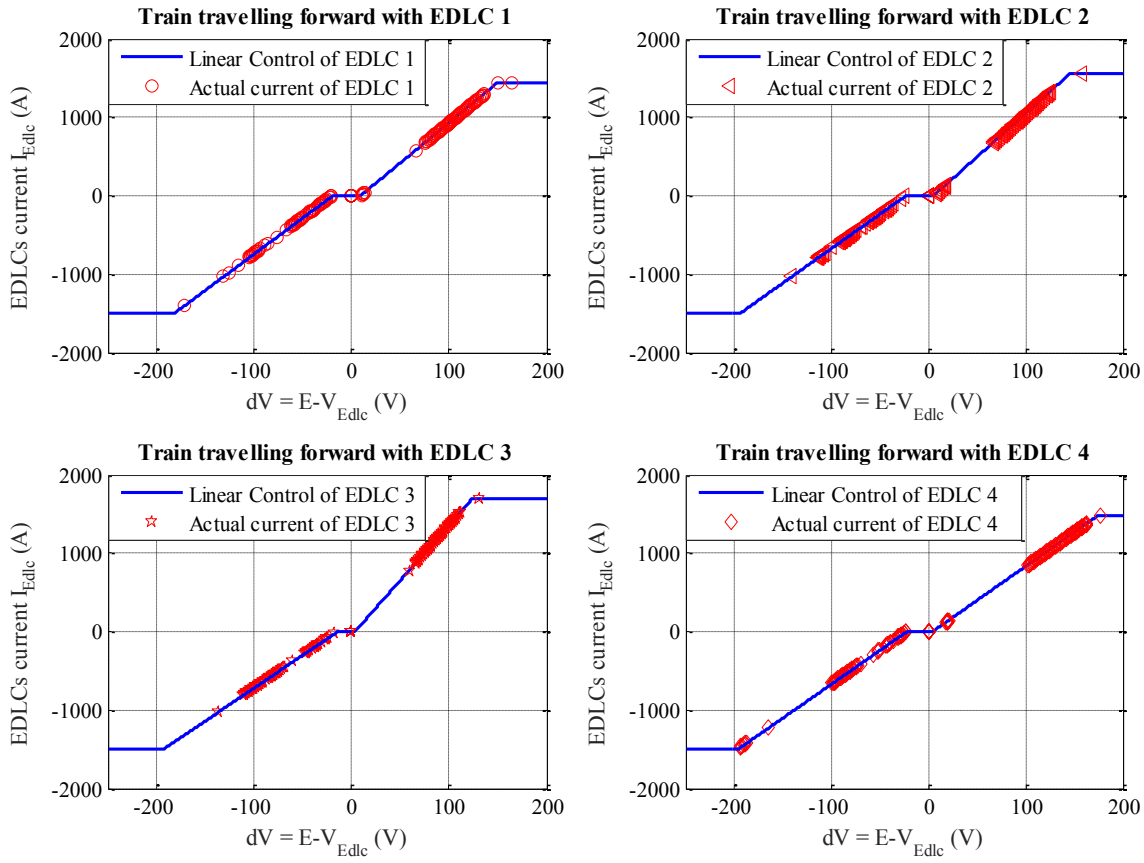

Figure 5.8: Characteristic of piece-wise linear SOC control of stationary EDLCs for the 1st round-trip of the train travelling forward: all EDLCs start from 50% SOC

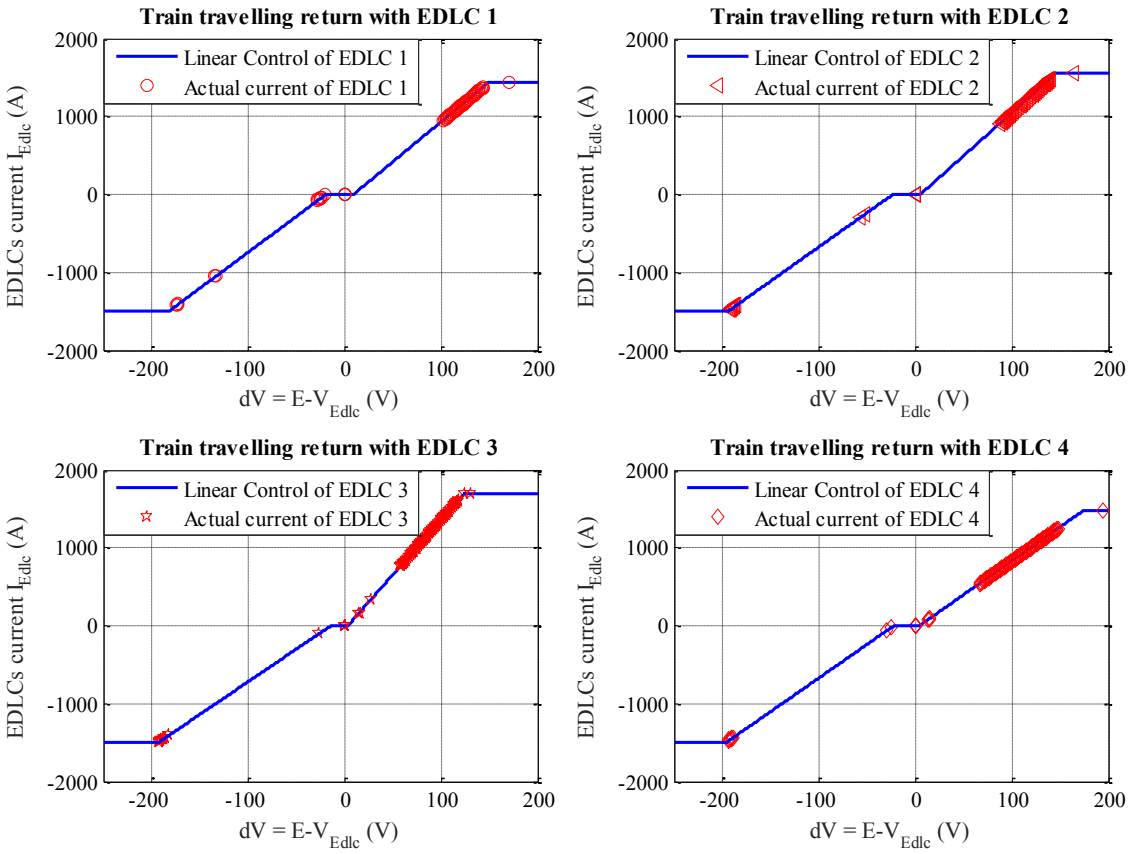

Figure 5.9: Characteristic of piece-wise linear SOC control of stationary EDLCs for the 1st round-trip of the return journey: all EDLCs start from 50% SOC

Finally, a third case with initial SOC of 0% has been simulated for two round-trips of the train, as shown in Figure 5.10. The situation is similar to the case of initial SOC of 50%, although now the recharge of the EDLCs takes more time. In fact, All EDLCs are fully charged at the end of the first round-trip (after 44 km). The duty cycles of the SOC of all EDLCs are approaching the steady-state at the end of the first round-trip (after 44 km).

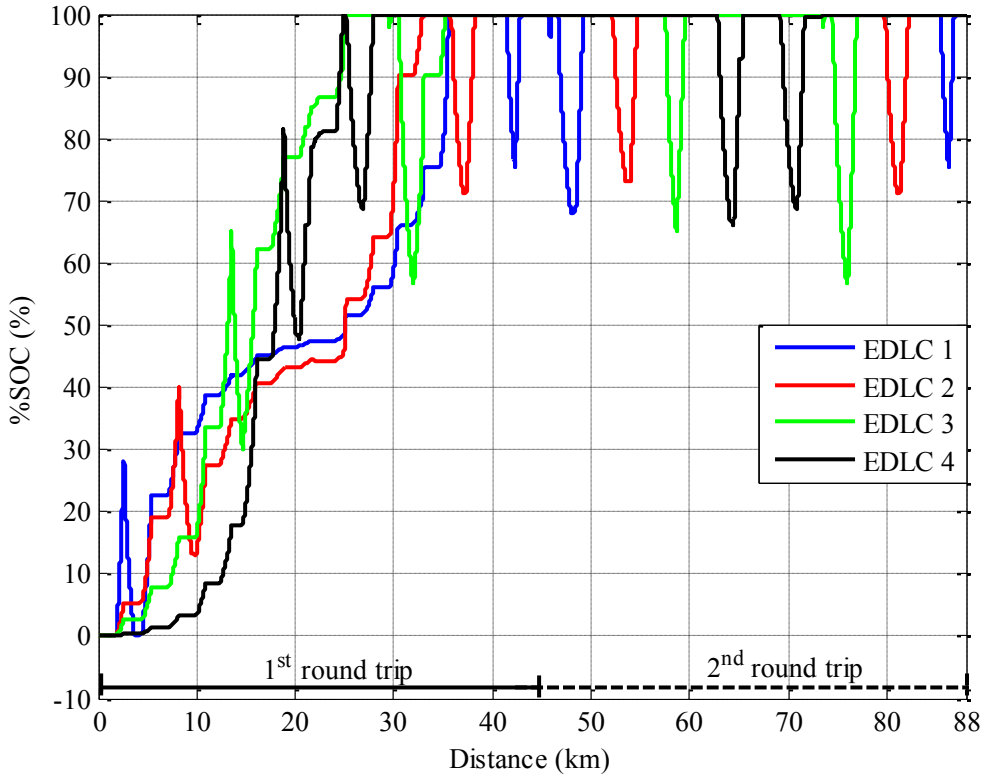

Figure 5.10: Percentage SOC of stationary EDLCs for the two round-trips of the train journey: all EDLCs start from 0% SOC and steady state of SOC at 100%

Figure 5.11 and Figure 5.12 present the characteristic of the piece-wise linear SOC control of EDLCs for an initial SOC of 0%. The results show that the characteristic of the piece-wise linear SOC control of stationary EDLCs is the same as in Figure 5.3 and Figure 5.4, but the EDLCs are recharged with a current lower than in the case of initial SOCs of 100%.

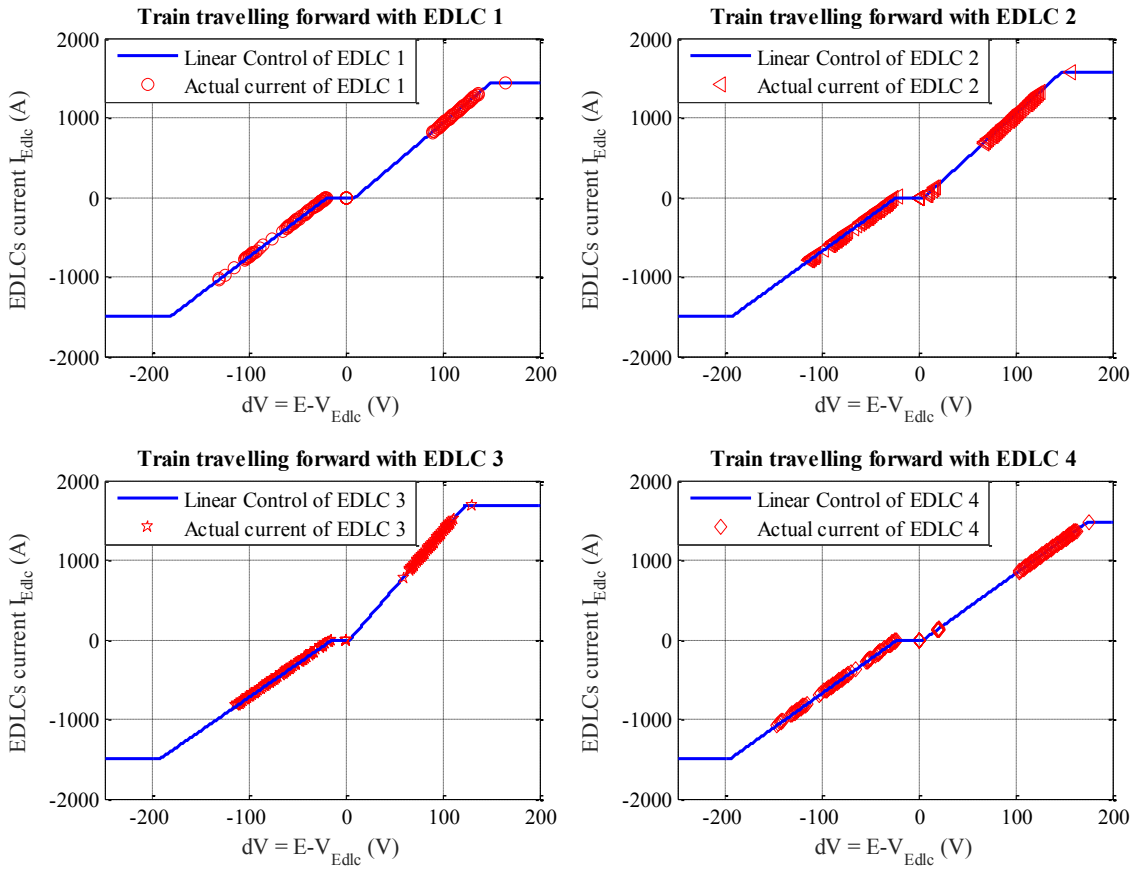

Figure 5.11: Characteristic of piece-wise linear SOC control of stationary EDLCs for the 1st round-trip of the train travelling forward: all EDLCs start from 0% SOC

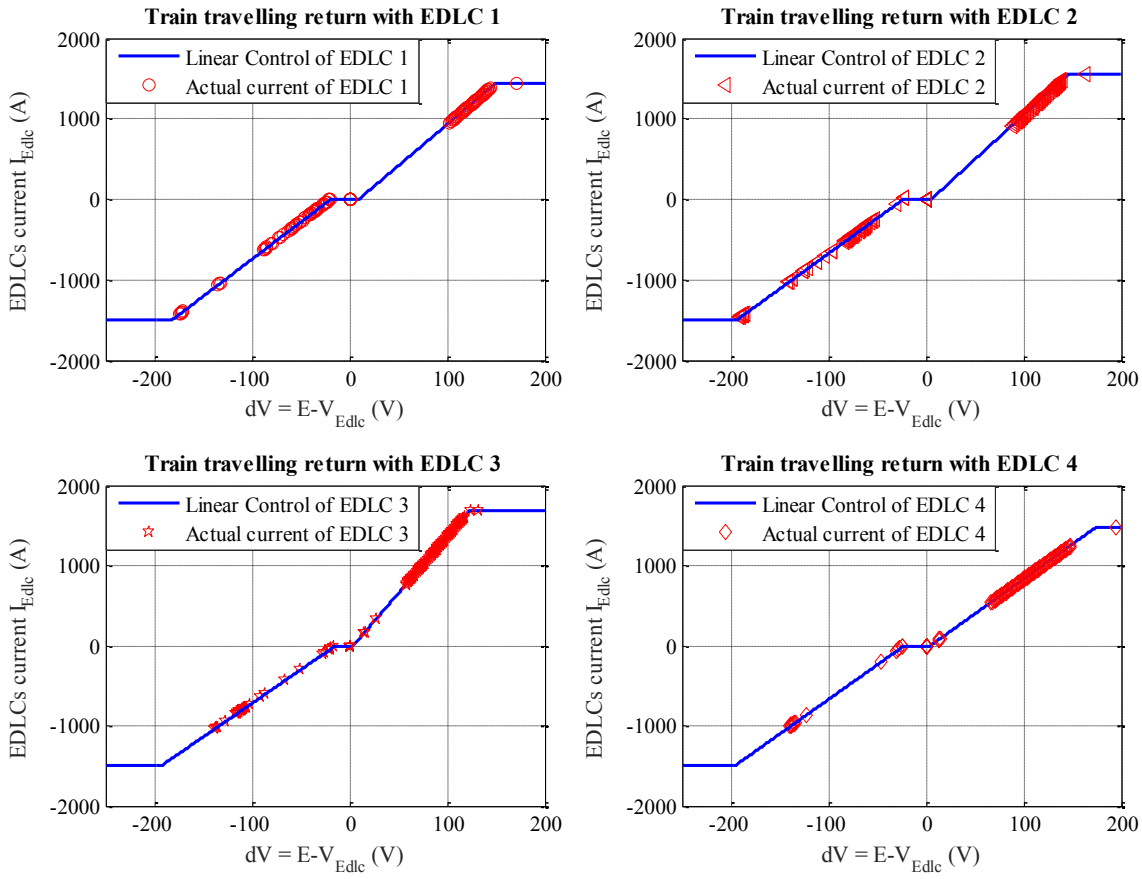

Figure 5.12: Characteristic of piece-wise linear SOC control of stationary EDLCs for the 1st round-trip of the return journey: all EDLCs start from 0% SOC

From these simulation results it is clear that the initial SOC is not an issue for the applicability of the proposed controller, because the discharge-recharge profiles of the EDLCs approach steady-state conditions within the end of the first round-trip of the train.

B. Steady state at 79% SOC

Based on the data in Table 5.1, the characteristics of piece-wise linear SOC control of stationary EDLCs of the train travelling forwards and in return with the initial SOC of 100%, 50% and 0% of the steady state at 100% SOC and the results in Figure 5.6, Figure 5.7 and Figure 5.10 shown that the steady state at 100% SOC is unaffected by the initial

SOC, because it can approach the steady-state conditions within the end of the first round-trip of the train.

The average SOC of EDLCs depends on the load demands of the train, and the criteria of the control algorithm. However, the load demands are unable to predict during the train in service, it relates to the number of passenger. Therefore, it is possible to change the SOC control in Figure 5.1 by modifying the minimum voltage deviation, $\Delta v_{d,\min}$ for discharging and $\Delta v_{c,\min}$ for charging energy which can be moved left and right between the nominal value by as follows:

$$\Delta v_{\min,1} = \Delta v_{\min,0} - K_{soc}\left(\mathrm{SOC}_{int} - \mathrm{SOC}_{ave}\right) \tag{5.26}$$

where $\Delta v_{\min,1}$ is an updated minimum voltage deviation, $\Delta v_{\min,0}$ is a nominal minimum voltage deviation, K_{soc} is a proportional gain and constant, SOC_{int} is an instantaneous SOC and SOC_{ave} is an average SOC.

An initial SOC of 100% has been chosen to find the optimal average steady state SOC of EDLCs. From (5.26), after several trials, the constant K_{soc} of each EDLC for discharging and charging energy are given in Table 5.2.

Table 5.2: The constant K_{soc} of each EDLC for discharging and charging energy

Mode	Discharging energy				Charging energy			
EDLC	$EDLC_1$	$EDLC_2$	$EDLC_3$	$EDLC_4$	$EDLC_1$	$EDLC_2$	$EDLC_3$	$EDLC_4$
K_{soc}	1	1	1	1	30	13	12	30

Based on (5.26), the percentage SOC of stationary EDLCs for two round-trips of the train journey of the average steady state SOC at 100% is shown in Figure 5.13. From the analysis, the optimal average steady state SOC is at 79%, which the percentage SOC of stationary EDLCs for two round-trips of the train journey shows in Figure 5.14.

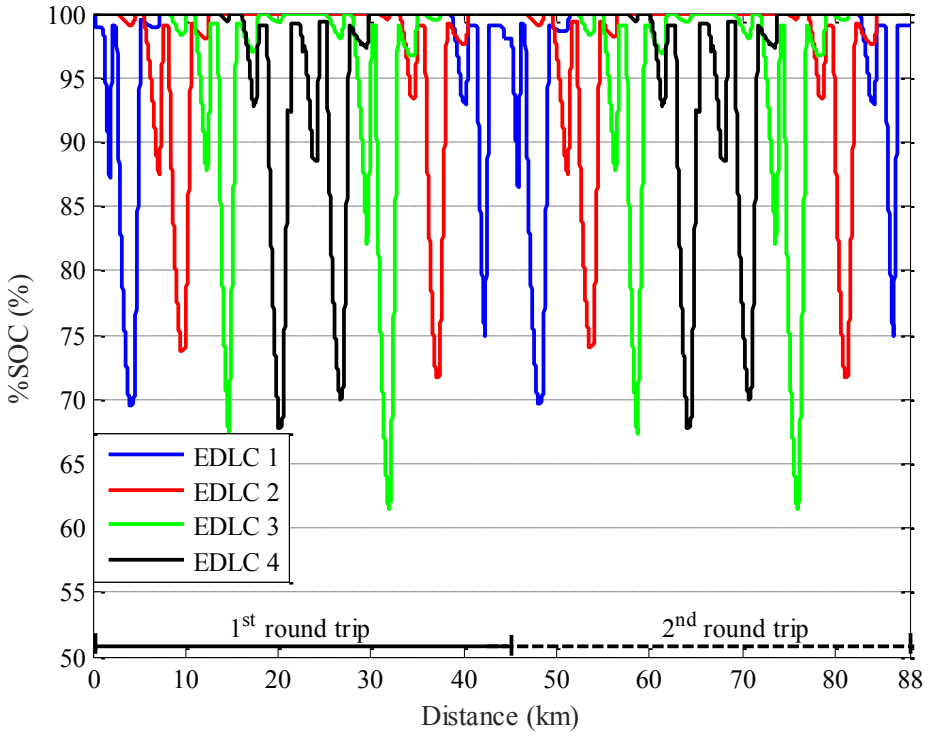

Figure 5.13: Percentage SOC of stationary EDLCs for two round-trips of the train journey: all EDLCs start from 100% SOC and the average steady state SOC at 100%

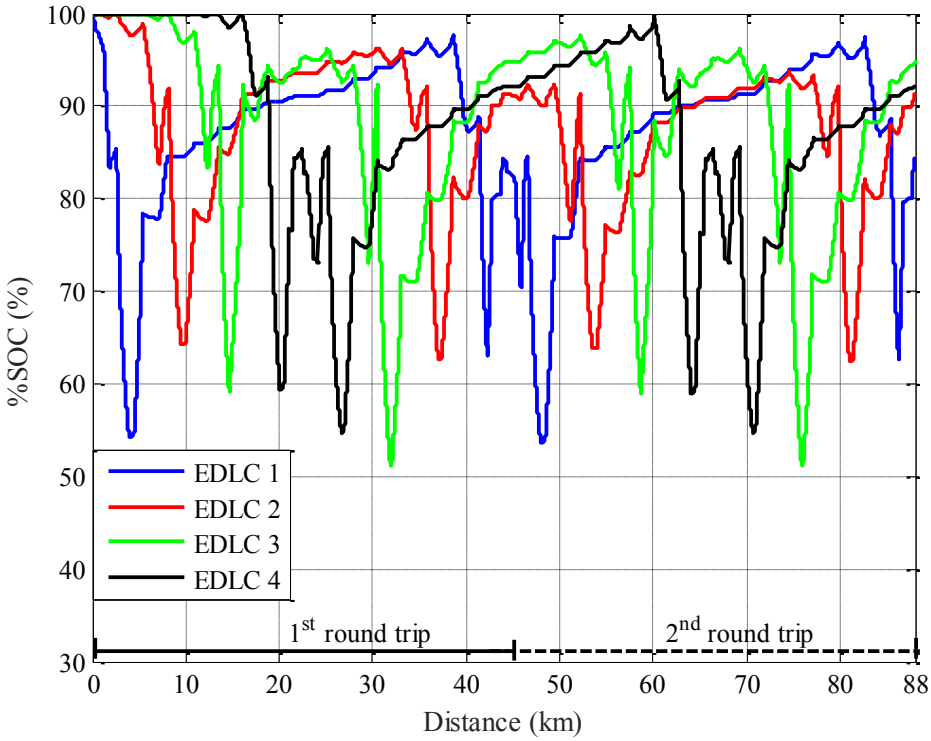

Figure 5.14: Percentage SOC of stationary EDLCs for two round-trips of the train journey: all EDLCs start from 100% SOC and the average steady state SOC at 79%

The percentage SOC of EDLCs with the steady state SOC at 100% in Figure 5.14 is always kept at 100% fully charged because the average SOC is defined as 100%. At some points that the percentage of SOC of all EDLCs are at 100% fully charged, therefore, the braking energy has to be dissipated by the braking resistance on-board. A 6.2% of braking resistance energy is drawn by the braking resistance in comparison with the substation energy of 1,012 kWh as shown in Figure 5.15.

In Figure 5.14, there are no percentages SOC of EDLCs approaching at 100% when the SOC is at the steady state after the first round-trip. This means that all EDLCs have reserved an extra storage for an extra energy from the uncertain braking of the single train. In practical applications, if there are SOC of one or two EDLCs approaching at 100% fully charged, the other three or two EDLCs that the SOC are not fully charged yet able to charge and extra energy from the uncertain braking of the single train. Therefore, there is a very small braking energy dissipated by the braking resistance. With the average steady state SOC at 79%, a 0.3% of the braking resistance energy is measured in comparison with the substation energy as shown in Figure 5.16.

From the analysis, there are also no percentages SOC of EDLCs below 50% with the average steady state SOC at 79%. At the SOC below 50%, EDLCs is charged energy with a half of the nominal voltage and double of the nominal current, this means that the internal loss of EDLCs will be increased by four time of the nominal condition.

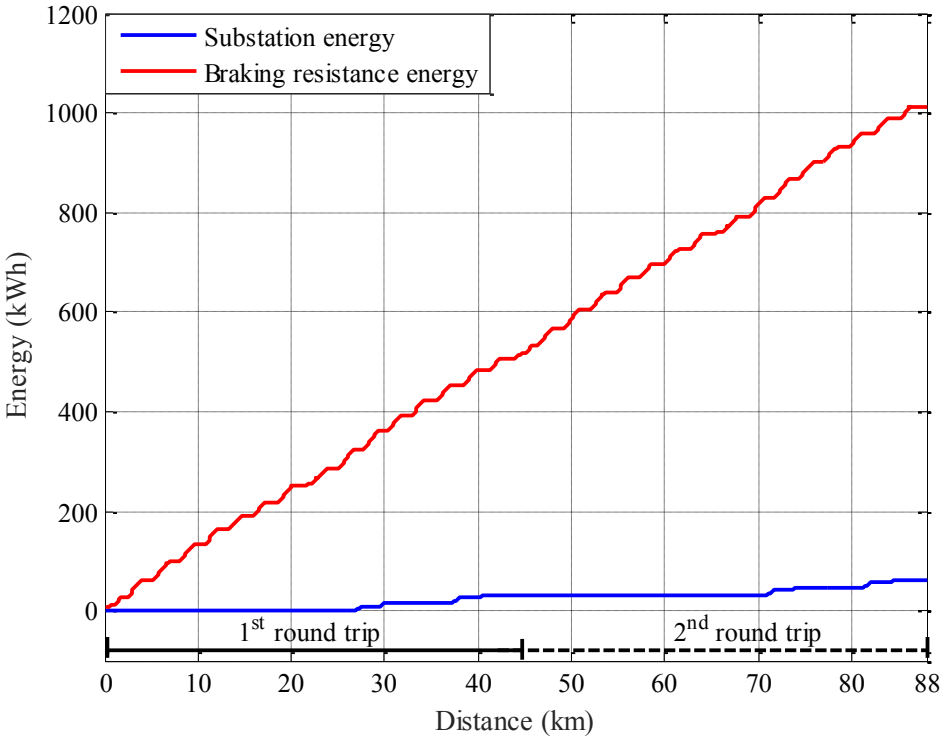

Figure 5.15: Substation energy and braking resistance energy for two round-trips of the train journey: all EDLCs start from 100% SOC and steady state of SOC at 100%

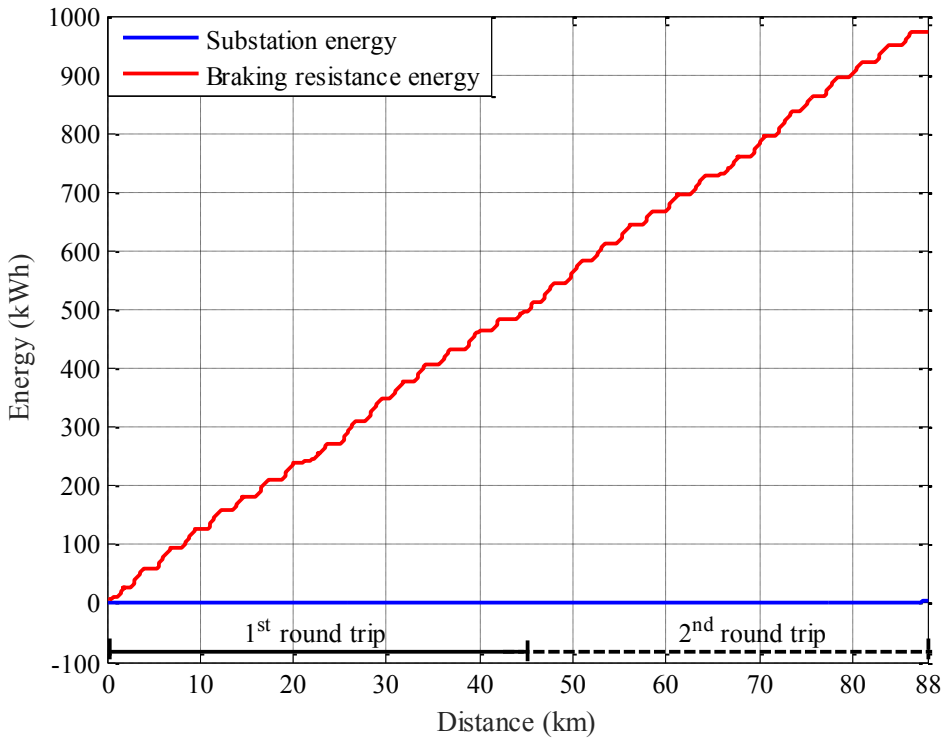

Figure 5.16: Substation energy and braking resistance energy for two round-trips of the train journey: all EDLCs start from 100% SOC and steady state of SOC at 100%

5.4.2 Evaluation by Variations of the Train Loading and Friction Force

To further verify the performance of the proposed controller, the characteristics of the train in terms of loading and friction force have been varied from the nominal conditions.

A. Variation of the train loading

Using the train data presented in Table 4.3, the weight of the train is 135.90 tonnes, with 4 cars and 272 seats. The dimensions of each coach are 19.83 m in length and 2.82 m in width. The average weight of a passenger is assumed to be 70 kg. Four main types of train loading have been considered in this work (Connor, 2011):

- AW0: empty weight;
- AW1: weight with seated passenger load;
- AW2: weight with average peak-hour passenger load, 4-5 passengers per m^2;
- AW3: crush loaded weight, where there are 6, 6-7 or 8 passengers per m^2 (8 passengers per m^2 preferred in this thesis).

The resulting train weights for each loading type are shown in Table 5.3.

Table 5.3: The train loading variation

Loading types	Total loading weights (tonnes)
AW0	135.90
AW1	154.94
AW2	233.06
AW3	280.10

Based on the results of the previous section, the stationary EDLCs reach steady-state conditions within one round-trip of the train motion; regardless of the initial SOC. Therefore, the following simulations are limited to one round-trip of the train to explore the effect of train loading variation.

Figure 5.17 shows the bar chart of the total energy supplied by the substations for the four loading conditions and initial SOCs of 100%, 50% and 0%, and the results are compared with the case without EDLCs. As expected, the total energy of the substations increases with the increments of train loading. When stationary EDLCs are employed and the initial SOCs are 100%, 50% and 0%, the average of the total energy supplied by the substations decreases for all 4 loading conditions by 27%, 27% and 26%, respectively. The energy support from the EDLCs is almost the same, regardless of the initial SOC.

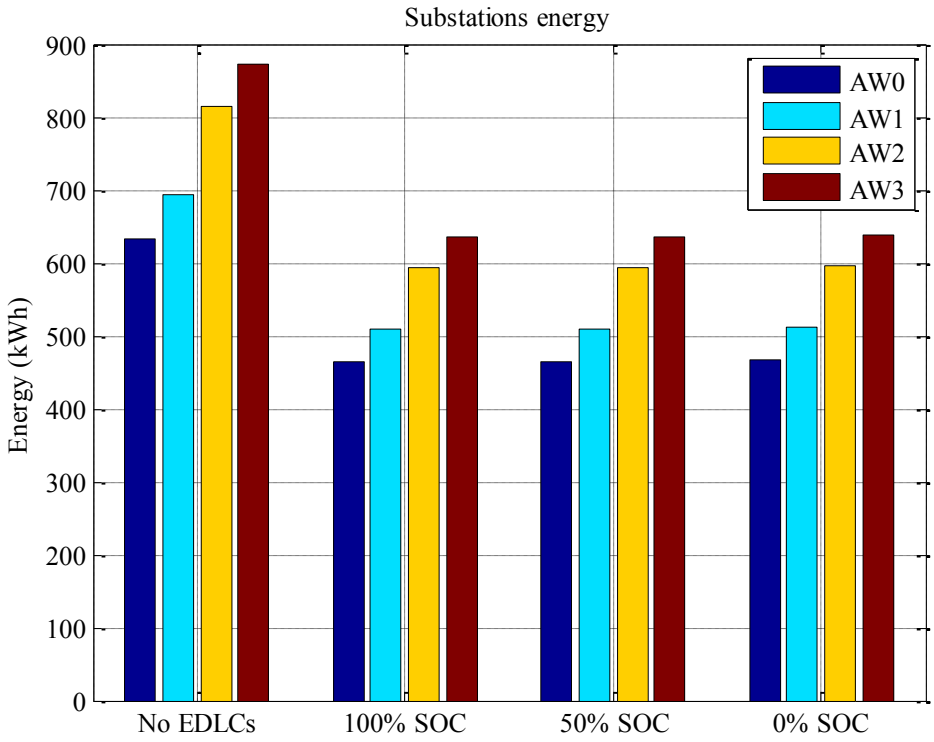

Figure 5.17: Total energy consumptions of the train loading variations with different initial SOC of stationary EDLCs

Figure 5.18 shows the bar chart of the total energy losses obtained from resistance of the rails and conducting rails and the on-board braking resistor (if all EDLCs are fully charged) based on the train loading variation tests and for initial SOCs of 100%, 50% and 0%, and without EDLCs. Also in this case, the total energy losses increase with the increments in train loading. When stationary EDLCs are employed and the initial SOCs

are 100%, 50% and 0%, the average total energy loss is reduced by 24%, 30% and 51%, respectively. This means that the lower the initial SOC is the lower the total energy losses. Obviously, this is valid only for the first round-trip before the EDLCs reach steady-state conditions. However, this result indicates that different control strategies could be adopted to deliberately keep the SOC of the EDLCs under 100% to reduce the energy losses. This is mainly because when the SOC of EDLCs is around 100%, there is a lower chance of recovering the regenerative braking energy and, hence, a more frequent use of the braking resistor.

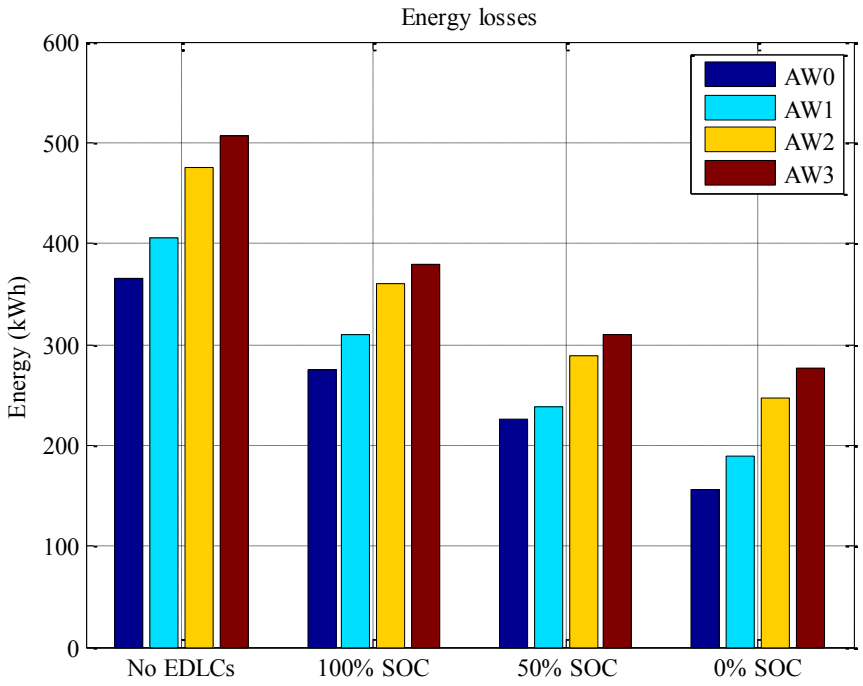

Figure 5.18: Energy losses of the train loading variations with different initial SOC of stationary EDLCs

B. Variation of the friction force

The friction force of a train is a function of the train speed, v, and can be mathematically modelled by the Davis equation, i.e. $F = a + bv + cv^2$, where a, b, and c are constant

coefficients. The increments of the friction force are modelled by increasing the Davis coefficients, as shown in Table 5.4.

Table 5.4: Variation of the friction force by increasing Davis coefficients

% Increasing	Davis coefficients		
	a	*b*	*c*
Normal condition	2.2024	0.0489	0.0043
20% increase	2.6429	0.0587	0.0051
60% increase	3.5238	0.0783	0.0069
100% increase	4.4048	0.0979	0.0086

Similar to the simulations with a variation of the train loading, only one round-trip of the train is simulated to verify the robustness of the piece-wise linear SOC control against variation in the friction force.

Figure 5.19 shows the bar chart of the total energy supplied by the substations when the friction force is varied for initial SOCs of 100%, 50% and 0%, and without the EDLCs. As expected, the energy supplied by the substations increases with the friction force from 633 kWh in the normal case to 711 kWh. The energy supplied by the substations, which the initial SOCs are 100%, 50% and 0%, is slightly affected by the increments in friction force and the average energy saving is equal to 27%, 27% and 26%, respectively.

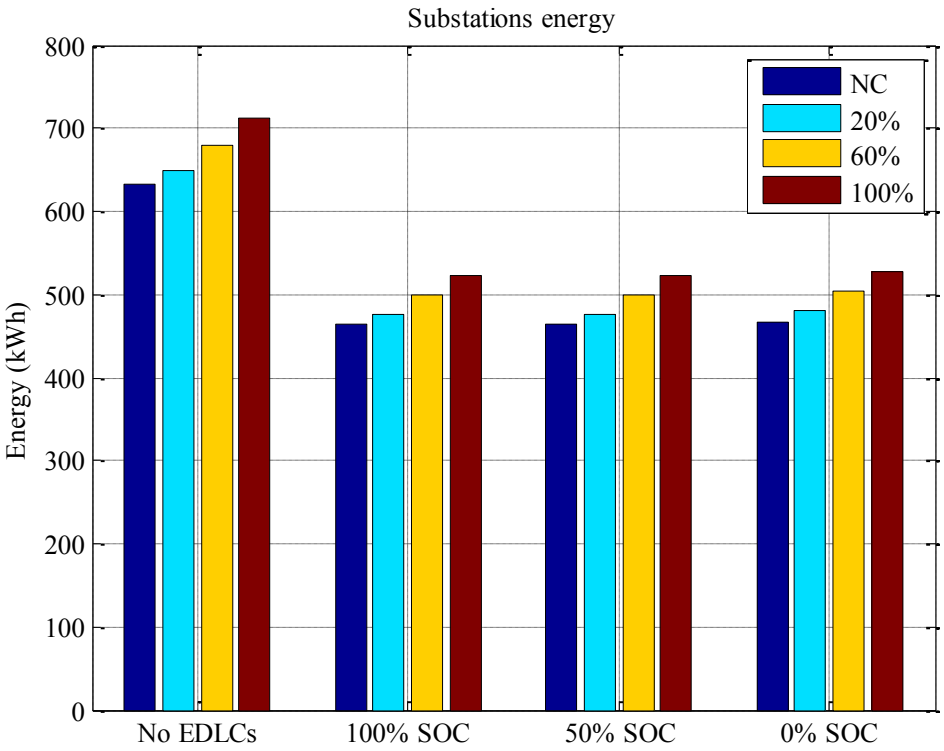

Figure 5.19: Total energy consumptions of the friction force variations with different initial SOC of stationary EDLCs

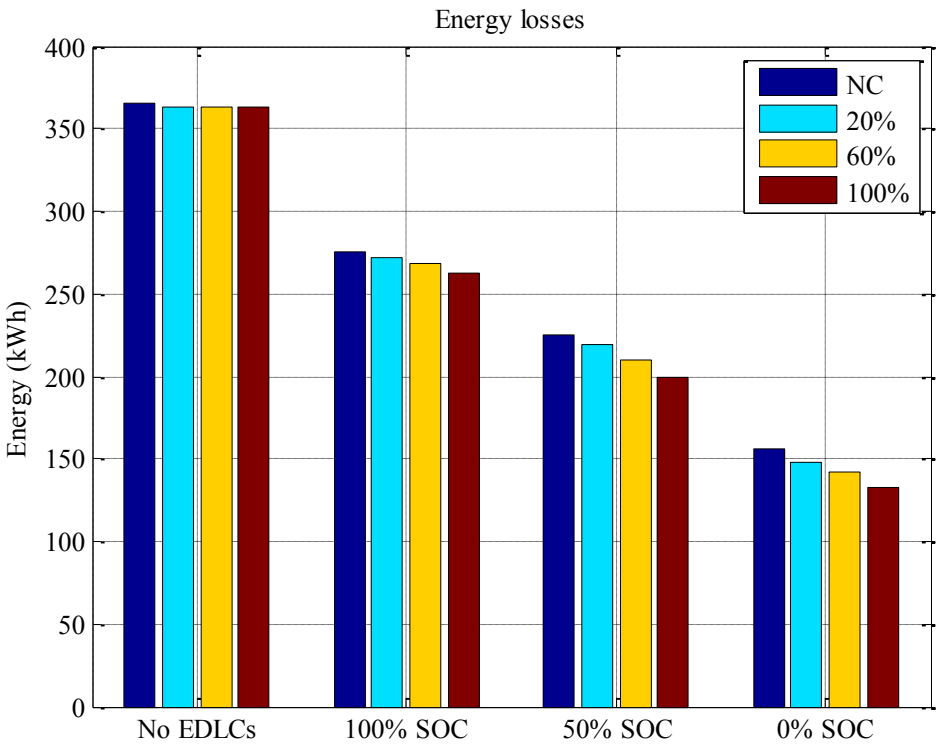

Figure 5.20: Energy losses of the friction force variations with different initial SOC of stationary EDLCs

Figure 5.20 shows the bar chart of the total energy losses from the resistance of rails and conducting rails and the on-board braking resistance (if all EDLCs are fully charged). The results show that the total energy losses without stationary EDLCs slightly decrease from 365 to 362 kWh with the incremental increases in friction force. The trend of total energy losses is more accentuated with the EDLCs, and it is slightly dependent on the initial SOC. The average of the total energy loss reductions for the initial SOCs of 100%, 50% and 0% are 24%, 41% and 60%, respectively. Again, this result indicates that having a low SOC of EDLCs at the beginning can be beneficial to reduce energy losses, and this benefit increases with the friction force.

C. Simultaneous variation of train loading and friction force

On the basis of the hypotheses of the two previous sections, there are four different train loading and friction force characteristics. For simplicity, only the worst case of the heaviest train loading and 100% increase in the friction force has been simulated to verify the proposed SOC control. Table 5.5 presents the results of the total energy supplied by the substations with and without stationary EDLCs, $E_{ss,edlc}$ and $E_{ss,noedlc}$, and also total the energy losses with and without stationary EDLCs, $E_{loss,edlc}$ and $E_{loss,noedlc}$, of one round-trip of the train journey based on 31 scenarios of initial SOCs of the stationary EDLCs. From the analysis of the results, it is interesting to note that the percentage reduction in energy consumption is basically independent of the initial SOC of the EDLCs, with a variation of only 1% between the best and worst case. On the other hand, the percentage reduction of total energy losses is more dependent on the initial SOC and is between 28-51%. The higher energy loss reduction is achieved with the lowest initial SOC of the stationary EDLCs. Additional diagrams of the percentage SOC of each EDLC with the

distance travelled by the train for one round-trip are shown in Appendix A for the 31 cases proposed. As for the results of the heaviest train loading and the highest friction force, it is important to note that the SOC of each stationary EDLC can approach the steady state of the full SOC within one round-trip of the train journey.

Table 5.5: The total energy consumptions and total energy losses for a round-trip of the train journey with the different scenarios of the initial SOC of each stationary EDLC

Cases	%SOC #1	%SOC #2	%SOC #3	%SOC #4	$E_{ss,noedlc}$ (kWh)	$E_{ss,edlc}$ (kWh)	% Reduction	$E_{loss,noedlc}$ (kWh)	$E_{loss,edlc}$ (kWh)	% Reduction
1	100	100	100	100	958	697	27	489	353	28
2	50	100	100	100	958	697	27	489	337	31
3	100	50	100	100	958	697	27	489	340	31
4	100	100	50	100	958	697	27	489	347	29
5	100	100	100	50	958	697	27	489	352	28
6	50	50	100	100	958	697	27	489	325	33
7	50	100	50	100	958	697	27	489	318	35
8	50	100	100	50	958	697	27	489	323	34
9	100	50	50	100	958	697	27	489	324	34
10	100	50	100	50	958	697	27	489	327	33
11	100	100	50	50	958	697	27	489	333	32
12	50	50	50	100	958	697	27	489	299	39
13	50	50	100	50	958	697	27	489	298	39
14	50	100	50	50	958	697	27	489	304	38
15	100	50	50	50	958	697	27	489	302	38
16	50	50	50	50	958	697	27	489	305	38
17	0	100	100	100	958	699	27	489	326	33
18	100	0	100	100	958	697	27	489	322	34
19	100	100	0	100	958	697	27	489	330	32
20	100	100	100	0	958	697	27	489	342	30
21	0	0	100	100	958	704	27	489	298	39
22	0	100	0	100	958	702	27	489	301	38
23	0	100	100	0	958	701	27	489	291	40
24	100	0	0	100	958	697	27	489	302	38
25	100	0	100	0	958	697	27	489	298	39
26	100	100	0	0	958	697	27	489	296	39
27	0	0	0	100	958	704	27	489	294	40
28	0	0	100	0	958	704	27	489	286	42
29	0	100	0	0	958	702	27	489	287	41
30	100	0	0	0	958	697	27	489	266	46
31	0	0	0	0	958	704	26	489	239	51

5.5 Summary

This chapter has presented a new piece-wise linear SOC control for stationary EDLCs to numerically validate the optimal design of the energy storage presented in Chapter 5. The

control action is divided into 5 areas to limit the storage current and it includes an idling zone to avoid continuous cycling of the storage when the line voltage is close to the nominal value. The model of the DC railway network has been modified to take into account that all the substations are electrically connected together. For the simulations, the rated voltages, currents and energy capacities of the stationary EDLCs are obtained from the optimisation algorithm described in the previous chapters.

The proposed controller is evaluated with normal conditions of train motion with the average steady state SOC of the EDLCs at 100% and 79%. The results show that the average steady state SOC at 79% is more efficient than the steady state SOC at 100% in terms of low braking resistance energy. This is because it has a greater available capacity to discharge either the uncertain or certain braking energy, and this, therefore, reduces the use of the braking resistance.

The robustness of the control has also been simulated against variations of the train loading and friction force, and with the different initial SOC of EDLCs and the steady state of the SOC at only 100%. The simulations show that the SOC of EDLCs is independent of the different initial SOC with the proposed controller. The SOC of EDLCs with any initial SOC can approach the steady state at 100% within only one round-trip of the train motion. In addition, the average reduction of the energy supplied by substations is 26 – 27% for both variations in the train loading and the friction force and with the different initial SOC of the EDLCs. The energy loss reductions are most significantly achieved by the lowest initial SOC of the EDLCs with an increase in friction force.

Chapter 6 Conclusions and Future Works

6.1 General Summary of Contents

The major findings and contributions based on the objectives presented in Section 1.4 are outlined in the following sections.

6.1.1 Model of the DC Electrified Railway System with Stationary EDLCs

The review of the technical literature has shown that energy storage devices have been used in light railway systems to improve the performance and efficiency in terms of energy consumption reduction, total energy loss reduction, voltage profile regulation, peak current reduction and catenary-free operations for trains (available only with on-board storage devices). The energy stored by energy storage devices is regenerated from train braking, whereas, in the absence of storage, the regenerative braking energy is normally dissipated by on-board braking resistors. Although several energy storage device technologies have been applied to electrified railway systems, EDLCs have been chosen in this thesis due to their high power density, quick recharging and discharging times and long life cycles. With reference to the installation, stationary EDLCs have been chosen to avoid modifications to the rolling stock and to ensure that the same storage can be used for multiple trains, with the aim of installing a lower total capacity of energy storage. This choice has led to the problem of finding the optimal locations and capacities for the EDLCs. In order to tackle this problem, a model of the railway electrification system and rolling stock, including a model of the DC substations and trains, both with and without stationary EDLCs, has been developed.

The major findings and contributions of this part of the research are:

1. The development of an electric dynamic model of the railway with two substations and a light railway vehicle travelling between the two substations;
2. The development of an electric dynamic model of the traction motors taking into account the torque speed characteristic;
3. The development of an electric dynamic model of the stationary EDLCs including the power converter.

6.1.2 Optimal Design of the Stationary EDLCs

The position and capacity of the EDLCs have been optimised for the case of a railway with 5 substations and 4 stations between the substations for a total track length of 22 km. The objective function of the optimisation algorithm aims to minimise the energy consumption of substations and the energy losses of the return rails, conducting rails and the on-board braking resistors. The definition of the objective function indicated the problem of finding the best set of weight coefficients. In order to find the best weight coefficients, an optimisation algorithm based on GA and PSO has been applied. The optimisation process produced the locations and the capacities of the EDLCs, which were then used to design the actual number of EDLC modules to be connected in series and parallel, starting from commercially available modules.

The major findings and contributions of this part of the research are:

1. Calculation of the best set of weight coefficients of the objective function using GA and PSO algorithms. The study has shown that both algorithms produce

similar results, but the PSO algorithm is quicker than GA with the same population size and number of generations;

2. Calculation of the optimal position and capacitance of the EDLCs for each section of the railway. For all sections, the optimal position is close to the middle station, or around the middle of the track between two adjacent substations;
3. Calculation of the energy saving with the optimal EDLCs. The simulation study has shown that the total energy consumption of the substations can be reduced by 42%. In addition, total energy losses can be reduced by 72%.

6.1.3 Piece-wise Linear SOC Control of Stationary EDLCs

A piece-wise linear SOC control has been proposed for the optimised EDLCs. The boundary of each current and voltage in the linear SOC control have been taken from the optimisation algorithm. The control has been tested with different initial SOCs and variable train loading and friction force.

The major findings and contributions of this part of the research are:

1. Definition of the linear equation of the controller for the different operating areas, including an idling area to avoid oscillation around the nominal line voltage.
2. Verification of the discharge-recharge cycles of the EDLCs for different scenarios and variation of the train loading and friction force. The simulation study has indicated a reduction of the total energy consumption by 26 – 27%. In addition, the total energy losses seem to be reduced more effectively for low initial SOCs of the stationary EDLCs.

6.2 Future Works

6.2.1 Further Works to Investigate the Assumptions

Based on the assumptions of the research presented in Chapter 1, the STS used in this thesis has an error due to the large step size of the discrete distance (10 m). However, decreasing that step size to a more realistic size for single train services can reduce the error. In addition, the algorithm used for the optimisation method to design the optimal capacitances and positions of EDLCs could be evaluated on other routes of the DC light railway system with varied positions of stationary EDLCs less than 500 metres apart, possibly every 10 -50 metres, for a more realistic case study of the practical use of EDLCs in DC light railway systems. It is also planned that the optimal steady state of the SOC of EDLCs should be studied in the future works.

6.2.2 Optimal Design of Stationary EDLCs with the Multi-Train Simulator

In order to limit the computational effort, this study used only a single-train simulator (STS) to predict the tractive effort and velocity profile of the train. However, for practical services, there is usually more than one train travelling simultaneously and there are two tracks. Therefore, the methodology for the design of the stationary EDLCs could be applied to a more realistic scenario using the Multi-Train Simulator (MTS(b)), which would take into account the effect of simultaneous acceleration and braking of trains which could help to further reduce the capacity of the energy storage.

6.2.3 Study on Bi-Directional DC-DC Converter Control

The DC-DC bi-directional converter used to connect the EDLCs to the electrified line is assumed to be ideal in this work, i.e. the currents and voltages at the terminal of the converters are instantaneously equal to their reference values. As a further development, a more in-depth analysis of the bi-directional DC-DC converter is needed. This includes the definition of the converter topology capable of matching the maximum current and voltage required for this application. Furthermore, a study on the stability of the controller is also needed to see if there is any interference with the proposed piece-wise linear SOC controller.

6.2.4 Experiments on a Scale Model

This simulation study has predicted a substantial energy saving using stationary EDLCs. A demonstration on a scale model of the DC electrified railway system with stationary EDLCs could give further support to this result and a more detailed insight on the influence of real losses of the different components. The small-scale simulator should include EDLC modules, a bi-directional DC-DC converter, a traction drive and a rotating inertia simulating the mass of the train. The experimental study would give further recommendations on the practical applicability of the proposed optimal design and associated SOC control of the EDLCs.

References

ADAMUTHE, A. C., MANE, S. U. & THAMPI, G. T. Genetic algorithmic approach for security personnel scheduling. International Conference on Communication, Information & Computing Technology (ICCICT), 19-20 October 2012 Mumbai, India. 1-6.

ADINOLFI, A., LAMEDICA, R., MODESTO, C., PRUDENZI, A. & VIMERCATI, S. S. 1998. Experimental assessment of energy saving due to trains regenerative braking in an electrified subway line. *IEEE Transaction on Power Delivery,* 4**,** 1536-1541.

ALBRECHT, T. 2004. Reducing power peaks and energy consumption in rail transit systems by simultaneous train running time control. *Journal of Advanced Transportation,* 15**,** 885-894.

ALLÈGRE, A. L., BOUSCAYROL, A., DELARUE, P., BARRADE, P., E., C. & EL-FASSI, S. 2010. Energy storage system with supercapacitor for an innovative subway. *IEEE Transactions on Industrial Electronics,* 57**,** 4001-4012.

ALVES, P. T. & PIRES, C. L. Energy saving strategy in São Paulo Metro. IET Conference on Railway Traction Systems (RTS 2010) , 13- 15 April 2010 Birmingham, UK. IET, 1-4.

AMJADI, Z. & WILLIAMSON, S. S. Review of alternate energy storage systems for hybrid electric vehicles. IEEE on Electrical Power & Energy Conference (EPEC), 22-23 Oct 2009 Montreal, QC. IEEE, 1-7.

AMPOFO, F., MAIDMENT, G. G. & MISSENDEN, J. F. 2011. Application of groundwater cooling scheme for London Underground network. *International Journal Refrigeration,* 34**,** 2042-2049.

ARABAS, J. & KOZDROWSKI, S. 2001. Applying an evolutionary algorithm to telecommunication network design. *IEEE Transactions on Evolutionary Computation,* 5**,** 309-322.

ARENAS, D., CHEVRIER, R., RODRIGUEZ, J. & DHAENENS, C. Application of a co- evolutionary genetic algorithm to solve the periodic railway timetabling problem. Proceedings of 2013 International Conference on Industrial Engineering and Systems Management (IESM), 28-30 October 2013 Rabat, Morocco. 1-7.

BAETENSA, R., JELLEA, B. P. & GUSTAVSEND, A. 2010. Properties, requirements and possibilities of smart windows for dynamic daylight and solar energy control in buildings: A state-of-the-art review. *Solar Energy Materials and Solar Cells,* 94**,** 87-105.

BAJWA, A., WILLIAMS, T. & STUCHLY, M. A. Design of broadband radar absorbers with genetic algorithm. IEEE International Symposium of Antennas and Propagation Society, 2001. 672-675.

BARRERO, R., MIERLO, J. V. & TACKOEN, X. 2008. Energy savings in public transport. *IEEE Vehicle Technology Magazine.*

BARRERO, R., TACKOEN, X. & MIERLO, J. V. 2010. Stationary or onboard energy storage systems for energy consumption reduction in a metro network. *Proceedings of the Institution of Mechanical Engineers, Part F: Journal of Rail and Rapid Transit,* 224**,** 207-225.

BARSALI, S., GIGLIOLI, R., POLI, D. & VELLUCCI, F. Demand Response of urban transport systems: a help for deploying the new Smart Grid paradigm. Cigré International Symposium The Electric Power System of the Future - Integrating supergrids and microgrids, 13-15 September 2011 Bologna, Italy.

BATTISTELLI, L., CICCARELLI, F., LAURIA, D. & PROTO, D. Optimal design of DC electrified railway stationary storage system. International Conference on Clean Electrical Power – ICCEP 2009, 2009 Capri, Italy.

BATTISTELLI, L., FANTAUZZI, M., IANNUZZI, D. & LAURIA, D. Generalized approach to design supercapacitor-based storage devices integrated into urban mass transit systems. 3rd International conference on clean electrical power: renewable energy resources impact – ICCEP 2011, 2011 Ischia, Italy.

BEDWANI, W. A. & ISMAIL, O. M. 2001. Genetic optimization of variable structure pid control systems. *ACS/IEEE International Conference on Computer Systems and Applications.*

BERA, R., MANDAL, D., KAR, R. & GHOSHAL, S. P. Application of improved Particle Swarm Optimization technique for thinning of concentric hexagonal array antenna. Fourth World Congress on Information and Communication Technologies (WICT), 8-11 Dec. 2014 Bandar Hilir, Malaysia. IEEE, 188-193.

BOCHARNIKOV, Y. V., TOBIAS, A. M. & ROBERTS, C. Reduction of train and net energy consumption using genetic algorithms for Trajectory Optimisation. IET Conference on Railway Traction Systems (RTS 2010) , 13- 15 April 2010 Birmingham, UK. 1-5.

BOCHARNIKOV, Y. V., TOBIAS, A. M., ROBERTS, C., HILLMANSEN, S. & GOODMAN, C. J. 2007. Optimal driving strategy for traction energy saving on DC suburban railways. *IET Electric Power Applications* 1**,** 675 – 682.

BOCKLISCH, T. Hybrid energy storage systems for renewable energy applications. 9th International Renewable Energy Storage Conference, IRES 2015, 2015. Elsevier, 103 – 111

BOIZUMEAU, J. R., LEGUAY, P. & NAVARRO, E. 2011. Braking energy recovery at the Rennes metro. *Workshop on braking energy recovery systems–Ticket to Kyoto Project.* Bielefeld, Germany.

BOLUND, B., BERNHOFF, H. & LEIJON, M. 2005. Flywheel energy and power storage systems. *Renewable and Sustainable Energy Reviews,* 11**,** 235–258.

BOMBARDIER- TRANSPORTATION 2009. MITRAC Energy Saver. *EcoActive Technology, Propulsion & Controls.*

BOSCO, G. L. A genetic algorithm for image segmentation. Proceedings of 11th International Conference on Image Analysis and Processing, 2001. 262-266.

BOYLESTAD, R. L. 2007. *Introductory Circuit Analysis*, Pearson Prentice Hall.

BREEZE, P. 2014. *Chapter 10 – Power System Energy Storage Technologies*, Elsevier B.V.

BRENNA, M., FOIADELLI, F., TIRONI, E. & ZANINELLI, D. Ultracapacitors application for energy saving in subway transportation systems. International Conference on Clean Electrical Power – ICCEP 2007, 2007 Capri, Italy.

BUDDE-MEIWES., H., DRILLKENS, J., LUNZ, B., MUENNIX, J., ROTHGANG, S., KOWAL, J. & SAUER, D. U. 2013. A review of current automotive battery

technology and future prospects. *Journal of Automobile Engineering,* 227**,** 761-776.

CARRUTHERS, J. J., CALOMFIRESCU, M., GHYS, P. & PROCKAT, J. 2009. The application of a systematic approach to material selection for the lightweighting of metro vehicles. *Proc IMechE Part F: J. Rail and Rapid Transit,* 223**,** 427-437.

CASTILLO, O., MONTIEL, O., SEPULVEDA, R. & MELIN, P. Application of a breeder genetic algorithm for system identification in an adaptive finite impulse response filter. Proceedings of The 3rd NASA/ DoD Workshop on Evolvable Hardware, 2001. 146-153.

CHEN, H., CONG, T. N., YANG, W., TAN, C., LI, Y. & DING, Y. 2009a. Progress in electrical energy storage system - a critical review. *Progress in Natural Science,* 19**,** 291 – 312.

CHEN, J. F., LIN, R. L. & LIU, Y. C. 2005. Optimization of an MRT train schedule – reducing maximum traction power by using genetic algorithms. *IEEE Transactions on Power Systems,* 20**,** 1366-1372.

CHEN, P. H., CHEN, L. M., LIU, A. & CHEN, A. C. Application of Particle Swarm Optimization to Hydro Generation Scheduling. International Conference on Energy and Environment Technology, ICEET '09. , 16- 18 Oct. 2009b Guilin, Guangxi, China. IEEE, 541-544.

CHEN, Q., GUO, W. & LI, C. Railway Passenger Volume Forecast by GA-SA-BP Neural Network. International Workshop on Intelligent Systems and Applications (ISA 2009), 23-24 May 2009c Wuhan, China. 1-4.

CHRISTEN, T. & CARLEN, M. W. 2000. Theory of Ragone plots. *Power Sources,* 91**,** 210–216.

CHYMERA, M., RENFREW, A. & BARNES, M. Analyzing the potential of energy storage on electrified transit systems. 8th World Congress of Railway Research – WCRR 2008, 2008 Seoul, South Korea.

CHYMERA, M., RENFREW, A. C., BARNES, M. & HOLDEN, J. 2011. Simplified power converter for integrated traction energy storage. *IEEE Vehicle Technology,* 60**,** 1374–1383.

CICCARELLI, F., IANNUZZI, D. & TRICOLI, P. 2012. Control of metro- trains equipped with onboard supercapacitors for energy saving and reduction of power peak demand. *Transportation Research Part C: Emerging Technologies,* 24**,** 36-49.

CITADIS. 2005. Available: http://www.ccm.nl/pdf/Citadis%20Rotterdam%20as%20Flywheel%20Demonstrator.pdf, 2005].

CONNOR, P. 2011. *Railway Passenger Vehicle Capacity* [Online]. RTWP Infopaer No 2.

CORDON, O., HERRERA, F. & VILLAR, P. 2001. Generating the knowledge base of a fuzzy rule- based system by the genetic learning of the database. *IEEE Transactions on Fuzzy Systems,* 9**,** 667-674.

CORNIC, D. Efficient recovery of braking energy through a reversible dc substation. 9th World Congress on Railway Research – WCRR 2011, 2011 Lille, France.

DANG, M., WANG, Z. & QIAN, F. A new particle swarm optimization and the application in the soft sensor modeling. 8th IEEE International Conference on Control and Automation (ICCA), 9- 11 June 2010 Xiamen, China. IEEE, 1175 - 1177.

DAŞ, M. T., DÜLGER, L. C. & DAŞ, G. S. Robotic applications with Particle Swarm Optimization (PSO) . International Conference on Control, Decision and Information Technologies (CoDIT) , 6- 8 May 2013 Hammamet, Tunisia. IEEE, 160-165.

DESTRAZ, B., BARRADE, P., RUFER, A. & KLOHR, M. Study and simulation of the energy balance of an urban transportation network. 2007 European conference on power electronics and applications, 2007 Aalborg, Denmark.

DOMÍNGUEZ, M., CUCALA, A. P., FERNÁNDEZ, A., PECHARROMÁN, R. R. & BLANQUER, J. Energy efficiency on train control – design of metro ATO driving and impact of energy accumulation devices. 9th World Congress on Railway Research – WCRR 2011, 2011 Lille, France.

DOUGLAS, H., ROBERTS, C., HILLMANSEN, S. & SCHMID, F. 2015. An assessment of available measures to reduce traction energy use in railway networks. *Energy Conversion and Management,* 16**,** 1149–1165.

DOUGLAS, H., WESTON, P., KIRKWOOD, D., HILLMANSEN, S. & ROBERTS, C. 2016. Method for validating the train motion equations used for passenger rail vehicle simulation. *Rail and Rapid Transit,* 0**,** 1-15.

DUNN, B., KAMATH, H. & TARASCON, J. M. 2011. Electrical energy storage for the grid: A battery of choices. *Science,* 334**,** 928 – 935.

FALVO, M., LAMEDICA, R., BARTONI, R. & MARANZANO, G. 2011. Energy management in metrotransit systems: an innovative proposal toward an integrated and sustainable urban mobility system including plug- in electric vehicles. *Electrical Power System Research,* 81**,** 2127-2138.

FALVO, M. C., LAMEDICA, R. & RUVIO, A. Energy storage application in trolley-buses lines for a sustainable urban mobility. Electrical Systems for Aircraft, Railway and Ship Propulsion (ESARS), 16-18 Oct. 2012 Bologna, Italy. IEEE, 1-6.

FARANDA, R. & LEVA, S. Energetic sustainable development of railway stations. Power Engineering Society General Meeting, 2007, 24-28 June 2007 Tampa, FL, USA. IEEE, 1-6.

FETCENKO, M. A. 2005. 22nd International Seminar & Exhibit on Primary and Secondary Batteries. Ft. Lauderdale, FL.

FOIADELLI, F., ROSCIA, M. & ZANINELLI, D. Optimization of storage devices for regenerative braking energy in subway systems. IEEE Power Engineering Society General Meeting – PES 2006, 2006 Montreal, Canada.

GARCIA-TABARES, L., IGLESIAS, J., LAFOZ, M., MARTINEZ, J. C., VAZQUEZ, C. & TOBAJAS, C. Development and testing of a 200 MJ/350 kW kinetic energy storage system for railways applications. 9th World Congress on Railway Research – WCRR 2011, 2011 Lille, France.

GELMAN, V. 2009. Braking energy recuperation. *IEEE Vehicle Technology Magazine.*

GHOFRANI, M., ARABALI, A., ETEZADI-AMOLI, M. & FADALI, M. S. 2013. Energy Storage Application for Performance Enhancement of Wind Integration. *IEEE Transactions on Power Systems,* 28**,** 4803 - 4811.

GIBBARD, H. F. 1993. Nickel metal hydride battery technology. *Conference Record, WESCON/'93.* . San Francisco, CA: IEEE.

GLICKENSTEIN, H. 2013. Contactless payment debuts on London's busses, new and improved railways around the world: Williams hybrid power and Alstom transport

to partner on energy storage technology for trams. *IEEE Vehicle Technology Magazine (IEEE Press),* 8**,** 19–25.

GOH, C. & LI, Y. GA automated design and synthesis of analog circuits with practical constraints. Proceedings of the 2001 Congress on Evolutionary Computation, 2001. 170-177.

GONZALEZ- GIL, A. , PALACIN, R. & BATTY, P. 2013. Sustainable urban rail systems: Strategies and technologies for optimal management of regenerative braking energy. *Energy Conversion and Management,* 75**,** 374–388.

GONZALEZ-GIL, A., PALACIN, R. & BATTY, P. 2015. Optimal energy management of urban rail systems: Key performance indicators. *Energy Conversion and Management,* 90**,** 282–291.

GONZALEZ-GIL, A., PALACIN, R., BATTY, P. & POWELL, J. P. 2014. A systems approach to reduce urban rail energy consumption. *Energy Conversion and Management,* 80**,** 509-524.

GOODMAN, C. J. 2010. Overview of electric railway systems and the calculation of train performance. *IET Professional Development Course on Electric Traction Systems.* London, UK: IET.

GRAINGER, J. J. 1994. *Power system analysis,* New York; London, McGraw-Hill.

GRIMBLEBY, J. B. Automatic analogue circuit synthesis using genetic algorithms. IEE Proceedings on Circuits, Devices and Systems, December 2000. 319-323.

GUNSELMANN, W. Technologies for increased energy efficiency in railway systems. European Conference on Power Electronics and Applications, 11- 14 Sept 2005 Dresden, Germany. IEEE.

HAMMAR, A., VENET, P., LALLEMAND, R., COQUERY, G. & ROJAT, G. 2010. Study of Accelerated Aging of Supercapacitors for Transport Applications. *IEEE Transactions on Industrial Electronics* 57**,** 3972 - 3979.

HAYASHIYA, H., HARA, D., TOJO, M., WATANABE, K., HINO, M., SUZUKI, T., OKAMOTO, H., TAKAHASHI, H., KATO, T. & TESHIMA, M. Lithium-ion battery installation in traction power supply system for regenerative energy utilization: Initial report of effect evaluation after half a year operation. 16th International on Power Electronics and Motion Control Conference and Exposition (PEMC), 21-24 September 2014 Antalya, Turkey. IEEE, 119 - 124.

HENNING, U., THOOLEN, F., LAMERTH, M., BERNDT, J., LOHNER, A. & JANIG, N. 2005. Ultra low emission vehicle – transport advanced propulsion. *Electrical Engineering: Railway Electrical Service Representative,* 20**,** 33-39.

HEO, J. H., PARK, G. P., YOON, Y. T., PARK, J. K. & LEE, S. S. Application of particle swarm optimization for an optimal maintenance strategy in transmission systems. IEEE Power and Energy Society General Meeting, 24-29 July 2011 San Diego, CA. IEEE, 1-7.

HILLMANSEN, S. & ROBERTS, C. 2007. Energy storage devices in hybrid railway vehicles: A kinematic analysis. *Proceedings of the Institution of Mechanical Engineers, Part F: Journal of Rail and Rapid Transit* 221**,** 135-143.

HO, M. H., CHIU, C. C. & LIAO, S. H. 2012. Optimisation of channel capacity for multiple-input multiple-output smart antenna using a particle swarm optimiser. *IET Communications,* 6**,** 2645 - 2653.

HOANG, H. H., POLIS, M. P. & HAURIE, A. 2003. Reducing energy consumption through trajectory optimization for a metro network. *IEEE Transactions on Automatic Control,* 20**,** 590 - 595.

HOLLAND, J. H. 1975. *Adaptation in Natural and Artificial Systems,* Ann Arbor, MI, University ofMichigan Press.

HOU, P., HU, W., SOLTANI, M. & CHEN, Z. 2015. Optimized Placement of Wind Turbines in Large-Scale Offshore Wind Farm Using Particle Swarm Optimization Algorithm. *IEEE Transactions on Sustainable Energy* 6**,** 1272 - 1282.

HUSSEIN, F., KHARMA, N. & WARD, R. Genetic algorithms for feature selection and weighting: A review and study. Proceedings of 6th International Conference on Document Analysis and Recognition, 2001. 1240-1244.

HUTCHISON, G. I., ZAHAWI, B., HARMER, K., STEDALL, B. & GIAOURIS, D. Synchronous machine parameter identification using particle swarm optimization. 5th IET International Conference on Power Electronics, Machines and Drives (PEMD 2010), 19-21 April 2010 Brighton, UK. IET, 1-4.

HUYNH , D. C. & DUNNIGAN, M. W. Parameter estimation of an induction machine using a chaos particle swarm optimization algorithm. 5th IET International Conference on Power Electronics, Machines and Drives (PEMD 2010), 19-21 April 2010a Brighton, UK. IET, 1-6.

HUYNH , D. C. & DUNNIGAN, M. W. 2010b. Parameter estimation of an induction machine using advanced particle swarm optimisation algorithms. *IET Electric Power Applications* 4**,** 748 - 760.

IANNUZZI, D. Improvement of the energy recovery of traction electrical drives using supercapacitors. 13th Power Electronics and Motion Control Conference, 2008 (EPE-PEMC 2008), 17-20 May 2008 Poznan, Poland. 933 - 938.

IANNUZZI, D., CICCARELLI, F. & LAURIA, D. 2012a. Stationary ultracapacitors storage device for improving energy saving and voltage profile of light transportation networks. *Transportation Research Part C: Emerging Technologies,* 21**,** 321-327.

IANNUZZI, D., LAURIA, D. & CICCARELLI, F. 2013. Wayside ultracapacitors storage design for light transportation systems: a multiobjective optimization approach. *International Review of Electrical Engineering (IREE),* 8**,** 190-199.

IANNUZZI, D., LAURIA, D. & TRICOLI, P. 2012b. Optimal design of stationary supercapacitors storage devices for light electrical transportation systems. *Optimization and Engineering,* 13**,** 698-704.

IANNUZZI, D. & TRICOLI, P. Metro trains equipped onboard with supercapacitors: a control technique for energy saving. International Symposium Power Electronics, Electrical Drives, Automation and Motion (SPEEDAM), 14–16 June 2010 Pisa, Italy. 750-756.

IANNUZZI, D. & TRICOLI, P. Supercapacitor state of charge control based on changeover finite state controller for metro-train applications. ICCEP 2011–3rd international conference on clean electrical power: renewable energy resources impact, 2011 Ischia, Italy.

IANNUZZI, D. & TRICOLI, P. 2012. Speed-based state-of-charge tracking control for metro trains with onboard supercapacitors. *IEEE Power Electrononics,* 27**,** 2129-2140.

IEEE 2004. 112-2004 - IEEE Standard Test Procedure for Polyphase Induction Motors and Generators. IEEE.

IGLESIAS, I. J., MARTINEZ, J. C., TOBAJAS, C., LAFOZ, M., TABARÉS, L. G. & COAUTHORS, C. V. A kinetic energy storage system for railways applications. Eighth World Congress on Railway Research, 18–22 May 2008 Coex, Seoul, Korea. 1-10.

ISHAQUE, K., SALAM, Z. & SHAMSUDIN, A. Application of particle swarm optimization for maximum power point tracking of PV system with direct control method. IECON 2011 - 37th Annual Conference on IEEE Industrial Electronics Society, 7-10 Nov. 2011 Melbourne, VIC. IEEE, 1214 - 1219.

ISHAQUE , K., SALAM, Z., TAHERI, H. & SHAMSUDIN, A. Maximum Power Point Tracking for PV system under partial shading condition via particle swarm optimization. IEEE on Applied Power Electronics Colloquium (IAPEC), 18-19 April 2011 Johor Bahru, Malaysia. IEEE, 5-9.

JEONG, I. B., PARK, C. S., NA, K. I., HAN, S. & KIM, J. H. Particle swarm optimization-based central patter generator for robotic fish locomotion. IEEE Congress of Evolutionary Computation (CEC), 5-8 June 2011a New Orleans, LA. IEEE, 152 - 157.

JEONG, W., KON, S. B., PARK, D. & JUNG, W. S. Efficient energy management for onboard battery-driven light railway vehicle. 9th World Congress on Railway Research – WCRR 2011, 2011b Lille, France.

JONES, E., RUNKLE, P., DASGUPTA, N., COUCHMAN, L. & CARIN, L. 2001. Genetic algorithm wavelet design for signal classification. *IEEE Transactions on Pattern Analysis and Machine Intelligence,* 23**,** 890-895.

JORDEHI, A. R., JASNI, J., A., W. N. I. & KADIR, M. Z. A. A. Particle swarm optimisation applications in FACTS optimisation problem. IEEE 7th International on Power Engineering and Optimization Conference (PEOCO), 3-4 June 2013 Langkawi, Malaysia. IEEE, 193 - 198.

KAWASAKI. 2008. Kawasaki Heavy Industries. *Scope Quarterly Newsletter*, January 2008.

KENNEDY, J. & EBERHART, R. C. 1995. Particle swarm optimization. *IEEE International Conference on Neural Networks*. Perth, Australia.

KENNEDY, J. & EBERHART, R. C. 2001. *Swarm Intelligence,* San Francisco, CA, Morgan Kaufmann.

KEZUNOVIC, M. & LIAO, Y. Fault location estimation based on matching the simulated and recorded waveforms using genetic algorithms. IEE International Conference on Developments in Power System Protection, 2001. 399-402.

KIM, G. & LEE, H. A study on the application of ESS on Seoul Metro line 2. International conference on information and multimedia technology, 2009 Jeju Island, South Korea.

KIM, K. S. & BYOUNG-TAK, Z. Evolutionary learning of web-document structure for information retrieval. Proceedings of the 2001 Congress on Evolutionary Computation, 2001. 2, 1253-1260.

KIN, C. C., TAT, T. H., TONG, L. & KIN, L. T. Medical image registration and model construction using genetic algorithms. Proceedings of International Workshop on Medical Imaging and Augmented Reality, 2001. 174-179.

KONDO, K. 2010. Recent Energy Saving Technologies on Railway Traction Systems. *IEEJ TRANSACTIONS ON ELECTRICAL AND ELECTRONIC ENGINEERING,* 5**,** 298–303.

KONISHI, T., HASE, S. & NAKAMICHI, Y. 2004. Energy storage system for DC electrified railway using EDLC. *In:* QUARTERLY REPORT OF RAILWAY TECHNICAL RESEARCH INSTITUTE (RTRI), J. (ed.).

KONISHI, T., MORIMOTO, H., AIHARA, T. & TSUTAKAWA, M. 2010. Fixed energy storage technology applied for DC electrified railway. *IEE Journal on Electrical Electronic Engineering,* 5**,** 270-277.

KOUZOU, A., MAHMOUDI, M. O. & BOUCHERIT, M. S. Application of SHE-PWM for seven- level inverter output voltage enhancement based on Particle Swarm Optimization. 7th International Multi- Conference on Systems Signals and Devices (SSD), 27-30 June 2010 Amman, Jordan. IEEE, 1-6.

KURZWEIL, P. 2015. *Chapter 19 – Electrochemical Double-layer Capacitors*, Elsevier B.V.

LACOTE, F. 2005. Rolling Stock and Manufacturers (part 2): Alstom – future trends in railway transportation. *Japan Railway & Transport Review 42' (East Japan Railway Culture Foundation (EJRCF), 2005)***,** 4-9.

LAM, S. S. A genetic fuzzy expert system for stock market timing. Proceedings of the 2001 Congress on Evolutionary Computation, 2001. 410-417.

LEE, C. K., KIM, D. H. & JUN, W. S. Study on the energy saving running technology and its CO_2 reduction effect of railway vehicle. 9th World Congress on Railway Research – WCRR 2011, 2011a Lille, France.

LEE, H., SONG, J., LEE, H., LEE, C., JANG, G. & KIM, G. 2011b. Capacity optimization of the supercapacitor energy storages on DC railway system using a railway powerflow algorithm. *International Journal of Innovative Computing, Information and Control (IJICIC),* 1**,** 2739-2753.

LEE, H. M. A study on development of ESS installed in DC railway system. International Conference on Control, Automation and Systems, 27– 30 October 2010 Gyeonggi– do, Korea. 804-806.

LHOMME, W., DELARUE, P., BARRADE, P., BOUSCAYROL, A. & RUFER, A. 2005. Design and control of a supercapacitor storage system for traction applications. *IAS annual meeting of IEEE industry applications society.* Hong Kong, China.

LI, H. J. & HENNESSY, T. 2013. European town microgrid and energy storage application study. *IEEE PES Innovative Smart Grid Technologies (ISGT)*. Washington, DC: IEEE.

LI, J., WEI, W. & HE, Y. Optimization of online timetable re-scheduling in high-speed train services based on PSO. International Conference on Transportation, Mechanical, and Electrical Engineering (TMEE), 16-18 Dec. 2011 Changchun, China. IEEE, 1896 - 1899.

LI, Y., TANG, X. & LIU, J. Application of particle swarm optimization algorithm in soft sensor modeling. ICEMI '09. 9th International Conference on Electronic Measurement & Instruments, 16-19 Aug. 2009 Beijing, China. IEEE, 2-920 - 2-924.

LIU, J., CAI, B. G. & WANG, J. Particle swarm optimization for integrity monitoring in BDS/ DR based railway train positioning. IEEE Congress on Evolutionary Computation (CEC), 6-11 July 2014 Beijing, China. 792-797.

LIU, J. & SHI, T. A new two- stages PSO algorithm for railway trajectory planning on GIS system. 17th International IEEE Conference on Intelligent Transportation Systems (ITSC), 8-11 Oct. 2014 Qingdao, China. IEEE, 2768-2773.

LIU, W., LUAN, Z., Y., Y., GAN, R. & ZHAO, H. The application of the improved Particle Swarm Optimization on dynamic economic dispatch of power system with wind farms. IEEE Region 10 Conference (TENCON 2015) 1-4 Nov. 2015 Macao. IEEE, 1-6.

LÓPEZ-LÓPEZ, A., PECHARROMÁN, R. R., PILO DE LA PUENTE, E., CUCALA, A. P. & FERNÁNDEZ-CARDADOR, A. Analysis of energy-saving strategies in railway power supply systems. 9th World Congress on Railway Research – WCRR 2011, 2011 Lille, France.

LU, S., HILLMANSEN, S., HO, T. K. & ROBERTS, C. 2013. Single-Train Trajectory Optimization. *IEEE Transactions on Intelligent Transportation Systems* 14**,** 743 - 750.

MAHER, B. 2006. Ultracapacitors provide cost and energy savings for public transportation applications. *Battery Power Product Technology.*

MAN, K. F., TANG, K. S., KWONG, S. & HALANG, W. A. 1997. *Genetic Algorithms for Control and Signal Processing,* London, Springer-Verlag.

MANGANARO, G. 2000. Genetic algorithms for vlsi design, layout, and test automation: Reviews. *IEEE Circuits and Devices Magazine.*

MEESAD, P. & YEN, G. G. A hybrid intelligent system for medical diagnosis. Proceedings of International Joint Conference on Neural Networks, 2001. 2558-2563.

MEINERT, M. New mobile energy storage system for rolling stock. 13th European Conference Power Electronics and Applications (EPE), 8–10 September 2009 Barcelona, Spain. 1-10.

MELIN, P. & CASTILLO, O. Intelligent control of nonlinear dynamical systems with a neuro-fuzzy-genetic approach. Proceedings of International Joint Conference on Neural Networks, 2001. 515-520.

MELLITT, B., MOUNEIMNE, Z. S. & GOODMAN, C. J. Simulation study of DC transit systems with inverting substations. Electric Power Applications, IEE Proceedings B, 1984. 38-50.

MIN-HUANG, H., MING-CHUN, C., YUE-SHAN, C. & SHYAN-MING, Y. A ga-based dynamic personalized filtering for internet search service on multi-search engine. Canadian Conference on Electrical and Computer Engineering, 2001. 270-276.

MINAMI, M., SUZUKI, H., AGBANHAN, J. & ASAKURA, T. Visual servoing to fish and catching using global/local ga search. Proceedings of 2001 IEEE/ASME International Conference on Advanced Intelligent Mechatronics, 2001. 183-188.

MIR, L., ETXEBERRIA-OTADUI, I., PEREZ DE ARENAZA, I., SARASOLA, I. & NIEVA, T. A Supercapacitor based light rail vehicle: system design and operations modes. IEEE Energy Conversion Congress and Exposition – ECCE 2009, 2009 San Jose, USA.

MIRANDA, V. & FONSECA, N. EPSO-evolutionary particle swarm optimization, a new algorithm with applications in power systems. Asia Pacific. IEEE/ PES on Transmission and Distribution Conference and Exhibition, 6-10 Oct. 2002. IEEE, 745 - 750.

MITSUKURA, Y. , FUKUMI, N. & AKAMATSU, N. Proceedings of IJCNN International Joint Conference on Neural Networks, 2001. 2253-2257.

MIYATAKE, M. & MATSUDA, K. 2009. Energy saving speed and charge/ discharge control of a railway vehicle with on- board energy storage by means of an optimization model. *IEEJ Transactions on Electrical and Electronic Engineering,* 4**,** 771-778.

MOLLER, R. & ZEIPELT, R. Automatic segmentation of 3d- mri data using a genetic algorithm. Proceedings of International Workshop on Medical Imaging and Augmented Reality, 2001. 278-281.

MORITA, G. , KONISHI, T. , HASE, S. , NAKAMICHI, Y. , NARA, H. & T. , U. Verification tests of electric double- layer capacitors for static energy storage system in DC electrified railway. SPEEDAM 2008 – international symposium on power electronics, electrical drives, automation and motion, 2008 Ischia, Italy.

MOSKOWITZ, J. P. & COHUAU, J. L. STEEM: ALSTOM and RATP experience of supercapacitors in tramway operation. Conference on Vehicle Power and Propulsion Conference (VPPC), 1–3 September 2010 Lille, France. IEEE, 1-5.

NAGAMINE, M. , KATO, H. & NISHI, Y. Characteristics of new lithium ion rechargeable batteries. 33rd Battery Symposium, 16- 18 September 1992 Tokyo, Japan. 83-84.

NASRI, A., MOGHADAM, M. F. & MOKHTARI, H. Timetable optimization for maximum usage of regenerative energy of braking in electrical railway systems. SPEEDAM 2010 – international symposium on power electronics, electrical drives, automation and motion, 2010 Pisa, Italy.

NICK, Z. Z. & THEMIS, P. 2001. Web search using a genetic algorithm. *IEEE Internet Computing,* 5**,** 18-26.

OGASA, M. 2010a. Application of energy storage technologies for electric railway vehicles – examples with hybrid electric railway vehicles. *IEEJ Transactions on Electrical and Electronic Engineering,* 5**,** 304-311.

OGASA, M. Onboard storage in Japanese electrified lines. 14th International Conference on Power Electronics and Motion Control (EPE/PEMC), 6-8 September 2010b Ohrid, Bulgaria. 9-16.

OGASA, M. & TAGUCHI, Y. Power electronics technologies for a lithium ion battery tram. Power Conversion Conference – Nagoya (PCC'07), 2-4 April 2007 Nagoya, Japan. 1369–1375.

OGURA, K., NISHIMURA, K., MATSUMURA, T., TONDA, C., YOSHIYAMA, E. & ANDRIANI, M. Test results of a high capacity wayside energy storage system using Ni-MH batteries for DC electric railway at New York City Transit. IEEE green technologies conference – green 2011, 2011 Baton Rouge, USA.

OKUI, A., HASE, S., SHIGEEDA, H., KONISHI, T. & YOSHI, T. Application of energy storage system for railway transportation in Japan. Proceeding International Conference Power Electronics Conference (IPEC), 21–24 June 2010 Sapporo, Japan. 3117–3123.

ORTEGA, J. M. & IBAIONDO, H. Kinetic energy recovery on railway systems with feedback to the grid. 9th World Congress on Railway Research – WCRR 2011, 2011 Lille, France.

OTEVREL, V. & OLIVA, L. Comparison of Real-coding Genetic Algorithm with Particle Swarm Optimization on the bandgap bandwidth maximization problem. 17th International Conference Radioelektronika, 24-25 April 2007 Brno, Czech Republic. IEEE, 1-4.

OVSHINSKY, S. R., FETCENKO, M. A. & ROSS, J. 1993. Science. 20.

PEÑA-ALCARAZ, M., FERNÁNDEZ, A., CUCALA, A. P., RAMOS, A. & PECHARROMÁN, R. R. 2011. Optimal underground timetable design based on power flow for maximizing the use of regenerative-braking energy. *Proceedings of the Institution of Mechanical Engineers, Part F: Journal of Rail and Rapid Transit,* 226**,** 397-408.

PIERRE, D. A. 1969. *Optimisation theory with applications,* Bozeman, Montana, John Wiley & Sons, Inc.

POIRIER, E., GHRIBI, M. & KADDOURI, A. Loss minimization control of induction motor drives based on genetic algorithms. IEEE International Electric Machines and Drives Conference, 2001. 475-478.

RADCLIFFE, P., WALLACE, J. S. & SHU, L. H. Stationary applications of energy storage technologies for transit systems. IEEE Electric Power and Energy Conference (EPEC), 25–27 August 2010 Halifax, NS, Canada. 1-7.

RAINES, K. M. Underground Passenger Comfort: Rethinking the current thermal and lighting standards. PLEA2009 - 26th Conference on Passive and Low Energy Architecture, 22-24 June 2009 Quebec City, Canada.

RATNIYOMCHAI, T. , HILLMANSEN, S. & TRICOLI, P. Optimal capacity and positioning of stationary supercapacitors for light rail vehicle systems. Proceeding on International Symposium Power Electronic Electrical Drives, Automation and Motion (SPEEDAM), 18-20 June 2014a Ischia, Italy. 807-812.

RATNIYOMCHAI, T., HILLMANSEN, S. & TRICOLI, P. 2014b. Recent developments and applications of energy storage devices in electrified railways. *IET Electrical System in Transportation,* 4**,** 9-22.

RATNIYOMCHAI, T., HILLMANSEN, S. & TRICOLI, P. Energy Loss Minimisation by Optimal Design of Stationary Supercapacitors for Light Railways. Proceeding on 5th International Conference on Clean Electrical Power: Renewable Energy Resources Impact, 16-18 June 2015 Taormina, Italy. 528-534.

RAY, R. N., CHATTERJEE, D. & GOSWAMI, S. K. 2009. Harmonics elimination in a multilevel inverter using the particle swarm optimisation technique. *IET Power Electronics* 2**,** 646 - 652.

RICHARDSON, M. B. Flywheel energy storage system for traction applications. IEEE international conference on power electronics, machines and drives, 2002 Bath, UK.

RSSB 2010. Research Programme, Engineering, phase 2: OHL electrification gaps. *Energy storage systems for railway application.*

RUFER, A. Energy storage for railway systems, energy recovery and vehicle autonomy in Europe. International Conference on Power Electronics Conference (IPEC), 21–24 June 2010 Sapporo, Japan. 3124–3127.

RUFER, A., HOTELLIER, D. & BARRADE, P. 2004. A supercapacitor-based energy storage substation for voltage compensation in weak transportation networks. *IEEE Transaction on Power Delivery,* 19**,** 629-636.

SALAMEH, Z. 2014. *Chapter 4 – Energy Storage*, Elsevier B.V. .

SEKIJIMA, Y., KUDO, Y., INUI, M., MONDEN, Y., TODA, S. & AOYAMA, I. Development of energy storage system for DC electric rolling stock applying electric double layer capacitor. 7th World Congress on Railway Research, 4–7 June 2006 Fairmont the Queen Elizabeth Montreal, Canada. 1-7.

SELAMAT, H. & BILONG, S. D. A. Optimal controller design for a railway vehicle suspension system using Particle Swarm Optimization. 9th Asian on Control Conference (ASCC), 23-26 June 2013 Istanbul, Turkey. IEEE, 1-5.

SHARMA, P. & BHATTI, T. S. 2010. A review on electrochemical double-layer capacitors. *Energy Conversion and Management,* 51**,** 2901–2912.

SHINDO, T. & JIN'NO, K. Switching angles optimization of single phase PWM DC-AC inverter by particle swarm optimizations. 6th International Conference on Soft Computing and Intelligent Systems (SCIS) and 13th International Symposium on Advanced Intelligent Systems (ISIS), 20-24 Nov. 2012 Kobe, Japan. IEEE, 65-70.

SHIONUMA, K., YOKOKAWA, M. & NAGAURA, T. Characteristics of lithium ion rechargeable battery. Proceeding of Abstracts 32nd Battery Symposium, 9-11 September 1991 Kyoto, Japan. 33-34.

SIEMENS. SITRAS SES Static energy storage systems based on double layer capacitor technology – the gateway to high efficient improvement of mass transit power

supply. 2nd UIC Railway Energy Efficiency Conference, 4– 5 February 2004 Paris, France.

SIEMENS 2012. Simotics low-voltage motors. *In:* SIEMENS (ed.) *Catalog D 81.1.*

SON, K., NOH, S., KWON, K., CHOI, J. & LEE, E. K. Line voltage regulation of urban transit systems using supercapacitors. IEEE 6th International on Power Electronics and Motion Control Conference 2009 (IPEMC '09) 17-20 May 2009 Wuhan, China. IEEE, 933 - 938.

SONG, J., ZHENG, H. & ZHANG, L. Application of particle swarm optimization algorithm and genetic algorithms in beam broadening of phased array antenna. International Symposium on Signals, Systems and Electronics, 17-20 Sept. 2010 Nanjing, China. IEEE, 1-4.

SRIKAEW, A. 2009. *Computational Intelligence,* Suranaree University of Technology.

SRINIVASAN, D., LONG, C. R. & PENG, P. Y. Hybrid fuzzy logic-genetic algorithm technique for automated detection of traffic incidents on freeways. Proceedings of 2001 IEEE Intelligent Transportation Systems, 2001. 352-357.

STEINER, M., KLOHR, M. & PAGIELA, S. Energy storage system with UltraCaps on board of railway vehicles. European Conference Power Electrics and Application, 2–5 September 2007 Aalborg, Denmark. 1-10.

STEINER, M. & SCHOLTEN, J. Energy storage on board of DC fed railway vehicles. IEEE annual Power Electronics Specialists Conference – PESC, 2004 Aachen, Germany.

STEWART, E., WESTON, P., HILLMANSEN, S. & ROBERTS, C. The Merseyrail Energy Monitoring Project. 9th World congress on railway research - WCRR 2011, 2011 Lille, France.

SUN, S., LI, Y. & XU, H. Energy Consumption Optimization for High-Speed Railway Based on Particle Swarm Algorithm. Fourth International Conference on Computational Intelligence and Communication Networks (CICN), 3-5 Nov. 2012 Mathura, India. IEEE, 879-882.

TEYMOURFAR, R., ASAEI, B., IMAN-EINI, H. & NEJATI-FARD, R. 2012. Stationary super-capacitor energy storage system to save regenerative braking energy in a metro line. *Energy Conversion and Management,* 56**,** 206-214.

THOMPSON, J. A., MAIDMENT, G. G. & MISSENDEN, J. F. 2006. Modelling low-energy cooling strategies for underground railways. *Apply Energy,* 83**,** 1152-1162.

TSAIS, P.-J. & CHAN, L. I. 2013. *11 - Nickel-based batteries: materials and chemistry*, Woodhead Publishing

TZENG, J., EMERSON, R. & MOY, P. 2006. Composite Flywheel Development for Energy Storage Composite science technology.

VALLE, Y. D., VENAYAGAMOORTHY, G. K., MOHAGHEGHI, S., HERNANDEZ, J. C. & HARLEY, R. G. 2008. Particle Swarm Optimization: Basic Concepts, Variants and Applications in Power Systems. *IEEE Transactions on Evolutionary Computation,* 12**,** 171 - 195.

VATANKHAH, R., ETEMADI, S., HONARVAR, M., ALASTY, A., BOROUSHAKI, M. & VOSSOUGHI, G. Online velocity optimization of robotic swarm flocking using particle swarm optimization (PSO) method. ISMA '09. 6th International Symposium on Mechatronics and its Applications, 23-26 March 2009 Sharjah, UAE. IEEE, 1-6.

VAZQUEZ, S., LUKIC, S. M., GALVAN, E., FRANQUELO, L. G. & CARRASCO, J. M. 2010. Energy Storage Systems for Transport and Grid Applications. *IEEE Transactions on Industrial Electronics,* 57**,** 3881 - 3895.

VISIOLI, A. Optimal tuning of pid controllers for integral and unstable processes. IEE Proceedings of Control Theory and Applications, March 2001. 180-184.

WALHA, C. , BEZINE, H. & ALIMI, A. M. A Multi- Objective Particle Swarm Optimization approach to robotic grasping. International Conference on Individual and Collective Behaviors in Robotics (ICBR), 15-17 Dec. 2013 Sousse, Tunisia. IEEE, 120-125.

WANG, K. 2013. Calculus of Variation: An Introduction to Isoperimetric Problems. The University of Sydney SSP Working Seminars, MATH2916.

WANG, S., ZHAO, P. & QIAO, K. Study on passenger train stopping scheme based on improved Particle Swarm Optimization algorithm. IEEE International Conference on Intelligent Computing and Intelligent Systems (ICIS 2009), 20-22 Nov. 2009 Shanghai, China. IEEE, 821-826.

WARIN, Y., LANSELLE, R. & THIOUNN, M. Active substation. 9th World Congress on Railway Research – WCRR 2011, 2011 Lille, France.

WASIAK, I., PAWELEK, R. & MIENSKI, R. 2014. Energy storage application in low-voltage microgrids for energy management and power quality improvement. *IET Generation, Transmission & Distribution,* 8.

WEI, L. , QUNZHAN, L. & BING, T. Energy Saving Train Control for Urban Railway Train with Multi- population Genetic Algorithm. International Forum on Information Technology and Applications (IFITA '09) , 15- 17 May 2009 Chengdu, China. 58-62.

WEILE, D. S. & MICHIELSSEN, E. 2001. The control of adaptive antenna arrays with genetic algorithms using dominance and diploidy. *IEEE Transactions on Antennas and Propagation,* 49**,** 1424-1433.

WHEELER, P. Voltage regulation application of a kinetic energy storage system. 2nd International Conference on Power Electronics, Machines and Drives (PEMD), 31 March–2 April 2004. 605–608.

WONG, Y. K., CHUNG, T. S. & LAI, W. M. 2000. Application of genetic algorithm in reactive power/voltage control-problem. *International Conference on Advances in Power System Control, Operation and Management.*

WU, D., FEI, W., LUK, P. C. K. & XIA, B. Design considerations of outer-rotor permanent magnet synchronous machines for in-wheel electric drivetrain using particle swarm optimization. 7th IET International Conference on Power Electronics, Machines and Drives (PEMD 2014), 8-10 April 2014 Manchester, UK. IET, 1-6.

XIANGZHENG, X., BAICHAO, C. & FANGCHENG, G. Electrical Railway Active Power Filter Research Based on Genetic Algorithms. IEEE International Conference on Control and Automation (ICCA 2007), 30 May - 1 June 2007 Guangzhou, China. 1465-1468.

YAMAZAKI, Y., AIYOSHIN, V., KRASILNIKOVA, J. & KRASILNIKOV, I. Adaptive-intelligent control by neural-network and genetic-algorithm systems and its application. Proceedings of Second International Conference on Knowledge-Based Intelligent Electronic Systems, 1998. 230-239.

YANG, X. S. 2010. *Nature-Inspired Metaheuristic Algorithms* UK, Luniver Press.

YANG, Y., CHEN, R., YU, J. & CHEN, R. Improved Particle Swarm Optimization Based Fault Diagnosis Approach for Power Electronic Devices. 2009 WRI Global Congress on Intelligent Systems 19-21 May 2009 Xiamen, China. IEEE, 183 - 187.

YASSIN, I. M., TAIB, M. N., RAHIM, N. A., SALLEH, M. K. M. & ABIDIN, H. Z. Particle Swarm Optimization for NARX structure selection — Application on DC motor model. IEEE Symposium on Industrial Electronics & Applications (ISIEA), 3-5 Oct. 2010 Penang, Malaysia. IEEE, 456 - 462.

YE, Y., SHARMA, R. & GARG, P. An integrated power management strategy of hybrid energy storage for renewable application. IECON 2014 - 40th Annual Conference of the IEEE Industrial Electronics Society, Oct. 29 2014-Nov. 2014 Dallas, TX. IEEE, 3088 - 3093.

YONG-HUA, S. & IRVING, M. R. 2001. Optimisation techniques for electrical power systems iI. heuristic optimisation methods. *Power Engineering Journal,* 15**,** 151-160.

YU, T. F. & PENG, C. H. Application of an improved Particle Swarm Optimization to economic load dispatch in power plant. 3rd International Conference on Advanced Computer Theory and Engineering (ICACTE), 20-22 Aug. 2010 Chengdu, China. IEEE, V2-619 - V2-624.

YUAN, X., YANG, D. & LIU, H. MPPT of PV system under partial shading condition based on adaptive inertia weight particle swarm optimization algorithm. IEEE International Conference on Cyber Technology in Automation, Control, and Intelligent Systems (CYBER), 8-12 June 2015 Shenyang, China. IEEE, 729 - 733.

ZHAN, Z. H. & ZHANG, J. Orthogonal learning particle swarm optimization for power electronic circuit optimization with free search range. IEEE Congress of Evolutionary Computation (CEC), 5-8 June 2011 New Orleans, LA. IEEE, 2563 - 2570.

ZHAO, Y., LI, X., LI, Y. & JI, H. Resource allocation for high-speed railway downlink MIMO- OFDM system using quantum- behaved particle swarm optimization. IEEE International Conference on Communications (ICC) , 9- 13 June 2013 Budapest, Hungary. IEEE, 2343 - 2347.

ZHU, X., ZHANG, W., WANG, Y. & LIANG, H. Optimal dispatch of wind farm based on particle swarm optimization algorithm. IEEE International Conference on Power System Technology (POWERCON), Oct. 30 2012-Nov. 2012 Auckland, New Zealand. IEEE, 1-5.

Appendix A: Additional Results

The results of the percentage SOC of each stationary EDLC with the train travelling two round trips in 31 scenarios of the initial SOC of the stationary EDLCs are as shown in Figures A.1 to A.31. The sequence of the title in each figure is the number of the scenario based on Table 5.5 and the %SOC of stationary EDLCs 1 – 4.

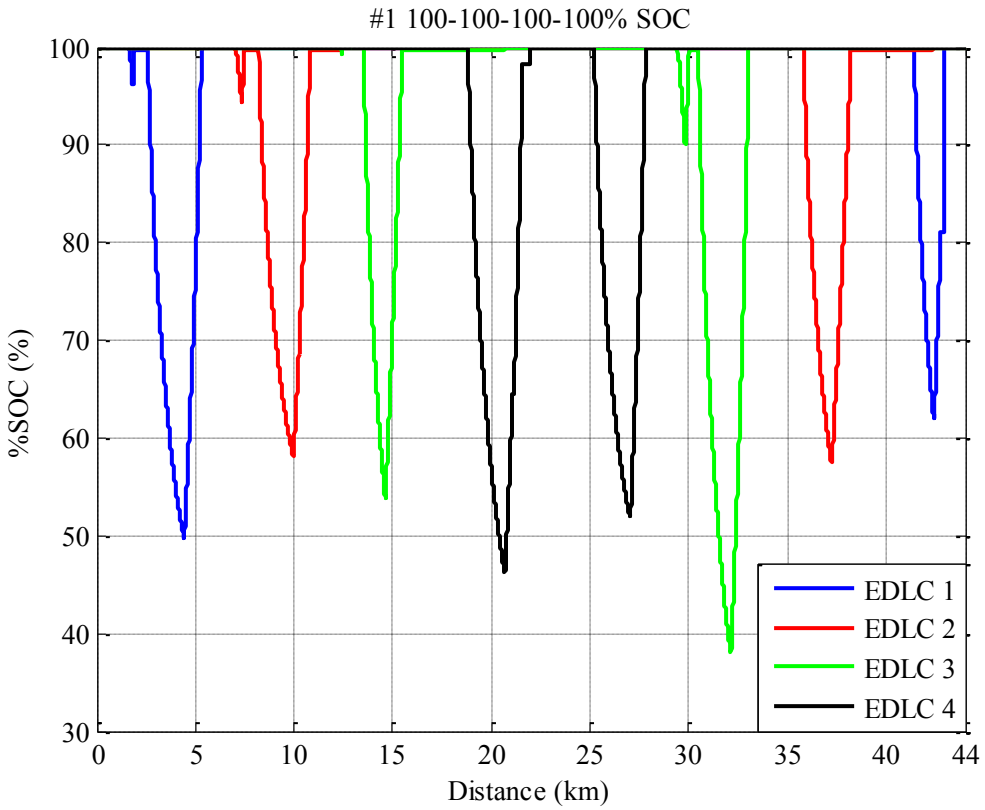

Figure A.1: Scenario 1, %SOC of 100, 100, 100 and 100 of stationary EDLCs

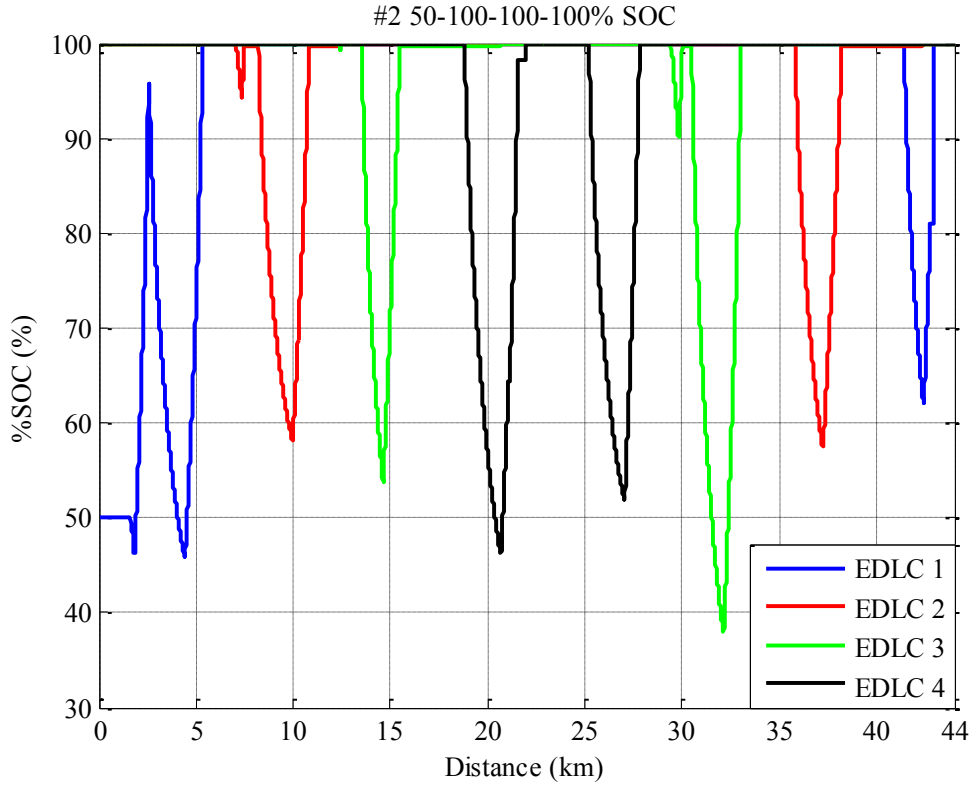

Figure A.2: Scenario 2, %SOC of 50, 100, 100 and 100 of stationary EDLCs

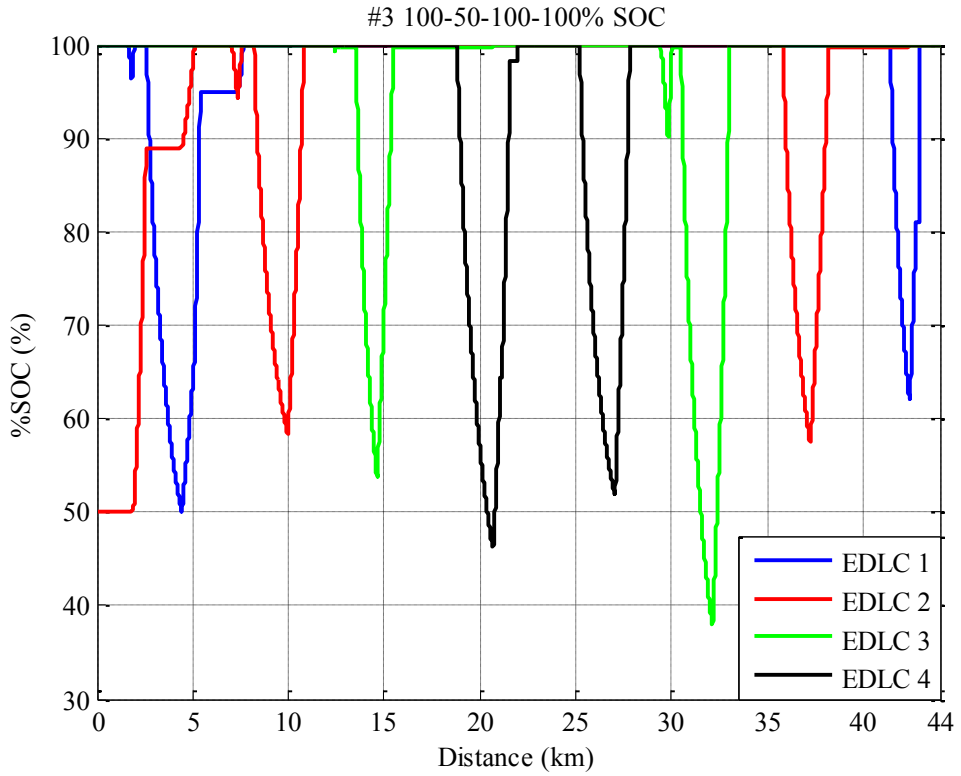

Figure A.3: Scenario 3, %SOC of 100, 50, 100 and 100 of stationary EDLCs

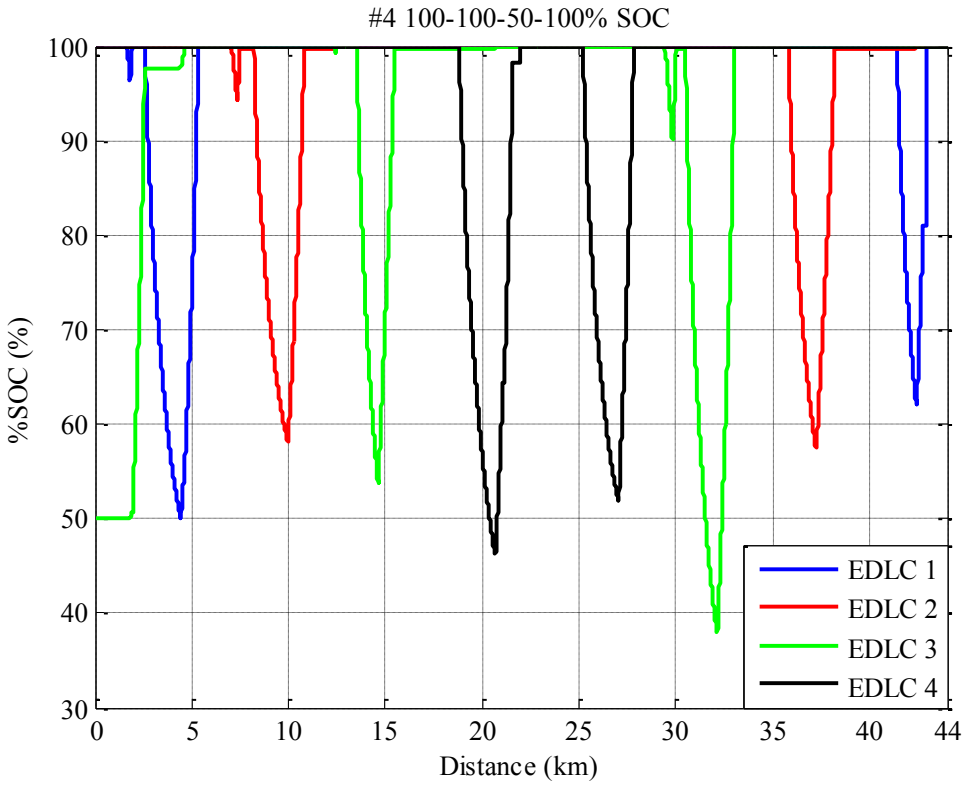

Figure A.4: Scenario 4, %SOC of 100, 100, 50 and 100 of stationary EDLCs

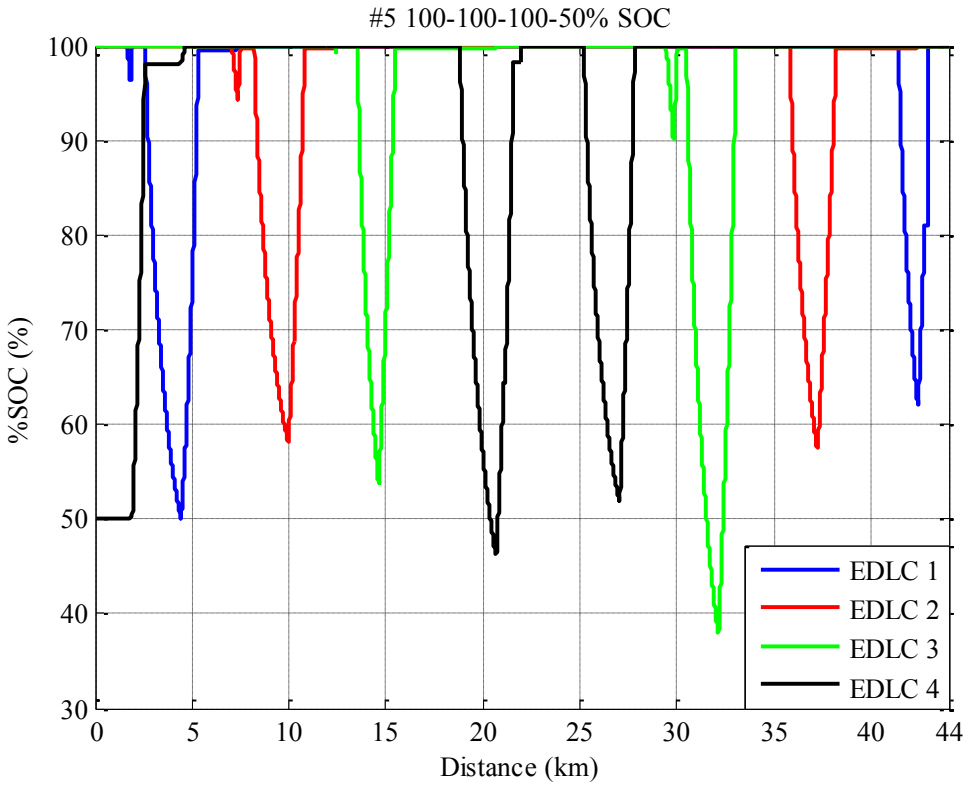

Figure A.5: Scenario 5, %SOC of 100, 100, 100 and 50 of stationary EDLCs

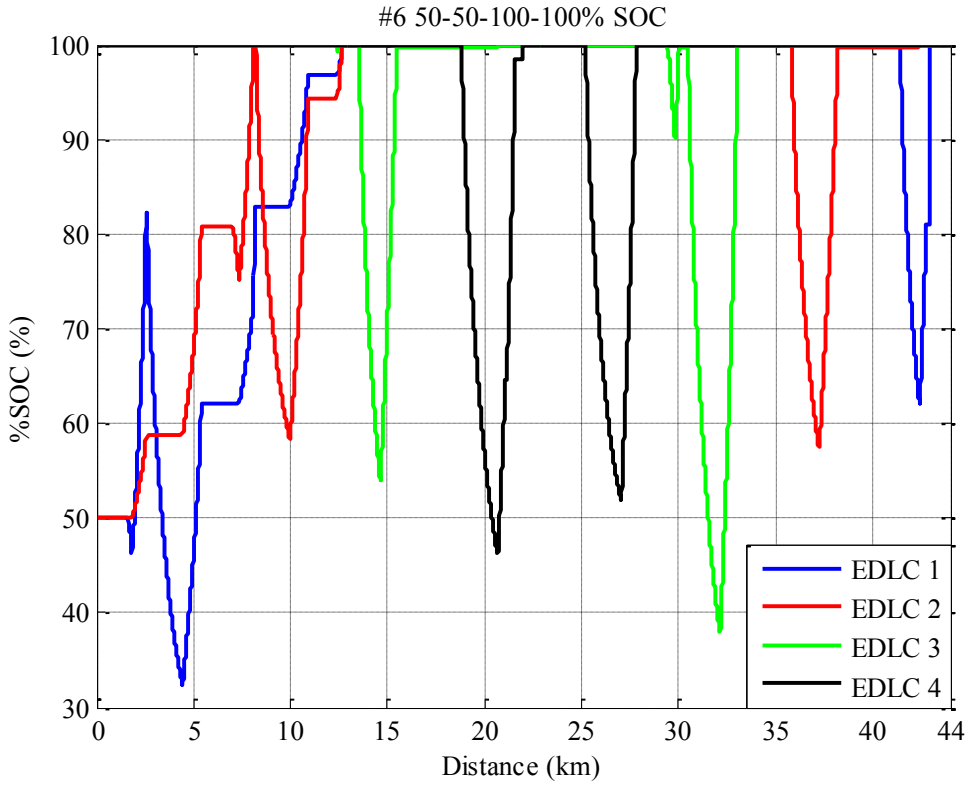

Figure A.6: Scenario 6, %SOC of 50, 50, 100 and 100 of stationary EDLCs

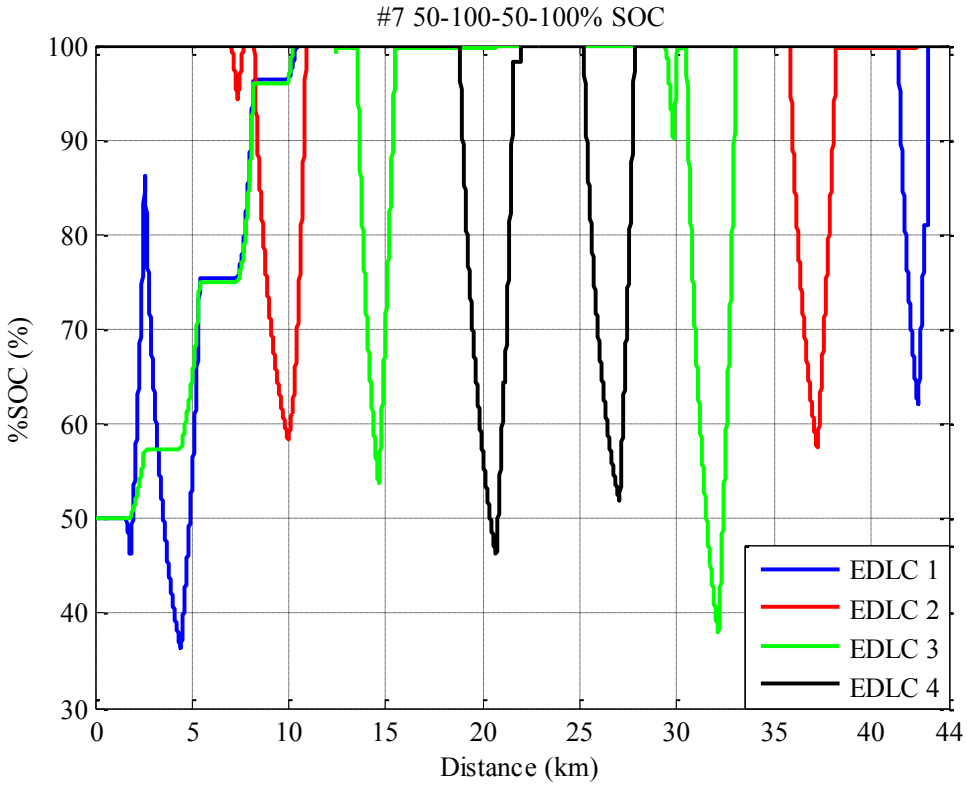

Figure A.7: Scenario 7, %SOC of 50, 100, 50 and 100 of stationary EDLCs

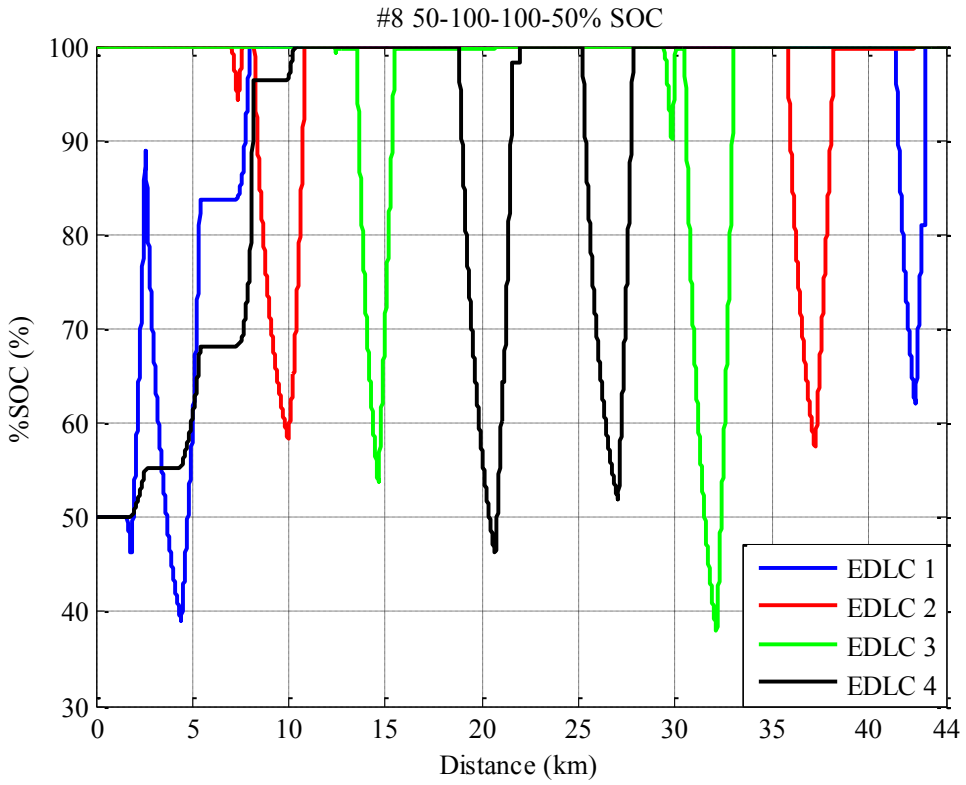

Figure A.8: Scenario 8, %SOC of 50, 100, 100 and 50 of stationary EDLCs

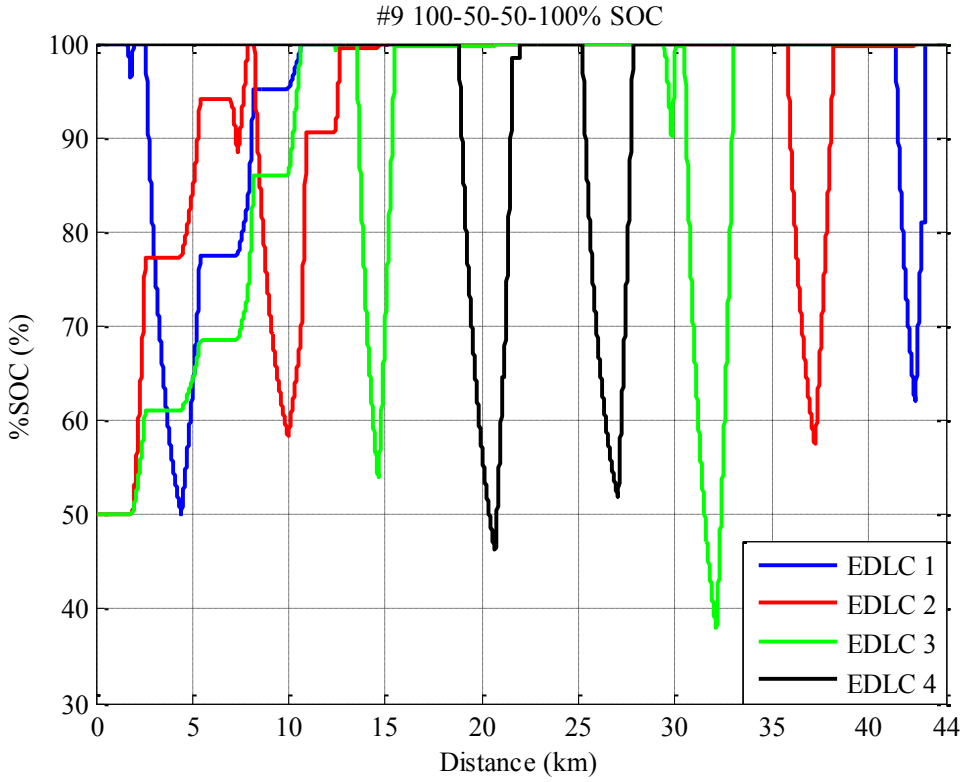

Figure A.9: Scenario 9, %SOC of 100, 50, 50 and 100 of stationary EDLCs

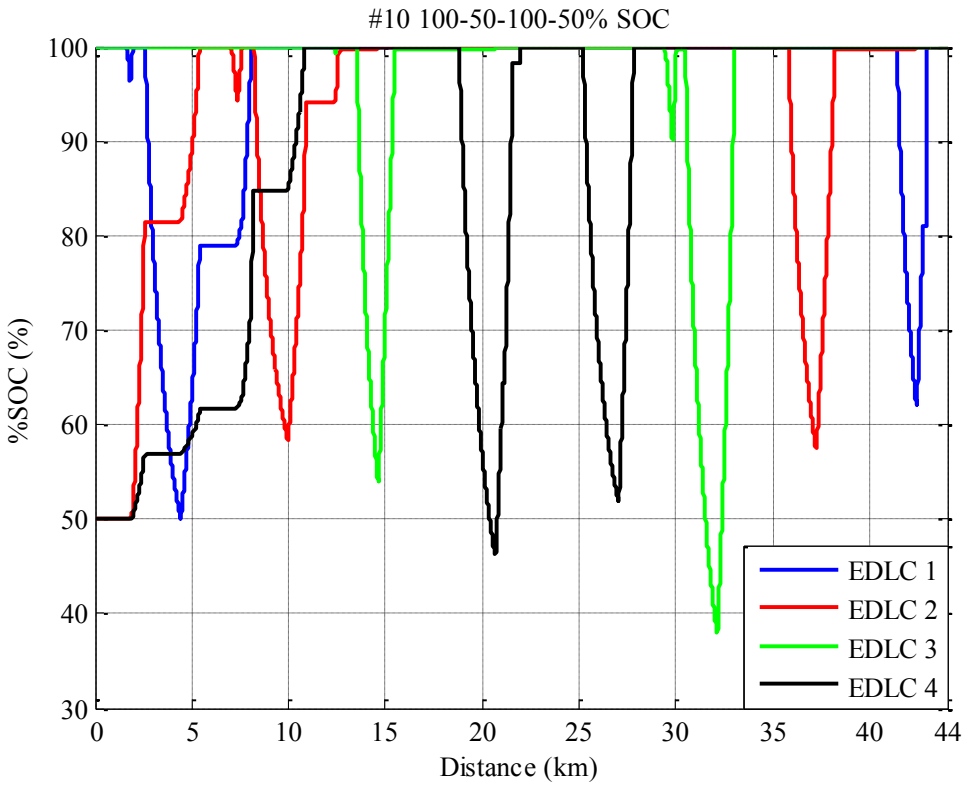

Figure A.10: Scenario 10, %SOC of 100, 50, 100 and 50 of stationary EDLCs

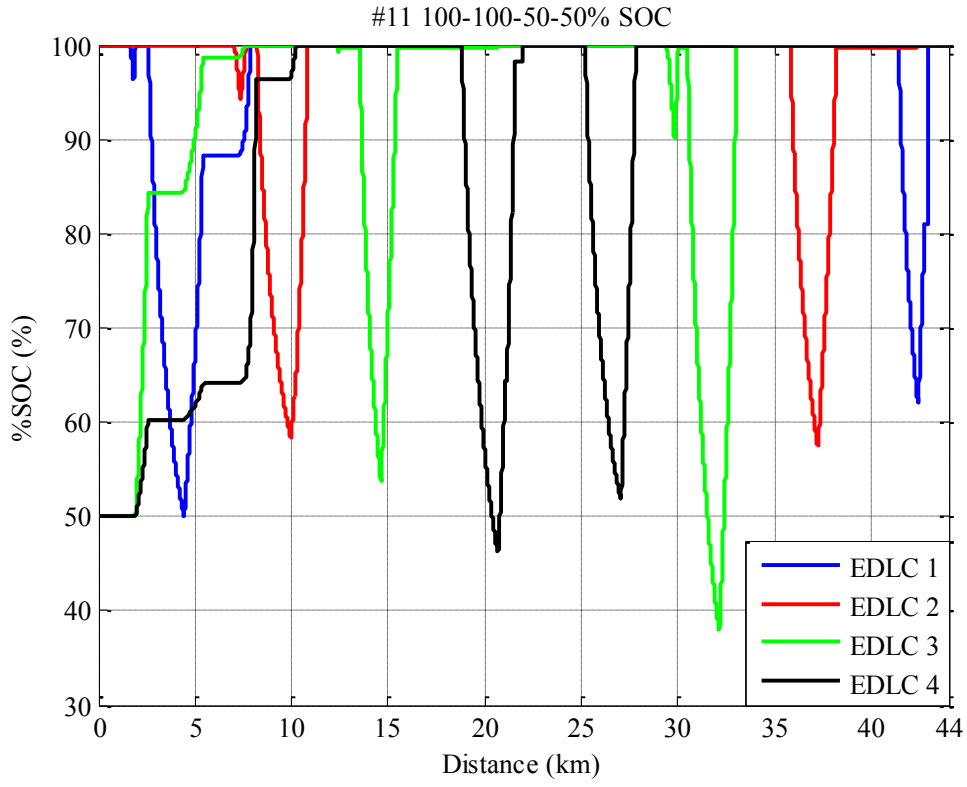

Figure A.11: Scenario 11, %SOC of 100, 100, 50 and 50 of stationary EDLCs

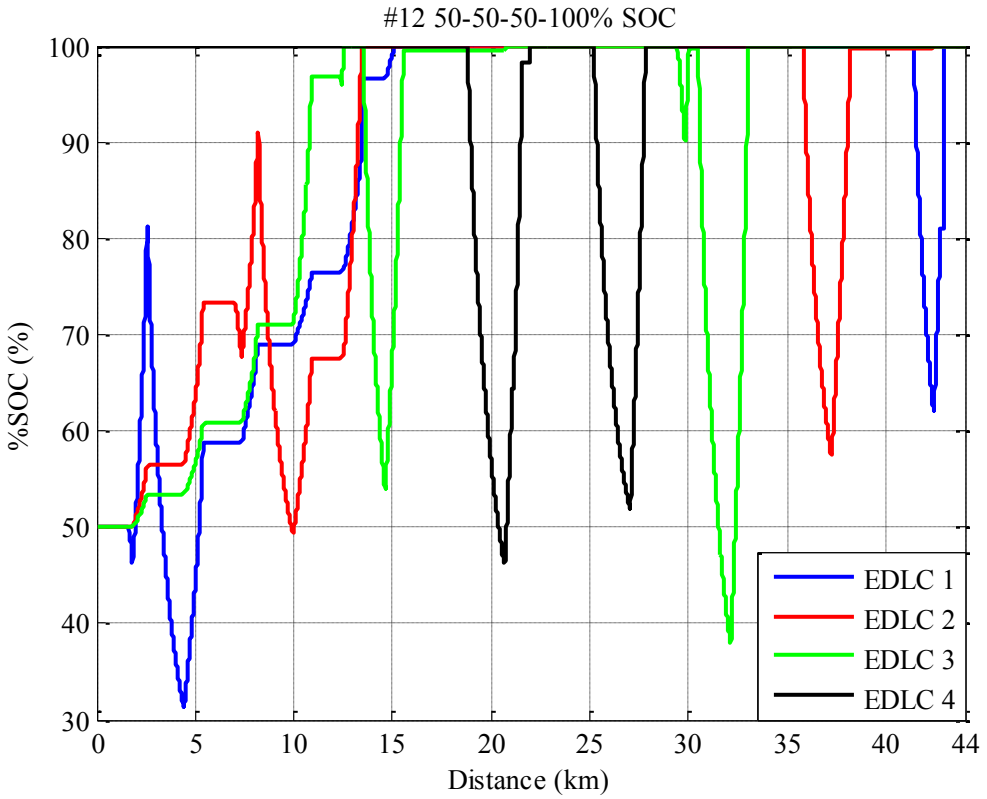

Figure A.12: Scenario 12, %SOC of 50, 50, 50 and 100 of stationary EDLCs

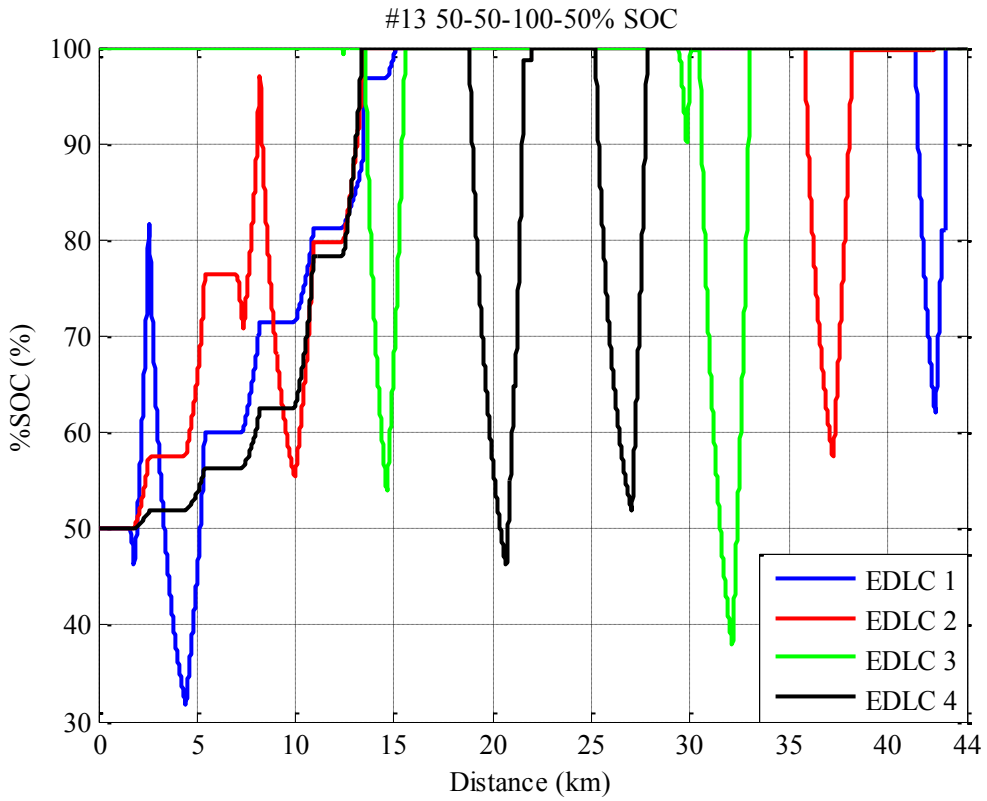

Figure A.13: Scenario 13, %SOC of 50, 50, 100 and 50 of stationary EDLCs

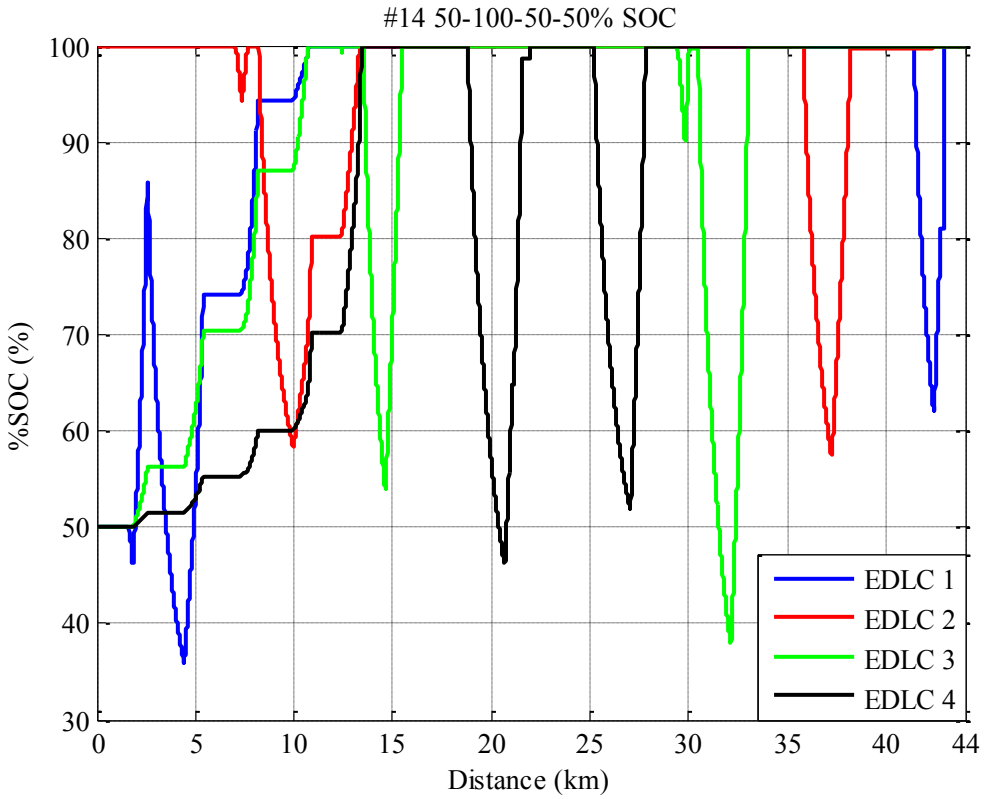

Figure A.14: Scenario 14, %SOC of 50, 100, 50 and 50 of stationary EDLCs

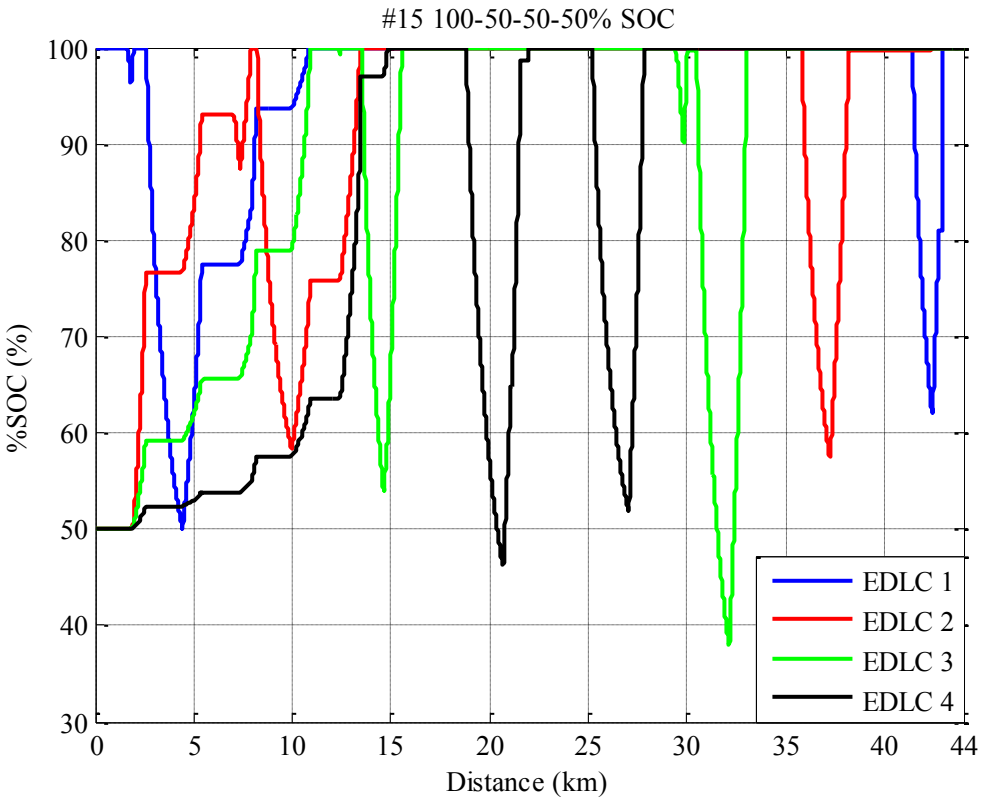

Figure A.15: Scenario 15, %SOC of 100, 50, 50 and 50 of stationary EDLCs

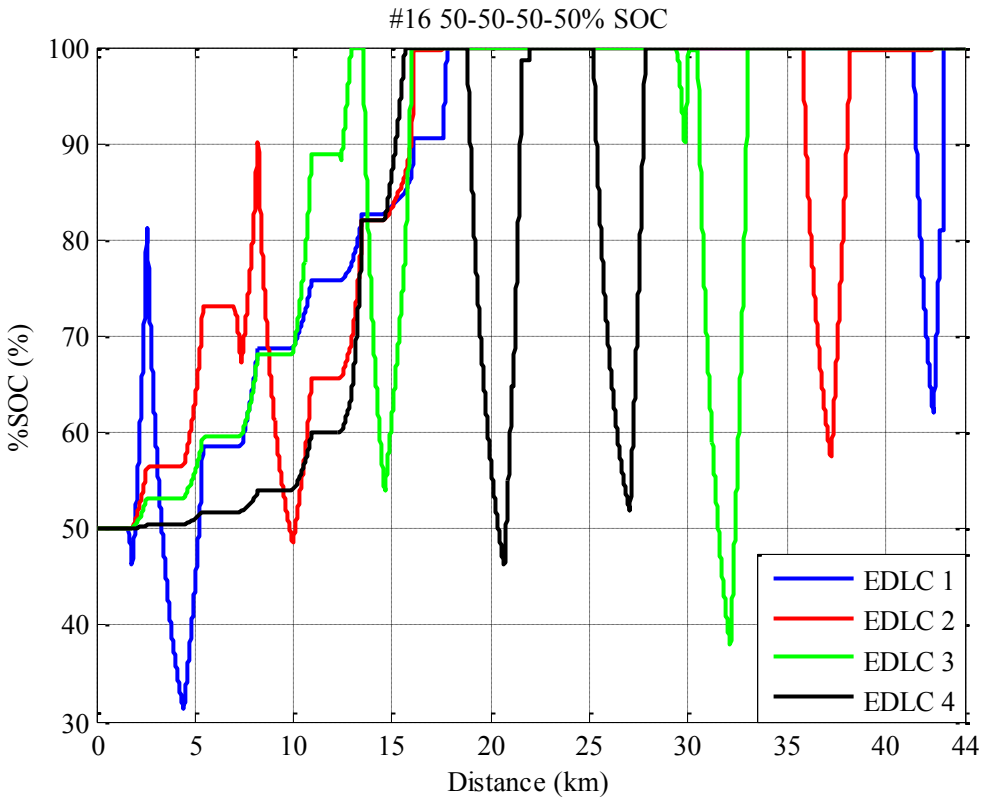

Figure A.16: Scenario 16, %SOC of 50, 50, 50 and 50 of stationary EDLCs

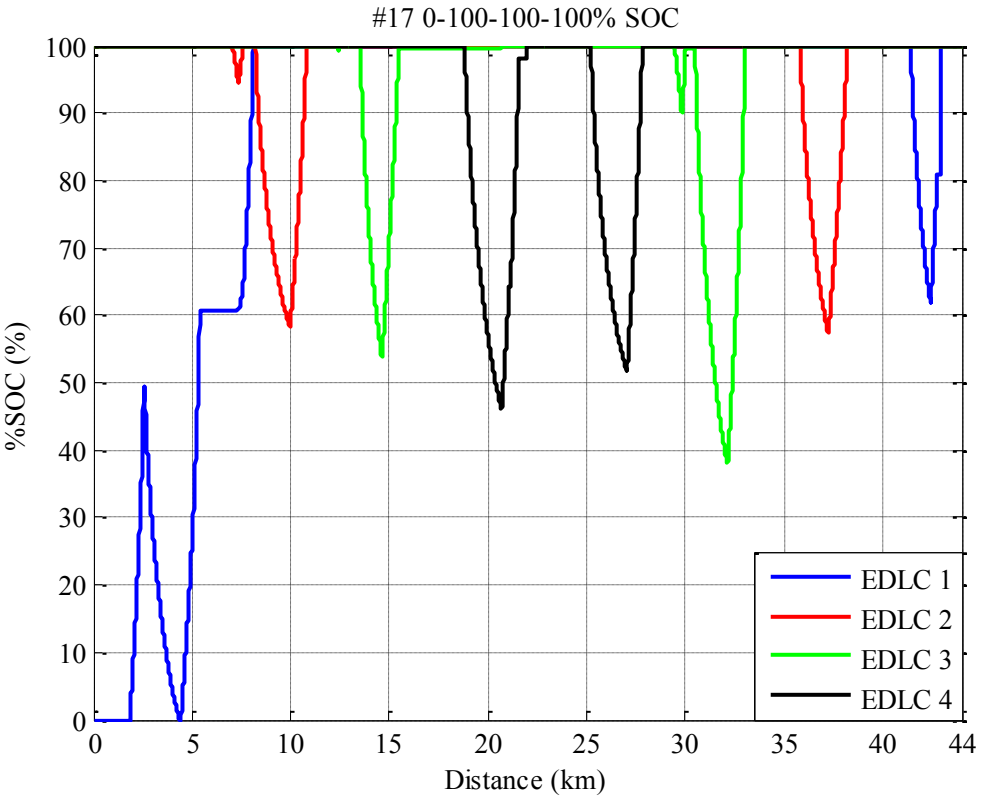

Figure A.17: Scenario 17, %SOC of 0, 100, 100 and 100 of stationary EDLCs

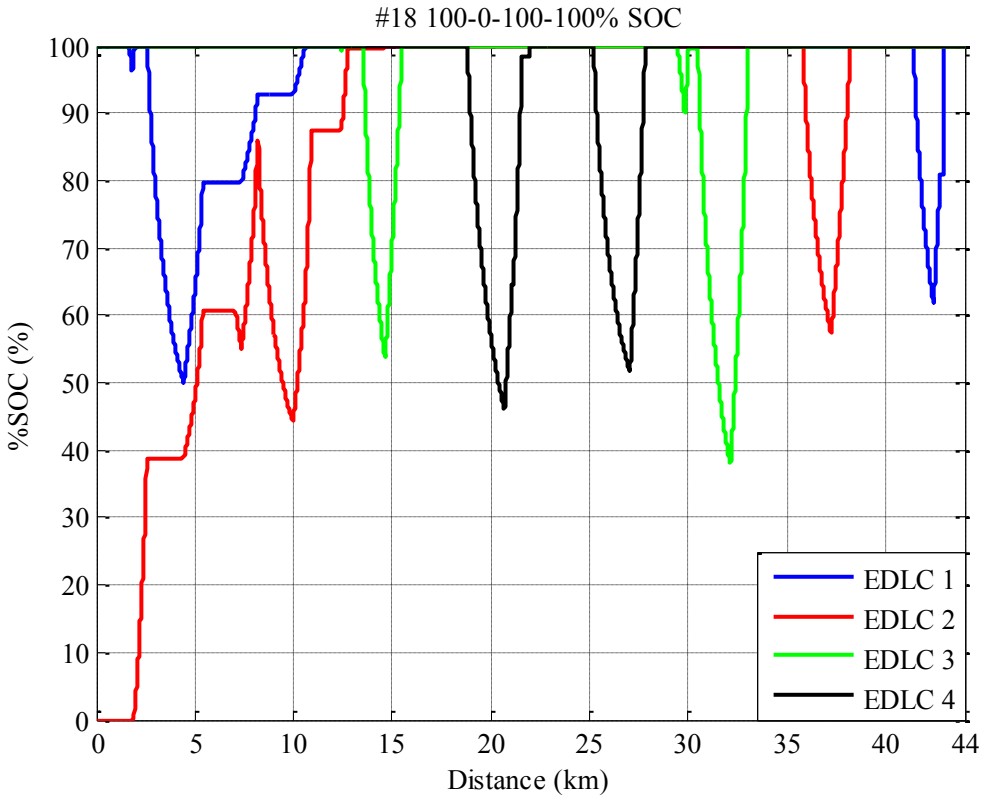

Figure A.18: Scenario 18, %SOC of 100, 0, 100 and 100 of stationary EDLCs

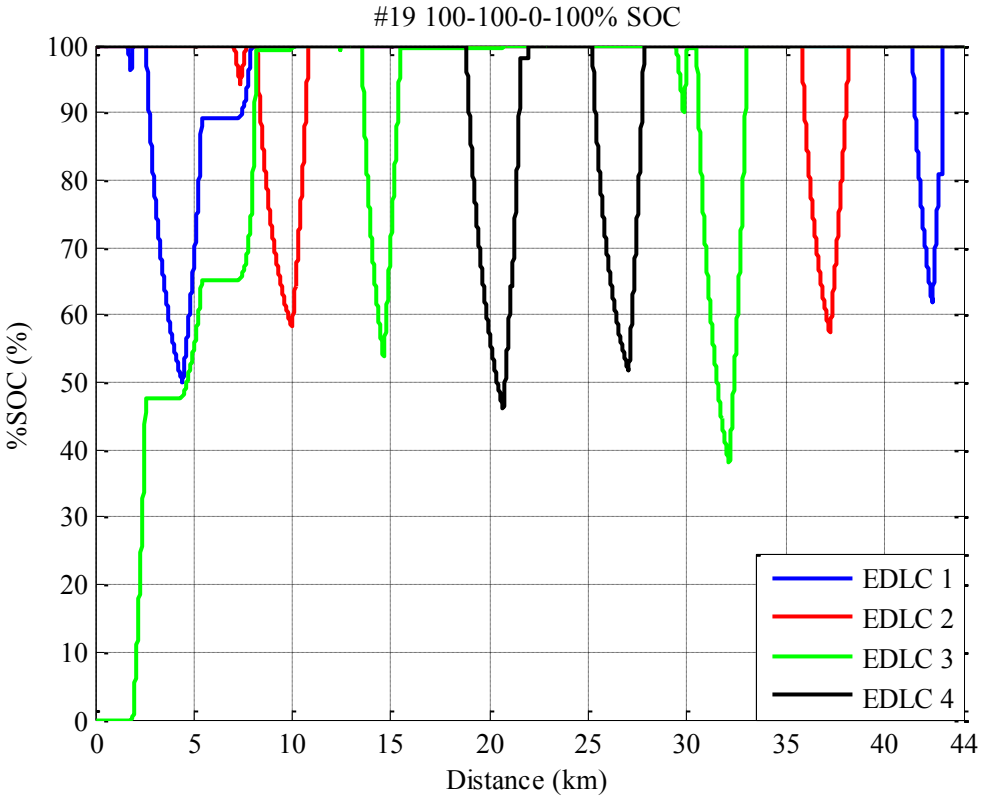

Figure A.19: Scenario 19, %SOC of 100, 100, 0 and 100 of stationary EDLCs

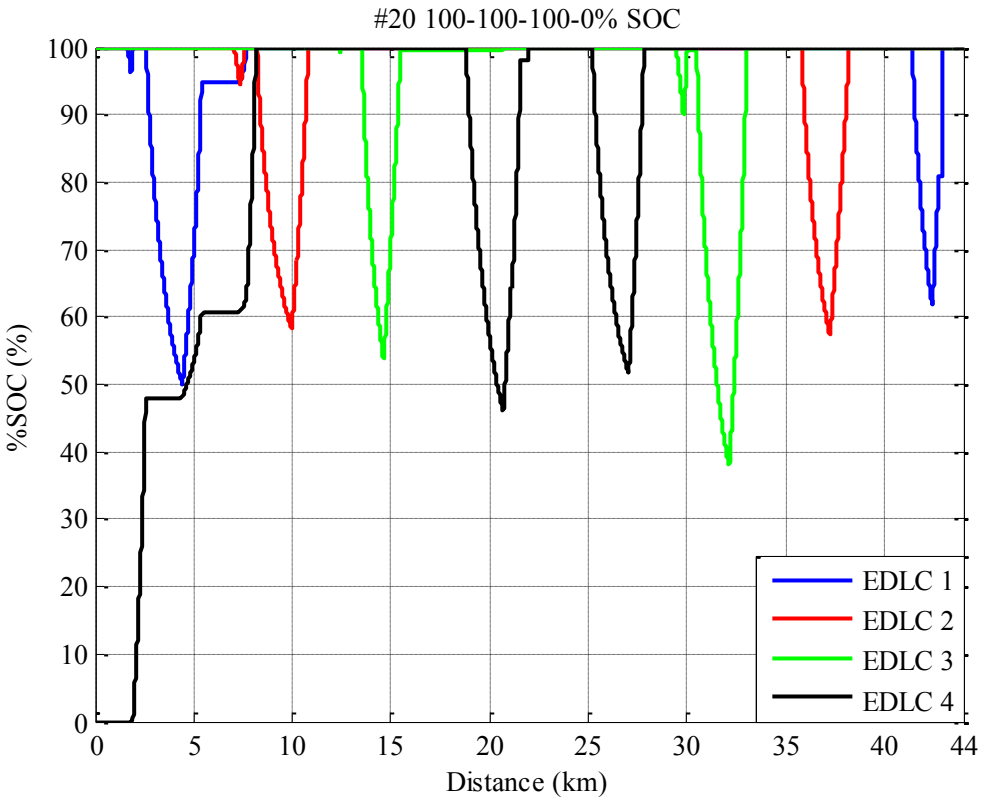

Figure A.20: Scenario 20, %SOC of 100, 100, 100 and 0 of stationary EDLCs

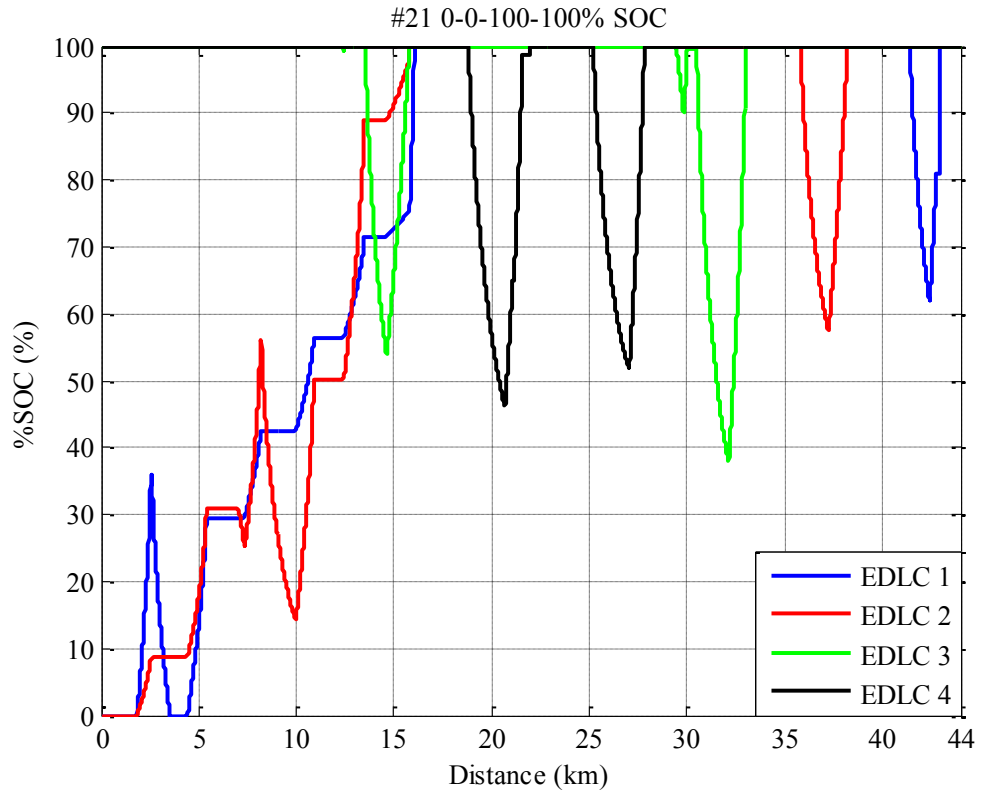

Figure A.21: Scenario 21, %SOC of 0, 0, 100 and 100 of stationary EDLCs

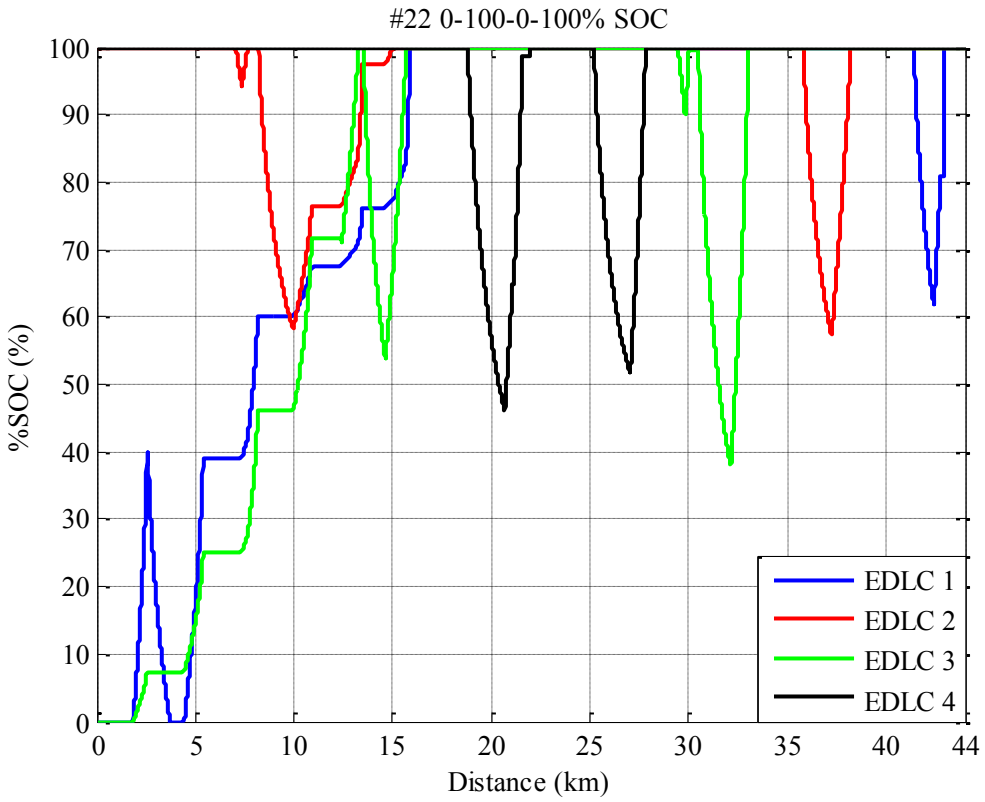

Figure A.22: Scenario 22, %SOC of 0, 100, 0 and 100 of stationary EDLCs

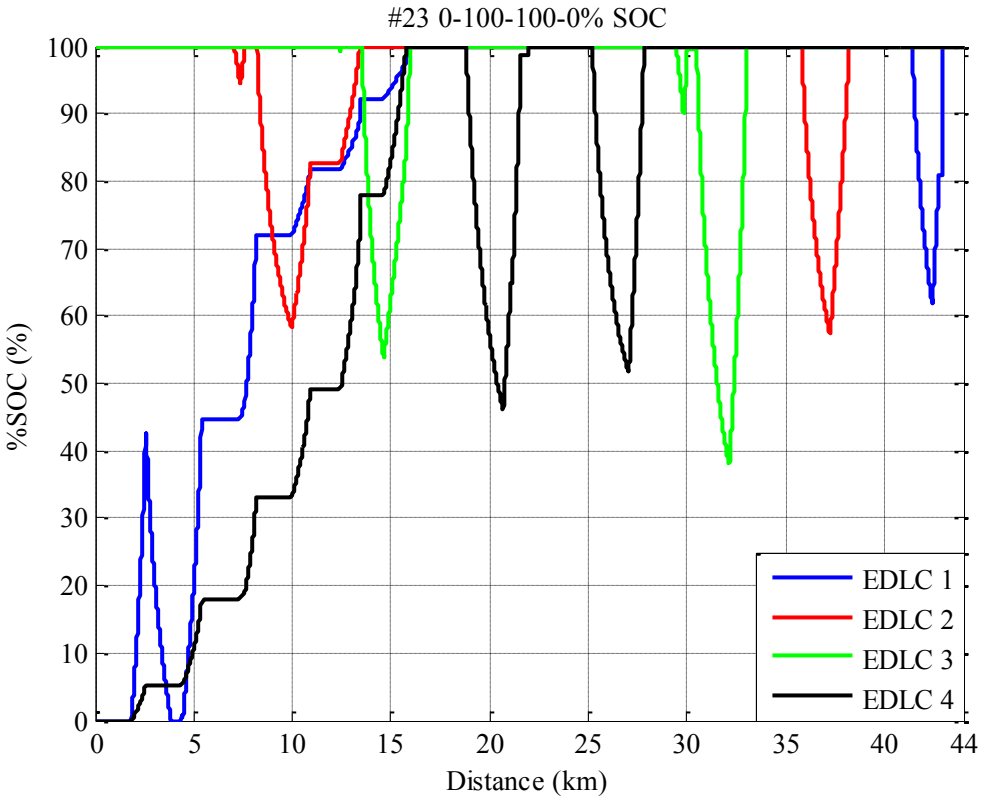

Figure A.23: Scenario 23, %SOC of 0, 100, 100 and 0 of stationary EDLCs

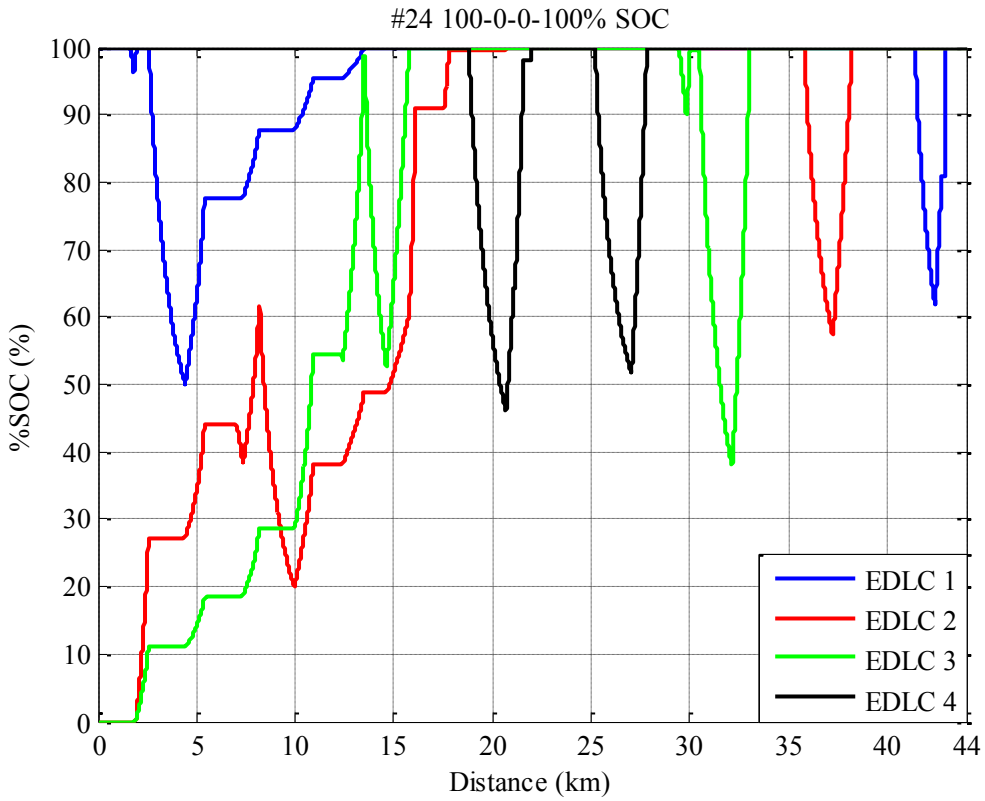

Figure A.24: Scenario 24, %SOC of 100, 0, 0 and 100 of stationary EDLCs

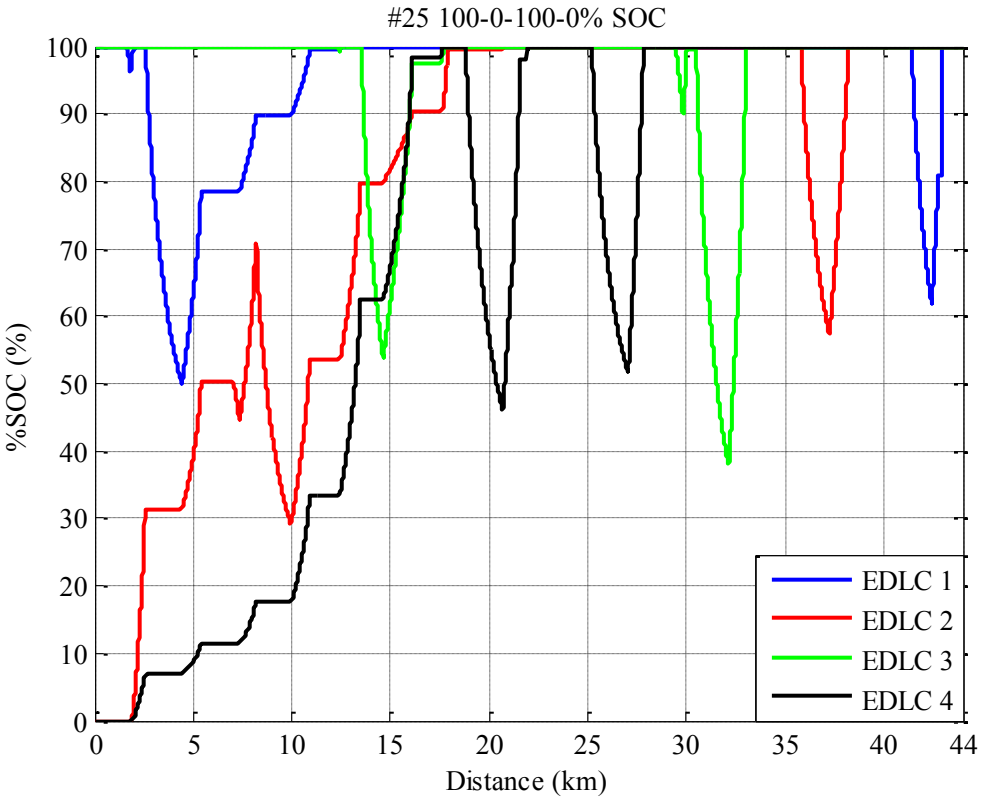

Figure A.25: Scenario 25, %SOC of 100, 0, 100 and 0 of stationary EDLCs

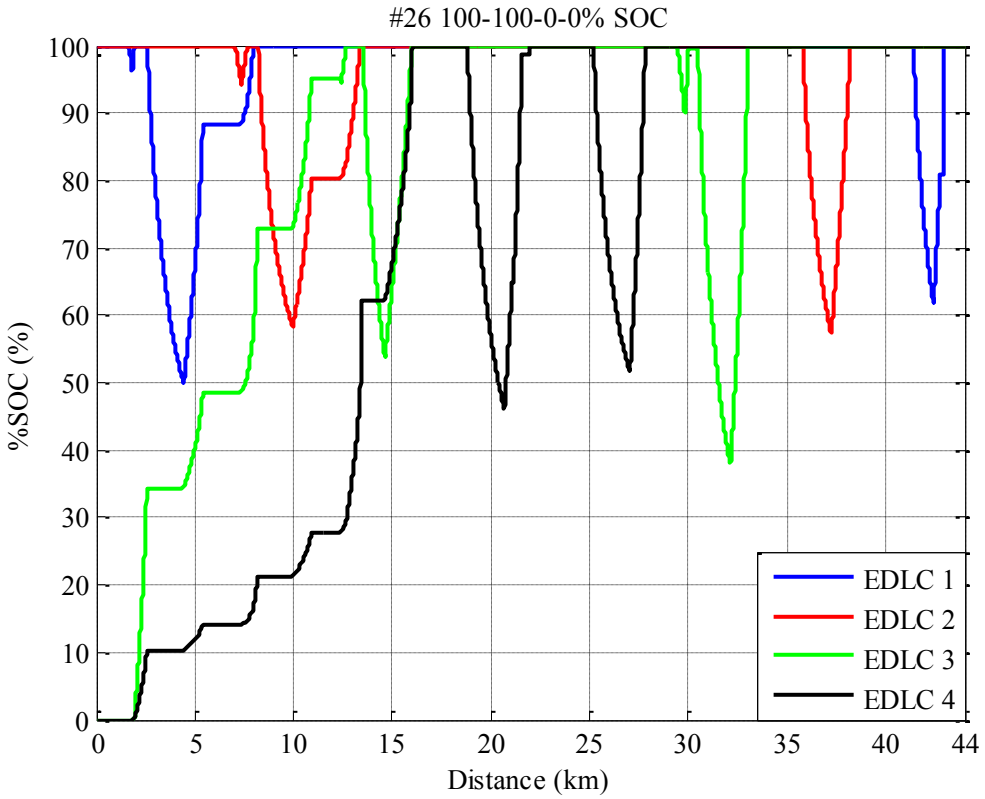

Figure A.26: Scenario 26, %SOC of 100, 100, 0 and 0 of stationary EDLCs

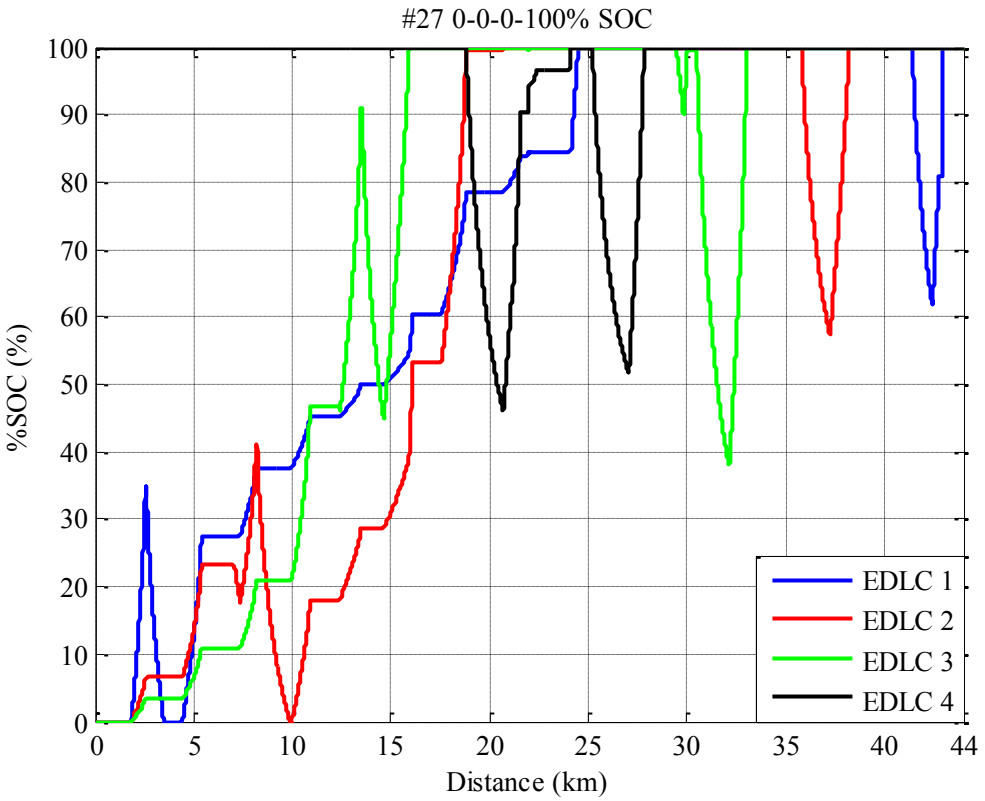

Figure A.27: Scenario 27, %SOC of 0, 0, 0 and 100 of stationary EDLCs

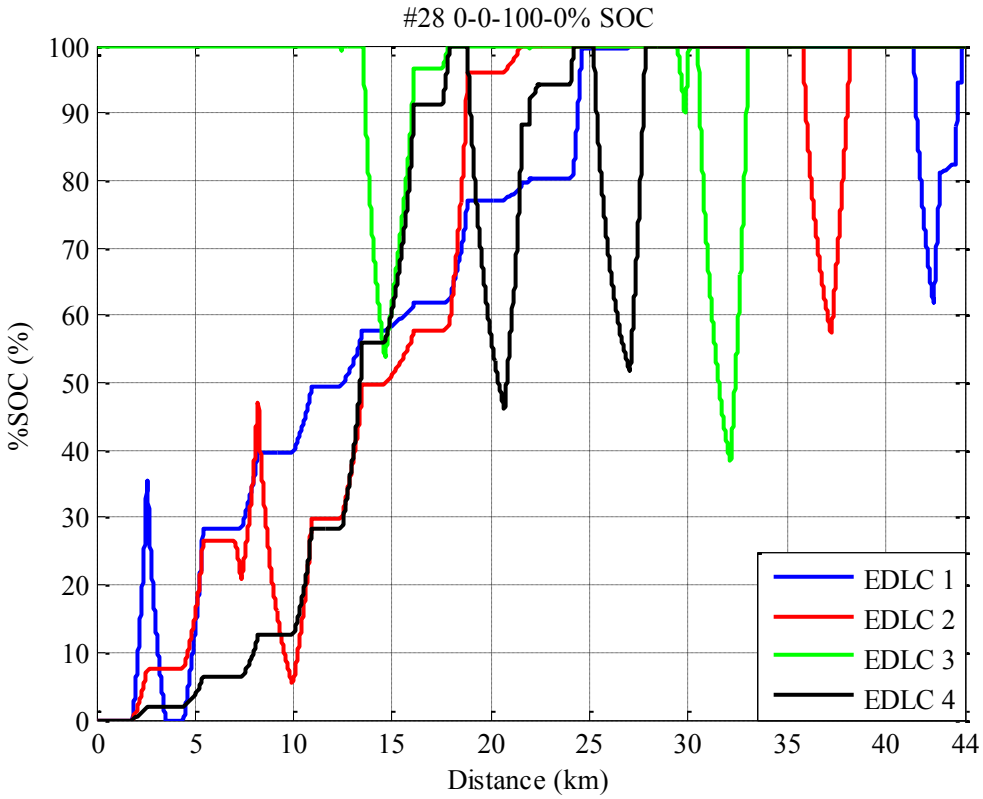

Figure A.28: Scenario 28, %SOC of 0, 0, 100 and 0 of stationary EDLCs

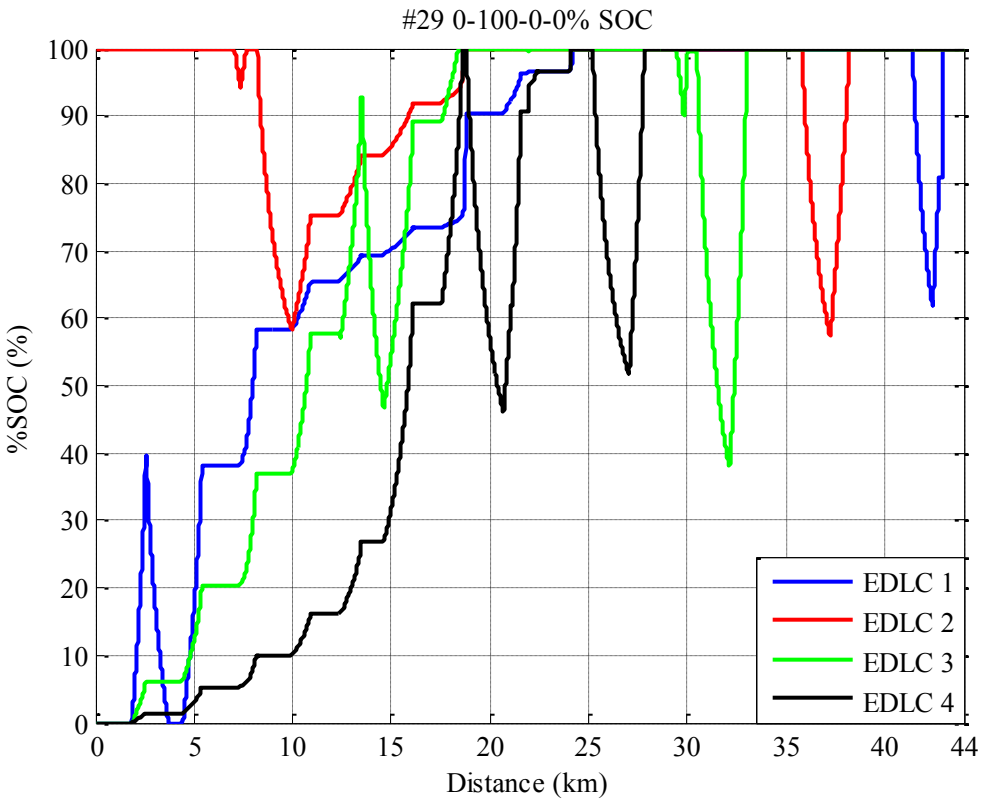

Figure A.29: Scenario 29, %SOC of 0, 100, 0 and 0 of stationary EDLCs

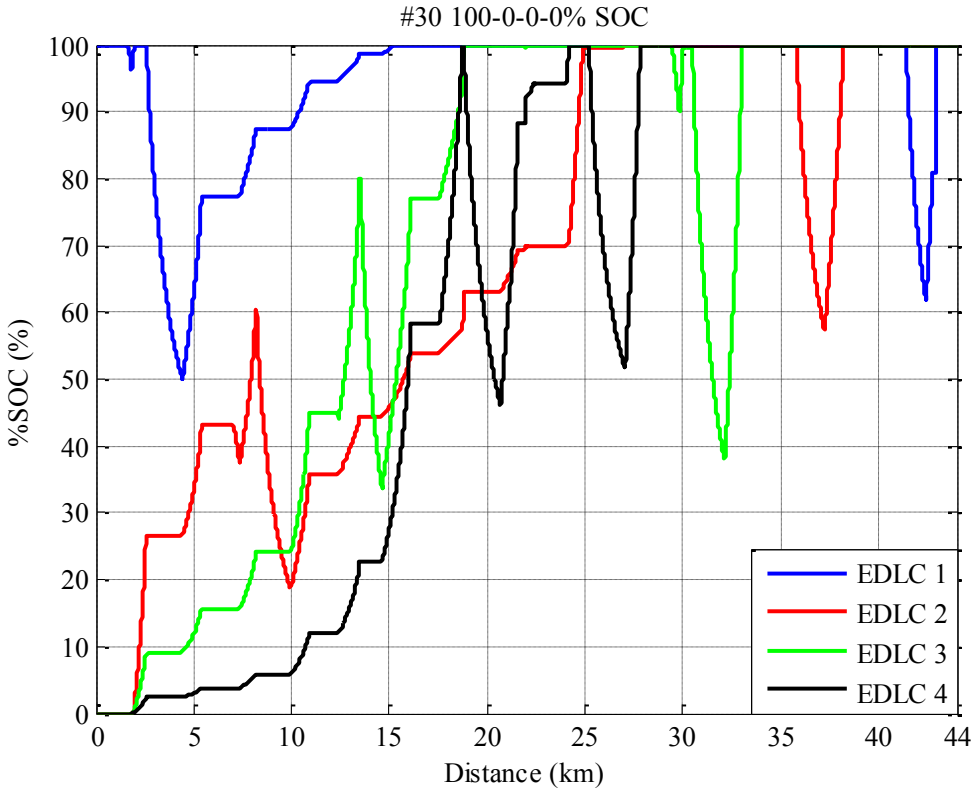

Figure A.30: Scenario 30, %SOC of 100, 0, 0 and 0 of stationary EDLCs

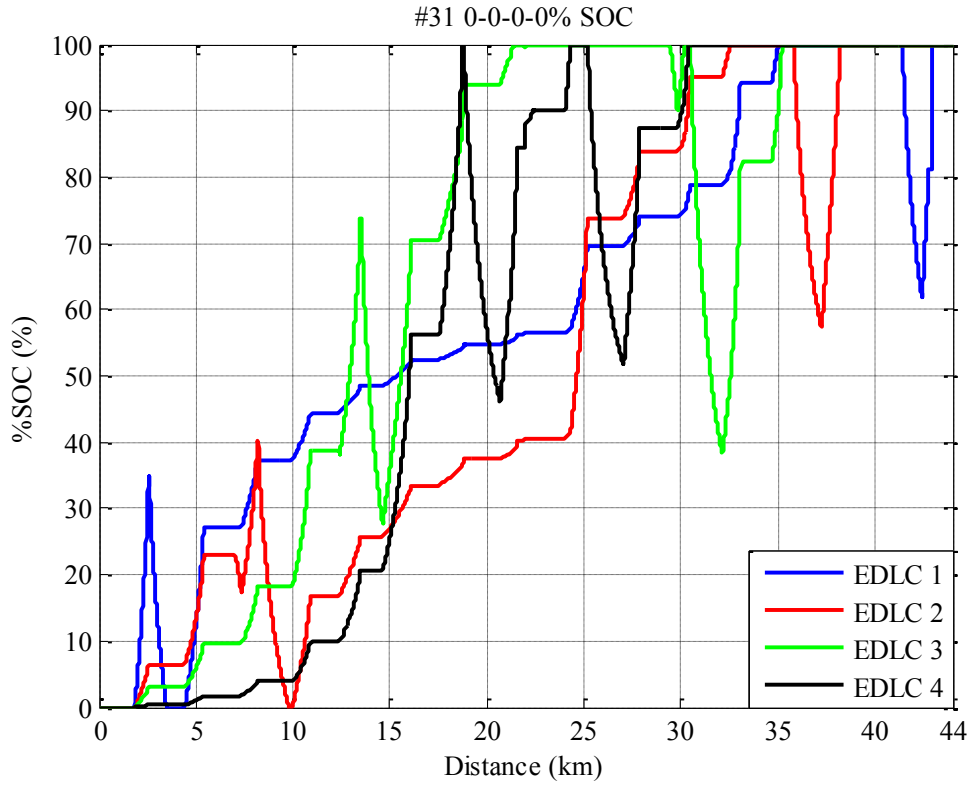

Figure A.31: Scenario 31, %SOC of 0, 0, 0 and 0 of stationary EDLCs

Appendix B: Publications

1. Ratniyomchai, T., Hillmansen, S. and Tricoli, P. (2014). Recent developments and applications of energy storage devices in electrified railways. *IET Electrical System in Transportation,* 4**,** 9-20.

2. Ratniyomchai, T., Hillmansen, S. and Tricoli, P. (2014) Published. Optimal capacity and positioning of stationary EDLCs for light rail vehicle systems. Proceeding on International Symposium Power Electronic Electrical Drives, Automation and Motion (SPEEDAM), 18-20 June 2014a Ischia, Italy. 807-812.

3. Ratniyomchai, T., Hillmansen, S. and Tricoli, P. (2015) Published. Energy Loss Minimisation by Optimal Design of Stationary EDLCs for Light Railways. Proceeding on 5th International Conference on Clean Electrical Power: Renewable Energy Resources Impact, 16-18 June 2015 Taormina, Italy. 528-534.

4. Ratniyomchai, T., Hillmansen, S. and Tricoli, P. (2016) Published. Energy Consumptions and Losses Minimisation for a Round-Trip of a Light Railway Journey by Optimal Design of Stationary Super Capacitors. Proceeding on Asian Conference on Engineering and Natural Sciences (ACENS), 1-3 February 2016, Fukuoka, Japan. 751-754.